Nonlinear wave structures in multispecies plasmas

by

PALTU HALDER

THESIS SUBMITTED IN FULFILLMENT OF
THE REQUIREMENTS FOR THE DEGREE OF
DOCTOR OF PHILOSOPHY (SCIENCE)
at

JADAVPUR UNIVERSITY
188, Raja S. C. Mallick Road, Kolkata - 700 032
West Bengal, India
June, 2024

যাদবপুর বিশ্ববিদ্যালয়

FACULTY OF SCIENCE
DEPARTMENT OF MATHEMATICS

JADAVPUR UNIVERSITY
Kolkata - 700 032, India
Telephone : 91 (33) 2457 2269

CERTIFICATE FROM THE SUPERVISOR

This is to certify that the thesis entitled **"Nonlinear wave structures in multispecies plasmas"**submitted by Sri **Paltu Halder** who got his name registered on **September 11, 2019** for the award of Ph.D. (Science) degree of **JADAVPUR UNIVERSITY**, is absolutely based upon his own work under the supervision of Prof. Anup Bandyopadhyay, Department of Mathematics, Jadavpur University, Kolkata- 700 032, West Bengal, India and that neither this thesis nor any part of it has been submitted for either any degree/diploma or any other academic award anywhere before.

Anup Bandyopadhyay
07/06/2024
.....

Prof. Anup Bandyopadhyay
(Signature of the Supervisor date with official seal)

Professor
DEPARTMENT OF MATHEMATICS
Jadavpur University
Kolkata – 700 032, West Bengal

Dedicated To

My Parents
&
Younger Sister

Table of Contents

Acknowledgements

Foremost, I would like to express my sincere gratitude to my guide, Prof. Anup Bandyopadhyay for the continuous support of my Ph.D. study and research, for his patience, motivation, enthusiasm and immense knowledge. His guidance helped me in all the time of research and writing of this thesis. I shall remain grateful forever to him for his affection, inspiration and valuable advice.

Secondly, I would like to acknowledge my sincere thanks to Dr. Sankirtan Sardar, Guru Ghasidas Vishwavidyalaya, Chhattisgarh, India and Dr. Sandip Dalui, Vellor Institute of Technology, Chennai, India for their advice and enlightening comments at different stages of my research works.

My sincere thanks also goes to the Heads of the Department of Mathematics, Jadavpur University, for giving me adequate facilities during the tenure of my research works. They rendered their support whenever it was needed. I also shall remain indebted to the teachers and staff for their kind help, despite many adverse circumstances.

I would like to express my thanks to Mrs. Jaba Bandyopadhyay, Dr. Animesh Das, Dr. Jayasree Das, Dr. Sk. Anarul Islam, Dr. Ashesh Paul, Dr. Debdatta Debnath and Ms. Rittika Pain for their constant encouragement and fruitful discussions to complete this work.

My very special thanks goes to Dr. Nibedita Pradhan, for standing beside me in all my ups and downs during this Ph.D. tenure and for her continuous support in various stages.

Last but not the least, I would like to thank my family: my grand mother, father, mother, uncles, aunts, elder and younger sisters for their endless love and support at every step of my life.

I greatly appreciate the financial support offered by CSIR Fellowship Scheme, HRDG, Government of India.

Date :

Place : Jadavpur, Kolkata Paltu Halder

List of published/ communicated papers

1. ***Dust-ion acoustic solitary waves in a collisionless magnetized five components plasma***

   P. Halder, A. Bandyopadhyay, S. Dalui, S. Sardar

   Z Naturforsch. A, **77**, pp 659 (15 pages) (2022)

   https://doi.org/10.1515/zna-2021-0287

2. ***Instability of dust-ion acoustic solitary waves in a collisionless magnetized five components plasma***

   P. Halder, A. Bandyopadhyay, S. Sardar

   Indian J Phys. **98**, pp 771 (13 pages) (2024)

   https://doi.org/10.1007/s12648-023-02839-0

3. ***Arbitrary amplitude dust-ion acoustic nonlinear and supernonlinear wave structures in a magnetized five components plasma***

   P. Halder, S. Dalui, S. Sardar, A. Bandyopadhyay

   Eur. Phys. J. Plus, **138**, pp. 734 (20 pages)(2023)

   https://doi.org/10.1140/epjp/s13360-023-04359-6

4. ***Modulation instability of obliquely propagating dust-ion acoustic waves in five components magnetized plasma***

   P. Halder, A. Bandyopadhyay, S. Dalui, S. Sardar

   Communicated

5. ***Arbitrary amplitude dust-ion acoustic solitary structures in five components unmagnetized plasma***

   P. Halder, A. Bandyopadhyay, S. Sardar

   Plasma Phys. Rep., **49**, pp. 467 (17 pages) (2023)

   https:// DOI: 10.1134/S1063780X22601225

6. ***Arbitrary amplitude DIA nonlinear wave structures at*** $M = M_c$ ***in an unmagnetized five components plasma***

   P. Halder, A. Bandyopadhyay, S. Dalui, S. Sardar

   Communicated

Abstract

In this thesis, we have considered the following problems on dust ion acoustic (DIA) waves in a collisionless magnetized / unmagnetized five components electron-positron-ion-dust (e-p-i-d) plasma consisting of warm adiabatic ions, static negatively charged dust particulates, nonthermal hot electrons, isothermal cold electrons and nonthermal positrons.

Problem-1: Here, we have derived a Korteweg-de Vries-Zakharov-Kuznetsov (KdV-ZK) equation to study the nonlinear behaviour of DIA waves in a collisionless magnetized five components plasma. It is found that the coefficient of the nonlinear term of the KdV-ZK equation vanishes along different family of curves in different compositional parameter planes. In this situation, to describe the nonlinear behaviour of DIA waves, we have derived a modified KdV-ZK (MKdV-ZK) equation. When the coefficients of the nonlinear terms of both KdV-ZK and MKdV-ZK equations are simultaneously equal to zero, then we have derived a further modified KdV-ZK (FMKdV-ZK) equation which effectively describes the nonlinear behaviour of DIA waves. Analytically and numerically, we have investigated the solitary wave solutions of different evolution equations propagating obliquely to the direction of the external static uniform magnetic field. We have also discussed the effect of different parameters of the system on solitary waves obtained from the different evolution equations.

Problem-2: Here, we have discussed the stability of DIA solitary waves obtained from the KdV-ZK and different modified KdV-ZK equations which have been derived in **Problem-1**. We have used the small-k perturbation expansion method of Rowlands and Infeld [J. Plasma Phys. 3, 567 (1969); 8, 105 (1972); 10, 293 (1973); 33, 171 (1985)] to analyze the stability of the steady state solitary wave solutions of the KdV-ZK equation and different modified KdV-ZK equations. In this method, we want to find a nonlinear dispersion relation of the nonlinear evolution equation connecting the lowest order of the wave frequency and the wave number. This nonlinear dispersion relation helps to analyze the

stability of solitary structures of the KdV-ZK equation and different modified KdV-ZK equations. We have found the instability condition and the growth rate of instability up to the lowest order of wave number. We have analyzed graphically the growth rate of instability of solitary waves of different evolution equations with respect to different parameters of the plasma system.

Problem-3: In this problem, we have considered the quasi-neutrality condition instead of the Poisson equation along with other hydrodynamic conservation equations as described in **Problem-1** to investigate the nonlinear behaviour of arbitrary amplitude DIA waves. We have applied the Sagdeev pseudo-potential approach and phase portrait analysis to confirm the existence of different DIA nonlinear wave structures. The plasma system contains eleven parameters and the nonlinear wave structures have been studied through the compositional parameter space consisting of these eleven parameters. The effects of these parameters on the amplitude of the nonlinear wave structures have also been investigated. We have extensively discussed the existence of negative potential solitary waves (NPSWs), positive potential solitary waves (PPSWs), positive potential supersolitons (PPSSs), negative potential double layers (NPDLs) and supernonlinear periodic waves. We have also analyzed the coexistence of PPSWs and NPSWs, coexistence of NPSWs and PPSSs, coexistence of NPDL and PPSSs. For increasing values of some parameters, there exists a sequence of NPSWs converging to the double layer solution of the same polarity, whereas it is also observed that a sequence of NPSWs converging to the double layer solution for decreasing values of some other set of parameters involved in the system. Therefore, the amplitude of the NPDL solution can be regarded as an upper bound of the amplitude of the sequence of the NPSWs. The dependence of the amplitudes of the PPSWs and PPSSs on the different parameters of the system has also been critically investigated.

Problem-4: Here, we have derived a nonlinear Schrödinger equation to study the modulation instability of DIA waves propagating obliquely to the direction of the uniform static magnetic field in the plasma system as defined in **Problem-1**. The nonlinear dispersion relation of the modulated DIA waves has been analyzed

to study the instability regions in the parameter planes. This nonlinear dispersion relation has also been used to investigate the maximum modulational growth rate of instability of the modulated DIA waves. We have discussed the effect of different parameters of the system on the existence of the instability regions and the maximum growth rate of instability.

Problem-5: In this problem, the energy integral derived by using Sagdeev pseudo-potential technique has been analyzed to investigate the existence of arbitrary amplitude DIA solitons including double layers and supersolitons in a collisionless unmagnetized plasma system whose constituents are same as given in **Problem-1**. The graphical analysis of Sagdeev pseudo-potential shows the existence of PPSSs along with positive potential double layers (PPDLs) and PPSWs whereas in the negative potential side, the system does not support negative potential supersolitons (NPSSs) but the existence of NPDLs, NPSWs, the coexistence of both PPSWs and NPSWs, and supernonlinear periodic waves have been established. To explain the existence of different DIA solitary structures, phase portraits of the dynamical system corresponding to the different DIA solitary structures have been drawn. With the help of phase portraits, the transition of PPSWs just before and just after the formation of PPDL has been discussed. We have discussed the effect of different parameters of the system on the amplitude of the different DIA solitary structures including supersolitons.

Problem-6: Here, we have investigated the arbitrary amplitude DIA nonlinear wave structures at the acoustic (sonic) speed $M = M_c$ in a collisionless unmagnetized plasma system as defined in **Problem-5**. The present plasma system confirms the existence of NPSWs, PPSWs and NPDLs at the acoustic speed $M = M_c$. We have studied the effect of different parameters of the system on the amplitude of PPSWs, NPSWs and NPDLs at $M = M_c$. We have also analyzed the difference between various DIA nonlinear wave structures at supersonic speed, subsonic speed and sonic speed through phase portraits of the dynamical system corresponding to nonlinear DIA wave structures.

List of Notations/Symbols/Terminologies

- IA wave : Ion acoustic wave.
- DIA wave : Dust-ion acoustic wave.
- DA wave : Dust acoustic wave.
- Korteweg-de Vries-Zakharov-Kuznetsov equation : KdV-ZK equation
- Modified KdV-ZK equation : MKdV-ZK equation
- Further Modified KdV-ZK equation : FMKdV-ZK equation
- NPSW : Negative potential solitary wave.
- PPSW : Positive potential solitary wave.
- NPDL : Negative potential double layer.
- PPDL : Positive potential double layer.
- PPSS : Positive potential supersolitons.
- NLSE : Nonlinear Schrödinger equation
- MI : Modulational instability
- e-i plasma : Electron-ion plasma.
- e-p-i plasma : Electron-positron-ion plasma.
- e-i-d plasma : Electron-ion-dust plasma.
- e-p-i-d plasma : Electron-positron-ion-dust plasma.
- n_{i0} : Unperturbed number density of ions.
- n_{c0} : Unperturbed number density of nonthermal electrons.
- n_{s0} : Unperturbed number density of isothermal electrons.
- n_{p0} : Unperturbed number density of positrons.
- n_{d0} : Unperturbed number density of dust grains.
- T_i : The average temperature of ions.
- T_{ce} : The average temperature of nonthermal electrons.

- T_{ce} : The average temperature of isothermal electrons.
- T_p : The average temperature of positrons.
- T_{pef} relation : $\frac{n_{c0}}{T_{ce}} + \frac{n_{s0}}{T_{se}} + \frac{n_{p0}}{T_p} = \frac{n_{c0} + n_{s0} - n_{p0} + Z_d n_{d0}}{T_{pef}}$.
- m_i : The mass of an ion.
- Z_d : The number of unit negative charges residing on a dust grain surface.
- N_{d0} : $Z_d n_{d0}$.
- $-e$: The charge of an electron.
- β_e : The nonthermal parameter associated with the nonthermal velocity distribution of electrons.
- β_p : The nonthermal parameter associated with the nonthermal velocity distribution of positrons.
- n_{sc} : $\frac{n_{s0}}{n_{c0}}$
- n_{pc} : $\frac{n_{p0}}{n_{c0}}$
- n_{dc} : $\frac{N_{d0}}{n_{c0}}$
- σ : $\frac{T_i}{T_{pef}}$.
- σ_{sc} : $\frac{T_{se}}{T_{ce}}$.
- σ_{pc} : $\frac{T_p}{T_{ce}}$.
- M : Mach number.
- M_c : Lower bound of the Mach number for the existence of solitary structures for the supersonic case, i.e., for $M > M_c$.

Introduction

This thesis presents some nonlinear problems on dust ion acoustic (DIA) waves in a collisionless five components magnetized or unmagnetized plasma system consisting of adiabatic warm ions, negatively charged static dust grains, nonthermal electrons defined by Cairns *et al.* [1], isothermal electrons and nonthermal positrons. We have investigated the existence of different DIA solitary wave solutions of different nonlinear evolution equations, which are valid in different compositioal parameter spaces, i.e., we have derived different nonlinear evolution equations by considering different conditions on the parameters of the system. One of the important parts of this thesis is to investigate the stability of these solitary wave solutions obtained from different evolution equations. We have also investigated the arbitrary amplitude DIA nonlinear waves including solitons of both polarities, double layers, supersolitons and supernonlinear periodic waves in the same five components collisionless magnetized or unmagnetized plasma system. In an another problem, we have investigated the modulation instability of obliquely propagating DIA waves in a collisionless magnetized five components plasma system. In this section, our aim is to present the overall scenario of this thesis by considering the following points:

- A brief review of the development of small amplitude solitary waves and their stability analysis
- A brief review of the development of arbitrary amplitude solitary waves
- A brief review of the development of modulational instability
- Different nonthermal distributions
- Satellite observations
- Different methods used in the present thesis
- Overview of each chapter

A brief review of the development of small amplitude solitary waves and their stability analysis

Solitary wave is a nonlinear wave whose shape and size remains unchanged during its propagation. There are many applications of these nonlinear waves in different areas of physics such as fluid dynamics, condensed matter physics, nonlinear optics and plasma dynamics. In 1895, Korteweg & De Vries [2] developed a theory of solitary waves by considering a nonlinear partial differential equation. In 1949, Walter H. Munk [3] summarized different properties of solitary waves. In 1958, Adlam & Allen [4] investigated solitary waves in a collisionless magnetized plasma. In 1965, Zabusky & Kruskal [5] discovered that the solitary waves retain their identity after the collision and they have used the term soliton instead of solitary wave. In 1966, Washimi & Tanuiti [6] investigated the one-dimensional long-time asymptotic behavior of small but finite amplitude ion acoustic (IA) waves. They have demonstrated the presence of solitons by deriving the Kortweg-de Vries (KdV) equation. In 1974, Tran [7] investigated the IA solitary waves in a two-ion species plasma with a finite ion temperature by deriving a KdV equation. He found that a finite ion temperature produces fast as well as slow IA solitary waves. In 1975, Das and Tagare [8] studied the same problem with oppositely charged ions by deriving a KdV equation. They clearly mentioned that rarefactive solitary waves can propagate only if the initial concentration of negative ions is greater than a critical value. In 1977, Goswami and Buti [9] used the reductive perturbation method to derive a multi-dimensional modified KdV equation which describes the propagation of a finite amplitude drift wave in a collisional plasma. In 1984, Watanabe [10] considered a plasma system consisting of positive ion, negative ion and electrons to study the nonlinear IA waves. He had clearly mentioned that when the density of negative ion reaches a critical value, the nonlinear coefficient of the KdV equation vanishes. In this situation, he established that the IA wave can be described by a modified KdV equation. The evolution equation with quadratic and cubic nonlinearities had been used to study the nonlinear behaviour of IA waves in this situation. Tagare and Reddy [11, 12] examined the effect of ion temperature on IA solitons in a

warm, two-ion plasma consisting of positive ions, negative ions and hot electrons. In 1988, Verheest [13] investigated IA solitons in a plasma consisting of isothermal electrons and a number of adiabatic ion species by considering the reductive perturbation method. He clearly mentioned that nonlinear behaviour of IA waves can be described by a modified KdV equations with cubic nonlinearities when the coefficient of the nonlinear term of the KdV equation vanishes. In 1989, Das and Verheest [14] studied on IA solitons in a low-β magnetized plasma consisting of adiabatic positive and negative ion species along with isothermal electrons. They derived a three dimensions KdV equation, also known as the Korteweg-de Vries-Zakharov-Kuznetsov (KdV-ZK) equation. They have used the small-k perturbation expansion method of Rowlands and Infeld [15–18] to study the stability of solitary wave solutions at the lowest order of wave number, i.e., for long-wavelength plane-wave perturbation. Several authors [14, 19–49] have used this method [15–18] to investigate the stability of different types of solitary waves and double layers. Several authors [24, 26, 50–55] investigated different nonlinear properties of IA solitons by considering nonthermal electrons as prescribed by Cairns *et al.* [1]. By considering the effect of different parameters of different plasma systems, several authors [56–62] studied the nonlinear behaviour of IA waves.

A brief review of the development of arbitrary amplitude solitary waves

Sagdeev [63] established a very important mechanical analogy to describe the nonlinear dynamics of IA waves through a single equation known as energy integral, which can be regarded as the motion of a particle in one dimension. In fact, shifting all the equations describing the nonlinear behaviour of IA waves in a wave frame, he is able to form the following equation:

$$\phi_{\xi\xi} + V'(\phi) = 0 \Leftrightarrow \frac{1}{2}(\phi_\xi)^2 + V(\phi) = 0, \tag{1}$$

where he has used a suitable transformation of the coordinate axis without making any perturbation of the dependent variables. This equation can be regarded as the equation of motion of a pseudo-particle of unit mass under the action of

the force field $-V'(\phi)$, where ϕ is the position of the pseudo-particle at time ξ with velocity $\frac{d\phi}{d\xi}$. The magnitude of the velocity of the particle is $\sqrt{-2V(\phi)}$. If $V(0) = V'(0) = 0$, then the particle is in equilibrium at the point $\phi = 0$. If $V''(0) < 0$, then using the Energy Test of Stability, one can conclude that the particle is in unstable equilibrium at $\phi = 0$. Therefore, if the particle is slightly displaced from its unstable position of equilibrium then it moves away from $\phi = 0$ and it continues its motion until there exists a $\phi_m \neq 0$ such that $V(\phi_m) = 0$. If $V'(\phi_m) > 0$ (for $\phi_m > 0$) or $V'(\phi_m) < 0$ (for $\phi_m < 0$) then the pseudo-particle at $\phi = \phi_m$ is under the action of an attracting force towards $\phi = 0$. Consequently, the particle oscillates between $0 < \phi < \phi_m$ for $(\phi_m > 0)$ or $\phi_m < \phi < 0$ for $(\phi_m < 0)$. This oscillation propagates in a wave frame moving with a dimensionless velocity M, known as Mach number. If the oscillation propagates along the positive direction of ϕ axis, then we have positive potential solitary waves and if the oscillation propagates along the negative direction of ϕ axis, then we have negative potential solitary structures. This is the mechanical analogy of solitary waves as given by Sagdeev [63]. Using this mechanical analogy, Shukla & Yu [64] investigated nonlinear IA waves in a magnetized plasma. In small amplitude limit, they have derived an energy integral which describes nonlinear IA waves propagating obliquely making an angle to the direction of the external magnetic field. Shukla & Yu [64] established a relationship between the angle of propagation, the soliton's speed, and its amplitude. Additionally, they derived an exact analytical formula for the electric field in the small amplitude limit. In 1980, Buti [65] studied a plasma composed of cold ions together with both hot and cold electrons. They derived an energy integral for a pseudo-particle. In 1986, Bharuthram and Shukla [66] presented a theory for a double layer in a plasma consisting of cold ions and two distinct groups of hot electrons obeying Boltzmann-Maxwellian distribution. The double layer solutions can also be described from the mechanical analogy of Sagdeev [63]. Here, if $V(\phi_m) = 0$ and $V'(\phi_m) = 0$, then the velocity as well as the force acting on the pseudo-particle both are simultaneously equal to zero and consequently, the particle can not be reflected at $\phi = 0$ because for this case there is no oscillation of the particle. In this situation, the solution obtained from energy integral is known as double layer

solution. This theory describes conditions under which large amplitude stationary double layers can exist. The IA solitons and double layers for arbitrary amplitude were investigated by Baboolal *et al.* [67, 68] in a plasma system consisting of two different species of ions and two distinct populations of isothermal electrons of different temperatures. Using the Sagdeev pseudo-potential formalism, large dust-acoustic (DA) waves have been studied by Verheest [69] in a multispecies plasma model with cold negative dust in the presence of hot nonthermal Cairns distributed positive ions and cold Boltzmann positive ions. Verheest and others [70–74] have studied different types of large amplitude solitary waves including supersolitons by considering different plasma systems. Dubinov *et al.* [75] applied Sagdeev pseudo-potential method to study the nonlinear wave structures. They have investigated the nonlinear and supernonlinear wave structures in five components collisionless unmagnetized electron-positron-ion-dusty (e-p-i-d) plasma consisting of positive ions and negative ions species. Several authors [75–84] have considered collisionless four components e-p-i-d plasma systems to discuss different arbitrary amplitude nonlinear wave structures in unmagnetized e-p-i-d plasma. Choi *et al.* [85] studied arbitrary amplitude IA solitary structures in a magnetized collisionless dusty plasma. They solved this problem using Sagdeev's pseudo-potential method. In another study, Choi *et al.* [86] explored the impact of ion pressure on IA solitary structures. Dubinov *et al.* [87] showed that large amplitude stationary electrostatic waves are possible in symmetric unmagnetized pair plasmas. Later, Dubinov and others [88–90] have defined the large amplitudes solitons including supersoliton and supernonlinear periodic structures. Das *et al.* [91] investigated DIA solitary waves and double layers in a dusty plasma system. The system contains adiabatic warm ions, nonthermal electrons, and negatively charged static dust grains. They have analyzed different types of solitary structures by considering the entire compositional parameters space. Several authors [92–101] have studied various arbitrary amplitude nonlinear wave structures by considering different magnetized plasma systems. Verheest and Hellberg [102] observed a positive potential DA solitary structure at the sonic speed in a collisionless, unmagnetized plasma system. This was the first observation of a DA solitary structure at the sonic speed. Later, Das *et al.* [103] analytically proved

ten important theorems for the existence of solitary structures at the sonic speed for any unmagnetized plasma system. With the help of these theorems of Das *et al.* [103], Paul *et al.* [83] studied DIA solitary structures at the sonic speed in a collisionless unmagnetized e-p-i-d plasma system with warm ions, Cairns-distributed electrons, Maxwellian-distributed positrons, and negatively charged static dust grains. For the first time, Debnath and Bandyopadhyay [101] studied IA solitary waves at acoustic speed in a collisionless magnetized plasma.

A brief review of the development of modulational instability

In 1968, Taniuti & Washimi [104] derived a nonlinear Schrödinger equation to investigate modulational instability (MI) of finite amplitude hydromagnetic waves in a magnetized cold plasma. Later, Taniuti and Yajima [105] studied the nonlinear Schrödinger equation (NLSE) from a set of complex nonlinear partial differential equations, where they used the perturbation method to derive the NLSE. Using this perturbation method, Asano *et al.* [106] derived a NLSE for electron plasma system which describes the nonlinear wave modulation. In 1972, Kako [107] made a thorough investigation on the nonlinear modulation of waves in a cold magnetized plasma. In an another paper, Kako *et al.* [108] explored the nonlinear modulation of electromagnetic waves that propagate parallel to external magnetic field giving special emphasis to the contribution of resonant particles at the group velocity. After that Kako [109] considered MI of IA waves in both magnetized and unmagnetized plasma. The plasma system was composed of cold ions and isothermal electrons. Ichikawa & Kako [110] focused on the nonlinear wave modulation of quasi-monochromatic electromagnetic waves in a magnetized plasma. In this investigation, they have also considered the effect of resonant particles at the group velocity. Kakutani and Sugimoto [111] used the Krylov-Bogoliubov-Mitropolsky (KBM) perturbation method to derive a NLSE for the nonlinear modulation of IA and magneto-acoustic waves in a collisionless plasma consisting of cold ions and isothermal electrons. Murtaza and Salahuddin [112] studied the modulation of IA waves in a magnetized plasma consisting of cold ions and isothermal electrons. Several authors [113–130] investigated the modulation instability of IA waves in different plasma systems in a collisionless unmagnetized/

magnetized plasma systems consisting of different types of particles. In the papers [131, 132], authors have considered an unmagnetized five components plasma system with positive ions, nonextensive positrons and two electron species at different temperatures having nonextensive distribution and dust grains. Guo *et al.* [131] have studied MI of the planar and nonplanar IA waves by considering negative and positive dust grains. By considering the same plasma model, and using the reductive perturbation method [105, 106] El-Kalaawy [132] has derived a modified NLSE which describes the low-frequency modulation of IA waves. Watanabe [133] and Ikezi *et al.* [134] conducted experiments to investigate the MI of a nonlinear ion wave packet.

Different nonthermal distributions

A. Kappa distribution: This is a long high-energy-tailed non-Maxwellian distribution, which has the property that the number of particles in phase space far away from the point $v = 0$ is much greater than the number of particles in the same region for the Maxwellian-Boltzmann distribution, where v is the velocity of the particles in phase space. The Kappa distribution was used by Binsack [135] and Vasyliunas [136]. Since then, several authors [70, 137–153] have used this distribution in various studies of plasma physics.

B. Cairns distribution: This is a modified Maxwellian-Boltzmann distribution, which has the property that the number of particles in phase space in the neighbourhood of the point $v = 0$ is much smaller than the number of particles in the same region for the Maxwellian-Boltzmann distribution [154]. In fact, the number of electrons in the neighbourhood of $v = 0$ decreases for increasing values of the nonthermal parameter associated with the distribution. Consequetly, the distribution function develops wings for increasing values of the nonthermal parameter and at the same time, the center density in phase space drops [155]. It is also simple to check that these two wings are symmetrical about the point $v = 0$. So, the Cairns distribution describes the flattening of the distribution in phase space in the neighbourhood of the point $v = 0$. Several authors [1, 21, 50, 79, 81, 91, 94, 103, 154, 156–167] have used this distribution to study various nonlinear properties of plasma dynamics.

C. Combined Kappa-Cairns distribution: As reported by Debnath and Bandyopadhyay [100], the combined Kappa-Cairns distribution describes the possible deviation of Kappa distribution in the neighbourhood of the point $v = 0$ with the help of Cairns distribution. This distribution follows the properties of Kappa distribution as well as the properties of Cairns distribution. Specifically, (1) this distribution follows the properties of Kappa distribution, i.e., the number of particles in phase space far away from the point $v = 0$ is much greater than the number of particles in the same region for the Boltzmann-Maxwellian distribution and (2) this distribution follows the properties of Cairns distribution, i.e., the number of particles in phase space in the neighbourhood of the point $v = 0$ is much smaller than the number of particles in the same region for the Kappa distribution. The number of electrons in the neighbourhood of $v = 0$ decreases for increasing values of the nonthermal parameter associated with the distribution. Consequently, the distribution function develops wings for increasing values of the nonthermal parameter and at the same time, the center density in phase space drops. Debnath and Bandyopadhyay [100] have clearly explained these two properties with the figure 1 in their paper. It is also simple to check that these two wings are symmetrical about the point $v = 0$. Therefore, this distribution describes the flattening of the Kappa distribution in the neighbourhood of the point $v = 0$. So, this distribution is nothing but the Cairns distribution when the Kappa distribution is taken as the background distribution.

D. Nonextensive nonthermal velocity distribution: Instead of Kappa distribution if we take q- nonextensive distribution as the background distribution, then considering the deviation in the neighbourhood of the point $v = 0$ by using the Cairns distribution, we get nonthermal q- nonextensive velocity distribution. This was first used by Tribeche *et al.* [168] to study IA solitary waves in a plasma consisting of cold ions and nonthermal nonextensive electrons.

Satellite Observations

The presence of e-p-i-d plasma has been detected in interstellar medium [169–171], in the remnants of supernova explosions [172], in the galactic centre [169], around pulsars [173], in the Milky Way [171]. Also this e-p-i-d plasma may exist in the Earth's magnetosphere and in the Earth's ionosphere. These regions contain positrons [174, 175] and highly charged dust grains [172]. The observation of various spacecraft missions [176–180, 180–186] indicates the existence of two electron species of different temperatures (cold and hot) at the auroral region. More specifically Viking satellite [176, 177] and Freja satellite [187] indicate coexistence of energetic electrons and isothermal electrons in the auroral region of the Earth's upper ionosphere. But there is no proper technique for the construction of the velocity distribution function of the energetic particles in the space plasma and consequently, we have used different non-Maxwellian velocity distributions to express the behaviour of the energetic particles. Cairns [1] distributed nonthermal model for the lighter species is one of the widely used non-Maxwellian model and this distribution can describe a population of fast energetic particle.

In this present thesis, we have considered an e-p-i-d plasma system, where electron species is divided into two distinct populations of electrons at different temperatures. From this point of view, i.e., as the two distinct populations of electrons follow two different distributions, we can consider the present plasma system as five components plasma. In fact, based on the assumption that the above mentioned species of electrons are physically separate in the phase space by external or self-consistent fields [188], then these two species of electrons can be taken as two distinct species of electrons. So, we can conclude that there may exist five components e-p-i-d plasmas in the auroral region of the upper Earth's ionosphere, which contains nonthermal hot electrons and isothermal cold electrons. In future, next generation satellites may be able to distinguish astrophysical plasmas having five components as considered in this thesis.

Moslem *et al.* [189] have considered a five components dusty plasma system consisting of positively charged dust grains, Maxwellian electrons, and ions including solar wind streaming electrons and protons. They have used this plasma

model in Jupiters magnetosphere to investigate the dynamics of the dust grains and solar wind streaming electrons and protons. Afterward, Al-Yousef *et al.* [190] have considered the same plasma model of Moslem *et al.* [189] to investigate the arbitrary amplitude dust-acoustic waves in the Jupiter atmosphere for a distance greater than $15R_j$, where R_j (= 71398 km) is the distance from the center of the Jupiter. Considering the reports as mentioned in the papers [189] and [190], and considering the mechanism for the formation of positrons from protons as mentioned by Gusev *et al.* [174, 175], we can conclude that there may exist five components e-p-i-d plasmas in the Jupiter atmosphere for a distance greater than $15R_j$.

Again, several authors [189–192] have considered dusty plasmas of five components consisting of positive dust grains, ions and isothermal or superthermal electrons including solar wind streaming protons and electrons. Finally, they [189–192] concluded that the results are applicable in Jupiter's atmosphere by considering the five components positively charged dusty plasma model. Although, several authors have used their model in Jupiter's atmosphere by considering positively charged dust grains, there are many research papers in the existing literature, where authors [193–197] have described their results in Jupiter's atmosphere for both polarities dusty plasma model. So, the plasma systems of this thesis may be applicable to study the nonlinear waves in the upper ionosphere of Earth and in Jupiter's atmosphere.

Different Methods Used in the Present Thesis

In this thesis, we have used the following methods:

- **Sagdeev Pseudo Potential Technique [63]**
- **Reductive Perturbation Method [198]**
- **Generation of Different Harmonics Through Perturbation Method [106]**
- **Tanh Method of Malfliet and Hereman [199]**

- **Small-k Perturbation Expansion Method of Rowlands & Infeld [15–18]**
- **Numerical Method for Phase Portrait**
- **Different Methods of Applied Mathematics**

Overview of Each Chapter

Chapter-1

In this **chapter**, we have studied the nonlinear behaviour of small amplitude DIA waves in a collisionless magnetized five components dusty plasma consisting of warm adiabatic ions, nonthermal hot electrons, isothermal cold electrons, nonthermal positrons and static negatively charged dust particulates.

- To discuss the nonlinear behaviour of the small amplitude DIA waves, we have derived the following KdV - ZK equation:

$$\phi_{\tau}^{(1)} + AB_1\phi^{(1)}\phi_{\zeta}^{(1)} + \frac{1}{2}A\phi_{\zeta\zeta\zeta}^{(1)} + \frac{1}{2}AD(\phi_{\eta\eta}^{(1)} + \phi_{\xi\xi}^{(1)})_{\zeta} = 0, \tag{2}$$

  where A, B_1 and D are functions of the parameters of the plasma system.

- The nonlinear behaviour of DIA waves can be described by the KdV-ZK equation (2) only when the coefficient of the nonlinear term of the KdV-ZK equation does not vanish, i.e., $B_1 \neq 0$. But when $B_1 = 0$, the coefficient of the nonlinear term of the KdV-ZK equation (2) vanishes along different families of curves in the compositional parameter planes and for this case, we have derived the following modified KdV-ZK (MKdV-ZK) equation to describe the nonlinear behaviour of the DIA waves:

$$\phi_{\tau}^{(1)} + AB_2(\phi^{(1)})^2\phi_{\zeta}^{(1)} + \frac{1}{2}A\phi_{\zeta\zeta\zeta}^{(1)} + \frac{1}{2}AD(\phi_{\eta\eta}^{(1)} + \phi_{\xi\xi}^{(1)})_{\zeta} = 0, \tag{3}$$

  where B_2 is a function of the parameters of the plasma system. The nonlinear behaviour of DIA waves can be described by the MKdV-ZK equation only when $B_1 = 0$ but $B_2 \neq 0$. But we see that the coefficient of the nonlinear term of the MKdV-ZK equation (3) vanishes along different family

of curves in the compositional parameter plane. In this situation, i.e., when $B_1 = 0$ and $B_2 = 0$, neither KdV-ZK equation nor MKdV-ZK equation can describe the nonlinear behaviour of the DIA waves and for this case, we have derived the following further modified KdV-ZK (FMKdV-ZK) equation:

$$\phi_{\tau}^{(1)} + AB_3(\phi^{(1)})^3\phi_{\zeta}^{(1)} + \frac{1}{2}A\phi_{\zeta\zeta\zeta}^{(1)} + \frac{1}{2}AD(\phi_{\eta\eta}^{(1)} + \phi_{\xi\xi}^{(1)})_{\zeta} = 0, \tag{4}$$

where B_3 is a function of the parameters of the plasma system.

- We have investigated the validity of the different evolution equations by considering different compositional parameter planes.

- We have studied the solitary wave solutions of different evolution equations propagating obliquely to the direction of the external static uniform magnetic field.

- We have investigated the effect of different parameters on the solitary wave solutions of different evolution equations.

Chapter-2

This **chapter** can be regarded as an extension of Chapter-1 in the following direction:

In this **chapter**, we have discussed the stability of DIA solitary waves obtained from the KdV-ZK equation and different modified KdV-ZK equations derived in **Chapter-1**.

We have used the small-k perturbation expansion method of Rowlands and Infeld [15–18] to analyze the stability of the steady state solitary wave solutions of the KdV-ZK equation and different modified KdV-ZK equations. In this method, we want to find a nonlinear dispersion relation of the nonlinear evolution equations connecting the lowest order of ω and k, where ω is the wave frequency and k is the wave number. This nonlinear dispersion relation helps to analyze the stability of solitary structures of the KdV-ZK equation and different modified KdV-ZK equations.

- For the first time, we have studied the instability of DIA solitary waves in a five components e-p-i-d plasma with the help of the small-k perturbation expansion method of Rowlands and Infeld.

- We have found the instability condition and the growth rate of instability up to the lowest order of wave number (k). We have graphically analyzed the growth rate of instability of different evolution equations with respect to different parameters of the present plasma system.

- In this **chapter**, our aim is to study the stability of the steady state solitary wave solutions of the different nonlinear evolution equations by considering the perturbation in the form $\Phi_0(Z)+q_1(\xi,\eta,\tau,Z)$, where $\Phi_0(Z)$ is the steady state solitary wave solution of the evolution equation and $q_1(\xi,\eta,\tau,Z)$ is the perturbed quantity with respect to $\Phi_0(Z)$ as steady state solitary wave solution.

- In this **chapter**, we have considered the long-wavelength plane-wave perturbation and consequently, the wave number is the small parameter of the system and so, the general prescription is to express the perturbed quantity in a power series of the wave number k.

- Considering $\Phi_0(Z)$ as a steady state, our aim is to express the wave frequency ω as a function of the wave number k. For linearized case, it is possible to express ω as a function of k, but for nonlinear evolution equation with $\Phi_0(Z)$ as a steady state, it is not possible to express ω as a function of k. For this reason, we also expand ω in a power series of k by considering k is small enough.

- For the first time, we have derived the consistency condition for the existence of solutions of a sequence of differential equations connected with the perturbed field variable with respect to the steady state solitary wave solutions of the different evolution equations by considering Lagrange's identity and this consistency condition helps to study the instability of the DIA solitary waves up to the lowest order of the wave number.

- In this **chapter**, we are not only interested to analyze the stability of soliton as given by several authors [200–206] by considering several methods, but also interested to find the growth rate of instability. The consistency condition helps to find the growth rate of instability.

- We have discussed the effects of parameters involved in the plasma system on the instability condition and the growth rate of instabilities for the KdV solitons and different modified KdV solitons.

- Finally, we have compared the result of the stability analysis of DIA solitons described in this chapter for magnetized e-p-i-d plasma with the stability analysis of DIA solitons for unmagnetized e-p-i-d plasma as presented by Sardar *et al.* [45].

- It is found that DIA solitary waves in a collisionless **magnetized** e-p-i-d plasma obtained from the KdV-ZK equation and different modified KdV-ZK equations having the nonlinear term of the form $(\phi^{(1)})^r \phi_\zeta^{(1)}$ are unstable for $r < 4$ at the lowest order of the wave number. Although Sardar *et al.* [45] have shown that DIA solitary waves described by the three-dimensional KP and different modified KP equations having the nonlinear term of the form $\frac{\partial}{\partial \xi}\left((\phi^{(1)})^r \phi_\xi^{(1)}\right)$ in a collisionless **unmagnetized** e-p-i-d plasma are stable for $r < 4$, where ξ is the stretched space coordinate in the paper of Sardar *et al.* [45]. They have also used the same small-k perturbation expansion method of Rowlands and Infeld [15–18].

- Analytically the instability conditions and the growth rate of instability at the lowest order of the wave number have been derived for the KdV-ZK soliton and different modified KdV-ZK solitons using the consistency condition.

- We have also numerically studied the growth rate of instabilities of the KdV-ZK soliton and different modified KdV-ZK solitons.

Chapter-3

In this **chapter**, we have considered the same plasma system as mentioned in **Chapter-1** but we have considered the quasi-neutrality condition instead of the Poisson equation along with the other hydrodynamic conservation equations as described in **Chapter-1** to investigate the nonlinear behaviour of arbitrary amplitude dust ion acoustic waves in a collisionless five components magnetized e-p-i-d plasma giving special emphases on the following points:

- To discuss the nonlinear behaviour of the arbitrary amplitude dust ion acoustic waves in a collisionless magnetized plasma with warm adiabatic ions, nonthermally distributed positrons, negative immobile dust particles, and two distinct species of electrons with isothermally and nonthermally distributed, we have derived the following energy integral:

$$\frac{1}{2}\left(\frac{d\phi}{d\xi}\right)^2 + V(\phi) = 0, \tag{5}$$

where $V(\phi)$ is a function of ϕ, M and other parameters of the plasma system. Here M is the normalized (dimensionless) velocity of the wave frame. In fact, we have used the following steps to get the energy integral (5)

[**1**] To derive the energy integral (5), all hydrodynamic conservation equations consisting of continuity equation for ions, the equation of conservation of momentum for ion fluids and the equation of conservation of pressure equation for ions are shifted in a wave frame moving with a normalized velocity M.

[**2**] To consider a wave frame moving with a velocity M, the general prescription is to consider the following transformation:

$$\xi = m_x x + n_y y + l_z z - Mt,$$

where $m_x,\ n_y,\ l_z$ are the direction cosines of the direction of the moving wave frame and we have also normalized the space coordinates $x,\ y,\ z$ and time t by appropriate length and appropriate time.

[**3**] Finally, using the quasi-neutrality condition and the appropriate boundary conditions for solitary structures, we get the energy integral (5).

- We have seen that the system supports the existence of PPSWs, PPSSs, NPSWs and NPDLs along with the coexistence of different solitary structures and supernonlinear periodic waves. The curve $V(\phi)$ with respect to ϕ and the phase portraits of the dynamical system defined by

$$\frac{d\phi}{d\xi} = \theta, \qquad \frac{d\theta}{d\xi} = -V^{'}(\phi) \tag{6}$$

confirm the existence of different solitary wave structures including double layers, supersolitons and super-nonlinear periodic waves. The coupled system of equations (6) can easily be obtained by differentiating (5) with respect to ϕ and then putting $\frac{d\phi}{d\xi} = \theta$.

- It is observed that NPSW and PPSS exist simultaneously and also it is found NPDL and PPSS exist simultaneously.

- Two distinct types of supernonlinear periodic waves as mentioned by Dubinov and others [89, 90] have been observed in this magnetized plasma system.

- We have investigated the effect of different parameters of te system on the amplitude of different solitary structures.

Chapter-4

In this **chapter**, we have considered the same plasma system as mentioned in **Chapter-1**. Considering the generation of different Harmonics through the perturbation method, we have derived the following nonlinear Schrödinger equation to study the modulational instability of DIA waves propagating obliquely to the direction of the uniform static magnetic field.

$$i\frac{\partial\phi_1^{(1)}}{\partial\tau} + P\frac{\partial^2\phi_1^{(1)}}{\partial\xi^2} + Q|\phi_1^{(1)}|^2\phi_1^{(1)} = 0, \tag{7}$$

where P and Q are the functions of parameters of the system.

The nonlinear dispersion relation of the modulated DIA wave has been analyzed to study the instability regions in the parameter plane. The nonlinear dispersion relation of the modulated DIA waves obtained from the NLSE (7) is given by the following equation:

$$\Omega^2 = [PK^2]^2\left(1 - \frac{2Q|\phi_0|^2}{PK^2}\right), \tag{8}$$

where Ω and K are, respectively, the wave frequency and wave number of modulated DIA waves.

From the equation (8), it is simple to check that

- modulated DIA wave is always modulationally stable for $PQ < 0$.
- modulated DIA wave is stable or unstable according to whether $K \geq K_c$ or $K < K_c$ if $PQ > 0$, where $K_c = \sqrt{\frac{2Q|\phi_0|^2}{P}}$.

Using only these two conditions, we have investigated the effect of parameters on the stable and unstable regions of the modulated DIA waves and when modulated DIA wave is unstable then we have also investigated the maximum growth rate of instability of the modulated DIA wave.

Chapter-5

In this **chapter**, we have considered a collisionless unmagnetized five components plasma system whose constituents are same as given in **Chapter-1**, i.e., the system contains two distinct species of electrons at different temperatures - one is nonthermally distributed hot electrons and another one is Boltzmann-Maxwellian distributed cold electrons, warm adiabatic ions, nonthermally distributed positrons and negatively charged immobile dust grains. Using the Sagdeev pseudo-potential technique, we have derived an energy integral. To derive the energy integral, we follow similar steps as given in problem **Chapter-3**. But here instead of quasi-neutrality condition, we have used the Poisson equation. The structure of the energy integral is same as given in equation (5). The coupled equations obtained by differentiating the energy integral (5) are also same as the coupled equations given in (6). Here also M (Mach number) is the dimensionless velocity of the wave frame normalized by the linearized DIA speed (c_s).

We have observed the existence of positive potential solitary waves (PPSWs), negative potential solitary waves (NPSWs), the coexistence of both PPSWs and NPSWs, negative potential double layers (NPDLs), positive potential double layers (PPDLs), supersolitons, and super-nonlinear periodic waves.

- We have seen that for the supersonic speed of the waves ($M > M_c$), the origin (0, 0) is an unstable equilibrium point, whereas for the subsonic speed of the waves ($M < M_c$), the origin (0, 0) is a stable equilibrium point, where M_c is a lower bound M for the existence of supersonic solitary structures, i.e., supersonic solitary structure exists only when $M > M_c$. Therefore, there does not exist any solitary structure if $M < M_c$.

- In this chapter, we have investigated the solitary structures for supersonic speed only and we have also considered super-nonlinear periodic waves for subsonic speed only. We have not considered any wave structure for sonic speed.

- We have seen that every minimum value of the potential function $V(\phi)$ corresponds to a stable equilibrium point, whereas the maximum value of potential function $V(\phi)$ corresponds to an unstable equilibrium point.

- We have seen that every closed curve about any stable equilibrium point corresponds to a periodic wave solution, whereas a separatrix that appears to pass through the unstable equilibrium point at the origin (0, 0) enclosing a stable equilibrium point corresponds to a solitary wave.

- The separatrix through (0, 0) which encloses more than one separatrices and more than one stable equilibrium points corresponds to supersolitons.

- For the subsonic speed ($M < M_c$), the super-nonlinear periodic wave exists only when there exists a separatrix passes through a non-zero unstable equilibrium point enveloping another separatrix that appears to pass through another non-zero unstable equilibrium point. The inner separatrix encloses at least two stable equilibrium points, one of which is (0, 0). Any closed

curves within inner and outer separatrices are due to super-nonlinear periodic waves.

- We have found that there exists a smooth transition from one solitary structure to another solitary structure as PPSW (before the formation of PPDL) $\rightarrow$ PPDL $\rightarrow$ PPSS $\rightarrow$ PPSW (after the formation of PPDL). This smooth transition has been observed for the present five components plasma model, which confirms the existence of a sequence of supersolitons.

- We have also investigated the effect of different parameters of the system on the amplitude of different solitary waves.

Chapter-6

In this **chapter**, we have investigated arbitrary amplitude dust ion acoustic nonlinear wave structures at $M = M_c$ in a collisionless unmagnetized five components electron-positron-ion-dusty (e-p-i-d) plasma system as considered in **Chapter -5**. The present plasma system confirms the existence of negative potential and positive potential solitary structures. We have also observed the existence of negative potential double layers (NPDLs) at the acoustic speed $M = M_c$. In this **chapter**, we have studied the effects of different parameters of the system on the amplitude of the positive potential solitary waves (PPSWs), negative potential solitary waves (NPSWs) and negative potential double layers. We have also analyzed the difference between the various DIA nonlinear wave structures at supersonic speed, subsonic speed and sonic speed by considerig the phase portraits of the dynamical system corresponding to nonlinear DIA wave structures.

- We have seen that for subsonic speed (supersonic speed) of the waves $M < M_c (M > M_c)$ the origin (0, 0) is a stable (unstable) equilibrium point, whereas, for sonic speed ($M = M_c$), the origin (0, 0) is the point of inflexion.

- From the phase portrait of DIA double layers at sonic speed, we have seen the separatrix of the phase portrait tends to pass through an unstable equilibrium point which starts and ends at the point of inflexion. This separatrix encloses at least one stable equilibrium point.

The schematic diagram of this thesis can be represented as follows.

The Schematic Diagram of The Present Thesis

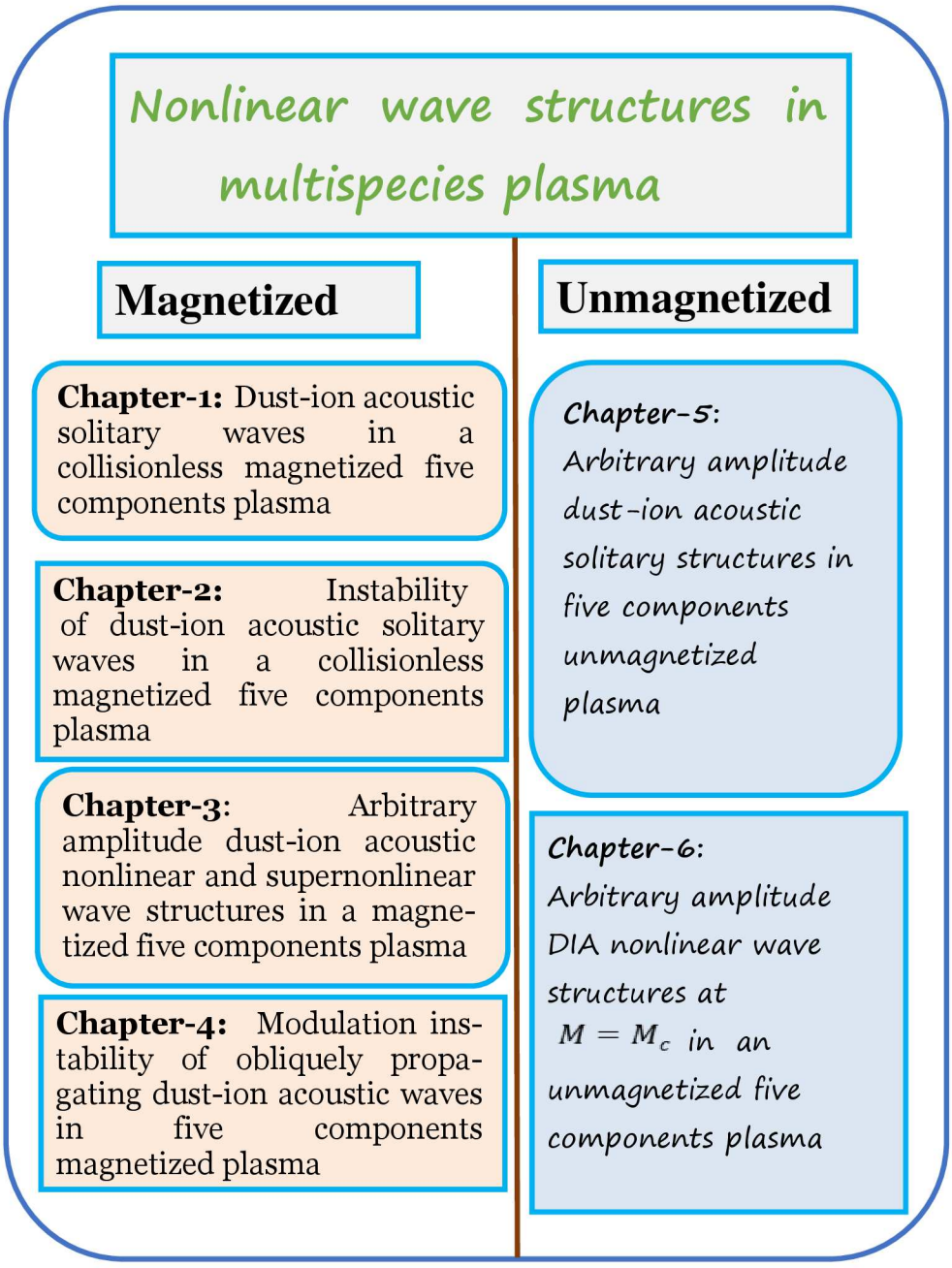

Chapter 1

Dust-ion acoustic solitary waves in a collisionless magnetized five components plasma *

In this **chapter**, we have derived a Korteweg-de Vries-Zakharov-Kuznetsov (KdV-ZK) equation to study the nonlinear behaviour of dust-ion acoustic waves in a collisionless magnetized five components dusty plasma consisting of warm adiabatic ions, nonthermal hot electrons, isothermal cold electrons, nonthermal positrons and static negatively charged dust particulates. It is found that the coefficient of the nonlinear term of the KdV-ZK equation vanishes along different family of curves in different compositional parameter planes. In this situation, to describe the nonlinear behaviour of dust-ion acoustic waves, we have derived a modified KdV-ZK (MKdV-ZK) equation. When the coefficients of the nonlinear terms of both KdV-ZK and MKdV-ZK equations are simultaneously equal to zero, then we have derived a further modified KdV-ZK (FMKdV-ZK) equation which effectively describes the nonlinear behaviour of dust-ion acoustic waves. Analytically and numerically, we have investigated the solitary wave solutions of different evolution equations propagating obliquely to the direction of the external static uniform magnetic field. We have seen that the amplitude of the KdV soliton strictly increases with increasing β_e, whereas the amplitude of the MKdV soliton strictly decreases with increasing β_e, where β_e is the nonthermal parameter associated with the hot electron species. Also, there exists a critical value $\beta_r^{(c)}$ of β_e such that the FMKdV soliton exists within the interval $\beta_r^{(c)} < \beta_e \leq \frac{4}{7}$, whereas the FMKdV soliton does not exist within the interval $0 < \beta_e < \beta_r^{(c)}$. We have also discussed the effect of different parameters of the system on solitary waves obtained from the different evolution equations.

*This chapter has been published in ***Zeitschriftfr Naturforschung A 77, 659 (2022); https://doi.org/10.1515/zna-2021-0287**

1.1 Introduction

The presence of dust particles in the electron-ion plasma modifies the propagation properties of nonlinear ion acoustic waves. These plasma systems are observed in various astrophysical environments such as asteroid zones, the planetary rings, the interstellar medium, comets, Earth's ionosphere and Earth's magnetosphere [207–212]. Several authors [100, 213–217] studied the nonlinear behaviour of ion acoustic (IA) / dust acoustic (DA) / dust-ion acoustic (DIA) waves in different plasma systems by considering one electron species or two electron species of different temperatures (cold and hot). Again, along with these dusty plasma systems, there are various astrophysical sites, viz., interstellar medium [169–171], in the remnants of supernova explosions [172], in the galactic centre [169], around pulsars [173], in the Milky Way [171] and interior regions of accretion disks near neutron stars and magnetars [77] in which existence of significant amount of positrons is observed. Thus, four components electron-positron-ion-dust (e-p-i-d) plasma is formed in these astrophysical sites. Also this e-p-i-d plasma may exist in the Earth's magnetosphere and in the Earth's ionosphere these regions contain positrons [174, 175] and highly charged dust grains [172]. Beside these astrophysical sites, e-p-i-d plasma can also be found in laboratory experiments [77, 173]. Several authors [45, 56, 75–82, 131, 148, 218–222] investigated dynamics of IA or DIA waves in e-p-i-d plasmas. Some authors [80, 81, 221, 223] studied different e-p-i-d plasma systems by considering the nonthermal electrons and positrons.

On the other hand, two electron species of different temperatures (cold and hot) exist in various space plasmas [178, 224] and also in laboratories [225–228]. Several authors [66–68, 229–235] investigated different nonlinear structures of IA waves in different plasmas. Most of the authors have considered two electron species, where both the electron species are Boltzmann-Maxwellian distributed isothermal electrons but their temperatures are different. The observation of

various spacecraft missions [176–180, 180–186] indicate the existence of two electron species of different temperatures (cold and hot) at the auroral region. More specifically Viking satellite [176, 177] and Freja satellite [187] indicate coexistence of energetic electrons and isothermal electrons in the auroral region of the Earth's upper ionosphere. But there is no proper technique for the construction of the velocity distribution function of the energetic particles in the space plasma and consequently we have used different non-Maxwellian velocity distributions to express the behaviour of the energetic particles. Cairns [1] distributed nonthermal model for the lighter species is one of the widely used non-Maxwellian model and this distribution can describe a population of fast energetic particle. Considering an isothermal species of electrons and another species of nonthermal Cairns distributed electrons, several authors [94, 97, 98, 124–126, 163] theoretically studied dynamical properties of IA waves in a collisionless unmagnetized / magnetized plasma.

Again, analyzing the electric field measurements collected by S3-3 satellite, Temerin *et al.* [178] reported the existence of small amplitude IA solitary waves and double layers in collisionless magnetized auroral plasma. They concluded that these small amplitude double layers are responsible for the fine structures of auroral kilometric radiation. Viking satellite [176] measurements also confirm the presence of small amplitude solitary waves and weak double layers in the auroral region of the ionosphere. Dovner *et al.*[187] reported the occurrence of solitary waves in the auroral zone of the upper ionosphere. The Polar satellite [236] observation also indicates the presence of small and large amplitude solitary waves and double layers in the auroral acceleration region. Ergun *et al.* [183, 184] reported that FAST satellite observation indicates large group of solitary waves of same polarity in the auroral zone may responsible for generating diverging electrostatic shocks associated with the electron acceleration in those regions of our atmosphere. Mcfadden *et al.* [180] observed IA solitary waves in the auroral region from the FAST measurement data and reported that these waves may have

effect on the particle acceleration mechanism.

Recently, Moslem *et al.* [189] have considered a five components dusty plasma system consisting of positively charged dust grains, Maxwellian electrons and ions including solar wind streaming electrons and protons. They have used this plasma model in the Jupiters magnetosphere to investigate the dynamics of the dust grains and solar wind streaming electrons and protons. Afterward Al-Yousef *et al.* [190] have considered the same plasma model of Moslem *et al.* [189] to investigate the arbitrary amplitude dust-acoustic waves in the Jupiter atmosphere for a distance greater than $15R_j$, where R_j (= 71398 km) is the distance from the center of the Jupiter. Guo *et al.* [131] have investigated modulational instability of ion acoustic waves in a collisionless unmagnetized five components plasma consisting of cold ions, q-nonextensive positrons, negatively or positively fixed charged immobile dust grains and two groups of q-nonextensive electrons having different temperatures. EL-Kalaawy [132] has investigated conservation laws and bright soliton solution of ion-acoustic waves in the same five components plasma system considered by Guo *et al.* [131]. Considering the reports as mentioned in the papers [189] and [190], and considering the mechanism for the formation of positrons from protons as mentioned by Gusev *et al.* [174, 175], we can conclude that there may exist five components e-p-i-d plasmas in the Jupiter atmosphere for a distance greater than $15R_j$.

Again, there are number of papers in four components e-p-i-d plasmas [45–47, 56, 75–83, 127–129, 148, 169–172, 218–223, 237–249]. In the above mentioned papers [45–47, 56, 75–83, 127–129, 148, 169–172, 218–223, 237–249], the existence of different four components e-p-i-d plasmas has been confirmed in different astrophysical regions but the authors have considered one species of electrons only. But we have already mentioned that two different species of electrons at different temperatures are common in space plasmas [176–187]. In the present **chapter**, we have considered an e-p-i-d plasma system, where electron species is divided into two distinct populations of electrons at different temperatures. From this point of

view, i.e., as the two distinct populations of electrons follow two different distributions, we can consider the present plasma system as five components plasma. So, we can conclude that there may exist five components e-p-i-d plasmas in the auroral region of the upper Earth's ionosphere, which contains nonthermal hot electrons and isothermal cold electrons. In future, next generation satellites may be able to distinguish astrophysical plasmas having five components as considered in this **chapter**.

In this present **chapter**, we have considered a fully ionized collisionless magnetized five components e-p-i-d plasma system consisting of warm adiabatic ions, nonthermally distributed positrons and negatively charged immobile dust grains and two electron species of different temperatures, a cooler one with a population of Boltzmann-Maxwellian distributed and hotter one with a nonthermal distribution of Cairns *et al.* [1]. So, the plasma system as considered in the present **chapter** is different from the plasma systems as mentioned in the papers of Paul *et al.*[81], Guo *et al.* [131], Paul and Bandyopadhyay [79] and Banerjee and Maitra [80] in the following directions:

- Paul *et al.* [81] considered a collisionless unmagnetized four components e-p-i-d plasma system consisting of warm adiabatic ions, nonthermally distributed electrons, nonthermally distributed positrons and negatively charged immobile dust grains. In the present chapter, we have considered an extra cold electron species and the plasma system is under the action of static uniform magnetic field.

- The plasma systems as mentioned in the papers of Paul and Bandyopadhyay [79], Banerjee and Maitra [80] and Paul *et al.* [81] are unmagnetized but in the present **chapter**, we have considered magnetized plasma.

- In the papers of Paul and Bandyopadhyay [79], Banerjee and Maitra [80] and Paul *et al.* [81], the authors have considered only one nonthermal population of electrons but in this present **chapter**, we have considered two

electron species of different temperatures - one electron species is isothermal and other is nonthermal.

- In the papers of Paul and Bandyopadhyay [79], Banerjee and Maitra [80] and Paul *et al.* [81], the authors have investigated arbitrary amplitude DIA solitary structures by using the Sagdeev Pseudo Potential method whereas in this present **chapter** we have investigated the small amplitude DIA solitary structures by considering the reductive perturbation method.

- On the other hand, Guo *et al.* [131] considered a five components plasma system, where both the electron species and positron species follow the q-nonextensive velocity distributions and this plasma system is free from any external uniform static magnetic field. They have investigated the modulational instability (MI) of the IA waves in a collisionless unmagnetized five components e-p-i-d plasma.

In the present plasma system, we have investigated the nonlinear behaviour of DIA waves by considering the following points:

- Starting from the equation of continuity of ions, equation of motion of ion fluid, equation of pressure of ion fluid and the Poisson equation, we have derived a Korteweg-de Vries-Zakharov-Kuznetsov (KdV-ZK) equation by considering appropriate stretchings of space coordinates and time, and appropriate perturbation expansions of the dependent variables.

- When the coefficient of the nonlinear term of the KdV-ZK equation is zero, then to describe the nonlinear behaviour of DIA waves, we have derived a modified KdV-ZK (MKdV-ZK) equation.

- When the coefficients of the nonlinear terms of both KdV-ZK and MKdV-ZK equations are simultaneously equal to zero, then we have derived a further modified KdV-ZK (FMKdV-ZK) equation to describe the nonlinear behaviour of DIA waves.

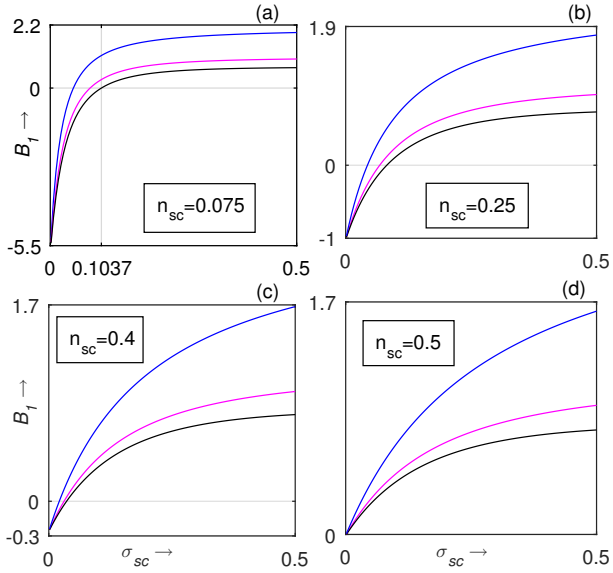

Figure 1.1: B_1 is plotted against σ_{sc} for $\gamma = 5/3$, $\sigma = 0.001$, $n_{pc} = 0.09$, $n_{dc} = 0.1$, $\beta_e = 0.2$, $\beta_p = 0.25$ and for (a) $n_{sc} = 0.075$, (b) $n_{sc} = 0.25$, (c) $n_{sc} = 0.4$ and (d) $n_{sc} = 0.5$. Here Blue, magenta and black curves of each figure correspond to $\sigma_{pc} = 0.1$, $\sigma_{pc} = 0.25$ and $\sigma_{pc} = 0.5$, respectively. Figures 1.1(a), 1.1(b) and 1.1(c) show the existence of points $\sigma_{sc}^{(c)}$ such that $B_1 = 0$ for some values of σ_{pc} whereas figure 1.1(d) shows that $B_1 > 0$ for all values of σ_{pc} and for all σ_{sc} lying within the interval $(0, 0.5)$. In particular, for $n_{sc} = 0.075$ and $\sigma_{pc} = 0.5$, the value of $\sigma_{sc}^{(c)}$ is 0.1037 (approx.).

- We have investigated the validity of the different evolution equations by considering different compositional parameter planes.

- We have studied the solitary wave solutions of different evolution equations propagating obliquely to the direction of the external static uniform magnetic field.

- We have investigated the effect of different parameters on the solitary wave solutions of different evolution equations.

So, this problem can be considered as new problem in the present five components plasma system.

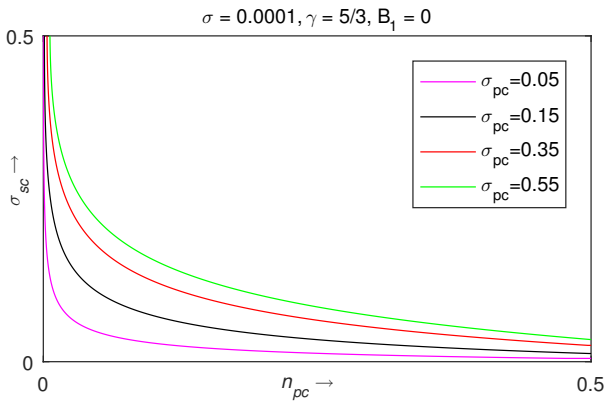

Figure 1.2: When $B_1 = 0$, σ_{sc} is plotted against n_{pc} for $\gamma = 5/3$, $\sigma = 0.0001$, $n_{sc} = 0.15$, $n_{dc} = 0.1$, $\beta_e = 0.5$ and $\beta_p = 0.15$, and for different values of σ_{pc}. Here magenta, black, red and green curves correspond to $\sigma_{pc} = 0.05$, $\sigma_{pc} = 0.15$, $\sigma_{pc} = 0.35$ and $\sigma_{pc} = 0.55$, respectively.

1.2 Basic Equations

We consider a fully ionized collisionless magnetized five components plasma system consisting of warm adiabatic ions, two different species of electrons at different temperatures, a cooler one with a population of Boltzmann-Maxwellian distributed and hotter one with a nonthermal distribution of Cairns *et al.* [1], nonthermally distributed positrons and negatively charged immobile dust grains. The basic equations of the present plasma system are given by

$$\frac{\partial n_i}{\partial t} + \overrightarrow{\nabla}.(n_i \overrightarrow{u_i}) = 0, \tag{1.2.1}$$

$$\left(\frac{\partial}{\partial t} + \overrightarrow{u_i}.\overrightarrow{\nabla}\right)\overrightarrow{u_i} + \frac{\sigma}{n_i}\overrightarrow{\nabla} P_i + \overrightarrow{\nabla}\phi - \omega_c(\overrightarrow{u_i} \times \hat{z}) = 0, \tag{1.2.2}$$

$$\frac{\partial P_i}{\partial t} + (\overrightarrow{u_i}.\overrightarrow{\nabla})P_i + \gamma P_i(\overrightarrow{\nabla}.\overrightarrow{u_i}) = 0, \tag{1.2.3}$$

$$\nabla^2\phi = n_{ce} + n_{se} - n_p - n_i + Z_d n_{d0}. \tag{1.2.4}$$

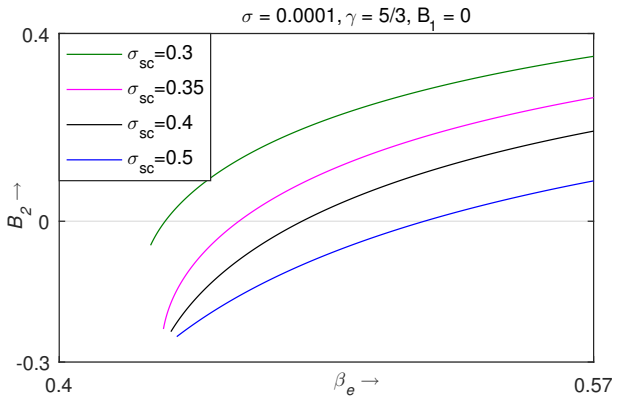

Figure 1.3: When $B_1 = 0$, B_2 is plotted against β_e for $\gamma = 5/3$, $\sigma = 0.0001$, $n_{pc} = 0.002$, $n_{dc} = 0.1$, $\sigma_{pc} = 0.15$ and $\beta_p = 0.25$, and for different values of σ_{sc}. Here green, magenta, black and blue curves correspond to $\sigma_{sc} = 0.3$, $\sigma_{sc} = 0.35$, $\sigma_{sc} = 0.4$ and $\sigma_{sc} = 0.5$, respectively.

Here, we have considered the warm plasma model to study the effect (analytically and numerically) of ion temperature and the pressure of ion fluid. In fact, neglecting the effects of viscosity, thermal conductivity and energy transfer due to collisions, one can express the pressure law through the equation (1.2.3). This warm plasma model can be reduced to a cold plasma model by considering the approximation $\sigma = \frac{T_i}{T_{pef}} << 1$ ($\Rightarrow \sigma \approx 0$). Again, using the equation (1.2.1), the pressure equation for ion fluid (1.2.3) can be written in the following form:

$$P_i = n_i^{\gamma}, \tag{1.2.5}$$

where γ is the ratio of the specific heat at constant pressure to the specific heat at constant volume.

Equations (1.2.1), (1.2.2), (1.2.3) and (1.2.4) are, respectively, the equation of continuity of ions, the equation of motion of ion fluid, the equation of pressure of ion fluid and the Poisson equation. Here, we have assumed that the uniform static magnetic field is directed along the z-axis. To get a consistent system of nonlinear equations, we have added the following equations along with the equations (1.2.1) - (1.2.4) to describe the nonlinear behaviour of the DIA waves:

$$n_{ce} = \overline{n}_{c0}(1 - \beta_e\sigma_c\phi + \beta_e\sigma_c^2\phi^2)\exp(\sigma_c\phi), \tag{1.2.6}$$

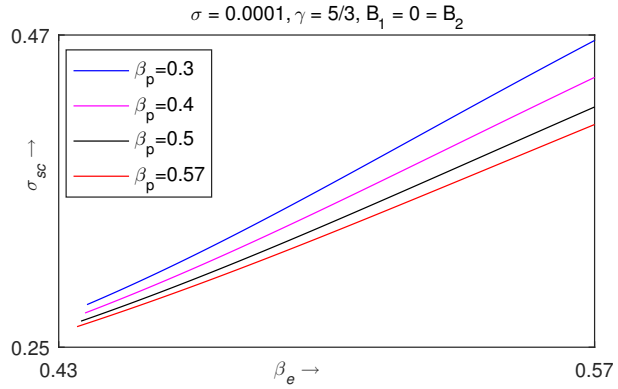

Figure 1.4: When $B_1 = 0 = B_2$, σ_{sc} is plotted against β_e for $\gamma = 5/3$, $\sigma = 0.0001$, $n_{pc} = 0.001$, $n_{dc} = 0.1$, $\sigma_{pc} = 0.1$ and for different values of β_p. Here blue, magenta, black and red curves correspond to $\beta_p = 0.3$, $\beta_p = 0.4$, $\beta_p = 0.5$ and $\beta_p = 0.57$, respectively.

$$n_{se} = \overline{n}_{s0}\exp(\sigma_s\phi), \tag{1.2.7}$$

$$n_p = \overline{n}_{p0}(1 + \beta_p\sigma_p\phi + \beta_p\sigma_p^2\phi^2)\exp(-\sigma_p\phi), \tag{1.2.8}$$

$$n_d = \overline{n}_{d0}, \tag{1.2.9}$$

$$n_{i0} - n_{c0} - n_{s0} + n_{p0} - Z_d n_{d0} = 0. \tag{1.2.10}$$

The equations (1.2.6), (1.2.7), (1.2.8) are, respectively, the equations for the number densities of hot electron species, cold electron species and hot positron species. Equation (1.2.9) indicates that the number density of dust grain is constant and equation (1.2.10) is the charge neutrality condition at the equilibrium state. In equations (1.2.1) - (1.2.10), we have used the following terminologies: $n_i, n_{ce}, n_{se}, n_p, n_d, \overrightarrow{u_i} = (u, v, w), \phi, P_i, (x, y, z)$ and t are the ion number density, the nonthermal electron number density, the isothermal electron number density, the nonthermal positron number density, the number density of dust grains, the ion fluid velocity, the electrostatic potential, the ion pressure, the spatial variables, and time, respectively. These are normalized by $n_{i0}, n_{i0}, n_{i0}, n_{i0}, n_{i0}$, c_s, $\frac{K_B T_{pef}}{e}, n_{i0}K_B T_i, (\lambda_D, \lambda_D, \lambda_D)$ and ω_p^{-1}, respectively. n_{i0}, n_{c0}, n_{s0} and n_{p0} are

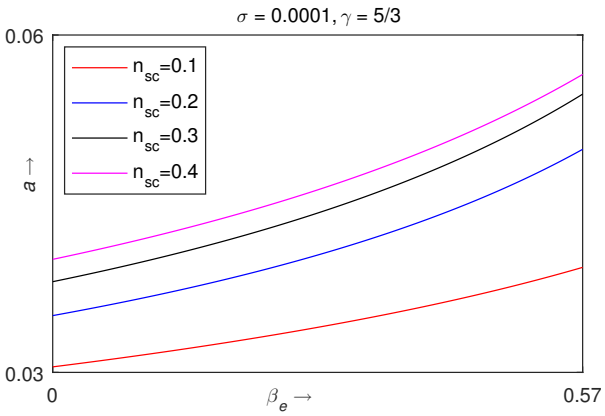

Figure 1.5: The amplitude (a) of the KdV soliton is plotted against β_e for $\gamma = 5/3$, $\sigma = 0.0001$, $n_{pc} = 0.09$, $n_{dc} = 0.1$, $\sigma_{sc} = 0.25$, $\sigma_{pc} = 0.2$, $\beta_p = 0.25$, $\theta = 45^\circ$ and for different values of n_{sc}. Here red, blue, black and magenta curves correspond to $n_{sc} = 0.1$, $n_{sc} = 0.2$, $n_{sc} = 0.3$ and $n_{sc} = 0.4$, respectively.

the equilibrium number densities of ions, nonthermal electrons, isothermal electrons, and nonthermal positrons, respectively. β_e and β_p are the nonthermal parameters associated with the nonthermal velocity distributions of hot electrons and positrons, respectively. Z_d is the number of electrons residing on the dust grain surface, $-e$ is the charge of an electron and $\gamma\left(=\frac{5}{3}\right)$ is the ratio of two specific heats and K_B is the Boltzmann constant. Here $\overrightarrow{\nabla} = \hat{x}\frac{\partial}{\partial x} + \hat{y}\frac{\partial}{\partial y} + \hat{z}\frac{\partial}{\partial z}$, $\overline{n}_{p0} = \frac{n_{p0}}{n_{i0}}, \overline{n}_{c0} = \frac{n_{c0}}{n_{i0}}, \overline{n}_{s0} = \frac{n_{s0}}{n_{i0}}, \overline{n}_{d0} = \frac{n_{d0}}{n_{i0}}$, $\sigma = \frac{T_i}{T_{pef}}, \sigma_c = \frac{T_{pef}}{T_{ce}}, \sigma_s = \frac{T_{pef}}{T_{se}}, \sigma_p = \frac{T_{pef}}{T_p}$, ω_c (the ion cyclotron frequncy) $= \frac{eB_0}{m_i c}$, $\omega_p = \sqrt{\frac{4\pi e^2 n_{i0}}{m_i}}$, λ_D (Debye length of the present plasma system) $= \sqrt{\frac{K_B T_{pef}}{4\pi e^2 n_{i0}}}$ and $c_s = \sqrt{\frac{K_B T_{pef}}{m_i}}$, where m_i is the mass of an ion. T_i, T_{ce}, T_{se} and T_p are the average temperature of ion, nonthermal electrons, isothermal electrons and nonthermal positrons, respectively. T_{pef} is given by the following expression:

$$\frac{n_{c0}}{T_{ce}} + \frac{n_{s0}}{T_{se}} + \frac{n_{p0}}{T_p} = \frac{n_{c0} + n_{s0} - n_{p0} + Z_d n_{d0}}{T_{pef}}. \tag{1.2.11}$$

Therefore, the charge neutrality condition (1.2.10) and the equation (1.2.11) can be written as

$$\overline{n}_{c0} + \overline{n}_{s0} + \overline{n}_{p0} + \overline{N}_{d0} = 1, \tag{1.2.12}$$

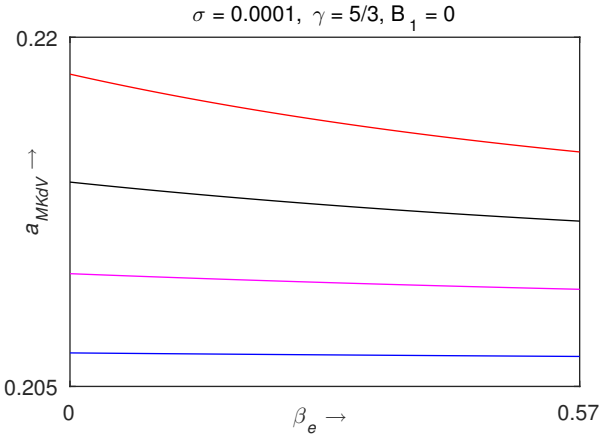

Figure 1.6: The amplitude of the MKdV soliton is plotted against β_e for $\gamma = 5/3$, $\sigma = 0.0001$, $n_{pc} = 0.002$, $n_{dc} = 0.1$, $\sigma_{pc} = 0.15$, $\beta_p = 0.25$, $\theta = 15^\circ$ and for different values of σ_{sc}. Here blue, magenta, black and red curves correspond to $\sigma_{sc} = 0.01$, $\sigma_{sc} = 0.02$, $\sigma_{sc} = 0.03$ and $\sigma_{sc} = 0.04$, respectively.

$$\overline{n}_{c0}\sigma_c + \overline{n}_{s0}\sigma_s + \overline{n}_{p0}\sigma_p = 1, \tag{1.2.13}$$

where $Z_d n_{d0} = N_{d0} \iff Z_d \overline{n}_{d0} = \overline{N}_{d0}$. Introducing the new parameters : $n_{sc} = \frac{n_{s0}}{n_{c0}}, n_{pc} = \frac{n_{p0}}{n_{c0}}, n_{dc} = \frac{N_{d0}}{n_{c0}}, \sigma_{sc} = \frac{T_{se}}{T_{ce}}, \sigma_{pc} = \frac{T_p}{T_{ce}}$, and the expressions of $\overline{n}_{c0}, \overline{n}_{s0}, \overline{n}_{p0}, \overline{N}_{d0}, \sigma_c, \sigma_s$, and, σ_p can be simplified as follows:

$$\overline{n}_{c0} = \frac{1}{1 + n_{sc} - n_{pc} + n_{dc}}, \tag{1.2.14}$$

$$\overline{n}_{s0} = \frac{n_{sc}}{1 + n_{sc} - n_{pc} + n_{dc}}, \tag{1.2.15}$$

$$\overline{n}_{p0} = \frac{n_{pc}}{1 + n_{sc} - n_{pc} + n_{dc}}, \tag{1.2.16}$$

$$\overline{N}_{d0} = \frac{n_{dc}}{1 + n_{sc} - n_{pc} + n_{dc}}, \tag{1.2.17}$$

$$\sigma_c = \frac{(1 + n_{sc} - n_{pc} + n_{dc})\sigma_{sc}\sigma_{pc}}{\sigma_{sc}\sigma_{pc} + n_{sc}\sigma_{pc} + n_{pc}\sigma_{sc}}, \tag{1.2.18}$$

$$\sigma_s = \frac{(1 + n_{sc} - n_{pc} + n_{dc})\sigma_{pc}}{\sigma_{sc}\sigma_{pc} + n_{sc}\sigma_{pc} + n_{pc}\sigma_{sc}}, \tag{1.2.19}$$

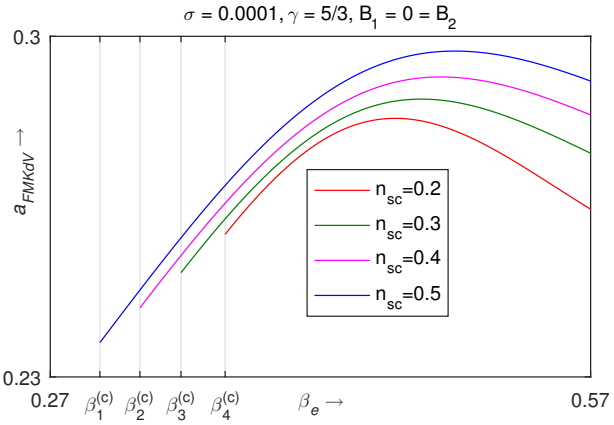

Figure 1.7: The amplitude of the FMKdV soliton is plotted against β_e for $\gamma = 5/3$, $\sigma = 0.0001$, $n_{dc} = 0.1$, $\sigma_{pc} = 0.25$, $\beta_p = 0.2$, $\theta = 15^\circ$ and for different values of n_{sc}. Here red, green, magenta and blue curves correspond to $n_{sc} = 0.2$, $n_{sc} = 0.3$, $n_{sc} = 0.4$ and $n_{sc} = 0.5$, respectively.

$$\sigma_p = \frac{(1 + n_{sc} - n_{pc} + n_{dc})\sigma_{sc}}{\sigma_{sc}\sigma_{pc} + n_{sc}\sigma_{pc} + n_{pc}\sigma_{sc}}. \tag{1.2.20}$$

Expanding n_{ce}, n_{se} and n_p as given in (1.2.6), (1.2.7) and (1.2.8), respectively, and, keeping terms up to ϕ^4, the Poisson equation (1.2.4) can be written as follows:

$$\begin{aligned}
\nabla^2\phi &= 1 - n_i \\
&+ [(1-\beta_e)\overline{n}_{c0}\sigma_c + \overline{n}_{s0}\sigma_s + (1-\beta_p)\overline{n}_{p0}\sigma_p]\phi \\
&+ \frac{\overline{n}_{c0}\sigma_c^2 + \overline{n}_{s0}\sigma_s^2 - \overline{n}_{p0}\sigma_p^2}{2}\phi^2 \\
&+ \frac{(1+3\beta_e)\overline{n}_{c0}\sigma_c^3 + \overline{n}_{s0}\sigma_s^3 + (1+3\beta_p)\overline{n}_{p0}\sigma_p^3}{6}\phi^3 \\
&+ \frac{(1+8\beta_e)\overline{n}_{c0}\sigma_c^4 + \overline{n}_{s0}\sigma_s^4 - (1+8\beta_p)\overline{n}_{p0}\sigma_p^4}{24}\phi^4.
\end{aligned} \tag{1.2.21}$$

The linear dispersion relation of the dust-ion acoustic wave for the present five components plasma system can be written as

$$\frac{k_\perp^2}{\omega^2 - \omega_c^2} + \frac{k_\parallel^2}{\omega^2} = \frac{1}{M_D^2}\left[\frac{1 + \lambda_D^2 k^2}{1 + \frac{\sigma\gamma}{M_s^2}\lambda_D^2 k^2}\right], \tag{1.2.22}$$

where $k^2 = (k_\perp^2 + k_\parallel^2)$, $M_D^2 = M_s^2 c_s^2$ and

$$M_s^2 = V^2 = \sigma\gamma + \frac{1}{1 - \beta_e\overline{n}_{c0}\sigma_c - \beta_p\overline{n}_{p0}\sigma_p}.$$

Here, ω and k are, respectively, the wave frequency and wave number of the plane wave perturbation. For low frequency domain ($\omega << \omega_c$), the dispersion relation (1.2.22) can be written in the following form:

$$\frac{k^2}{\omega^2} = \frac{1}{M_D^2}\left[\frac{1+\lambda_D^2 k^2}{1+\frac{\sigma\gamma}{M_s^2}\lambda_D^2 k^2}\right]. \tag{1.2.23}$$

Using the equation (1.2.5), the equation of motion ion fluid (1.2.2) can be written in the following form:

$$\left(\frac{\partial}{\partial t} + \overrightarrow{u}_i.\overrightarrow{\nabla}\right)\overrightarrow{u}_i + \sigma\gamma n_i^{\gamma-2}\overrightarrow{\nabla}n_i + \overrightarrow{\nabla}\phi - \omega_c(\overrightarrow{u}_i \times \hat{z}) = 0. \tag{1.2.24}$$

1.3 Derivation of different evolution equations

To derive the different evolution equations, we make the following stretchings of space coordinates and time:

$$(\xi, \eta, \zeta) = \epsilon^{\frac{1}{2}}(x, y, z - Vt), \tau = \epsilon^{\frac{3}{2}}t, \tag{1.3.1}$$

where ϵ is a small parameter measuring the weakness of the dispersion and V is a constant.

1.3.1 KdV-ZK equation

We have applied the following perturbation expansions of the dependent variables to derive the KdV-ZK equation :

$$F = F^{(0)} + \epsilon^p F^{(p)}, G = G^{(0)} + \epsilon^{\frac{p}{2}+1}G^{(p)}, \tag{1.3.2}$$

where repeated index implies summation over that index, $F = n_i, \phi, w$ with $n_i^{(0)} = 1$, $\phi^{(0)} = 0$, $w^{(0)} = 0$ and $G = u, v$ with $u^{(0)} = 0$, $v^{(0)} = 0$. Substituing stretchings and perturbation expansions given in the equations (1.3.1) and (1.3.2) in the equations (1.2.1), (1.2.4), and (1.2.24) and equating the coefficients of the

different power of ϵ, we get a set of equations. From this set of equations, we have derived the following KdV-ZK equation:

$$\phi_{\tau}^{(1)} + AB_1\phi^{(1)}\phi_{\zeta}^{(1)} + \frac{1}{2}A\phi_{\zeta\zeta\zeta}^{(1)} + \frac{1}{2}AD(\phi_{\eta\eta}^{(1)} + \phi_{\xi\xi}^{(1)})_{\zeta} = 0, \tag{1.3.3}$$

where

$$A = \frac{1}{V}(V^2 - \sigma\gamma)^2, \tag{1.3.4}$$

$$B_1 = \frac{1}{2}\left[\frac{3V^2 + \sigma\gamma(\gamma - 2)}{(V^2 - \sigma\gamma)^3} - (\overline{n}_{c0}\sigma_c^2 + \overline{n}_{s0}\sigma_s^2 - \overline{n}_{p0}\sigma_p^2)\right], \tag{1.3.5}$$

$$D = \left[1 + \frac{V^4}{\omega_c^2(V^2 - \sigma\gamma)^2}\right]. \tag{1.3.6}$$

The nonlinear behaviour of DIA waves can be described by the KdV-ZK equation (1.3.3) only when the coefficient of the nonlinear term of the KdV-ZK equation does not vanish, i.e., $B_1 \neq 0$. But when $B_1 = 0$, the coefficient of the nonlinear term of the KdV-ZK equation (1.3.3) vanishes along different family of curves in the compositional parameter planes.

From the expression of B_1 as given in (1.3.5), it is clear that B_1 is a function of n_{sc}, n_{pc}, n_{dc}, σ_{sc}, σ_{pc}, β_e and β_p for any prescribed value of γ, σ, i.e., $B_1 = B_1(n_{sc}, n_{pc}, n_{dc}, \sigma_{sc}, \sigma_{pc}, \beta_e, \beta_p)$. Therefore, in figure 1.1, B_1 is plotted against σ_{sc} for $\gamma = 5/3$, $\sigma = 0.001$, $n_{pc} = 0.09$, $n_{dc} = 0.1$, $\beta_e = 0.2$, $\beta_p = 0.25$ and for (a) $n_{sc} = 0.075$, (b) $n_{sc} = 0.25$, (c) $n_{sc} = 0.4$ and (d) $n_{sc} = 0.5$. Here, blue, magenta and black curves of each figure correspond to $\sigma_{pc} = 0.1$, $\sigma_{pc} = 0.25$ and $\sigma_{pc} = 0.5$, respectively. From figure 1.1(a)-(c), we see that there exists a value $\sigma_{sc}^{(c)}$ of σ_{sc} such that $B_1 = 0$ at σ_{sc}=$\sigma_{sc}^{(c)}$, and more specifically, $B_1 < 0$ for $\sigma_{sc} < \sigma_{sc}^{(c)}$ and $B_1 > 0$ for $\sigma_{sc} > \sigma_{sc}^{(c)}$. Again, from figure 1.1(d), we see that $B_1 > 0$ for all values of σ_{pc}. Now, from figure 1.1, it is obvious that there exists a region R_I = $\{(n_{sc}, n_{pc}, n_{dc}, \sigma_{sc}, \sigma_{pc}, \beta_e, \beta_p) : B_1(n_{sc}, n_{pc}, n_{dc}, \sigma_{sc}, \sigma_{pc}, \beta_e, \beta_p) \neq 0\}$ such that each point of R_I satisfies the condition $B_1(n_{sc}, n_{pc}, n_{dc}, \sigma_{sc}, \sigma_{pc}, \beta_e, \beta_p)$ $\neq 0$. On the other hand there must exist a collection of points from the entire parameter plane such that every point of the collection must satisfy the equation

$B_1(n_{sc},\ n_{pc},\ n_{dc},\ \sigma_{sc},\ \sigma_{pc},\ \beta_e,\ \beta_p) = 0$ and consequently for these values of the parameters n_{sc}, n_{pc}, n_{dc}, σ_{sc}, σ_{pc}, β_e and β_p, we cannot use the KdV-ZK evolution equation to investigate the nonlinear dynamics of DIA solitary waves. To confirm the existence of a region $R_{II} = \{(n_{sc},\ n_{pc},\ n_{dc},\ \sigma_{sc},\ \sigma_{pc},\ \beta_e,\ \beta_p) : B_1(n_{sc},\ n_{pc},\ n_{dc},\ \sigma_{sc},\ \sigma_{pc},\ \beta_e,\ \beta_p) = 0\}$ in the entire parameter plane, we consider the following figure in different parameter planes.

Now, the coefficient B_1 can be considered as functions of n_{pc} and σ_{sc} for any suitable values of other parameters and consequently, $B_1 = 0$ gives a functional relationship between n_{pc} and σ_{sc}. Now, for $B_1 = 0$, this functional relationship between n_{pc} and σ_{sc} is plotted in figure 1.2, for different values of σ_{pc}. Here, magenta, black, red and green curves correspond to $\sigma_{pc} = 0.05$, $\sigma_{pc} = 0.15$, $\sigma_{pc} = 0.35$ and $\sigma_{pc} = 0.55$, respectively.

So, figure 1.2, confirms the existence of the region R_{II} in the parameter space such that each point of R_{II} satisfies the equation $B_1(n_{sc},\ n_{pc},\ n_{dc},\ \sigma_{sc},\ \sigma_{pc},\ \beta_e,\ \beta_p) = 0$. Therefore, for $B_1(n_{sc},\ n_{pc},\ n_{dc},\ \sigma_{sc},\ \sigma_{pc},\ \beta_e,\ \beta_p) = 0$ or for $(n_{sc},\ n_{pc},\ n_{dc},\ \sigma_{sc},\ \sigma_{pc},\ \beta_e,\ \beta_p) \in R_{II}$, it is necessary to modify the KdV-ZK equation to investigate the nonlinear behaviour of DIA waves. In this situation, the nonlinear behaviour of DIA waves cannot be described by the KdV-ZK equation.

1.3.2 MKdV-ZK equation

We have applied the following perturbation expansions of the dependent variables to derive the MKdV-ZK equation when $B_1 = 0$:

$$F = F^{(0)} + \epsilon^{\frac{p}{2}} F^{(p)}, G = G^{(0)} + \epsilon^{\frac{p+1}{2}} G^{(p)}, \tag{1.3.7}$$

where repeated index implies summation over that index, $F = n_i, \phi, w$ with $n_i^{(0)} = 1$, $\phi^{(0)} = 0$, $w^{(0)} = 0$ and $G = u, v$ with $u^{(0)} = 0$, $v^{(0)} = 0$. Substituing stretchings and perturbation expansions given in the equations (1.3.1) and (1.3.7) in the equations (1.2.1), (1.2.4), and (1.2.24) and equating the coefficients of the different power of ϵ, we get a set of equations. From this set of equations, we

have derived the following MKdV-ZK equation:

$$\phi_{\tau}^{(1)} + AB_2(\phi^{(1)})^2\phi_{\zeta}^{(1)} + \frac{1}{2}A\phi_{\zeta\zeta\zeta}^{(1)} + \frac{1}{2}AD(\phi_{\eta\eta}^{(1)} + \phi_{\xi\xi}^{(1)})_{\zeta} = 0, \tag{1.3.8}$$

where

$$\begin{aligned} B_2 &= \frac{1}{4}\Bigg[\{15V^4 + V^2\sigma(\gamma^3 + 13\gamma^2 - 18\gamma) \\ &+ \sigma^2(2\gamma^4 - 7\gamma^3 + 6\gamma^2)\} \times \frac{1}{(V^2 - \sigma\gamma)^5} \\ &- \{(1 + 3\beta_e)\overline{n}_{c0}\sigma_c^3 + \overline{n}_{s0}\sigma_s^3 + (1 + 3\beta_p)\overline{n}_{p0}\sigma_p^3\}\Bigg], \end{aligned} \tag{1.3.9}$$

and the expressions of A and D are same as given in equations (1.3.4) and (1.3.6), respectively.

The nonlinear behaviour of DIA waves can be described by the MKdV-ZK equation only when $B_1 = 0$ but $B_2 \neq 0$. In figure 1.3, for $\gamma = 5/3$, $\sigma = 0.0001$, $n_{pc} = 0.002$, $n_{dc} = 0.1$, $\sigma_{pc} = 0.15$ and $\beta_p = 0.25$, we have plotted B_2 against β_e for different values of σ_{sc} when $B_1 = 0$. Here green, magenta, black and blue curves of figure 1.3 correspond to $\sigma_{sc} = 0.3$, $\sigma_{sc} = 0.35$, $\sigma_{sc} = 0.4$ and $\sigma_{sc} = 0.5$, respectively. From figure 1.3, we have seen that the existence of B_2 decreases with increasing σ_{sc} provided $B_1 = 0$.

In figure 1.4, σ_{sc} is plotted against β_e when $B_1 = 0 = B_2$ for $\gamma = 5/3$, $\sigma = 0.0001$, $n_{pc} = 0.001$, $n_{dc} = 0.1$, $\sigma_{pc} = 0.1$ and for different values of β_p. Here blue, magenta, black and red curves correspond to $\beta_p = 0.3$, $\beta_p = 0.4$, $\beta_p = 0.5$ and $\beta_p = 0.57$ respectively. Again, we see that the coefficient of the nonlinear term of the MKdV-ZK equation (1.3.8) vanishes along different family of curves in the compositional parameter plane. In this situation i.e. when $B_1 = 0$ and $B_2 = 0$, neither KdV-ZK equation nor MKdV-ZK equation can describe the nonlinear behaviour of the DIA waves. In the next subsection, we have derived a FMKdV-ZK equation when $B_1 = 0$ and $B_2 = 0$.

1.3.3 FMKdV-ZK equation

We have applied the following perturbation expansions of the dependent variables to derive the FMKdV-ZK equation when $B_1 = 0$ and $B_2 = 0$:

$$F = F^{(0)} + \epsilon^{\frac{p}{3}} F^{(p)}, G = G^{(0)} + \epsilon^{\frac{p+4}{6}} G^{(p)}, \tag{1.3.10}$$

where repeated index implies summation over that index, $F = n_i, \phi, w$ with $n_i^{(0)} = 1$, $\phi^{(0)} = 0$, $w^{(0)} = 0$ and $G = u, v$ with $u^{(0)} = 0$, $v^{(0)} = 0$. Substituing stretchings and perturbation expansions given in the equations (1.3.1) and (1.3.10) in the equations (1.2.1), (1.2.4), and (1.2.24) and equating the coefficients of the different power of ϵ, we get a set of equations. From this set of equations, we have derived the following FMKdV-ZK equation:

$$\phi_\tau^{(1)} + AB_3(\phi^{(1)})^3\phi_\zeta^{(1)} + \frac{1}{2}A\phi_{\zeta\zeta\zeta}^{(1)} + \frac{1}{2}AD(\phi_{\eta\eta}^{(1)} + \phi_{\xi\xi}^{(1)})_\zeta = 0, \tag{1.3.11}$$

where

$$\begin{aligned} B_3 &= \frac{1}{12}\Bigg[\Bigg\{105V^6 + V^4\sigma(\gamma^4 + 21\gamma^3 + 161\gamma^2 - 174\gamma) \\ &+ V^2\sigma^2(8\gamma^5 + 53\gamma^4 - 162\gamma^3 + 108\gamma^2) \\ &+ \sigma^3(6\gamma^6 - 29\gamma^5 + 46\gamma^4 - 24\gamma^3)\Bigg\} \times \frac{1}{(V^2 - \sigma\gamma)^7} \\ &- \Bigg\{(1 + 8\beta_e)\overline{n}_{c0}\sigma_c^4 + \overline{n}_{s0}\sigma_s^4 - (1 + 8\beta_p)\overline{n}_{p0}\sigma_p^4\Bigg\}\Bigg], \end{aligned} \tag{1.3.12}$$

and the expressions of A and D are same as given in equations (1.3.4) and (1.3.6), respectively. The nonlinear behaviour of DIA waves can be described effectively by the FMKdV-ZK equation (1.3.11) only when $B_1 = B_2 = 0$ but $B_3 \neq 0$.

1.4 Obliquely propagating solitary wave solutions of the evolution equations

The evolution equations (1.3.3), (1.3.8) and (1.3.11) can be written in more compact form as follows:

$$\phi_{\tau}^{(1)} + AB_r(\phi^{(1)})^r\phi_{\zeta}^{(1)} + \frac{1}{2}A\phi_{\zeta\zeta\zeta}^{(1)} + \frac{1}{2}AD(\phi_{\eta\eta}^{(1)} + \phi_{\xi\xi}^{(1)})_{\zeta} = 0, \tag{1.4.1}$$

where $r = 1, 2, 3$. For a solitary wave solution of the equation (1.4.1) propagating at an angle δ with the external uniform static magnetic field directed along the z-axis, we make the following change of variable:

$$Z = \xi\sin\delta + \zeta\cos\delta - U\tau, \tag{1.4.2}$$

and for travelling wave solutions of (1.4.1), we set $\phi^{(1)} = \Phi(Z)$ in equation (1.4.1). Under the above mentioned change of coordinates and using equation (1.4.2), equation (1.4.1) transforms to the following equation:

$$-U\Phi' + a_r\Phi^r\Phi' + C\Phi''' = 0, \tag{1.4.3}$$

and we have used the notation Φ' for $\frac{d\Phi}{dZ}$. The expressions of a_r and C are given by the following equations:

$$a_r = AB_r\cos\delta, C = \frac{1}{2}A\cos\delta(\cos^2\delta + D\sin^2\delta). \tag{1.4.4}$$

Using the boundary conditions: $\Phi, \Phi', \Phi'' \to 0$ as $|Z| \to \infty$, the solitary wave solution of (1.4.3) can be written as follows:

$$\Phi = a\mathrm{sech}^{\frac{2}{r}}\left(\frac{Z}{\chi}\right), \tag{1.4.5}$$

where a and χ are given by the following equations:

$$a^r = \frac{(r+1)(r+2)U}{2a_r}, \chi^2 = \frac{4C}{r^2U}, \tag{1.4.6}$$

for $r = 1, 2, 3$.

1.5 Conclusions

In this present **chapter**, we have investigated small amplitude DIA solitary waves in a collisionless magnetized five components plasma consisting of warm adiabatic ions, nonthermal hot electrons, isothermal cold electrons, nonthermal positrons and static negatively charged dust particulates. The external magnetic field is static (time independent) and uniform (space independent).

Using reductive perturbation method, we have derived a KdV-ZK equation. This KdV-ZK equation is valid only when $B_1 \neq 0$, where B_1 is a factor of the coefficient of the nonlinear term of the KdV-ZK equation. We have seen that the coefficient of the nonlinear term of the KdV-ZK equation vanishes along different family of curves in different compositional parameter planes, viz., $n_{pc} - \sigma_{sc}$ plane. In this situation, we have derived a MKdV-ZK equation which describes the nonlinear behaviour of DIA waves along the family of curves where $B_1 = 0$. This MKdV-ZK equation is valid only when $B_1 = 0$ but $B_2 \neq 0$, where B_2 is a factor of the coefficient of the nonlinear term of the MKdV-ZK equation. Again, we have seen that the coefficients of the nonlinear terms of the KdV-ZK and MKdV-ZK equations are simultaneously equal to zero along different family of curves in different compositional parameter planes, viz., $\beta_e - \sigma_{sc}$ plane. In this context, we have derived a FMKdV-ZK equation which effectively describes the nonlinear behaviour of DIA waves. This FMKdV-ZK equation is valid only when $B_1 = 0$, $B_2 = 0$ and $B_3 \neq 0$, where B_3 is a factor of the coefficient of the nonlinear term of the FMKdV-ZK equation.

Numerically we have found the following results:

- For $r = 1$, in figure 1.5, the amplitude (a) of the KdV soliton is plotted against β_e for $\gamma = 5/3$, $\sigma = 0.0001$, $n_{pc} = 0.09$, $n_{dc} = 0.1$, $\sigma_{sc} = 0.25$, $\sigma_{pc} = 0.2$, $\beta_p = 0.25$, $\theta = 45^\circ$ and for different values of n_{sc}. Here red, blue, black and magenta curves correspond to $n_{sc} = 0.1$, $n_{sc} = 0.2$, $n_{sc} = 0.3$ and $n_{sc} = 0.4$, respectively. From this figure, we see that the amplitude of the KdV soliton increases with increasing n_{sc} and the amplitude of the KdV

soliton strictly increases with increasing β_e.

- For $r = 2$, in figure 1.6, the amplitude of the MKdV soliton is plotted against β_e for $\gamma = 5/3$, $\sigma = 0.0001$, $n_{pc} = 0.002$, $n_{dc} = 0.1$, $\sigma_{pc} = 0.15$, $\beta_p = 0.25$, $\theta = 15^\circ$ and for different values of σ_{sc}. Here blue, magenta, black and red curves correspond to $\sigma_{sc} = 0.01$, $\sigma_{sc} = 0.02$, $\sigma_{sc} = 0.03$ and $\sigma_{sc} = 0.04$ respectively. From figure 1.6, we see that the amplitude of the MKdV soliton increases with increasing σ_{sc} but the amplitude of the MKdV soliton strictly decreases with increasing β_e.

- For $r = 3$, in figure 1.7, the amplitude of the FMKdV soliton is plotted against β_e for $\gamma = 5/3$, $\sigma = 0.0001$, $n_{dc} = 0.1$, $\sigma_{pc} = 0.25$, $\beta_p = 0.2$, $\theta = 15^\circ$ and for different values of n_{sc} when $B_1 = 0 = B_2$. Here red, green, magenta and blue curves correspond to $n_{sc} = 0.2$, $n_{sc} = 0.3$, $n_{sc} = 0.4$ and $n_{sc} = 0.5$, respectively. From figure 1.7, we conclude that there exists a critical value $\beta_r^{(c)}$ of β_e such that FMKdV soliton exists for $\beta_r^{(c)} < \beta_e \leq \frac{4}{7}$ whereas the FMKdV soliton does not exist for $0 < \beta_e < \beta_r^{(c)}$. Finally, we have seen that the amplitude of the FMKdV soliton increases with increasing n_{sc} and also, the interval of existence of amplitude of the FMKdV soliton increases with increasing n_{sc}.

- In figure 1.8, the profile of the KdV soliton is plotted against Z in (a) for different values of n_{pc}, (b) for different values of n_{sc}, (c) for different values of β_p, (d) for different values of θ, (e) for different values of σ_{sc} and (f) for different values of σ_{pc}. In figure 1.8(a), red, blue and black curves correspond to $n_{pc} = 0.1$, $n_{pc} = 0.3$ and $n_{pc} = 0.5$, respectively. From figure 1.8(a), we have seen that there exist a critical value $n_{pc}^{(c)} (= 0.35)$ of n_{pc} such that for $0 < n_{pc} < n_{pc}^{(c)} = 0.35$ the amplitude of KdV soliton decreases with increasing n_{pc} and for $n_{pc}^{(c)} < n_{pc} < 0.9$ the amplitude of KdV soliton increases with increasing n_{pc}. In figure 1.8(b), red, blue and black curves correspond to $n_{sc} = 0.1$, $n_{sc} = 0.3$ and $n_{sc} = 0.5$, respectively. From

figure 1.8(b), we have seen that the amplitude of KdV soliton increases with increasing n_{sc}. In figure 1.8(c), red, blue and black curves correspond to $\beta_p = 0.05$, $\beta_p = 0.25$ and $\beta_p = 0.55$, respectively. From figure 1.8(c), we have seen that the amplitude of KdV soliton increases with increasing β_p. In figure 1.8(d), red, blue and black curves correspond to $\theta = 15^\circ$, $\theta = 45^\circ$ and $\theta = 75^\circ$, respectively. From figure 1.8(d), we have seen that the amplitude of KdV soliton increases with increasing θ. In figure 1.8(e), red, blue and black curves correspond to $\sigma_{sc} = 0.1$, $\sigma_{sc} = 0.2$ and $\sigma_{sc} = 0.4$, respectively. From figure 1.8(e), we have seen that the amplitude of KdV soliton decreases with increasing σ_{sc}. In figure 1.8(f), red, blue and black curves correspond to $\sigma_{pc} = 0.1$, $\sigma_{pc} = 0.2$ and $\sigma_{pc} = 0.4$, respectively. From figure 1.8(f), we have seen that the amplitude of KdV soliton increases with increasing σ_{pc}. From this figure, we can conclude that the amplitude of KdV soliton decreases with increasing σ_{sc} and n_{pc} for $0 < n_{pc} < n_{pc}^c = 0.35$ whereas the amplitude of KdV soliton increases with increasing β_e, n_{sc}, β_p, θ, σ_{pc} and n_{pc} for $n_{pc}^c = 0.35 < n_{pc} < 0.9$.

- In figure 1.9, the profile of the MKdV soliton is plotted against Z in (a) for different values of n_{pc}, (b) for different values of θ, (c) for different values of σ_{sc}, (d) for different values of σ_{pc}, (e) for different values of β_e and (f) for different values of β_p. Other values of the parameters are $\gamma = 5/3$, $\sigma = 0.0001$, $n_{dc} = 0.1$ and $\omega_c = 0.2$. In figure 1.9(a), black, red and blue curves correspond to $n_{pc} = 0.001$, $n_{pc} = 0.01$ and $n_{pc} = 0.0295$, respectively. From figure 1.9(a), we have seen that the amplitude of MKdV soliton increases with increasing n_{pc} within $0 < n_{pc} < 0.03$. In figure 1.9(b), black, red and blue curves correspond to $\theta = 15^\circ$, $\theta = 25^\circ$ and $\theta = 45^\circ$, respectively. From figure 1.9(b), we have seen that the amplitude of MKdV soliton increases with increasing θ. In figure 1.9(c), black, red and blue curves correspond to $\sigma_{sc} = 0.01$, $\sigma_{sc} = 0.03$ and $\sigma_{sc} = 0.05$, respectively. From figure 1.9(c), we have seen that the amplitude of MKdV soliton increases with increasing

σ_{sc}. In figure 1.9(d), black, red and blue curves correspond to $\sigma_{pc} = 0.04$, $\sigma_{pc} = 0.1$ and $\sigma_{pc} = 0.2$, respectively. From figure 1.9(d), we have seen that the amplitude of MKdV soliton decreases with increasing σ_{pc} within $0 < \sigma_{pc} < 0.25$. In figure 1.9(e), black, red and blue curves correspond to $\beta_e = 0.05$, $\beta_e = 0.15$ and $\beta_e = 0.45$, respectively. From figure 1.9(e), we have seen that the amplitude of MKdV soliton decreases with increasing β_e. In figure 1.9(f), black, red and blue curves correspond to $\beta_p = 0.05$, $\beta_p = 0.25$ and $\beta_p = 0.45$, respectively. From figure 1.9(f), we have seen that the amplitude of MKdV soliton decreases with increasing β_p. From this figure, we can conclude that the amplitude of MKdV soliton decreases with increasing β_e, β_p and σ_{pc} for $0 < \sigma_{pc} < 0.25$ whereas the amplitude of MKdV soliton increases with increasing θ, σ_{sc} and n_{pc} for $0 < n_{pc} < 0.03$.

- In figure 1.10, the profile of the FMKdV soliton is plotted against Z in (a) for different values of σ_{pc}, (b) for different values of θ, (c) for different values of β_e and (d) for different values of β_p. Other values of the parameters are $\gamma = 5/3$, $\sigma = 0.0001$, $n_{dc} = 0.1$ and $\omega_c = 0.2$. In figure 1.10(a), black, red and blue curves correspond to $\sigma_{pc} = 0.36$, $\sigma_{pc} = 0.45$ and $\sigma_{pc} = 0.53$, respectively. From figure 1.10(a), we have seen that the amplitude of FMKdV soliton increases with increasing σ_{pc} within $0.36 \leq \sigma_{pc} \leq 0.53$. In figure 1.10(b), black, red and blue curves correspond to $\theta = 15^\circ$, $\theta = 45^\circ$ and $\theta = 60^\circ$, respectively. From figure 1.10(b), we have seen that the amplitude of FMKdV soliton increases with increasing θ. In figure 1.10(c), black, red and blue curves correspond to $\beta_e = 0.47$, $\beta_e = 0.5$ and $\beta_e = 0.57$, respectively. From figure 1.10(c), we have seen that the amplitude of FMKdV soliton increases with increasing β_e within $0.47 \leq \beta_e \leq 0.57$. In figure 1.10(d), black, red and blue curves correspond to $\beta_p = 0.1$, $\beta_p = 0.3$ and $\beta_p = 0.55$, respectively. From figure 1.10(d), we have seen that the amplitude of FMKdV soliton decreases with increasing β_p. From this figure, we can conclude that the amplitude of FMKdV soliton decreases

with increasing β_p whereas the amplitude of FMKdV soliton increases with increasing θ, β_e where $0.47 \leq \beta_e \leq 0.57$ and σ_{pc} for $0.36 \leq \sigma_{pc} \leq 0.53$.

Although we have applied standard reductive perturbation method to derive KdV-ZK equation but we have considered the five components plasma system and one can investigate the effect of different parameters of the system on the stability of the solitary wave solutions of the different evolution equations. In this present **chapter**, we have not considered the stability analysis of the solitary structures obtained from the different evolution equations. This can be considered as a separate problem.

Again at critical compositions of the plasma model, the coefficient of the nonlinear term of the KdV-ZK equation is zero and for this case, the first equation of (1.4.6) shows that the amplitude of the solitary wave solution (1.4.5) for $r = 1$ is undefined because amplitude of the solitary wave solution (1.4.5) for $r = 1$ approaches to a large numerical value which is not possible for small amplitude limit. In this situation, i.e., when $B_1 = 0$, one can use MKdV-ZK equation to study the nonlinear behaviour of the DIA waves at critical composition of the plasma model for which $B_1 = 0$. On the other hand, when $B_1 = B_2 = 0$, the first equation of (1.4.6) shows that the amplitude of the solitary wave solution (1.4.5) for $r = 2$ is undefined because amplitude of the solitary wave solution (1.4.5) for $r = 2$ approaches to a large numerical value which is also untrue for small amplitude limit. In this situation, i.e., when $B_1 = B_2 = 0$, one can use FMKdV-ZK equation to study the nonlinear behaviour of the DIA waves at critical compositions for which $B_1 = B_2 = 0$. Alam *et al.* [215] reported that the amplitude of the KdV solitons goes to the infinite value, which then breaks down the validity of the reductive perturbation method. Therefore, more higher order nonlinear equation should be taken into account to get the formation of solitons around critical value.

Energy of solitary structure increases with increasing values of the amplitude of the solitary structures. A sequence of solitary waves of same polarity having

monotonically increasing amplitude converges to a double layer solution of same polarity provided that the later exists, i.e., the existence of a double layer solution implies that there must exist a sequence of solitary waves of same polarity converging to that double layer solution. On the other hand, Alfvén [172] reported that the formation of double layers in a plasma system releases an amount of energy which accelerates the charged particles of the system. In the present problem, we have considered the solitary structures only. To get the double layer solution for the same plasma system, it is necessary to consider the higher order nonlinearities to derive the more complicated evolution equation. This problem is beyond the scope of this present **chapter**.

In the present **chapter**, we have investigated the propagation properties of DIA waves in a collisionless five components e-p-i-d plasma system that can be found in the auroral zone of our atmosphere. So the results of our **chapter** regarding the existence of solitary waves can be applied to demonstrate the underlying mechanism of several physical phenomenon in the auroral region of the Earth such as auroral kilometric radiation, acceleration of energetic particles etc.

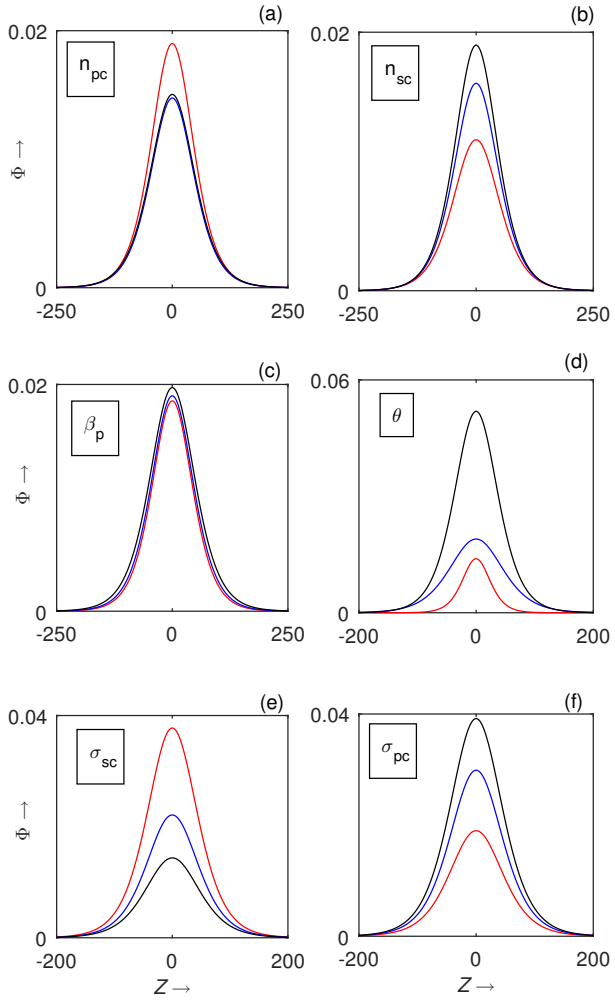

Figure 1.8: The profile of the KdV soliton is plotted against Z in (a) for different values of n_{pc} (red, blue and black curves correspond to $n_{pc} = 0.1$, $n_{pc} = 0.3$ and $n_{pc} = 0.5$, respectively), (b) for different values of n_{sc} (red, blue and black curves correspond to $n_{sc} = 0.1$, $n_{sc} = 0.3$ and $n_{sc} = 0.5$, respectively), (c) for different values of β_p (red, blue and black curves correspond to $\beta_p = 0.05$, $\beta_p = 0.25$ and $\beta_p = 0.55$, respectively), (d) for different values of θ (red, blue and black curves correspond to $\theta = 15^\circ$, $\theta = 45^\circ$ and $\theta = 75^\circ$, respectively), (e) for different values of σ_{sc} (red, blue and black curves correspond to $\sigma_{sc} = 0.1$, $\sigma_{sc} = 0.2$ and $\sigma_{sc} = 0.4$, respectively) and (f) for different values of σ_{pc} (red, blue and black curves correspond to $\sigma_{pc} = 0.1$, $\sigma_{pc} = 0.2$ and $\sigma_{pc} = 0.4$, respectively). Other values of the parameters are $\gamma = 5/3$, $\sigma = 0.0001$, $n_{dc} = 0.1$ and $\omega_c = 0.2$.

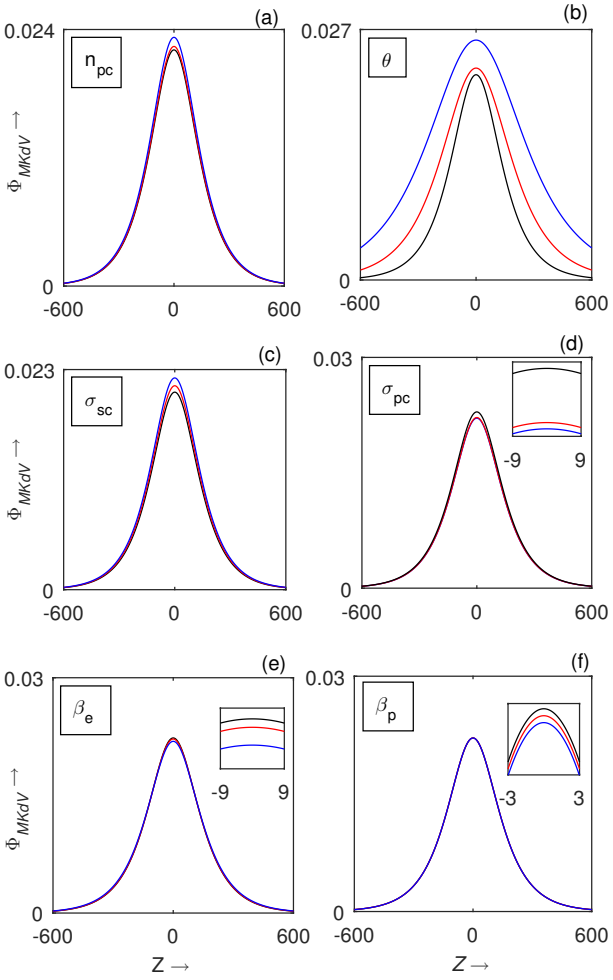

Figure 1.9: The profile of the MKdV soliton is plotted against Z in (a) for different values of n_{pc} (black, red and blue curves correspond to $n_{pc} = 0.001$, $n_{pc} = 0.01$ and $n_{pc} = 0.0295$ respectively), (b) for different values of θ (black, red and blue curves correspond to $\theta = 15^{\circ}$, $\theta = 25^{\circ}$ and $\theta = 45^{\circ}$, respectively), (c) for different values of σ_{sc} (black, red and blue curves correspond to $\sigma_{sc} = 0.01$, $\sigma_{sc} = 0.03$ and $\sigma_{sc} = 0.05$, respectively), (d) for different values of σ_{pc} (black, red and blue curves correspond to $\sigma_{pc} = 0.04$, $\sigma_{pc} = 0.1$ and $\sigma_{pc} = 0.2$, respectively), (e) for different values of β_e (black, red and blue curves correspond to $\beta_e = 0.05$, $\beta_e = 0.15$ and $\beta_e = 0.45$, respectively) and (f) for different values of β_p (black, red and blue curves correspond to $\beta_p = 0.05$, $\beta_p = 0.25$ and $\beta_p = 0.45$, respectively).

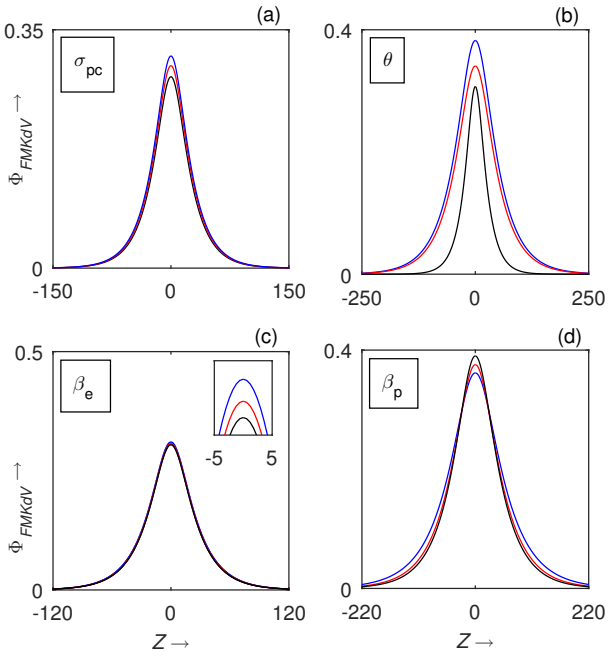

Figure 1.10: The profile of the FMKdV soliton is plotted against Z in (a) for different values of σ_{pc} (black, red and blue curves correspond to $\sigma_{pc} = 0.36$, $\sigma_{pc} = 0.45$ and $\sigma_{pc} = 0.53$, respectively), (b) for different values of θ (black, red and blue curves correspond to $\theta = 15°$, $\theta = 45°$ and $\theta = 60°$, respectively), (c) for different values of β_e (black, red and blue curves correspond to $\beta_e = 0.47$, $\beta_e = 0.5$ and $\beta_e = 0.57$, respectively) and (d) for different values of β_p (black, red and blue curves correspond to $\beta_p = 0.1$, $\beta_p = 0.3$ and $\beta_p = 0.55$, respectively).

Chapter 2

Instability of dust-ion acoustic solitary waves in a collisionless magnetized five components plasma [†]

In this **chapter**, we have discussed the stability of dust-ion acoustic (DIA) solitary waves obtained from the Korteweg-de Vries-Zakharov-Kuznetsov (KdV-ZK) equation and different modified KdV-ZK equations derived in **Chapter-1**, in a collisionless magnetized five components electron-positron-ion-dust (e-p-i-d) plasma system consisting of warm adiabatic ions, Cairns distributed nonthermal positrons, Maxwellian distributed cold isothermal electrons, Cairns distributed nonthermal electrons and negatively charged static dust grains. We have used the small-k perturbation expansion method of Rowlands and Infeld [J. Plasma Phys. **3**, 567 (1969); **8**, 105 (1972); **10**, 293 (1973); **33**, 171 (1985)] to analyze the stability of the steady state solitary wave solution of the KdV-ZK equation and different modified KdV-ZK equations. In this method, we want to find a nonlinear dispersion relation of the nonlinear evolution equation connecting the lowest order of ω and k, where ω is the wave frequency and k is the wave number. This nonlinear dispersion relation helps to analyze the stability of solitary structures of the KdV-ZK equation and different modified KdV-ZK equations. We have found the instability condition and the growth rate of instability up to the lowest order of wave number (k). We have graphically analyzed the growth rate of instability of different evolution equations with respect to different parameters of the present plasma system.

[†]This chapter has been published in ***Indian J. Phys.*** **98, 771 (2024); https://doi.org/10.1007/s12648-023-02839-0**

2.1 Introduction

In **Chapter-1**, we have studied small amplitude dust-ion acoustic (DIA) solitary structures in a magnetized five components collisionless electron-positron-ion-dust (e-p-i-d) plasma system consisting of warm adiabatic ions, Cairns distributed nonthermal positrons, Maxwellian distributed cold isothermal electrons, Cairns distributed nonthermal electrons and negatively charged static dust grains. They have derived a Korteweg-de Vries-Zakharov-Kuznetsov (KdV-ZK) equation and different modified KdV-ZK equations to investigate the solitary wave structures in different regions of compositional parameter spaces. Using the proper stretchings of space coordinates and time and appropriate perturbation expansions of the dependent field variables as given in **Chapter-1**, we have derived the following KdV-ZK equation:

$$\phi_{\tau}^{(1)} + AB_1\phi^{(1)}\phi_{\zeta}^{(1)} + \frac{1}{2}A\phi_{\zeta\zeta\zeta}^{(1)} + \frac{1}{2}AD(\phi_{\eta\eta}^{(1)} + \phi_{\xi\xi}^{(1)})_{\zeta} = 0, \tag{2.1.1}$$

where τ is the stretched time coordinate and ζ, η, ξ are the stretched spatial coordinates, $\phi^{(1)}$ is the first order perturbed part of electrostatic potential. Here A, B_1 and D are functions of the parameters of the present plasma system and the functional dependence of A, B_1 and D in terms of the parameters of the system are given in Appendix 1. The nonlinear behaviour of DIA waves can be described by the KdV-ZK equation (2.1.1) only when $B_1 \neq 0$. But when $B_1 = 0$, in **Chapter-1**, we have derived the following MKdV-ZK equation to study the nonlinearity of DIA waves:

$$\phi_{\tau}^{(1)} + AB_2(\phi^{(1)})^2\phi_{\zeta}^{(1)} + \frac{1}{2}A\phi_{\zeta\zeta\zeta}^{(1)} + \frac{1}{2}AD(\phi_{\eta\eta}^{(1)} + \phi_{\xi\xi}^{(1)})_{\zeta} = 0, \tag{2.1.2}$$

where the functional dependence of B_2 in terms of the parameters of the system is given in Appendix 2. The nonlinear behaviour of DIA waves can be described by the MKdV-ZK equation (2.1.2) only when $B_1 = 0$ but $B_2 \neq 0$. But when $B_1 = 0$ and $B_2 = 0$, in **Chapter-1**, we have derived the following FMKdV-ZK equation to study the nonlinearity of DIA waves:

$$\phi_{\tau}^{(1)} + AB_3(\phi^{(1)})^3\phi_{\zeta}^{(1)} + \frac{1}{2}A\phi_{\zeta\zeta\zeta}^{(1)} + \frac{1}{2}AD(\phi_{\eta\eta}^{(1)} + \phi_{\xi\xi}^{(1)})_{\zeta} = 0, \tag{2.1.3}$$

where the functional dependence of B_3 in terms of the parameters of the system is given in Appendix 3. The nonlinear behaviour of DIA waves can be described effectively by the FMKdV-ZK equation (2.1.3) only when $B_1 = B_2 = 0$ but $B_3 \neq 0$. In **Chapter-1**, we have also studied the obliquely propagating solitary wave solutions of the KdV-ZK equation, MKdV-ZK equation and FMKdV-ZK equation to describe the small amplitude nonlinear DIA wave structures in a magnetized five components collisionless e-p-i-d plasma system. On the other hand, a few years ago, Sardar *et al.* [45–47] studied the stabilities of DIA solitary wave solutions of three-dimensional Kadomtsev Petviashvilli (KP) equation and different modified KP equations in a collisionless unmagnetized e-p-i-d plasma system. So, in the present **chapter**, we have studied the instability analysis of solitary waves described by equations (2.1.1), (2.1.2) and (2.1.3). Here the instability analysis of different solitary structures described by different evolution equations have been considered by using the small-k perturbation expansion method of Rowlands and Infeld [15–18].

The nonlinear behaviours of the various wave structures and their stabilities are interesting topics for researchers. Several authors [14, 19–26, 28–49, 52, 200–206, 250–274] have derived different evolution equations to describe the nonlinear behaviours of the various wave structures and applying these stability methods, they have investigated the stabilities of different solitary wave solutions of different evolution equations in various plasma systems.

The small-k perturbation expansion method of Rowlands and Infeld [15–18] is used to investigate the stability of solitary waves at the lowest order of wave number, i.e., for long-wavelength plane-wave perturbation. Several authors [14, 19–26, 28–49] have used this method to investigate the stability of different types of solitary waves. In magnetized plasma, Laedke and Spatschek [251] have shown a transverse instability of ion acoustic (IA) soliton described by a two-dimensional KdV-ZK equation. Considering a magnetized electron-ion plasma model consisting of a isothermal electron species and a number of warm adiabatic ion species at

different temperatures, Das and Verheest [14] have derived a KdV-ZK equation and an MKdV-ZK equation in three dimensions to discuss the existence of solitary wave solutions of the KdV-ZK equation and the MKdV-ZK equation. Employing the small-k perturbation expansion method of Rowlands and Infeld [15–18], they have also analyzed the stability of the KdV solitons and MKdV solitons. Introducing nonthermal electrons in a magnetized electron-ion plasma with cold ions, Mamun and Cairns [21] have investigated the stability of the electrostatic solitary waves using the same small-k perturbation expansion method of Rowlands and Infeld. Bandyopadhyay and Das [24] have derived a KdV-ZK equation and an MKdV-ZK equation in three dimensions to study the stability of IA solitary waves by considering the same Rowlands and Infeld method. Later, Bandyopadhyay and Das [26] have also investigated the stability of coupled kinetic Alfvén waves and IA waves by considering the same Rowlands and Infeld method. Taking two different temperatures of electrons, one of them is nonthermally distributed hot electrons and another one is Boltzmann-Maxwellian distributed cold electrons, Islam *et al.* [34] have studied the stability of IA solitary wave solutions of a KdV-ZK equation and different modified KdV-ZK equations in a magnetized plasma. Applying the method of Rowlands and Infeld, Shahmohammadi and Dorranian [44] have studied the multi-dimensional instability of dust-acoustic solitary wave described by Zakharov-Kuznetsov (ZK) equation in a three-component magnetized dusty plasma model with hot dust grains, superthermal ions and electrons. Sardar *et al.* [45–47] have derived a three-dimensional KP equation and the different modified KP equations in a collisionless unmagnetized e-p-i-d plasma consisting of nonthermal electrons, isothermal positrons, warm adiabatic ions and static negatively charged dust grains. And they have studied the stabilities of DIA solitary wave solutions of the KP equation and different modified KP equations. Recently, considering a plasma model consisting of superthermal electrons, negatively and positively charged ions and immobile dust grains with negatively (or positively)

charged, Gao *et al.* [48] have studied the multi-dimensional instability of solitary waves of a three-dimensional ZK equation using the small-k perturbation expansion method of Rowlands and Infeld [15–18].

Several authors [25, 29, 52, 252, 255, 256, 258, 259, 261, 264, 269, 273] have studied the higher order growth rates of instability of solitary wave solutions by considering the multiple-scale perturbation expansion method of Allen and Rowlands [275, 276]. On the other hand, using the exponential rational function method, the extended direct algebraic method, the fractional direct algebraic methods, the modified extended mapping method, the extended $(\frac{G'}{G^2})$ expansion method and the modified extended direct algebraic method, several authors [200–206] have discussed the existence and stability of distinct types of wave solutions of different nonlinear evolution equations.

In this **chapter**, we have considered a five components e-p-i-d plasma system, which can be found in the Jupiter atmosphere or the auroral region of the upper Earth's ionosphere. In **Chapter-1**, we extensively discussed the existence of this plasma system in different astrophysical environments. In this **chapter**, we have considered the following schemes to discuss the stability of the small amplitude solitary wave solutions studied in **Chapter-1**:

- For the first time, we have studied the instability of DIA solitary waves in a five components e-p-i-d plasma with the help of the small-k perturbation expansion method of Rowlands and Infeld.

- In the present **chapter**, our aim is to study the stability of the steady state solitary wave solutions of the different nonlinear evolution equations by considering the perturbation in the form $\Phi_0(Z) + q_1(\xi, \eta, \tau, Z)$, where $\Phi_0(Z)$ is the steady state solitary wave solution of the evolution equation and $q_1(\xi, \eta, \tau, Z)$ is the perturbed quantity with respect to $\Phi_0(Z)$ as the steady state solitary wave solution.

- In the present **chapter**, we are considering the long-wavelength plane-wave

solutions of of the evolution equations and consequently, the wave number is the small parameter of the system. So, one can express each perturbed quantity in a power series of the wave number k.

- Considering $\Phi_0(Z)$ as a steady state solution, our aim is to express the wave frequency ω as a function of the wave number k. For linearized case, it is possible to express ω as a function of k, but for nonlinear evolution equation with $\Phi_0(Z)$ as steady state, it is not possible to express ω as a function of k. For this reason, we expand ω in powers of k by considering k is small.

- For the first time, we have derived the consistency condition for the existence of the solutions of a sequence of differential equations connected with the perturbed field variable with respect to the steady state solitary wave solutions of the different evolution equations by considering Lagrange's identity and this consistency condition helps to study the instability of the DIA solitary waves up to the lowest order of the wave number.

- In this **chapter**, we are not only interested to analyze the stability of soliton solution as given by several authors [200–206] by considering several methods, but also interested to find the growth rate of instability. The consistency condition helps to find the growth rate of instability.

- We have discussed the effects of parameters involved in the present plasma system on the instability condition and the growth rate of instabilities for the KdV solitons and different modified KdV solitons.

- Finally, we have compared the results obtained from the stability analysis of DIA solitons described in this **chapter** for magnetized e-p-i-d plasma with the stability analysis of DIA solitons for unmagnetized e-p-i-d plasma as presented by Sardar *et al.* [45].

- Here we have considered the lowest order stability analysis with respect to the wave number. In the future, we shall consider the same problem by

considering Allen and Rowlands method [275, 276] to find the higher order growth rate of the instability and the effects of different parameters of the system on the higher order growth rate of instability.

Therefore, the stability of the solitary waves solutions of DIA waves of the five components e-p-i-d plasma as obtained from equations (2.1.1), (2.1.2), (2.1.3) can be cosidered as a new problem.

2.2 Solitary wave solutions

Equations (2.1.1), (2.1.2) and (2.1.3) can be written in more compact form as

$$\frac{\partial\phi^{(1)}}{\partial\tau}+AB_r(\phi^{(1)})^r\frac{\partial\phi^{(1)}}{\partial\zeta}+\frac{1}{2}A\frac{\partial^3\phi^{(1)}}{\partial\zeta^3}+\frac{1}{2}AD\left(\frac{\partial^3\phi^{(1)}}{\partial\xi^2\partial\zeta}+\frac{\partial^3\phi^{(1)}}{\partial\eta^2\partial\zeta}\right)=0, \tag{2.2.1}$$

where $r = 1, 2$ and 3. Following **Chapter-1**, we substitute $\phi^{(1)} = \Phi_0(Z)$ in equation (2.2.1) to get the traveling wave solution of equation (2.2.1) propagating at an angle δ with the external uniform static magnetic field directed along the z-axis, where

$$Z = \xi\sin\delta+\zeta\cos\delta-U\tau. \tag{2.2.2}$$

Finally, we have obtained the following equation from the equation (2.2.1):

$$-U\Phi_0'+a_r\Phi_0^r\Phi_0'+C\Phi_0'''=0, \tag{2.2.3}$$

where

$$\Phi_0'\equiv\frac{d\Phi_0}{dZ},\ a_r=AB_r\cos\delta,\ C=\frac{Ab_1}{2}\cos\delta \tag{2.2.4}$$

with

$$b_1=(\cos^2\delta+D\sin^2\delta). \tag{2.2.5}$$

To obtain the soliton solution of (2.2.3), we have used the following boundary conditions [277]

$$\frac{d^n\Phi_0}{dZ^n}\to 0\ \text{ as }\ \mid Z\mid\to\infty\quad\text{for all }\ n=1,2,3,... \tag{2.2.6}$$

As electrostatic potential tends to 0 for $\mid Z \mid \rightarrow \infty$, we have

$$\Phi_0 \rightarrow 0 \quad \text{as} \quad \mid Z \mid \rightarrow \infty. \tag{2.2.7}$$

Using the boundary conditions (2.2.6) and (2.2.7), the solitary wave solution of (2.2.3) can be written in the following form:

$$\Phi_0 = a\text{sech}^{\frac{2}{r}}\left(\frac{Z}{\chi}\right), \tag{2.2.8}$$

where the amplitude (a) and the width (χ) of the soliton (2.2.8) are given by the following equations:

$$a^r = \frac{(r+1)(r+2)U}{2a_r} \quad \text{and} \quad \chi^2 = \frac{4C}{r^2U}. \tag{2.2.9}$$

For $r = 1$, $r = 2$ and $r = 3$, we get KdV solitons having profile sech^2, MKdV solitons having profile sech and FMKdV solitons having profile $\text{sech}^{2/3}$ respectively. In the next section, we have considered the stability analysis of the soliton solution (2.2.8).

2.3 Stability Analysis

To analyze the stability of solitary wave solution (2.2.8) of (2.2.1), we consider the following change of variables:

$$\xi^{'} = \xi\cos\delta - \zeta\sin\delta,\ \eta^{'} = \eta, \zeta^{'} = \xi\sin\delta + \zeta\cos\delta,\ \tau^{'} = \tau,\ Z = \zeta^{'} - U\tau^{'}. \tag{2.3.1}$$

Using the equation (2.3.1), the equation (2.2.1) can be written in the following form, where we have removed primes on the variables ξ, η and ζ:

$$\begin{aligned} &-U\frac{\partial\phi^{(1)}}{\partial Z} + \frac{\partial\phi^{(1)}}{\partial\tau} + a_r(\phi^{(1)})^r\frac{\partial\phi^{(1)}}{\partial Z} + \overline{a}_r(\phi^{(1)})^r\frac{\partial\phi^{(1)}}{\partial\xi} + C\frac{\partial^3\phi^{(1)}}{\partial Z^3} \\ &+b_2\frac{\partial^3\phi^{(1)}}{\partial\xi\partial Z^2} + b_3\frac{\partial^3\phi^{(1)}}{\partial\xi^2\partial Z} + b_4\frac{\partial^3\phi^{(1)}}{\partial\eta^2\partial Z} + b_5\frac{\partial^3\phi^{(1)}}{\partial\xi^3} + b_6\frac{\partial^3\phi^{(1)}}{\partial\xi\partial\eta^2} = 0, \end{aligned} \tag{2.3.2}$$

where

$$\overline{a}_r = -AB_r \sin\delta,\ b_2 = \frac{A}{2}\sin\delta\{D(2\cos^2\delta - \sin^2\delta) - 3\cos^2\delta\},$$
$$b_3 = \frac{A}{2}\cos\delta\{D(\cos^2\delta - 2\sin^2\delta) + 3\sin^2\delta\},\ b_4 = \frac{AD}{2}\cos\delta,$$
$$b_5 = -\frac{A}{2}\sin\delta(\sin^2\delta + D\cos^2\delta),\ b_6 = -\frac{AD}{2}\sin\delta.$$

Now, following the method of Rowlands and Infeld [15–18], we write $\phi^{(1)}$ as

$$\phi^{(1)} = \Phi_0(Z) + q_1(\xi, \eta, \tau, Z). \tag{2.3.3}$$

Using (2.3.3), the linearized equation with respect to q_1 obtained from the equation (2.3.2) can be written in the following form:

$$\left(\frac{\partial}{\partial\tau} + ra_r\Phi_0^{r-1}\frac{d\Phi_0}{dZ} + \overline{a}_r\Phi_0^r\frac{\partial}{\partial\xi} + b_5\frac{\partial^3}{\partial\xi^3} + b_6\frac{\partial^3}{\partial\xi\partial\eta^2}\right)q_1$$
$$+\left(-U + a_r\Phi_0^r + b_3\frac{\partial^2}{\partial\xi^2} + b_4\frac{\partial^2}{\partial\eta^2}\right)\frac{\partial q_1}{\partial Z} + \left(b_2\frac{\partial}{\partial\xi}\right)\frac{\partial^2 q_1}{\partial Z^2} + b_1\frac{\partial^3 q_1}{\partial Z^3} = 0. \tag{2.3.4}$$

For a long-wavelength plane-wave perturbation along a direction having direction cosines l_x, m_y, n_z, we can write

$$q_1(\xi, \eta, \tau, Z) = \overline{q}_1(Z)\exp[i\{k(l_x\xi + m_y\eta + n_zZ) - \omega\tau\}]. \tag{2.3.5}$$

Again, according to the small-k perturbation expansion method of Rowlands and Infeld [15–18], $\overline{q}_1(Z)$ and ω can be expanded as follows:

$$\overline{q}_1(Z) = \sum_{j=0}^{\infty} k^j q_1^{(j)}(Z), \quad \omega = \sum_{j=0}^{\infty} k^j\omega^{(j)} \tag{2.3.6}$$

with $\omega^{(0)} = 0$.

Substituting (2.3.5) and (2.3.6) into the equation (2.3.4) and equating different powers of k, we get the following sequence of equations:

$$U\frac{d}{dZ}(\aleph_1 q_1^{(j)}) = Q_1^{(j)}, \quad j = 0, 1, 2, ..., \tag{2.3.7}$$

where

$$\aleph_1 = -1 + \frac{a_r}{U}\Phi_0^r + \frac{C}{U}\frac{d^2}{dZ^2}$$

and the expressions of $Q_1^{(0)}$, $Q_1^{(1)}$ and $Q_1^{(2)}$ are given in Appendix 4.

The general solution of (2.3.7) can be written as

$$q_1^{(j)} = B_1^{(j)} f_1 + B_2^{(j)} g_1 + B_3^{(j)} h_1 + \frac{1}{C}\kappa^j, \tag{2.3.8}$$

where $B_1^{(j)}$, $B_2^{(j)}$ and $B_3^{(j)}$ are the integrating constants and f_1, g_1, h_1 and κ^j are given by

$$\begin{aligned} f_1 &= \frac{d\Phi_0}{dZ},\ g_1 = f_1 \int \frac{1}{f_1^2} dZ,\ h_1 = f_1 \int \frac{\Phi_0}{f_1^2} dZ, \\ \kappa^j &= f_1 \int \frac{\int \left(f_1 \int Q_1^{(j)} dZ \right) dZ}{f_1^2} dZ. \end{aligned} \tag{2.3.9}$$

From the first, second and third equations as given in (2.3.9), one can obtain the following results:

$$\lim_{|Z|\to\infty} (f_1, g_1, h_1) = \left(0, -\frac{\infty}{sign[a]}, -\frac{r^2\chi^2}{4} \right). \tag{2.3.10}$$

To solve (2.3.7), we have assumed that each $q_1^{(j)}$ is bounded and each $q_1^{(j)}$ vanishes as $\mid Z \mid \to \infty$. Under these assumptions, the solutions of the equation (2.3.7) for $j = 0$ and $j = 1$ can be written as

$$q_1^{(0)} = B_1^{(0)} f_1, \tag{2.3.11}$$

and

$$q_1^{(1)} = B_1^{(1)} f_1 + i B_1^{(0)} \left\{ \left(\frac{t_1}{rU} - \frac{t_3}{r a_r} \right) \Phi_0 + \left(\frac{Z t_1}{2U} - \frac{Z t_2}{2C} \right) \Phi_0^{'} \right\}, \tag{2.3.12}$$

where $t_1 = n_z U + \omega^{(1)}$, $t_2 = 3 n_z C + l_x b_2$ and $t_3 = n_z a_r + l_x \overline{a}_r$.

Now, for the operator $L = U\frac{d}{dZ}\aleph_1 = U\frac{d}{dZ}\Big(-1 + \frac{a_r}{U}\Phi_0^r + \frac{C}{U}\frac{d^2}{dZ^2} \Big)$ and for any function $v = v(Z)$ differentiable up to order three, the Lagrange's identity can be written as

$$\int v L q_1^{(j)} dZ - \int q_1^{(j)} L^* v dZ = R, \tag{2.3.13}$$

where the adjoint operator L^* and R are given by

$$L^* = -U\aleph_1 \frac{d}{dZ}, \tag{2.3.14}$$

and

$$R = Cq_1^{(j)}\frac{d^2v}{dZ^2} - C\frac{dq_1^{(j)}}{dZ}\frac{dv}{dZ} + U\left(\aleph_1 q_1^{(j)}\right)v. \tag{2.3.15}$$

If $q_1^{(j)}$ is a solution of (2.3.7), then Lagrange's identity (2.3.13) assumes the following form:

$$\int vQ_1^{(j)}dZ - \int q_1^{(j)}L^*vdZ = R. \tag{2.3.16}$$

Now, it is simple to check that $L^*\Phi_0 = 0$. Therefore, if we take $v = \Phi_0$, the equation (2.3.16) reduces to the following equation:

$$\int \Phi_0 Q_1^{(j)}dZ = R. \tag{2.3.17}$$

As Φ_0 is a soliton solution, using (2.2.6) and (2.2.7), it is simple to check that $R \to 0$ as $\mid Z \mid \to \infty$ and consequently, (2.3.17) reduces to the following consistency condition for the existence of the solution of equation (2.3.7)

$$\int_{-\infty}^{\infty} \Phi_0 Q_1^{(j)}dZ = 0 \quad \text{for } j = 0, 1, 2, \ldots. \tag{2.3.18}$$

This consistency condition can also be stated as follows [34]: For the existence of the solution of equation (2.3.7), the right hand side of the equation (2.3.7) must be perpendicular to the kernel of the operator adjoint to the operator L; this kernel, which must tend to 0 as $\mid Z \mid \to \infty$, is Φ_0 and hence one can obtain equation (2.3.18). One can easily check that the consistency condition (2.3.18) is satisfied for $j = 0$ and $j = 1$, whereas for $j = 2$, equation (2.3.18) gives the following quadratic equation of $\omega^{(1)}$

$$(n_zU + \omega^{(1)})^2 + S(n_zU + \omega^{(1)}) + T = 0, \tag{2.3.19}$$

where S and T are given in Appendix 5.

At the lowest order of the wave number k, the equation (2.3.5) can be written as

$$q_1(\xi, \eta, \tau, Z) = \overline{q}_1(Z)\exp[i\{k(l_x\xi + m_y\eta + n_zZ) - \omega^{(1)}k\tau\}]. \tag{2.3.20}$$

Now, if $\omega^{(1)}$ is complex, i.e., if imaginary part of $\omega^{(1)}$ (Im $\omega^{(1)}$) is not equal to zero (Im $\omega^{(1)} \neq 0$), then the two roots of $\omega^{(1)}$ of the quadratic equation (2.3.19) can be taken as

$$\omega^{(1)} = \omega_R^{(1)} \pm i\omega_I^{(1)} \quad \text{with} \quad \omega_I^{(1)} > 0. \tag{2.3.21}$$

Using (2.3.21), the equation (2.3.20) can be written as

$$q_1(\xi, \eta, \tau, Z) = \overline{q}_1(Z) \exp[ik\{(l_x\xi + m_y\eta + n_z Z) - \omega_R^{(1)}\tau\}] \exp[\pm\omega_I^{(1)} k\tau]. \tag{2.3.22}$$

From the equation (2.3.22), it is simple to check that

$$\mid q_1(\xi, \eta, \tau, Z) \mid = \mid \overline{q}_1(Z) \mid \exp[\pm\omega_I^{(1)} k\tau]. \tag{2.3.23}$$

From this equation, we can conclude that the perturbation at the order of the wave number grows exponentially for positive sign, whereas it decays exponentially for negative sign and totality of which shows that the perturbation grows exponentially and consequently, the steady state soliton solutions are not stable. Therefore, we see that the perturbation at the lowest order of the wave number grows exponentially with time if $\omega^{(1)}$ is complex, i.e., if the imaginary part of $\omega^{(1)}$(Im $\omega^{(1)}$) is not equal to zero, i.e., if Im $\omega^{(1)} \neq 0$ ($\Leftrightarrow$ Im $(\omega^{(1)} + n_z U) \neq 0$) and the condition Im $(\omega^{(1)} + n_z U) \neq 0$ implies that the discriminant of the quadratic equation (2.3.19) for the unknown $(\omega^{(1)} + n_z U)$ is less than zero and therefore, we have the following instability condition for the perturbation which grows exponentially with time at the lowest order of the wave number:

$$S^2 - 4T < 0. \tag{2.3.24}$$

If the above inequality holds good, then the growth rate of instability is given by

$$\Gamma = \sqrt{\frac{1}{4}(4T - S^2)}. \tag{2.3.25}$$

Simplifying (2.3.24) and (2.3.25), we get the following inequality and the equation for the growth rate of instability:

$$l_x^2\left(1 - \Lambda D \tan^2\delta\right) + b_1 m_y^2 > 0, \tag{2.3.26}$$

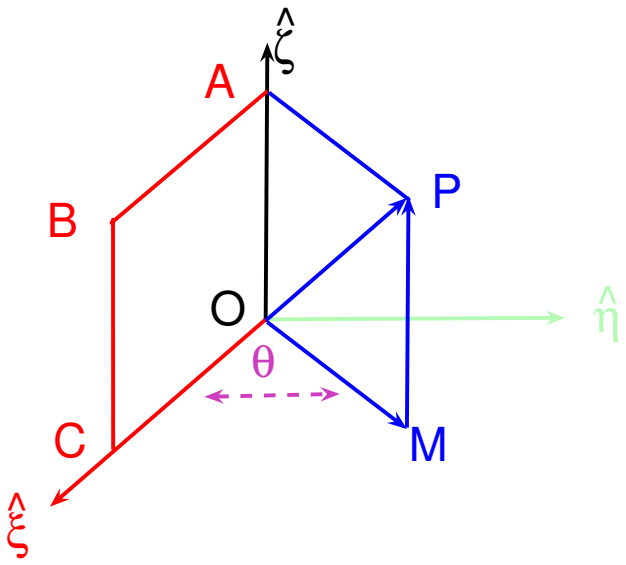

Figure 2.1: This figure shows that the perturbation given in a plane through ζ axis makes an angle θ with $\xi-\zeta$ plane along the direction of the unit vector $\vec{\mathbf{OP}}=\mathbf{l_x}\hat{\xi}+\mathbf{m_y}\hat{\eta}+\mathbf{n_z}\hat{\zeta}$. Here **OAPM** represents the plane of perturbation, **OABC** represents the $\xi-\zeta$ plane and θ is the angle between these two planes. Now, it is simple to check that the following equations hold good: $l_x=\sqrt{1-n_z^2}\cos\theta$ and $m_y=\sqrt{1-n_z^2}\sin\theta$.

$$\Gamma=\sqrt{\frac{4\Psi DU^2}{b_1^2}\left\{l_x^2\left(1-\Lambda D\tan^2\delta\right)+b_1m_y^2\right\}}, \tag{2.3.27}$$

where

$$\Psi=\frac{r^2}{16-r^2}\quad\text{and}\quad\Lambda=\frac{4+r}{4-r}. \tag{2.3.28}$$

The results obtained in (2.3.26) and (2.3.27) are similar to the results of Islam *et al.* [34].

Considering the perturbation as discussed in figure 2.1, the instability condition (2.3.26) and the growth rate of instability (2.3.27) can be written as

$$I_C>0, \tag{2.3.29}$$

$$\Gamma=\sqrt{\frac{4(1-n_z^2)\Psi DU^2}{b_1^2}I_C}, \tag{2.3.30}$$

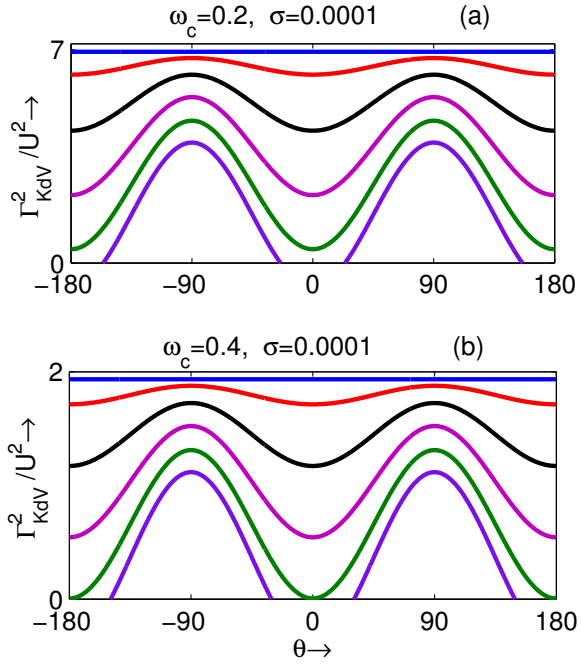

Figure 2.2: Each figure shows the variation of Γ^2_{KdV}/U^2 versus θ. In (a), blue, red, black, magenta, green and purple curves correspond to $\delta = 0^o$, $\delta = 2^o$, $\delta = 4^o$, $\delta = 6^o$, $\delta = 8^o$ and $\delta = 10^o$ respectively for $\omega_c = 0.2$, whereas in (b), blue, red, black, magenta, green and purple curves correspond to $\delta = 0^o$, $\delta = 4^o$, $\delta = 8^o$, $\delta = 12^o$, $\delta = 16^o$ and $\delta = 20^o$ respectively for $\omega_c = 0.4$. In both the figures, we take $\gamma = 5/3$, $\sigma = 0.0001$, $n_{pc} = 0.05$, $n_{sc} = 0.09$, $n_{dc} = 0.005$, $\sigma_{sc} = 0.09$, $\sigma_{pc} = 0.5$, $\beta_e = 0.4$ and $\beta_p = 0.1$.

where

$$I_C = \cos^2\theta\left(1 - \Lambda D\tan^2\delta\right) + b_1\sin^2\theta. \tag{2.3.31}$$

From the instability condition (2.3.26) or (2.3.29), we see that there is always instability if

$$|\,\delta\,| < \delta^c = \tan^{-1}\left[\sqrt{\frac{1}{\Lambda D}}\right]. \tag{2.3.32}$$

The maximum growth rate of instability can be obtained from equation (2.3.30) by taking $n_z = 0$.

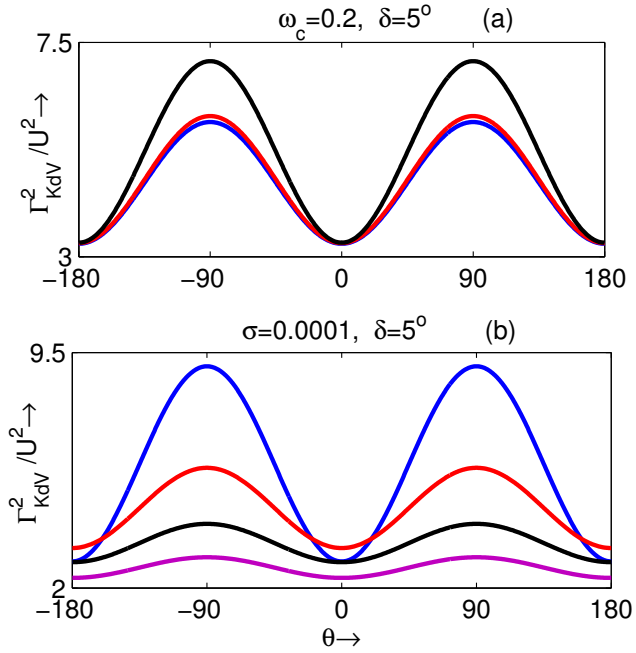

Figure 2.3: Each figure shows the variation of Γ^2_{KdV}/U^2 versus θ. In (a), blue, red and black curves correspond to $\sigma = 0.0001$, $\sigma = 0.01$ and $\sigma = 0.1$ respectively for $\omega_c = 0.2$ and $\delta = 5^o$, whereas in (b), blue, red, black and magenta curves correspond to $\omega_c = 0.15$, $\omega_c = 0.2$, $\omega_c = 0.25$ and $\omega_c = 0.3$ respectively for $\sigma = 0.0001$ and $\delta = 5^o$. In both the figures, we take $\gamma = 5/3$, $n_{pc} = 0.05$, $n_{sc} = 0.09$, $n_{dc} = 0.005$, $\sigma_{sc} = 0.09$, $\sigma_{pc} = 0.5$, $\beta_e = 0.4$ and $\beta_p = 0.1$.

2.3.1 Stability of the KdV Soliton

For KdV soliton ($r = 1$), the instability condition and the maximum growth rate of instability assume the following forms:

$$\cos^2\theta\left(1 - \frac{5}{3}D\tan^2\delta\right) + b_1\sin^2\theta > 0, \tag{2.3.33}$$

$$\Gamma^2_{KdV} = \frac{4DU^2}{15b_1^2}\left\{\cos^2\theta\left(1 - \frac{5}{3}D\tan^2\delta\right) + b_1\sin^2\theta\right\}. \tag{2.3.34}$$

We have analyzed graphically the inequality (2.3.33) and the equation (2.3.34) by considering $B_1 \neq 0$.

- Figure 2.2 (a) shows the variation of Γ^2_{KdV}/U^2 versus θ for $\omega_c = 0.2$, whereas figure 2.2 (b) shows the variation of Γ^2_{KdV}/U^2 versus θ for $\omega_c = 0.4$. In (a),

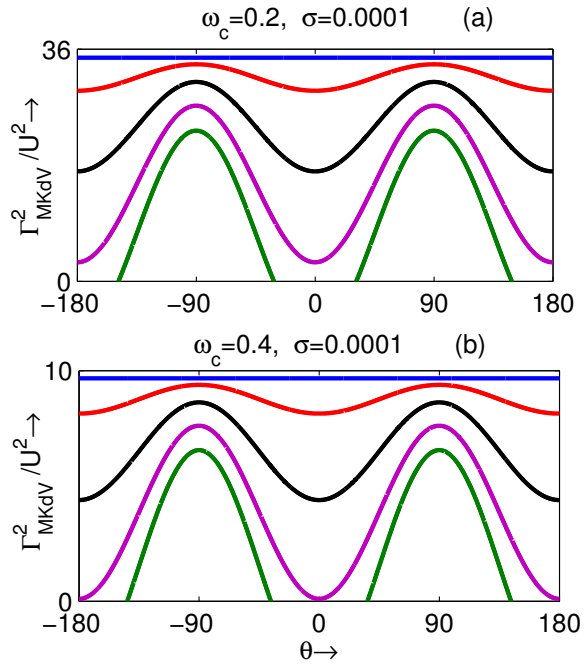

Figure 2.4: Each figure shows the variation of Γ^2_{MKdV}/U^2 versus θ. In (a), blue, red, black, magenta and green curves correspond to $\delta = 0^o$, $\delta = 2^o$, $\delta = 4^o$, $\delta = 6^o$ and $\delta = 8^o$ respectively for $\omega_c = 0.2$, whereas in (b), blue, red, black, magenta and green curves correspond to $\delta = 0^o$, $\delta = 4^o$, $\delta = 8^o$, $\delta = 12^o$ and $\delta = 16^o$ respectively for $\omega_c = 0.4$. In both the figures, we take $\gamma = 5/3$, $\sigma = 0.0001$, $n_{pc} = 0.05$, $n_{sc} = 0.09$, $n_{dc} = 0.005$, $\sigma_{sc} = 0.09$, $\sigma_{pc} = 0.5$, $\beta_e = 0.4$ and $\beta_p = 0.1$.

blue, red, black, magenta, green and purple curves correspond to $\delta = 0^o$, $\delta = 2^o$, $\delta = 4^o$, $\delta = 6^o$, $\delta = 8^o$ and $\delta = 10^o$ respectively, whereas in (b), blue, red, black, magenta, green and purple curves correspond to $\delta = 0^o$, $\delta = 4^o$, $\delta = 8^o$, $\delta = 12^o$, $\delta = 16^o$ and $\delta = 20^o$ respectively. In both the figures, we take $\gamma = 5/3$, $\sigma = 0.0001$, $n_{pc} = 0.05$, $n_{sc} = 0.09$, $n_{dc} = 0.005$, $\sigma_{sc} = 0.09$, $\sigma_{pc} = 0.5$, $\beta_e = 0.4$ and $\beta_p = 0.1$. From this figure, we have the following observations: (i) Γ^2_{KdV} is maximum when $\delta = 0^o$ and this value of Γ^2_{KdV} does not depend on θ, (ii) for any fixed value of δ, Γ^2_{KdV} is maximum when $\theta = 90^o$ or $\theta =$ any integral multiple of 90^o, (iii) there is always instability if $\theta = 90^o$ or $\theta =$ any integral multiple of 90^o, (iv) there is always instability if $\mid \delta \mid$ is less than δ^c, and for $\omega_c = 0.2$ and $\omega_c = 0.4$, the values δ^c are,

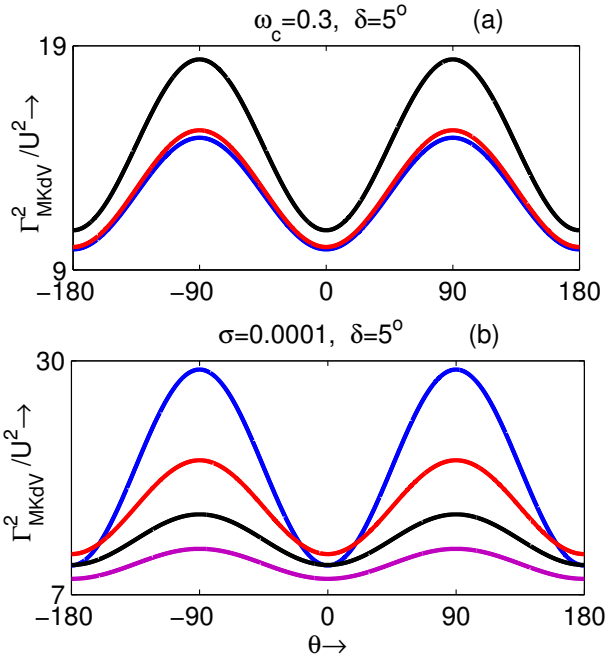

Figure 2.5: Each figure shows the variation of Γ^2_{MKdV}/U^2 versus θ. In (a), blue, red and black curves correspond to $\sigma = 0.0001$, $\sigma = 0.01$ and $\sigma = 0.1$ respectively for $\omega_c = 0.2$, whereas in (b), blue, red, black and magenta curves correspond to $\omega_c = 0.2$, $\omega_c = 0.25$, $\omega_c = 0.3$ and $\omega_c = 0.35$ respectively for $\sigma = 0.0001$. In both the figures, we take $\gamma = 5/3$, $n_{pc} = 0.05$, $n_{sc} = 0.09$, $n_{dc} = 0.005$, $\sigma_{sc} = 0.09$, $\sigma_{pc} = 0.5$, $\beta_e = 0.4$, $\beta_p = 0.1$ and $\delta = 5^o$.

respectively, 8.6367^o and 16.0476^o, which shows that δ^c increases with the increasing values of ω_c.

- Figure 2.3(a) shows the variation of Γ^2_{KdV}/U^2 against θ for different values of σ. Here blue, red and black curves correspond to $\sigma = 0.0001$, $\sigma = 0.01$ and $\sigma = 0.1$ respectively. Figure 2.3(a) shows that the growth rate of instability increases with increasing values of σ.

- Figure 2.3(b) shows the variation of Γ^2_{KdV}/U^2 against θ for different values of ω_c. Here blue, red, black and magenta curves correspond to $\omega_c = 0.15$, $\omega_c = 0.2$, $\omega_c = 0.25$ and $\omega_c = 0.3$ respectively. Figure 2.3(b) shows that the maximum value of Γ^2_{KdV} decreases with increasing values of ω_c.

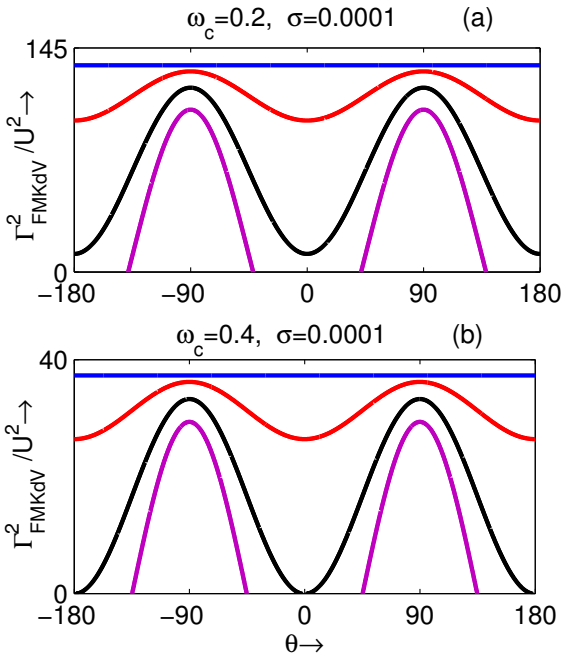

Figure 2.6: Each figure shows the variation of Γ^2_{FMKdV}/U^2 versus θ. In (a), blue, red, black and magenta curves correspond to $\delta = 0^o$, $\delta = 2^o$, $\delta = 4^o$ and $\delta = 6^o$ respectively for $\omega_c = 0.2$, whereas in (b), blue, red, black and magenta curves correspond to $\delta = 0^o$, $\delta = 4^o$, $\delta = 8^o$ and $\delta = 12^o$ respectively for $\omega_c = 0.4$. In both the figures, we take $\gamma = 5/3$, $\sigma = 0.0001$, $n_{pc} = 0.05$, $n_{sc} = 0.09$, $n_{dc} = 0.005$, $\sigma_{sc} = 0.09$, $\sigma_{pc} = 0.5$, $\beta_e = 0.4$ and $\beta_p = 0.1$.

- We have found that the variation of the maximum growth rate of instability is negligibly small with respect to the parameters n_{pc}, n_{sc}, n_{dc}, σ_{sc}, σ_{pc}, β_e and β_p.

2.3.2 Stability of the MKdV Soliton

For MKdV soliton ($r = 2$), the instability condition and the maximum growth rate of instability assume the following forms:

$$\cos^2\theta\left(1 - 3D\tan^2\delta\right) + b_1\sin^2\theta > 0, \tag{2.3.35}$$

$$\Gamma^2_{MKdV} = \frac{4DU^2}{3b_1^2}\left\{\cos^2\theta\left(1 - 3D\tan^2\delta\right) + b_1\sin^2\theta\right\}. \tag{2.3.36}$$

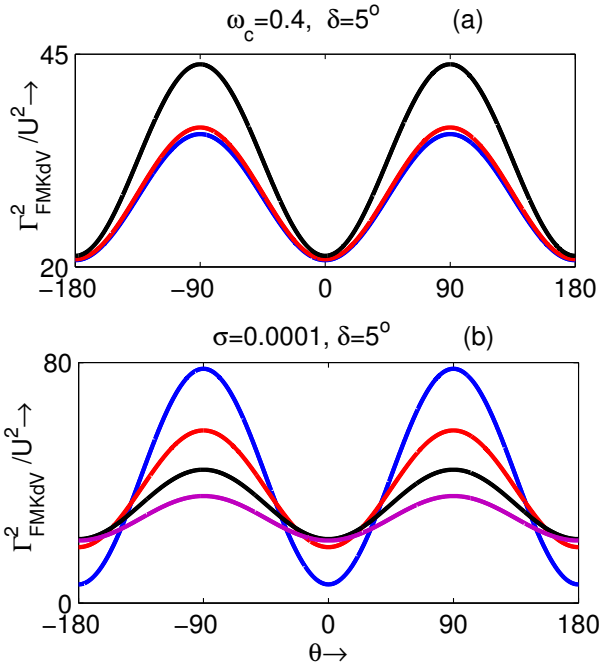

Figure 2.7: Each figure shows the variation of Γ^2_{FMKdV}/U^2 versus θ. In (a), blue, red and black curves correspond to $\sigma = 0.0001$, $\sigma = 0.01$ and $\sigma = 0.1$ respectively for $\omega_c = 0.2$, whereas in (b), blue, red, black and magenta curves correspond to $\omega_c = 0.25$, $\omega_c = 0.3$, $\omega_c = 0.35$ and $\omega_c = 0.4$ respectively for $\sigma = 0.0001$. In both the figures, we take $\gamma = 5/3$, $n_{pc} = 0.05$, $n_{sc} = 0.09$, $n_{dc} = 0.005$, $\sigma_{sc} = 0.09$, $\sigma_{pc} = 0.5$, $\beta_e = 0.4$, $\beta_p = 0.1$ and $\delta = 5^o$.

We have analyzed graphically the inequality (2.3.35) and the equation (2.3.36) by considering the conditions $B_1 = 0$ but $B_2 \neq 0$.

- Figure 2.4(a) shows the variation of Γ^2_{MKdV}/U^2 versus θ for $\omega_c = 0.2$, whereas figure 2.4(b) shows the variation of Γ^2_{MKdV}/U^2 versus θ for $\omega_c = 0.4$. In (a), blue, red, black, magenta and green curves correspond to $\delta = 0^o$, $\delta = 2^o$, $\delta = 4^o$, $\delta = 6^o$ and $\delta = 8^o$ respectively and in (b), blue, red, black, magenta and green curves correspond to $\delta = 0^o$, $\delta = 4^o$, $\delta = 8^o$, $\delta = 12^o$ and $\delta = 16^o$ respectively. In both the figures, we take $\gamma = 5/3$, $\sigma = 0.0001$, $n_{pc} = 0.05$, $n_{sc} = 0.09$, $n_{dc} = 0.005$, $\sigma_{sc} = 0.09$, $\sigma_{pc} = 0.5$, $\beta_e = 0.4$ and $\beta_p = 0.1$. From this figure, we have the following observations: (i) Γ^2_{MKdV} is maximum when $\delta = 0^o$ and this value of Γ^2_{MKdV} does not depend on θ,

(ii) for any fixed value of δ, Γ^2_{MKdV} is maximum when $\theta = 90^o$ or $\theta =$ any integral multiple of 90^o, (iii) there is always instability if $\theta = 90^o$ or $\theta =$ any integral multiple of 90^o, (iv) there is always instability if $\mid \delta \mid$ is less than δ^c, and for $\omega_c = 0.2$ and $\omega_c = 0.4$, the values δ^c are, respectively, 6.4591^o and 12.1008^o, which shows that δ^c increases with the increasing values of ω_c.

- Figure 2.5(a) shows the variation of Γ^2_{MKdV}/U^2 against θ for different values of σ. Here blue, red and black curves correspond to $\sigma = 0.0001$, $\sigma = 0.01$ and $\sigma = 0.1$ respectively. From figure 2.5(a), we see that the growth rate of instability increases with increasing values of σ.

- Figure 2.5(b) shows the variation of Γ^2_{MKdV}/U^2 against θ for different values of ω_c. Here blue, red, black and magenta curves correspond to $\omega_c = 0.2$, $\omega_c = 0.25$, $\omega_c = 0.3$ and $\omega_c = 0.35$ respectively. From figure 2.5(b), we see that the maximum value of Γ^2_{MKdV} decreases with increasing values of ω_c.

- We have found that the variation of the maximum growth rate of instability is negligibly small with respect to the parameters n_{pc}, n_{sc}, n_{dc}, σ_{sc}, σ_{pc}, β_e and β_p.

2.3.3 Stability of the FMKdV Soliton

For FMKdV soliton ($r = 3$), the instability condition and the maximum growth rate of instability assume the following forms:

$$\cos^2\theta\left(1 - 7D\tan^2\delta\right) + b_1\sin^2\theta > 0, \tag{2.3.37}$$

$$\Gamma^2_{FMKdV} = \frac{36DU^2}{7b_1^2}\left\{\cos^2\theta\left(1 - 7D\tan^2\delta\right) + b_1\sin^2\theta\right\}. \tag{2.3.38}$$

We have analyzed graphically the inequality (2.3.37) and the equation (2.3.38) by considering the conditions $B_1 = 0$, $B_2 = 0$ but $B_3 \neq 0$.

- Figure 2.6(a) shows the variation of Γ^2_{FMKdV}/U^2 versus θ for $\omega_c = 0.2$, whereas figure 2.6(b) shows the variation of Γ^2_{FMKdV}/U^2 versus θ for $\omega_c =$

0.4. In (a), blue, red, black and magenta curves correspond to $\delta = 0^o$, $\delta = 2^o$, $\delta = 4^o$ and $\delta = 6^o$ respectively. In (b), blue, red, black and magenta curves correspond to $\delta = 0^o$, $\delta = 4^o$, $\delta = 8^o$ and $\delta = 12^o$ respectively. In both the figures, we take $\gamma = 5/3$, $\sigma = 0.0001$, $n_{pc} = 0.05$, $n_{sc} = 0.09$, $n_{dc} = 0.005$, $\sigma_{sc} = 0.09$, $\sigma_{pc} = 0.5$, $\beta_e = 0.4$ and $\beta_p = 0.1$. From this figure, we have the following observations: (i) Γ^2_{FMKdV} is maximum when $\delta = 0^o$ and this value of Γ^2_{FMKdV} does not depend on θ, (ii) for any fixed value of δ, Γ^2_{FMKdV} is maximum when $\theta = 90^o$ or $\theta =$ any integral multiple of 90^o, (iii) there is always instability if $\theta = 90^o$ or $\theta =$ any integral multiple of 90^o, (iv) there is always instability if $\mid \delta \mid$ is less than δ^c, and for $\omega_c = 0.2$ and $\omega_c = 0.4$, the values δ^c are, respectively, 4.2387^o and 7.9896^o, which shows that δ^c increases with the increasing values of ω_c.

- Figure 2.7(a) shows the variation of Γ^2_{FMKdV}/U^2 against θ for different values of σ. Here blue, red and black curves correspond to $\sigma = 0.0001$, $\sigma = 0.01$ and $\sigma = 0.1$ respectively. Figure 2.7(a) shows that the growth rate of instability increases with increasing values of σ.

- Figure 2.7(b) shows the variation of Γ^2_{FMKdV}/U^2 against θ for different values of ω_c. Here blue, red, black and magenta curves correspond to $\omega_c = 0.25$, $\omega_c = 0.3$, $\omega_c = 0.35$ and $\omega_c = 0.4$ respectively. Figure 2.7(b) shows that the maximum value of Γ^2_{FMKdV} decreases with increasing values of ω_c.

- We have found that the variation of the maximum growth rate of instability is negligibly small with respect to the parameters n_{pc}, n_{sc}, n_{dc}, σ_{sc}, σ_{pc}, β_e and β_p.

It is important to note that we have drawn the growth rate of instability against the angle θ in figures 2.2-2.7 for different values of the parameters involved in the present system. From these figures, we see that the growth rate of instability either increases or decreases. If the growth rate of instability increases, the solitary wave solution becomes more unstable as t increases. On the other

hand, if the growth rate of instability decreases, then the solitary wave solution tends to be a stable one as t assumes a very large numerical value.

2.4 Conclusions

In this **chapter**, applying the small-k perturbation expansion method of Rowlands and Infeld [15–18], we have investigated the instability of DIA solitary wave in a collisionless magnetized five components e-p-i-d plasma system consisting of warm adiabatic ions, Cairns distributed nonthermal positrons, Maxwellian distributed cold isothermal electrons, Cairns distributed nonthermal electrons and negatively charged static dust grains. From this present **chapter**, we have found the following interesting facts:

- It is found that DIA solitary waves obtained from the KdV-ZK equation and different modified KdV-ZK equations having the nonlinear term of the form $(\phi^{(1)})^r \phi_\zeta^{(1)}$ are unstable for $r < 4$ at the lowest order of the wave number. Although Sardar *et al.* [45] have shown that DIA solitary waves described by the three-dimensional KP and different modified KP equations having the nonlinear term of the form $\frac{\partial}{\partial \xi}\left((\phi^{(1)})^r \phi_\xi^{(1)}\right)$ in a collisionless unmagnetized e-p-i-d plasma are stable for $r < 4$, where ξ is the stretched space coordinate in the paper of Sardar *et al.* [45]. They have also used the same small-k perturbation expansion method of Rowlands and Infeld [15–18].

- Analytically the instability conditions and the growth rate of instability at the lowest order of the wave number have been derived for the KdV-ZK soliton and different modified KdV-ZK solitons using the consistency condition.

- We have also numerically studied the growth rate of instabilities of the KdV-ZK soliton and different modified KdV-ZK solitons. We see that the growth rate of instability increases with increasing values of σ, whereas the

maximum growth rate of instability decreases with increasing values of ω_c for all solitons.

- We see that Γ attains its maximum values at $\theta = \pm(2n+1)\frac{\pi}{2}$ for any values of σ, δ and ω_c, where $n = 0, 1, 2, ...$

- It is also found that the variation of the maximum growth rate of instability is negligibly small with respect to the parameters n_{sc}, n_{pc}, n_{dc}, σ_{sc}, σ_{pc}, β_e and β_p.

Using the reductive perturbation method [198], in **Chapter-1**, we have derived different evolution equations. We have used the tanh method of Malfliet and Hereman [199] to find solitary wave solutions of different evolution equations. Finally, they analyzed the solitary wave solutions in different compositional parameter spaces. In future, one can also apply the Hirota bilinear method (HBM), the Laplace transform with the Adomian decomposition method (LADM), the auxiliary equation mapping method, the Unified Method (UM) and the Laplace homotopy transform method to study different types of solutions of evolution equations in the present plasma system. These methods have already been applied by several authors [278–289] to obtain different types of solutions of different equations. In future, one can also use the fractional calculus to derive the different nonlinear evolution equations and finally analyze the existence and stability of solitary wave solution of different nonlinear evolution equations. In future, the higher order growth rate of instability of DIA solitary waves in the present plasma system can be investigated by considering the multiple-scale perturbation expansion method of Allen and Rowlands [275, 276] and this can be treated as a separate problem. One can also consider the stability analysis of the above mentioned solutions.

The lowest order instability analysis of DIA solitary waves is helpful to characterize the stability character of the steady state solitary wave solutions of the KdV-ZK equation and different modified KdV-ZK equations as obtained

in **Chapter-1**. Finally, we want to mention that this type of five components plasma can be found in Jupiter's atmosphere and in the auroral region of the upper Earth's ionosphere.

Appendix 1

The expressions of A, B_1 and D are

$$A = \frac{1}{V}(V^2 - \sigma\gamma)^2, \tag{2.4.1}$$

$$B_1 = \frac{1}{2}\left[\frac{3V^2 + \sigma\gamma(\gamma-2)}{(V^2-\sigma\gamma)^3} - (\overline{n}_{c0}\sigma_c^2 + \overline{n}_{s0}\sigma_s^2 - \overline{n}_{p0}\sigma_p^2)\right], \tag{2.4.2}$$

$$D = \left[1 + \frac{V^4}{\omega_c^2(V^2-\sigma\gamma)^2}\right], \tag{2.4.3}$$

where

$$V^2 = \sigma\gamma + \frac{1}{1 - \beta_e\overline{n}_{c0}\sigma_c - \beta_p\overline{n}_{p0}\sigma_p}.$$

Here $\gamma(=\frac{5}{3})$ is the ratio of two specific heats, ω_c is the ion cyclotron frequency normalized by ion plasma frequency (ω_p), β_e and β_p are the nonthermal parameters associated with the nonthermal velocity distributions of hot electrons and positrons, respectively, and the expressions of $\overline{n}_{c0}, \overline{n}_{s0}, \overline{n}_{p0}, \overline{N}_{d0}, \sigma_c, \sigma_s$, and σ_p are given as follows:

$$(\overline{n}_{c0}, \overline{n}_{s0}, \overline{n}_{p0}, \overline{N}_{d0}) = \frac{1}{1 + n_{sc} - n_{pc} + n_{dc}}(1, n_{sc}, n_{pc}, n_{dc}), \tag{2.4.4}$$

$$(\sigma_c, \sigma_s, \sigma_p) = \frac{(1 + n_{sc} - n_{pc} + n_{dc})}{\sigma_{sc}\sigma_{pc} + n_{sc}\sigma_{pc} + n_{pc}\sigma_{sc}}(\sigma_{sc}\sigma_{pc}, \sigma_{pc}, \sigma_{sc}), \tag{2.4.5}$$

where $n_{sc} = \frac{n_{s0}}{n_{c0}}, n_{pc} = \frac{n_{p0}}{n_{c0}}, n_{dc} = \frac{N_{d0}}{n_{c0}}$, $\sigma = \frac{T_i}{T_{pef}}$, $\sigma_{sc} = \frac{T_{se}}{T_{ce}}$, $\sigma_{pc} = \frac{T_p}{T_{ce}}$ and T_{pef} is given by the following expression:

$$\frac{n_{c0}}{T_{ce}} + \frac{n_{s0}}{T_{se}} + \frac{n_{p0}}{T_p} = \frac{n_{c0} + n_{s0} - n_{p0} + Z_d n_{d0}}{T_{pef}}. \tag{2.4.6}$$

Here n_{j0} ($j = c$ for nonthermal electron, $j = s$ for itsohermal electron, $j = p$ for nonthermal positron and $j = d$ for dust particulates) is the equilibrium

number density of j-th species, T_{ce} (T_p) and T_{se} are the average temperatures of nonthermal electron (positron) and isothermal electron, respectively. The charge neutrality condition ($n_{i0} + n_{p0} = n_{c0} + n_{s0} + Z_d n_{d0}$) and the effective temperature equation (4.2.9) can be written as

$$\overline{n}_{c0} + \overline{n}_{s0} - \overline{n}_{p0} + \overline{N}_{d0} = 1, \tag{2.4.7}$$

$$\overline{n}_{c0}\sigma_c + \overline{n}_{s0}\sigma_s + \overline{n}_{p0}\sigma_p = 1, \tag{2.4.8}$$

where

$$Z_d n_{d0} = N_{d0} \Longleftrightarrow Z_d \overline{n_{d0}} = \overline{N}_{d0}.$$

Appendix 2

The expression of B_2 is

$$\begin{aligned} B_2 &= \frac{1}{4}\Big[\{15V^4 + V^2\sigma(\gamma^3 + 13\gamma^2 - 18\gamma) + \sigma^2(2\gamma^4 - 7\gamma^3 + 6\gamma^2)\} \times \frac{1}{(V^2 - \sigma\gamma)^5} \\ &- \{(1+3\beta_e)\overline{n}_{c0}\sigma_c^3 + \overline{n}_{s0}\sigma_s^3 + (1+3\beta_p)\overline{n}_{p0}\sigma_p^3\}\Big]. \end{aligned} \tag{2.4.9}$$

Appendix 3

The expression of B_3 is

$$\begin{aligned} B_3 &= \frac{1}{12}\Big[\Big\{105V^6 + V^4\sigma(\gamma^4 + 21\gamma^3 + 161\gamma^2 - 174\gamma) \\ &+ V^2\sigma^2(8\gamma^5 + 53\gamma^4 - 162\gamma^3 + 108\gamma^2) \\ &+ \sigma^3(6\gamma^6 - 29\gamma^5 + 46\gamma^4 - 24\gamma^3)\Big\} \times \frac{1}{(V^2 - \sigma\gamma)^7} \\ &- \Big\{(1+8\beta_e)\overline{n}_{c0}\sigma_c^4 + \overline{n}_{s0}\sigma_s^4 - (1+8\beta_p)\overline{n}_{p0}\sigma_p^4\Big\}\Big]. \end{aligned} \tag{2.4.10}$$

Appendix 4

The expressions of $Q_1^{(j)}$ of the equation (2.3.7) for $j = 0, 1$, and 2 are

$$Q_1^{(0)} = 0, \tag{2.4.11}$$

$$Q_1^{(1)} = it_1 q_1^{(0)} - it_2 \frac{d^2 q_1^{(0)}}{dZ^2} - it_3 \Phi_0^r q_1^{(0)}, \tag{2.4.12}$$

$$Q_1^{(2)} = i\omega^{(2)} q_1^{(0)} + it_1 q_1^{(1)} - it_2 \frac{d^2 q_1^{(1)}}{dZ^2} - it_3 \Phi_0^r q_1^{(1)} + t_4 \frac{dq_1^{(0)}}{dZ}, \tag{2.4.13}$$

where

$$t_4 = 3n_z^2 C + 2n_z l_x b_2 + l_x^2 b_3 + m_y^2 b_4. \tag{2.4.14}$$

Appendix 5

The coefficients of the equation (2.3.19) are

$$S = \frac{1}{r(4-r)} \left[\frac{4\{2(r+2) - (r+4)M_r\}}{r} \left(\frac{t_2}{\chi^2} \right) - \frac{2r\{4 + (r+1)(r+4)M_r\}}{(r+1)(r+2)} (a^r t_3) \right], \tag{2.4.15}$$

$$T = \frac{1}{r(4-r)} \left[16(1 - M_r) \left(U \frac{t_4}{\chi^2} \right) + \frac{16(M_r - 1)}{r^2} \left(\frac{t_2}{\chi^2} \right)^2 + \frac{8rM_r}{(r+1)(r+2)} (a^r t_3)^2 - \frac{8\{4 + (r^2 + r - 4)M_r\}}{r(r+1)(r+2)} \left(\frac{t_2}{\chi^2} \right) (a^r t_3) \right], \tag{2.4.16}$$

where

$$M_r = \frac{\int_{-\infty}^{\infty} N^{2+\frac{4}{r}} dZ}{\int_{-\infty}^{\infty} N^{\frac{4}{r}} dZ} \quad \text{with} \quad N = \operatorname{sech}\left(\frac{Z}{\chi} \right). \tag{2.4.17}$$

Chapter 3

Arbitrary amplitude dust-ion acoustic nonlinear and supernonlinear wave structures in a magnetized five components plasma [§]

In this **Chapter**, we have considered the quasi-neutrality condition instead of the Poisson equation along with other hydrodynamic conservation equations as described in **Chapter-1** to investigate the nonlinear behaviour of arbitrary amplitude DIA waves. We have applied the Sagdeev pseudo-potential approach and phase portrait analysis to confirm the existence of different DIA nonlinear wave structures in a collisionless magnetized plasma. The constituents of the present magnetized plasma are negative immobile dust particulates, non-isothermal positrons, nonthermal electrons, isothermal electrons and adiabatic warm ions. The plasma system contains eleven parameters and the nonlinear waves have been studied through the compositional parameter spaces consisting of these eleven parameters. The effects of these parameters on the amplitude of the nonlinear wave structures have also been investigated. We have extensively discussed the existence of negative potential solitary waves (NPSWs), positive potential solitary waves (PPSWs), positive potential supersolitons (PPSSs), negative potential double layers (NPDL) and supernonlinear periodic waves. We have also analyzed the coexistence of PPSWs and NPSWs, coexistence of NPSWs and PPSSs, coexistence of NPDL and PPSSs. For the increasing value of any one of the parameters n_{pc}, n_{sc} and σ_{sc}, there exists a sequence of NPSWs converging to the double layer solution of the same polarity, whereas it is observed that a sequence of NPSWs converging to the double layer solution for decreasing value of any one of the parameters β_e, σ_{pc} and l_z. Therefore, the amplitude of the NPDL solution can be regarded as an upper bound of the amplitude of the sequence of the NPSWs. The dependence of the amplitudes of the PPSWs and PPSSs on the different parameters of the system has also been critically investigated.

[§]This chapter has been published in ***Eur. Phys. J. Plus*, 138:734 (2023); https://doi.org/10.1140/epjp/s13360-023-04359-6**

3.1 Introduction

The different nonlinear properties of waves in electron-ion (e-i) plasmas are well-established in the literature. These nonlinear properties of waves in different unmagnetized e-i plasma systems have been studied by several authors [66, 67, 74, 163, 290–301]. Many of them have considered two electrons (two ions) species instead of one electron (ion) species. The presence of positron species (dust grains) along with the unmagnetized e-i plasma modifies the plasma model as electron-positron-ion (e-p-i) plasmas (electron-ion-dust (e-i-d) plasmas), whereas the presence of both positron species and a species of dust particulates along with the unmagnetized e-i plasma modify the plasma model as electron-positron-ion-dust (e-p-i-d) plasmas. Several authors [166, 302–314] have studied different nonlinear properties of waves by considering these e-p-i plasmas. Nonlinear wave structues in different e-i-d plasmas have been investigated by many authors [89, 91, 315–323]. Also considering the different unmagnetized e-p-i-d plasma systems of four or five components, several authors [45–47, 56, 75–84, 127, 131, 132, 148, 171, 218–220, 222, 223, 237, 238, 240–242, 245–247, 249, 324] have studied different characteristics of waves.

In magnetized plasma, small amplitude and arbitrary amplitude nonlinear wave structures have been investigated by many authors [14, 57, 62, 85, 86, 92–101, 128, 129, 164, 221, 222, 243, 244, 248, 325–354]. In a magnetized collisionless dusty plasma, arbitrary amplitude ion acoustic (IA) solitary structures have been considered by Choi *et al.* [85]. This problem was solved by considering Sagdeev pseudo-potential method. In another work, Choi *et al.* [86] investigated the effect ion pressure on IA solitary structures. To consider this effect, they have included the ion pressure term in the momentum equation of ion fluids. The obliquely propagating IA solitary waves in a collisionless magnetized dusty plasma have been studied by Maitra and Roychoudhury [92]. Shahmansouri and Alinejad [93]

have studied arbitrary amplitude DIA solitary waves in a collisionless magnetized dusty plasma by considering cold ion fluids, electrons of suprathermally distributed and stationary dust grains. Rufai *et al.* [94–97] have studied IA solitary waves by considering different e-i plasma systems. Considering two distinct species of electrons, Dalui *et al.* [98] have shown the existence of various solitary waves including double layers and supersolitons in a magnetized e-i plasma. Debnath and others [99, 100] have studied various IA solitary waves in a magnetized collisionless nonthermal dusty plasma. For the first time, they have studied the solitary waves in magnetized plasma by considering the compositional parameter spaces and they reported the transition of various solitary waves by considering the dynamical system corresponding to IA solitary waves. Again, for the first time in a collisionless magnetized plasma, Debnath and Bandyopadhyay [101] have studied IA solitary waves at the acoustic speed. Considering magnetized e-p-i-d plasmas, several authors [62, 129, 222, 248] have also studied small amplitude nonlinear waves properties.

In **Chapter-1**, we have considered a five components e-p-i-d plasmas. The components of this plasma system are negatively charged immobile dust particulates, non-isothermal positrons obeying Cairns distribution [1], isothermal electrons obeying Maxwellian distribution, non-isothermal electrons obeying Cairns distribution [1] and warm adiabatic ions and the plasma system is immersed in a uniform static magnetic field directed along z-axis. In **Chapter-1**, we have derived Kortewegde-Vries Zakharov-Kuznetsov (KdV-ZK) equation and different modified KdV-ZK equations to discuss the nonlinearity of the DIA waves in different parts of the compositional parameters space. The existence and validity of these evolution equations have been discussed by taking the effects of various parameters of the system. In this **chapter**, the same plasma system of **Chapter-1** has been taken to study the nonlinear wave structures including soliton of both polarities, double layers, supersolitons and supernonlinear periodic waves. In

Chapter-1, we have used the continuity equation of ions, the momentum equation of ions and the pressure equation of ions together with the Poisson equation to derive various evolution equations but in this **chapter**, the quasi-neutrality condition has been used rather than the Poisson equation. So, assuming the length scale of the solitary waves is greater than the Debye length or the gyroradius [85, 86], the quasi-neutrality condition has been taken instead to close the system of equations. We have applied the Sagdeev pseudo-potential technique to find the energy integral and this energy integral has guided us to investigate the existence of various types of nonlinear wave structures. We have found the coexistence of negative potential soliton with positive potential supersoliton and the coexistence of positive potential supersoliton with negative potential double layer. We have also found supernonlinear periodic wave solutions of DIA waves.

There are several articles [45–47, 56, 62, 76–84, 127, 129, 148, 171, 218–220, 222, 223, 237, 238, 240–242, 245–249] in four components magnetized and unmagnetized e-p-i-d plasma system and these e-p-i-d plasma systems have been observed in many astrophysical enviorements. But, Dalui *et al.* [126] have extensively studied the existence of plasma system with two different species of electrons, where the hotter species obeys the nonthermal Cairns distribution [1] and cooler one follows the Maxwell Boltzman distribution. In fact, if we assume that the above mentioned species of electrons are physically separate in the phase space by external or self-consistent fields [188], then these two species of electrons can be taken as two distint species of electron. On the basis of this assumption, two species of electrons have been considered by several authors [163, 290, 294, 311, 315, 355, 356] in different plasmas. This is the reason to take two different species of electrons in the existing e-p-i-d plasmas as discussed by many authors. This type of five components e-p-i-d plasma system has already been described In **Chapter-1**. Again, several authors [189–192] have considered dusty plasmas of five components consisting of positive dust grains, ions

and isothermal or superthermal electrons including solar wind streaming protons and electrons. Finally, they [189–192] concluded that the results are applicable in Jupiter's atmosphere by considering the five components positively charged dusty plasma model. Although, several authors have used their model in Jupiter's atmosphere by considering positively charged dust grains, there are many research papers in the existing literature, where authors [193–197] have described their results in Jupiter's atmosphere for both polarities dusty plasma model. So, the present model may be applicable to study the nonlinear waves in the upper ionosphere of Earth and in Jupiter's atmosphere.

To describe the difference between this **chapter** in comparison with the existing literature, we want to mention the following points:

- For the first time, we have investigated nonlinear and supernonlinear wave structures in a magnetized collisionless five components e-p-i-d plasma consisting of negatively charged static dust grains, nonthermal positrons, nonthermal electrons, isothermal electrons and warm adiabatic ions, whereas Dubinov *et al.* [75] have investigated the nonlinear and supernonlinear wave structures in five components collisionless unmagnetized e-p-i-d plasma consisting of two ion species (positive ions and negative ions). Dubinov *et al.* [75] applied Sagdeev pseudo-potential method to study the nonlinear wave structures.

- Again several authors [75–84] have considered collisionless four components e-p-i-d plasma system to discuss different arbitrary amplitude nonlinear wave structures in unmagnetized e-p-i-d plasma. But in this study, we have taken into consideration two species of electron at distinct temperatures along with positrons of nonthermally distributed, warm adiabatic ions and negatively charged immobile dust particulates in magnetized e-p-i-d plasma.

- In **Chapter-1**, we have taken into consideration the same plasma system to study the small amplitude solitary waves. But in this **chapter**, we have

considered arbitrary amplitude nonlinear wave structures in the same five components e-p-i-d plasma system by considering Sagdeev pseudo-potential approach. In this study, we have used quasi-neutrality condition in place of the Poisson equation based on the supposition that length scale of the solitary wave is larger than the Debye length or the gyroradius [85, 86], whereas in **Chapter-1**, we have applied the Poisson equation in place of quasi-neutrality condition to investigate the small amplitude solitary structures.

- The existence of e-p-i-d plasmas with five components has already been confirmed by numerous authors [75, 131, 132, 324] and in these papers, authors have investigated the existence of various solitary waves.

- This plasmas contains a large set of parameters and it is very difficult to handle the compositional parameter spaces containing a large set of parameters. So, in this respect, this problem is a challenging one. We have also considered the parameter's effect on the amplitudes of the various solitary waves.

3.2 Basic Equations

We consider a five components collisionless magnetised plasma system with warm adiabatic ions, nonthermally distributed positrons, negative immobile dust particles, and two distinct species of electrons with isothermally and nonthermally distributed. Here, we have considered weakly magnetized plasma and we have assumed that the magnetic pressure is much greater than the particle pressure and the ion cyclotron frequency is much greater than characteristic frequency. The continuity equation, the momentum equation and the pressure equation for ion fluid are given by

$$\frac{\partial n_i}{\partial t} + \overrightarrow{\nabla}.(n_i \overrightarrow{u_i}) = 0, \tag{3.2.1}$$

$$m_i n_i \left(\frac{\partial}{\partial t} + \overrightarrow{u_i}.\overrightarrow{\nabla} \right) \overrightarrow{u_i} + \overrightarrow{\nabla} P_i - n_i e(-\overrightarrow{\nabla}\phi + \frac{1}{C}\overrightarrow{u_i} \times B_0 \widehat{z}) = 0, \tag{3.2.2}$$

$$\frac{\partial P_i}{\partial t} + (\overrightarrow{u_i}.\overrightarrow{\nabla}) P_i + \gamma P_i (\overrightarrow{\nabla}.\overrightarrow{u_i}) = 0, \tag{3.2.3}$$

To close the above three equations, we have added the following equations:

$$n_i + n_p - n_{ce} - n_{se} - Z_d n_{d0} = 0. \tag{3.2.4}$$

$$n_{ce} = n_{c0} \left(1 - \beta_e \frac{e\phi}{K_B T_{ce}} + \beta_e \frac{e^2\phi^2}{K_B^2 T_{ce}^2} \right) \exp\left(\frac{e\phi}{K_B T_{ce}} \right), \tag{3.2.5}$$

$$n_{se} = n_{s0} \exp\left(\frac{e\phi}{K_B T_{se}} \right), \tag{3.2.6}$$

$$n_p = n_{p0} \left(1 + \beta_p \frac{e\phi}{K_B T_p} + \beta_p \frac{e^2\phi^2}{K_B^2 T_p^2} \right) \exp\left(- \frac{e\phi}{K_B T_p} \right), \tag{3.2.7}$$

$$n_d = n_{d0}. \tag{3.2.8}$$

The equations (3.2.4) - (3.2.8) are, respectively, the quasi-neutrality condition, the expression of number density of nonthermal electrons, the expression of number density of isothermal electrons, the expression of number density of nonthermal positrons and the expression of number density of dust grains. Here, the uniform static magnetic field B_0 is directed along the z-axis, C is the speed of light in vacuum, $\overrightarrow{u_i}$ is the ion fluid velocity, the electrostatic potential is ϕ, P_i represents the ion pressure, $-e$ represents the charge of an electron, m_i represents the ion mass, K_B is the Boltzmann constant, the ratio of two specific heats is $\gamma(= 5/3)$, n_α is the number density of α-th species of particle, where $\alpha = i$ for ion, $\alpha = p$ for nonthermal positron, $\alpha = ce$ for nonthermal electron, $\alpha = se$ for isothermal electron and $\alpha = d$ for dust particles. The equilibrium number density of the j-th species is n_{j0}, where $j = i$ for ion, $j = p$ for nonthermal positron, $j = c$ for nonthermal electron, $j = s$ for isothermal electron and $j = d$ for dust particles. The average temperatures of the k-th species is T_k, where $k = p$ for nonthermal

positron, $k = ce$ for nonthermal electron, $k = se$ for isothermal electron, β_e (β_p) is connected with the Cairns distributed electrons (positrons).

Based on the supposition that $m_d >> Z_d m_i$ (m_d represents the mass of a dust grain), following the prescription of Popel & Yu [357], it is simple to prove that the average velocity of the dust particulates is zero and dust density is a constant of motion. Although these facts has already been reported by Popel & Yu [357]. So, the present plasma model is essentially a dusty plasma, where we have not taken into consideration the variable-charge dust particulates effect, ionization effect, interaction of ions-dust effect, interaction of ion-neutral effect and effects originating from ion absorption by dust particulates. Numerous authors[358–373] have researched these effects. Several authors [72, 82, 91, 142, 331, 344, 374, 375] have considered this type of plasma system as dusty plasma system.

To get the bounded parameters of the system, we have considered the following normalization of the independent and dependent field variables: the spatial variables x, y, z are normalized by $\lambda_D \left(= \sqrt{\frac{K_B T_{pef}}{4\pi e^2 n_{i0}}} \right)$, time t is normalized by $\omega_p^{-1} \left(= \sqrt{\frac{m_i}{4\pi e^2 n_{i0}}} \right)$, ion fluid velocities u_x, u_y and u_z along x, y and z axis are normalized by $c_s \left(= \sqrt{\frac{K_B T_{pef}}{m_i}} \right)$, $\sigma = \frac{T_i}{T_{pef}}$, where the effective temperature T_{pef} is:

$$\frac{n_{c0}}{T_{ce}} + \frac{n_{s0}}{T_{se}} + \frac{n_{p0}}{T_p} = \frac{n_{c0} + n_{s0} - n_{p0} + Z_d n_{d0}}{T_{pef}}. \tag{3.2.9}$$

Again n_α is normalized by n_{i0}, ϕ is normalized by $\frac{K_B T_{pef}}{e}$, $\omega_c = (\frac{eB_0}{m_i C})$ is normalized by ω_p, P_i is normalized by $n_{i0} K_B T_i$. Assuming that Z_d is the amount of negative unit charges present on the dust grain surface, the normalized dimensionless equations may be expressed as follows:

$$\frac{\partial n_i}{\partial t} + \frac{\partial}{\partial x}(n_i u_x) + \frac{\partial}{\partial y}(n_i u_y) + \frac{\partial}{\partial z}(n_i u_z) = 0, \tag{3.2.10}$$

$$\frac{\partial u_x}{\partial t} + u_x \frac{\partial u_x}{\partial x} + u_y \frac{\partial u_x}{\partial y} + u_z \frac{\partial u_x}{\partial z} + \frac{\sigma}{n_i} \frac{\partial P_i}{\partial x} + \frac{\partial \phi}{\partial x} = \omega_c u_y, \tag{3.2.11}$$

$$\frac{\partial u_y}{\partial t} + u_x\frac{\partial u_y}{\partial x} + u_y\frac{\partial u_y}{\partial y} + u_z\frac{\partial u_y}{\partial z} + \frac{\sigma}{n_i}\frac{\partial P_i}{\partial y} + \frac{\partial \phi}{\partial y} = -\omega_c u_x, \tag{3.2.12}$$

$$\frac{\partial u_z}{\partial t} + u_x\frac{\partial u_z}{\partial x} + u_y\frac{\partial u_z}{\partial y} + u_z\frac{\partial u_z}{\partial z} + \frac{\sigma}{n_i}\frac{\partial P_i}{\partial z} + \frac{\partial \phi}{\partial z} = 0, \tag{3.2.13}$$

$$\frac{\partial P_i}{\partial t} + \left(u_x\frac{\partial P_i}{\partial x} + u_y\frac{\partial P_i}{\partial y} + u_z\frac{\partial P_i}{\partial z}\right) + \gamma P_i\left(\frac{\partial u_x}{\partial x} + \frac{\partial u_y}{\partial y} + \frac{\partial u_z}{\partial z}\right) = 0, \tag{3.2.14}$$

$$n_i + n_p - n_{ce} - n_{se} - Z_d n_{d0} = 0. \tag{3.2.15}$$

$$n_{ce} = \overline{n}_{c0}(1 - \beta_e\sigma_c\phi + \beta_e\sigma_c^2\phi^2)\exp(\sigma_c\phi), \tag{3.2.16}$$

$$n_{se} = \overline{n}_{s0}\exp(\sigma_s\phi), \tag{3.2.17}$$

$$n_p = \overline{n}_{p0}(1 + \beta_p\sigma_p\phi + \beta_p\sigma_p^2\phi^2)\exp(-\sigma_p\phi), \tag{3.2.18}$$

$$n_d = \overline{n}_{d0}. \tag{3.2.19}$$

Again, using the equation (3.2.10), the pressure equation for ion fluid (3.2.14) can be written as:

$$P_i = n_i^{\gamma}, \tag{3.2.20}$$

where γ is the ratio of two specific heat. Using equation (3.2.14), the equations (3.2.11), (3.2.12), (3.2.13) can be expressed as:

$$\frac{\partial u_x}{\partial t} + u_x\frac{\partial u_x}{\partial x} + u_y\frac{\partial u_x}{\partial y} + u_z\frac{\partial u_x}{\partial z} + \sigma\gamma n_i^{\gamma-2}\frac{\partial n_i}{\partial x} + \frac{\partial \phi}{\partial x} = \omega_c u_y, \tag{3.2.21}$$

$$\frac{\partial u_y}{\partial t} + u_x\frac{\partial u_y}{\partial x} + u_y\frac{\partial u_y}{\partial y} + u_z\frac{\partial u_y}{\partial z} + \sigma\gamma n_i^{\gamma-2}\frac{\partial n_i}{\partial y} + \frac{\partial \phi}{\partial y} = -\omega_c u_x, \tag{3.2.22}$$

$$\frac{\partial u_z}{\partial t} + u_x\frac{\partial u_z}{\partial x} + u_y\frac{\partial u_z}{\partial y} + u_z\frac{\partial u_z}{\partial z} + \sigma\gamma n_i^{\gamma-2}\frac{\partial n_i}{\partial z} + \frac{\partial \phi}{\partial z} = 0. \tag{3.2.23}$$

The charge neutrality condition at the unperturbed state (equilibrium state) can be written as

$$n_{i0} + n_{p0} = n_{c0} + n_{s0} + Z_d n_{d0}. \tag{3.2.24}$$

From equations (3.2.24) and (3.2.9), we get following two equations:

$$\overline{n}_{c0} + \overline{n}_{s0} - \overline{n}_{p0} + \overline{N}_{d0} = 1, \tag{3.2.25}$$

$$\overline{n}_{c0}\sigma_c + \overline{n}_{s0}\sigma_s + \overline{n}_{p0}\sigma_p = 1, \tag{3.2.26}$$

where $Z_d n_{d0} = N_{d0} \Longleftrightarrow Z_d \overline{n}_{d0} = \overline{N}_{d0}$.

Introducing the new parameters: $n_{ac} = \frac{n_{a0}}{n_{c0}}$ with $a = s, p, d$ and $\sigma_{hc} = \frac{T_g}{T_{ce}}$ with $h = s, p$ and $g = se, p$, we can express $\overline{n}_{c0}$, $\overline{n}_{s0}$, $\overline{N}_{d0}$, $\overline{n}_{p0}$, σ_p, σ_s and σ_c like this:

$$(\overline{n}_{c0}, \overline{n}_{s0}, \overline{n}_{p0}, \overline{N}_{d0}) = \Lambda(1, n_{sc}, n_{pc}, n_{dc}), \tag{3.2.27}$$

$$(\sigma_c, \sigma_s, \sigma_p) = \Gamma(\sigma_{sc}\sigma_{pc}, \sigma_{pc}, \sigma_{sc}), \tag{3.2.28}$$

where $\Lambda = \dfrac{1}{1 + n_{sc} - n_{pc} + n_{dc}}$ and $\Gamma = \dfrac{(1 + n_{sc} - n_{pc} + n_{dc})}{\sigma_{sc}\sigma_{pc} + n_{sc}\sigma_{pc} + n_{pc}\sigma_{sc}}$.

3.3 Energy Integral

In order to investigate the arbitrary amplitude DIA solitary structures travelling along a path with direction cosines (m_x, n_y, l_z), we consider the following transformation:

$$\xi = m_x x + n_y y + l_z z - Mt, \quad \text{with} \;\; m_x^2 + n_y^2 + l_z^2 = 1, \tag{3.3.1}$$

where M is the velocity of the wave frame normalized by c_s.

Using the same procedure of Debnath *et al.* [99], we have derived the equation known as energy integral with $V(\phi)$ as the Sagdeev pseudo-potential:

$$\frac{1}{2}\left(\frac{d\phi}{d\xi}\right)^2 + V(\phi) = 0, \tag{3.3.2}$$

where

$$V(\phi) = V(M, \phi) = -\frac{\displaystyle\int_0^{\phi} \frac{dS}{d\phi} F(\phi) d\phi}{\left(\dfrac{dS}{d\phi}\right)^2}, \tag{3.3.3}$$

$$S = \frac{M^2}{2n_i^2} + \frac{\sigma\gamma}{\gamma - 1} n_i^{\gamma-1} + \phi, \tag{3.3.4}$$

$$F(\phi) = \omega_c^2 \left[n_i - 1 - \frac{l_z^2}{M^2} n_i G_1(\phi) \right], \tag{3.3.5}$$

$$G_1(\phi) = \sigma(n_i^{\gamma} - 1) + \int_0^{\phi} n_i d\phi. \tag{3.3.6}$$

Equation (3.3.2) is known as energy integral. According to the terminology used by Sagdeev [63], equation (3.3.2) can be considered as the conservation of energy of a particle of mass unity, where the position of the particle at an instant of time ξ is ϕ and its velocity at that instant of time is $\frac{d\phi}{d\xi}$. So, the first term of (3.3.2) represents the kinetic energy, whereas the second term of the (3.3.2) can be considered as the potential energy. Now, differentation of (3.3.2) w.r.t. ϕ, gives $\frac{d^2\phi}{d\xi^2} = -V^{'}(\phi)$. Therefore, the velocity of the particle is $\sqrt{-2V(\phi)}$ and the force acting on the particle is $-V^{'}(\phi)$. The direction of this force is towards $\phi = 0$ (origin) if $V^{'}(\phi) > 0$ for $\phi > 0$ ($V^{'}(\phi) < 0$ for $\phi < 0$). Now, this particle is in equilibrium at the position ϕ if the velocity and the force acting on it are simultaneously equal to zero, i.e., if $V(\phi) = 0$ and $V^{'}(\phi) = 0$. If $\phi = 0$ is the position of the equilibrium, then we have $V(0) = 0$ and $V^{'}(0) = 0$. Now the stable and the unstable equlibrium of the particle at the origin depends on the sign of $V^{''}(0)$, and we have the following two cases.

Case-I [$V(0) = 0$, $V^{'}(0) = 0$ and $V^{''}(0) > 0$]: In this case, potential energy is minimum at $\phi = 0$. So, from the energy test of stability, we can conclude that $\phi = 0$ is a stable equilibrium position and consequently, if a particle with $\phi = 0$ is gently moved from its equilibrium position and then set free, it goes towards its equilibrium position. For this case, it is not possible to get any particle oscillation within $\phi \in (\min\{0, \phi_m\}, \max\{0, \phi_m\})$ for some $\phi_m > 0$ ($\phi_m < 0$) when the particle be slightly displaced in the positive (negative) direction of ϕ-axis and in this case, we get periodic solution only about the stable equilibrium point. As $V(\phi)$ can be considered as a function of ϕ and all the parameters of the system, we can write

$V(\phi) = V(M, \phi)$, then for the existence of a periodic wave solution of (3.3.2) about $\phi = 0$, we have $V(M, \phi) = 0$, $V^{'}(M, \phi) = 0$ and $V^{''}(M, \phi) > 0$ at $\phi = 0$.

Case-II [$V(0) = 0$, $V^{'}(0) = 0$ and $V^{''}(0) < 0$]: In this case, potential energy is maximum at $\phi = 0$ and then, from the energy test of stability, we can conclude that $\phi = 0$ is a unstable equilibrium position. Thus, if a particle is slightly moved towards the positive (negative) ϕ-axis then set free, it moves away from the point $\phi = 0$ and it keeps continues to move untill its velocity is exactly zero at $\phi = \phi_m > 0$ ($\phi = \phi_m < 0$). So, we have $V(\phi_m) = 0$, if in this position $V^{'}(\phi_m) > 0$ ($V^{'}(\phi_m) < 0$), the force acting on the particle is directed towards the origin and consequently, we have an oscillation of the particle within $0 < \phi < \phi_m$ ($\phi_m < \phi < 0$). Therefore, for the oscillation of the particle, we have $V(\phi_m) = 0$, $V^{'}(\phi_m) > 0$ ($V^{'}(\phi_m) < 0$) for $\phi_m > 0$ ($\phi_m < 0$). When such an oscillation is placed in a wave frame moving with a velocity M, then we get a nonlinear wave known as a positive potential soliton or negative potential soliton according to whether $\phi_m > 0$ or $\phi_m < 0$. Therefore, for the existence, of a positive (negative) potential soliton solution of (3.3.2), the following circumstances allow for the holding of conditions:

(i) $V(M, \phi) = V^{'}(M, \phi) = 0$ and $V^{''}(M, \phi) < 0$ at $\phi = 0$.

(ii) $V(M, \phi_m) = 0$, $V^{'}(M, \phi_m) > 0$ ($V^{'}(M, \phi_m) < 0$) for some M with $\phi_m > 0$ for the existence of a positive potential solitary wave ($\phi_m < 0$ for the existence of a negative potential solitary wave),

(iii) $V(M, \phi) < 0$ for all $0 < \phi < \phi_m (\phi_m < \phi < 0)$. This condition is required to define (3.3.2) for $\phi \in (\min\{0, \phi_m\}, \max\{0, \phi_m\})$.

For $\phi_m > 0$ ($\phi_m < 0$), the soliton is known as a positive (negative) potential solitary wave. Therefore, we see that for the existence of the solitary waves it is essential to exist a point $\phi_m (\neq 0)$ such that the the particle velocity at $\phi = \phi_m$ is equal to zero, but the force acting on the particle is not equal to zero. Now, if the force is also equal to zero, i.e., the particle at $\phi = \phi_m$ is in equilibrium,

then the particle will not come back again at the origin $\phi = 0$. In this case, it is impossible to get any soliton solution, but one can get a shock type solution known as a double layer (DL) solution. Therefore, for DL solution, the condition (ii) is replaced by $V(M, \phi_m) = 0,\ V^{'}(M, \phi_m) = 0,\ V^{''}(M, \phi_m) < 0$. For $\phi_m > 0$ ($\phi_m < 0$) DL is known as a positive (negative) potential DL. If there exists any soliton of the same polarity after the formation of DL, then the soliton is known as supersoliton. But, it is also possible to define supersoliton structures without the formation of DL of the same polarity. In fact, characteristics of supersoliton can be well defined through the separatrix of the phase portrait of the dynamical system corresponding to the system of coupled equations

$$\frac{d\phi}{d\xi} = \theta, \quad \frac{d\theta}{d\xi} = -V^{'}(\phi). \tag{3.3.7}$$

The system of equations (3.3.7) can be obtained by differentiating (3.3.2) with respect to ϕ. Differentiation of (3.3.2) with respect to ϕ gives a differential equation of second order and this second order differential equation can be split into (3.3.7). Following Dubinov and others [88–90] we have defined the supersoliton and supernonlinear periodic structures in the section 3.4.

Therefore, for the existence of any kind of solitary waves including DLs, $\phi = 0$ is the unstable equilibrium point of the pseudo particle associated with (3.3.2), i.e., $V(M, 0) = V^{'}(M, 0) = 0$ and $V^{''}(M, 0) < 0$. Using the equation (3.3.3), one can easily check that $V(M, 0) = 0$ and $V^{'}(M, 0) = 0$ are identically satisfied for any value of M but $V^{''}(M, 0) < 0$ imposes the following bounds of M:

$$M_c < M < M_s, \tag{3.3.8}$$

where

$$M_c = M_s l_z \tag{3.3.9}$$

and

$$M_s = \sqrt{\sigma\gamma + \frac{1}{1 - \beta_e \overline{n}_{c0}\sigma_c - \beta_p \overline{n}_{p0}\sigma_p}}. \tag{3.3.10}$$

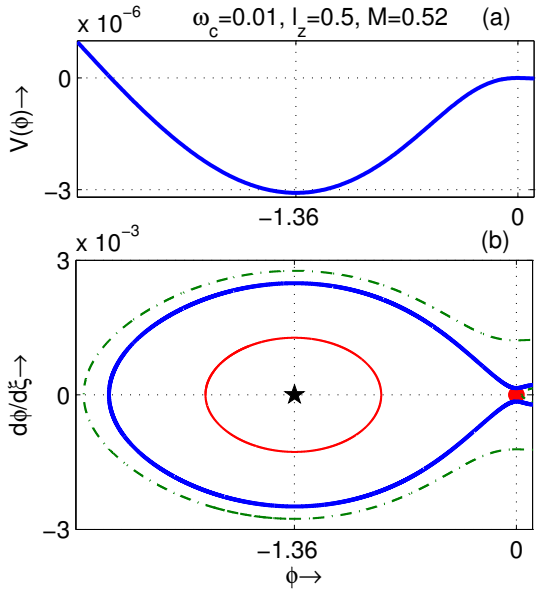

Figure 3.1: Drawings of $V(\phi)$ and the phase portrait of (3.3.7) are shown w.r.t. ϕ for $M = 0.52$, $\sigma = 0.001$, $\gamma = 5/3$, $n_{sc} = 0.5$, $n_{dc} = 0.01$, $n_{pc} = 0.09$, $\sigma_{pc} = 0.9$, $\sigma_{sc} = 0.07$, $\beta_p = 0.1$, $\beta_e = 0.25$, $\omega_c = 0.01$ and $l_z = 0.5$.

Debnath *et al.* [99] have extensively studied theoretically and also numerically the bounds of different solitary structures.

3.4 Phase Portraits

In this section, we have plotted $V(\phi)$ vs. ϕ curve (subplot (a)) and phase portrait (subplot (b)) of (3.3.7) by taking the same ϕ axis. Such figures establish a correspondence between $V(\phi)$ vs. ϕ and the separatrix of phase portrait. This one-one correspondence is necessary to establish the existence of the various nonlinear waves. To characterize the supernonlinear solitary structures, we follow the definition given by Dubinov and others [88–90]. In the phase portrait of the dynamical system (3.3.7), we have used bold black star to denote a stable fixed point, whereas we have used bold red circle to denote an unstable equilibrium point.

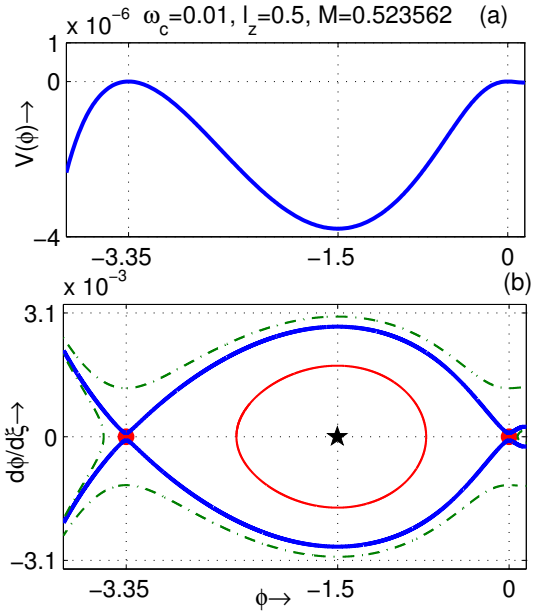

Figure 3.2: Drawings of $V(\phi)$ and the phase portrait of (3.3.7) are shown w.r.t. ϕ for $M = 0.523562$, $\sigma = 0.001$, $\gamma = 5/3$, $n_{sc} = 0.5$, $n_{dc} = 0.01$, $n_{pc} = 0.09$, $\sigma_{pc} = 0.9$, $\sigma_{sc} = 0.07$, $\beta_p = 0.1$, $\beta_e = 0.25$, $\omega_c = 0.01$ and $l_z = 0.5$.

Figure 3.1(b) represents the phase portrait of (3.3.7) corresponding to an NPSW. We have seen that there is a single separatrix, which seems to begin and end at (0, 0) and one stable fixed point (-1.3598, 0) is enclosed by the separatrix. Figure 3.1(a) establishes that $V(\phi)$ vs. ϕ corresponds to the separatrix of figure 3.1(b).

Figure 3.2(b) represents the phase portrait of (3.3.7) corresponding to an NPDL. We have seen that there is a single separatrix, which seems to go through the points $(0, 0)$ and $(-3.3506, 0)$, whereas one stable fixed point (-1.5022, 0) is enclosed by the separatrix. Figure 3.2(a) establishes that $V(\phi)$ vs. ϕ corresponds to the separatrix of the figure 3.2(b).

Figure 3.3(b) represents the phase portrait of (3.3.7) corresponding to a PPSW. We have seen that there is only one separatrix, which seems to begin and end at $(0, 0)$ and one stable fixed point $(0.476, 0)$ is enclosed by the separatrix. Figure 3.3(a) establishes that $V(\phi)$ vs. ϕ corresponds to the separatrix of

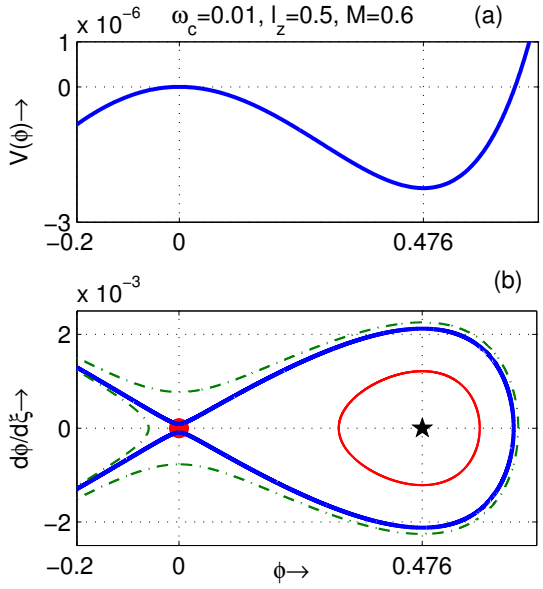

Figure 3.3: Drawings of $V(\phi)$ and the phase portrait of (3.3.7) are shown w.r.t. ϕ for $M = 0.6$, $\sigma = 0.001$, $\gamma = 5/3$, $n_{sc} = 0.5$, $n_{dc} = 0.01$, $n_{pc} = 0.09$, $\sigma_{pc} = 0.9$, $\sigma_{sc} = 0.07$, $\beta_p = 0.1$, $\beta_e = 0.25$, $\omega_c = 0.01$ and $l_z = 0.5$.

the figure 3.3(b).

In figure 3.4, profile of different solitary structures have been drawn. Figure 3.4(a) represents ϕ vs. ξ for negative potential solitary wave for $M = 0.52$, figure 3.4(b) represents ϕ vs. ξ for negative potential double layer for $M = 0.523562$ and figure 3.4(c) represents ϕ vs. ξ for positive potential solitary wave for $M = 0.6$. To draw these subplots, we have used $\sigma = 0.001$, $\gamma = 5/3$, $n_{sc} = 0.5$, $n_{dc} = 0.01$, $n_{pc} = 0.09$, $\sigma_{pc} = 0.9$, $\sigma_{sc} = 0.07$, $\beta_p = 0.1$, $\beta_e = 0.25$, $\omega_c = 0.01$ and $l_z = 0.5$. Figure 3.4(b) represents both "Z" type and "S" type double layers.

Figure 3.5(b) represents the phase portrait of (3.3.7) corresponding to simultaneous existence of NPDL and PPSW. We have seen that there is only one separatrix seems to go through the points $(0, 0)$ and $(-1.45, 0)$. The separatrix in the positive direction of ϕ-axis encloses stable fixed point $(0.42, 0)$ and the separatrix in the negative direction of ϕ-axis encloses stable fixed point $(-0.66, 0)$. Figures 3.5(a) and 3.5(b) simultaneously establish a corresponds between $V(\phi)$

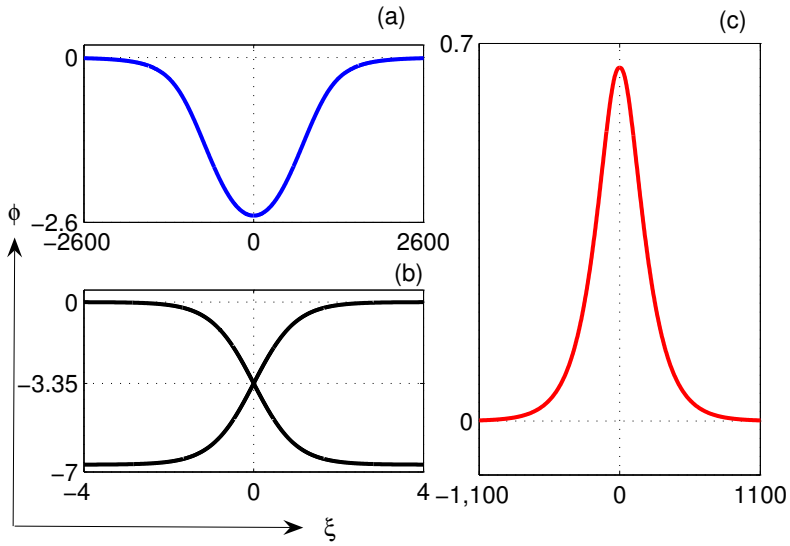

Figure 3.4: ϕ vs. ξ for $\sigma = 0.001$, $\gamma = 5/3$, $n_{sc} = 0.5$, $n_{dc} = 0.01$, $n_{pc} = 0.09$, $\sigma_{pc} = 0.9$, $\sigma_{sc} = 0.07$, $\beta_p = 0.1$, $\beta_e = 0.25$, $\omega_c = 0.01$ and $l_z = 0.5$. The blue curve correlates to $M = 0.52$, the black curve correlates to $M = 0.523562$ and the red curve correlates to $M = 0.6$.

vs. ϕ and the separatrix of phase portrait.

Figure 3.6(b) represents the phase portrait of (3.3.7) corresponding to the simultaneous existence of NPSW and a positive potential supersoliton (PPSS). The blue curve and sky blue curve demonstrate that there are two separatrices. The blue separatrix seems to begin and end at $(0, 0)$. The sky blue separatrix is enclosed by the blue separatrix. The sky blue separatrix seems to go through $(0.24835, 0)$ and it encloses two stable fixed points $(0.1911, 0)$ and $(0.4103, 0)$, whereas blue separatrix encloses a stable fixed point $(-0.19847, 0)$ in the negative direction. Figure 3.6(a) establishes that $V(\phi)$ vs. ϕ corresponds to the separatrix of the figure 3.6(b).

Figure 3.7(b) represents the phase portrait of (3.3.7) corresponding to the simultaneous existence of NPDL and positive potential supersoliton (PPSS). The blue curve and sky blue curve demonstrate that there are two separatrices. The

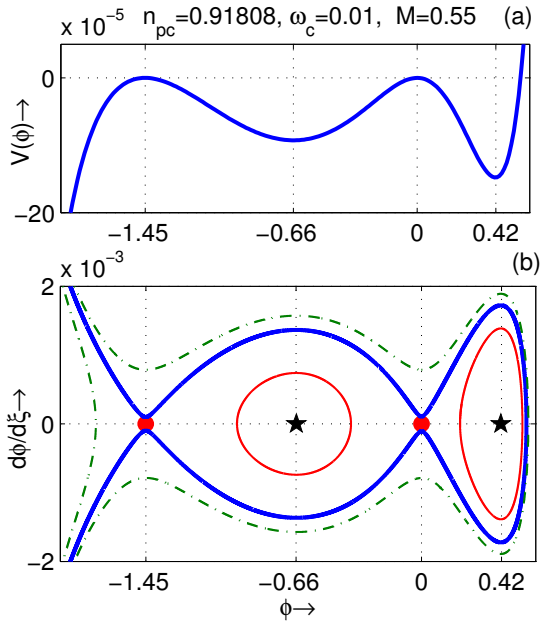

Figure 3.5: Drawings of $V(\phi)$ and the phase portrait of (3.3.7) are shown w.r.t. ϕ for $M = 0.55$, $\sigma = 0.001$, $\gamma = 5/3$, $n_{sc} = 0.05$, $n_{dc} = 0.1$, $n_{pc} = 0.91808$, $\sigma_{pc} = 0.09$, $\sigma_{sc} = 0.001$, $\beta_p = 0.1$, $\beta_e = 0.25$, $\omega_c = 0.01$ and $l_z = 0.5$.

blue separatrix seems to go through the points $(0, 0)$ and $(-0.45444, 0)$. The sky blue separatrix is enclosed by the blue separatrix. The sky blue separatrix seems to go through $(0.249, 0)$ and two stable fixed points $(0.19063, 0)$ and $(0.41058, 0)$ are enclosed by this separatrix, whereas blue separatrix encloses a stable fixed point $(-0.2025, 0)$ in the negative direction. Figure 3.7(a) establishes that $V(\phi)$ vs. ϕ corresponds to the separatrix of the figure 3.7(b).

Figure 3.8(b) represents the phase portrait of(3.3.7) corresponding to a PPSS. The blue curve and sky blue curve establish that there are two separatrices. The blue separatrix seems to go through the point $(0, 0)$. The sky blue separatrix is enclosed by the blue separatrix. The sky blue separatrix seems to go through the point $(0.25328, 0)$ and it contains two stable fixed points $(0.18431, 0)$ and $(0.41471, 0)$. Figure 3.8(a) establishes that $V(\phi)$ vs. ϕ corresponds to the separatrix of the figure 3.8(b).

In figure 3.9, profile of supersoliton has been shown for $M = 0.63$, $\sigma = 0.001$,

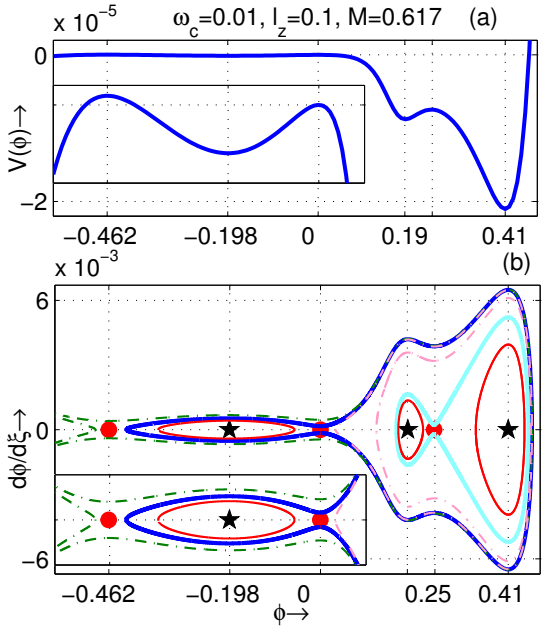

Figure 3.6: Drawings of $V(\phi)$ and the phase portrait of (3.3.7) are shown w.r.t. ϕ for $M = 0.617$, $\sigma = 0.001$, $\gamma = 5/3$, $n_{sc} = 0.04$, $n_{dc} = 0.001$, $n_{pc} = 0.2$, $\sigma_{pc} = 0.15$, $\sigma_{sc} = 0.01$, $\beta_p = 0.1$, $\beta_e = 0.25$, $\omega_c = 0.01$ and $l_z = 0.5$.

$\gamma = 5/3$, $n_{sc} = 0.04$, $n_{dc} = 0.001$, $n_{pc} = 0.2$, $\sigma_{pc} = 0.15$, $\sigma_{sc} = 0.01$, $\beta_p = 0.1$, $\beta_e = 0.25$, $\omega_c = 0.01$ and $l_z = 0.5$. This figure shows a dais-type soliton and this type of soliton has been reported by Das *et al.* [91].

Figure 3.10(b) represents the phase portrait of (3.3.7) corresponding to a PPSS. The blue curve and sky blue curve establish that there are two separatrices. The blue separatrix seems to go through $(0, 0)$. The sky blue separatrix is enclosed by the blue separatrix. The sky blue separatrix seems to go through the point $(0.201, 0)$, and it contains two stable fixed points $(0.158, 0)$ and $(0.332, 0)$. Figure 3.10(a) establishes that $V(\phi)$ vs. ϕ corresponds to the separatrix of the figure 3.10(b).

Figure 3.11(b) represents the phase portrait of (3.3.7) corresponding to the simultaneous existence of NPSW and PPSS. The blue curve and sky blue curve demonstrate that there are two separatrices. The blue separatrix seems to begin and end at $(0, 0)$. The sky blue separatrix is enclosed by the blue separatrix. The

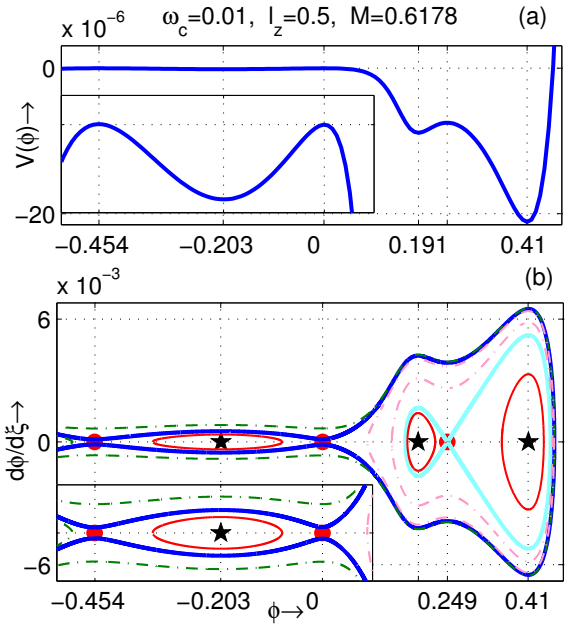

Figure 3.7: Drawings of $V(\phi)$ and the phase portrait of (3.3.7) are shown w.r.t. ϕ for $M = 0.6178$, $\sigma = 0.001$, $\gamma = 5/3$, $n_{sc} = 0.04$, $n_{dc} = 0.001$, $n_{pc} = 0.2$, $\sigma_{pc} = 0.15$, $\sigma_{sc} = 0.01$, $\beta_p = 0.1$, $\beta_e = 0.25$, $\omega_c = 0.01$ and $l_z = 0.5$.

sky blue separatrix seems to go through $(0.213, 0)$, and two stable fixed points $(0.14, 0)$ and $(0.35, 0)$ are enclosed by this separatrix, whereas blue separatrix encloses a stable fixed point $(-0.07, 0)$ in the negative direction. Figure 3.11(a) establishes that $V(\phi)$ vs. ϕ corresponds to the separatrix of the figure 3.11(b).

Figure 3.12(b) represents the phase portrait of (3.3.7) corresponding to the supernonlinear periodic wave. We have seen there is a single separatrix which seems to begin and end at $(0.128, 0)$ and two stable equilibrium points $(0, 0)$ and $(0.26, 0)$ are enclosed by the separatrix. Every closed curve (red curve) corresponds to the nonlinear periodic wave. A sequence of sky-blue closed curves surround the blue separatrix, and these closed curves are due to super-nonlinear periodic waves. Figure 3.12(a) establishes that $V(\phi)$ vs. ϕ corresponds to the separatrix of the figure 3.12(b).

Figure 3.13(b) represents the phase portrait of (3.3.7) corresponding to the supernonlinear periodic wave. We have seen that one separatrix (blue colour)

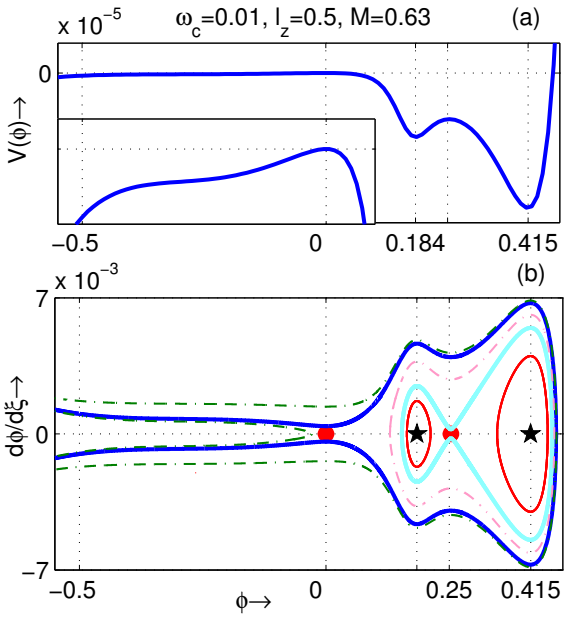

Figure 3.8: Drawings of $V(\phi)$ and the phase portrait of (3.3.7) are shown w.r.t. ϕ for $M = 0.63$, $\sigma = 0.001$, $\gamma = 5/3$, $n_{sc} = 0.04$, $n_{dc} = 0.001$, $n_{pc} = 0.2$, $\sigma_{pc} = 0.15$, $\sigma_{sc} = 0.01$, $\beta_p = 0.1$, $\beta_e = 0.25$, $\omega_c = 0.01$ and $l_z = 0.5$.

seems to begin and end at $(0.11908, 0)$ and another separatrix (magenta colour) seems to begin and end at $(0.062829, 0)$. Blue separatrix encloses two stable fixed points $(0.10192, 0)$ and $(0.1723, 0)$. The magenta colour separatrix encloses one stable fixed point $(0, 0)$ and envelopes the separatrix of blue colour. A sequence of closed sky-blue closed curves surrounding the blue separatrix that are due to super-nonlinear periodic waves. Figure 3.13(a) establishes that $V(\phi)$ vs. ϕ corresponds to the separatrix of the figure 3.13(b).

3.5 Results and Discussions

The amplitude variation of NPSWs has been displayed in figure 3.14 by taking the variation of (a) n_{pc}, (b) n_{sc}, (c) β_p, (d) β_e, (e) σ_{sc}, (f) σ_{pc}, (g) ω_c and (h) l_z, and fixed values of $\sigma(= 0.001)$, $\gamma(= 5/3)$, $n_{dc}(= 0.01)$ and $M(= 0.52)$. Figure 3.14(a) represents the variation of the amplitude of NPSW for various n_{pc} (for

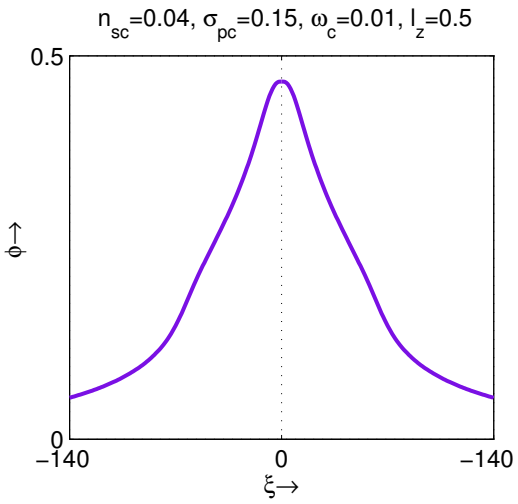

Figure 3.9: ϕ vs. ξ for $\sigma = 0.001$, $\gamma = 5/3$, $n_{sc} = 0.04$, $n_{dc} = 0.001$, $n_{pc} = 0.2$, $\sigma_{pc} = 0.15$, $\sigma_{sc} = 0.01$, $\beta_p = 0.1$, $\beta_e = 0.25$, $\omega_c = 0.01$ and $l_z = 0.5$. The purple curve corresponds to $M = 0.63$.

black curve $n_{pc} = 0.04$, for red curve $n_{pc} = 0.08$ and blue curve $n_{pc} = 0.09535$). Figure 3.14(a) states that the amplitude of NPSW grows with growing n_{pc} for $0 < n_{pc} < 0.09535$ for (n_{sc}, σ_{pc}, σ_{sc}, β_p, β_e, ω_c, l_z)=(0.5, 0.9, 0.07, 0.1, 0.25, 0.01, 0.5) and the system supports NPDL at $n_{pc} = 0.09535$ when (n_{sc}, σ_{pc}, σ_{sc}, β_p, β_e, ω_c, l_z)=(0.5, 0.9, 0.07, 0.1, 0.25, 0.01, 0.5).

Figure 3.14(b) represent the variation of the amplitude of NPSW for various n_{sc} (for black curve $n_{sc} = 0.45$, for red curve $n_{sc} = 0.5$ and for blue curve $n_{sc} = 0.5188$). Figure 3.14(b) states that the amplitude of NPSW grows with growing n_{sc} for $0.25 < n_{sc} < 0.5188$ for (n_{pc}, σ_{pc}, σ_{sc}, β_p, β_e, ω_c, l_z)=(0.09, 0.9, 0.07, 0.1, 0.25, 0.01, 0.5) and the system supports NPDL at $n_{sc} = 0.5188$ when (n_{pc}, σ_{pc}, σ_{sc}, β_p, β_e, ω_c, l_z)=(0.09, 0.9, 0.07, 0.1, 0.25, 0.01, 0.5).

Figure 3.14(c) represents the variation of the amplitude of NPSW for various β_p (for black curve $\beta_p = 0$, for red curve $\beta_p = 0.1$ and for blue curve $\beta_p = 0.5$). Figure 3.14(c) states that the amplitude of NPSW diminishes with growing β_p

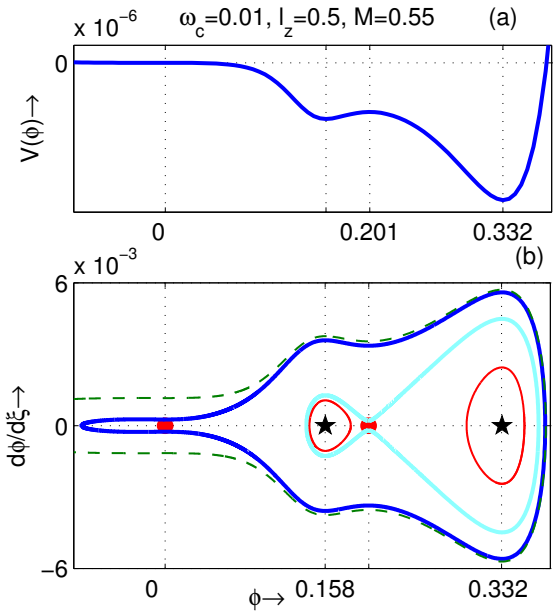

Figure 3.10: Drawings of $V(\phi)$ and the phase portrait of (3.3.7) are shown w.r.t. ϕ for $M = 0.55$, $\sigma = 0.001$, $\gamma = 5/3$, $n_{sc} = 0.05$, $n_{dc} = 0.005$, $n_{pc} = 0.05$, $\sigma_{pc} = 0.2$, $\sigma_{sc} = 0.01$, $\beta_p = 0.1$, $\beta_e = 0.25$, $\omega_c = 0.01$ and $l_z = 0.5$.

for $0 < \beta_p < 0.57$ for (n_{sc}, n_{pc}, σ_{pc}, σ_{sc}, β_e, ω_c, l_z)=(0.5, 0.09, 0.9, 0.07, 0.25, 0.01, 0.5), but the NPDL does not exist for any value of β_p when (n_{sc}, n_{pc}, σ_{pc}, σ_{sc}, β_e, ω_c, l_z)=(0.5, 0.09, 0.9, 0.07, 0.25, 0.01, 0.5).

Figure 3.14(d) represents the variation of the amplitude of NPSW for various β_e (for black curve $\beta_e = 0.23764$, for red curve $\beta_e = 0.3$ and for blue curve $\beta_e = 0.5$). Figure 3.14(d) states that the amplitude of NPSW diminishes with growing β_e for $0.23764 < \beta_e < 0.57$ for (n_{sc}, n_{pc}, σ_{pc}, σ_{sc}, β_p, ω_c, l_z)=(0.5, 0.09, 0.9, 0.07, 0.1, 0.01, 0.5) and the system supports NPDL at $\beta_e = 0.23764$ when (n_{sc}, n_{pc}, σ_{pc}, σ_{sc}, β_p, ω_c, l_z)=(0.5, 0.09, 0.9, 0.07, 0.1, 0.01, 0.5).

Figure 3.14(e) represents the variation of the amplitude of NPSW for various σ_{sc} (for black curve $\sigma_{sc} = 0.04$, for red curve $\sigma_{sc} = 0.06$ and for blue curve $\sigma_{sc} = 0.07158$). Figure 3.14(e) states that the amplitude of NPSW grows with growing σ_{sc} for $0 < \sigma_{sc} < 0.07158$ for (n_{sc}, n_{pc}, σ_{pc}, β_p, β_e, ω_c, l_z)=(0.5, 0.09, 0.9, 0.1, 0.25, 0.01, 0.5) and the system supports NPDL at $\sigma_{sc} = 0.07158$ when (n_{sc},

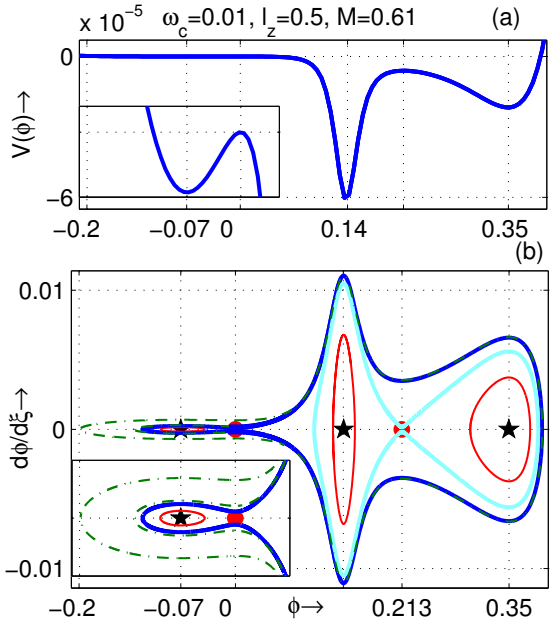

Figure 3.11: Drawings of $V(\phi)$ and the phase portrait of (3.3.7) are shown w.r.t. ϕ for $M = 0.61$, $\sigma = 0.001$, $\gamma = 5/3$, $n_{sc} = 0.05$, $n_{dc} = 0.005$, $n_{pc} = 0.05$, $\sigma_{pc} = 0.2$, $\sigma_{sc} = 0.01$, $\beta_p = 0.1$, $\beta_e = 0.25$, $\omega_c = 0.01$ and $l_z = 0.5$.

n_{pc}, σ_{pc}, β_p, β_e, ω_c, l_z)=(0.5, 0.09, 0.9, 0.1, 0.25, 0.01, 0.5).

Figure 3.14(f) represents the variation of the amplitude of NPSW for various σ_{pc} (for black curve $\sigma_{pc} = 0.8305$, for red curve $\sigma_{pc} = 0.85$ and for blue curve $\sigma_{pc} = 0.95$). Figure 3.14(f) states that the amplitude of NPSW diminishes with growing σ_{pc} for $0.8305 < \sigma_{pc} < 0.99$ for (n_{sc}, n_{pc}, σ_{sc}, β_p, β_e, ω_c, l_z)=(0.5, 0.09, 0.07, 0.1, 0.25, 0.01, 0.5) and the system supports NPDL at $\sigma_{pc} = 0.8305$ when (n_{sc}, n_{pc}, σ_{sc}, β_p, β_e, ω_c, l_z)=(0.5, 0.09, 0.07, 0.1, 0.25, 0.01, 0.5).

Figure 3.14(g) represents the variation of the amplitude of NPSW for various ω_c (for black curve $\omega_c = 0.01$, for red curve $\omega_c = 0.011$ and for blue curve $\omega_c = 0.012$). Figure 3.14(g) states that ω_c has no influence on the amplitude of NPSW for (n_{sc}, n_{pc}, σ_{pc}, σ_{sc}, β_p, β_e, l_z)=(0.5, 0.09, 0.9, 0.07, 0.1, 0.25, 0.5).

Figure 3.14(h) represents the variation of the amplitude of NPSW for various l_z (for black curve $l_z = 0.4966$, for red curve $l_z = 0.5$ and for blue curve $l_z = 0.51$). Figure 3.14(h) states that the amplitude of NPSW diminishes with growing l_z for

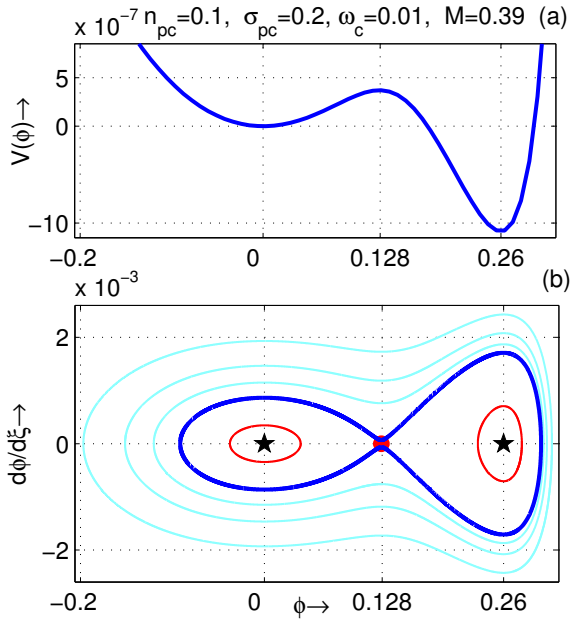

Figure 3.12: Drawings of $V(\phi)$ and the phase portrait of (3.3.7) are shown w.r.t. ϕ for $M = 0.39$, $\sigma = 0.001$, $\gamma = 5/3$, $n_{sc} = 0.05$, $n_{dc} = 0.01$, $n_{pc} = 0.1$, $\sigma_{pc} = 0.2$, $\sigma_{sc} = 0.01$, $\beta_p = 0.1$, $\beta_e = 0.25$, $\omega_c = 0.01$ and $l_z = 0.5$.

$0.4966 < l_z < 0.511$ for (n_{sc}, n_{pc}, σ_{pc}, σ_{sc}, β_p, β_e, ω_c)=(0.5, 0.09, 0.9, 0.07, 0.1, 0.25, 0.01) and the system supports NPDL at $l_z = 0.4966$ when (n_{sc}, n_{pc}, σ_{pc}, σ_{sc}, β_p, β_e, ω_c)=(0.5, 0.09, 0.9, 0.07, 0.1, 0.25, 0.01).

The amplitude variation of the coexistence of NPSWs and PPSWs has been displayed in figure 3.15 by taking the variation of (a) n_{pc}, (b) n_{sc}, (c) β_p, (d) β_e, (e) σ_{sc}, (f) σ_{pc}, (g) ω_c and (h) l_z, and $\sigma(= 0.001)$, $\gamma(= 5/3)$, $n_{dc}(= 0.1)$ and $M(= 0.55)$. Figure 3.15(a) represents the variation of the amplitude of the coexistence of NPSW and PPSW for various n_{pc} (for black curve $n_{pc} = 0.88$, for red curve $n_{pc} = 0.9$ and for blue curve $n_{pc} = 0.91808$). Figure 3.15(a) states that the amplitude of NPSW grows with growing n_{pc}, whereas the amplitude of PPSW diminishes with growing n_{pc} for $0.7 < n_{pc} < 0.91808$ for (n_{sc}, σ_{pc}, σ_{sc}, β_p, β_e, ω_c, l_z)=(0.05, 0.09, 0.001, 0.1, 0.25, 0.01, 0.5) and the system supports NPDL at $n_{pc} = 0.91808$ when (n_{sc}, σ_{pc}, σ_{sc}, β_p, β_e, ω_c, l_z)=(0.05, 0.09, 0.001, 0.1, 0.25, 0.01, 0.5).

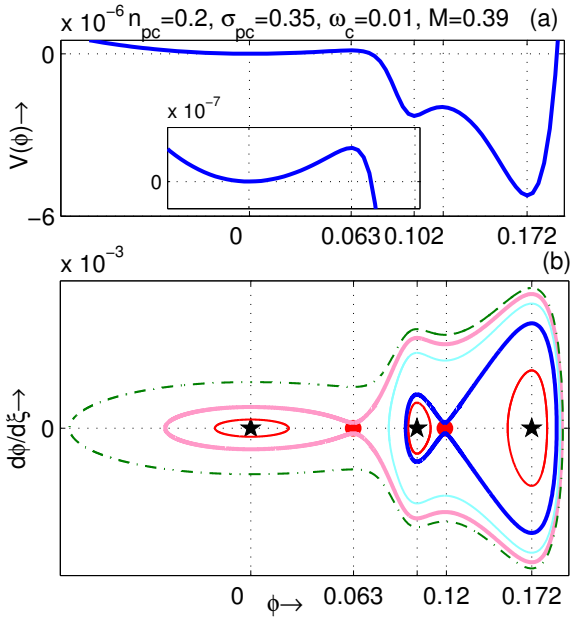

Figure 3.13: Drawings of $V(\phi)$ and the phase portrait of (3.3.7) are shown w.r.t. ϕ for $M = 0.39$, $\sigma = 0.001$, $\gamma = 5/3$, $n_{sc} = 0.01$, $n_{dc} = 0.01$, $n_{pc} = 0.2$, $\sigma_{pc} = 0.35$, $\sigma_{sc} = 0.007$, $\beta_p = 0.1$, $\beta_e = 0.25$, $\omega_c = 0.01$ and $l_z = 0.5$.

Figure 3.15(b) represents the variation of the amplitude of the coexistence of NPSW and PPSW for various n_{sc} (for black curve $n_{sc} = 0.04$, for red curve $n_{sc} = 0.07$ and for blue curve $n_{sc} = 0.08299$). Figure 3.15(b) states that the amplitude of NPSW grows with growing n_{sc}, whereas the amplitude of PPSW diminishes with growing n_{sc} for $0.0251 < n_{sc} < 0.08299$ for (n_{pc}, σ_{pc}, σ_{sc}, β_p, β_e, ω_c, l_z)=(0.9, 0.09, 0.001, 0.1, 0.25, 0.01, 0.5) and the system supports NPDL at $n_{sc} = 0.08299$ when (n_{pc}, σ_{pc}, σ_{sc}, β_p, β_e, ω_c, l_z)=(0.9, 0.09, 0.001, 0.1, 0.25, 0.01, 0.5).

Figure 3.15(c) represents the variation of the amplitude of the coexistence of NPSW and PPSW for various β_p (for black curve $\beta_p = 0$, for red curve $\beta_p = 0.1$ and for blue curve $\beta_p = 0.4$). Figure 3.15(c) states that both the amplitude of NPSW and PPSW diminishes with growing β_p for $0 < \beta_p < 0.57$ for (n_{sc}, n_{pc}, σ_{pc}, σ_{sc}, β_e, ω_c, l_z)=(0.05, 0.9, 0.09, 0.001, 0.25, 0.01, 0.5) and the system supports NPDL at $\beta_p = 0$ when (n_{sc}, n_{pc}, σ_{pc}, σ_{sc}, β_e, ω_c, l_z)=(0.05, 0.9, 0.09, 0.001, 0.25,

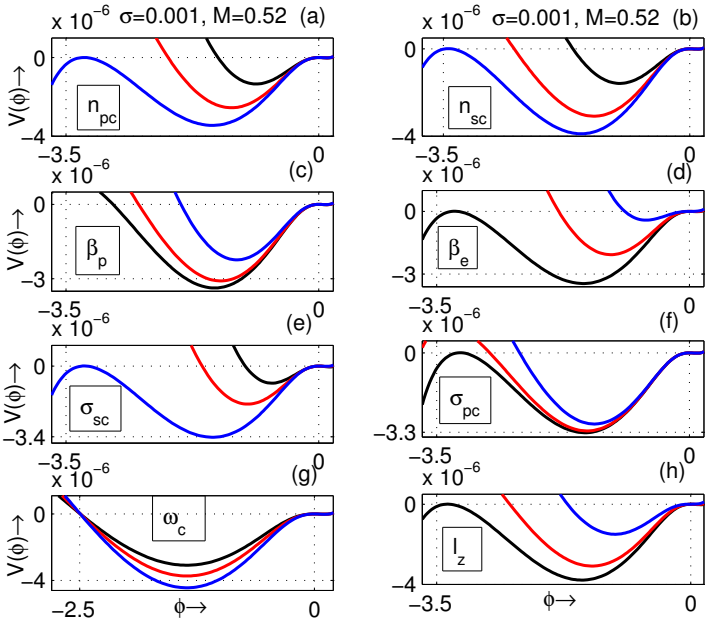

Figure 3.14: $V(\phi)$ vs. ϕ in (a) for various n_{pc}, (b) for various n_{sc}, (c) for various β_p, (d) for various β_e, (e) for various σ_{sc}, (f) for various σ_{pc}, (g) for various ω_c and (h) for various l_z with fixed values of σ, γ, n_{dc} and M.

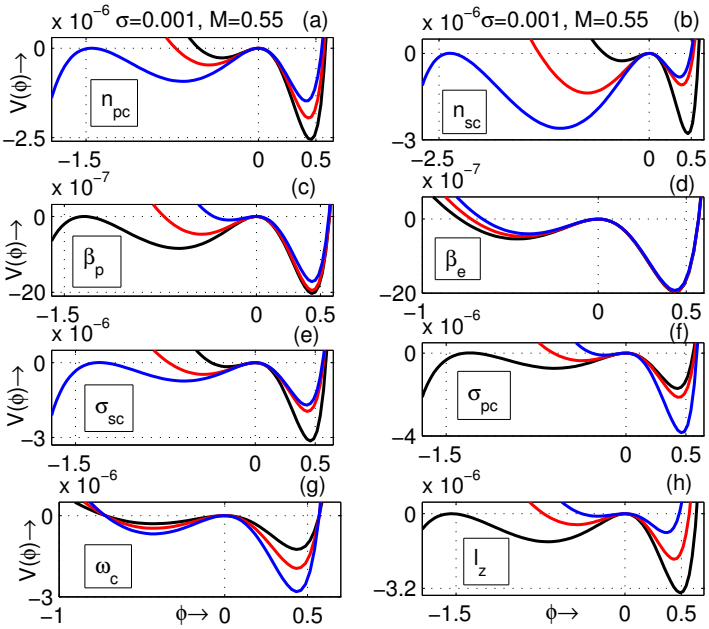

Figure 3.15: $V(\phi)$ vs. ϕ in (a) for various n_{pc}, (b) for various n_{sc}, (c) for various β_p, (d) for various β_e, (e) for various σ_{sc}, (f) for various σ_{pc}, (g) for various ω_c and (h) for various l_z with fixed values of γ, σ, n_{dc} and M.

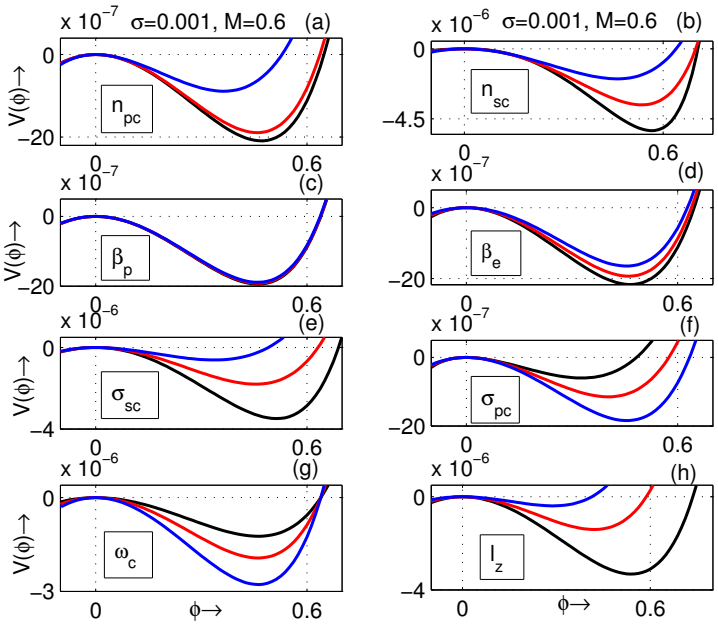

Figure 3.16: $V(\phi)$ vs. ϕ in (a) for various n_{pc}, (b) for various n_{sc}, (c) for various β_p, (d) for various β_e, (e) for various σ_{sc}, (f) for various σ_{pc}, (g) for various ω_c and (h) for various l_z with fixed values of γ, σ, n_{dc} and M.

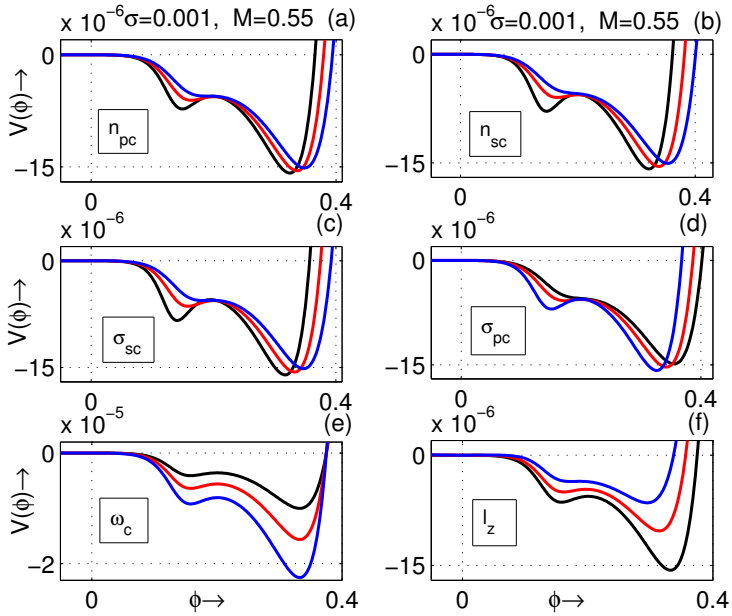

Figure 3.17: $V(\phi)$ vs. ϕ in (a) for various n_{pc}, (b) for various n_{sc}, (c) for various σ_{sc}, (d) for various σ_{pc}, (e) for various ω_c and (f) for various l_z with fixed values of γ, σ, n_{dc} and M.

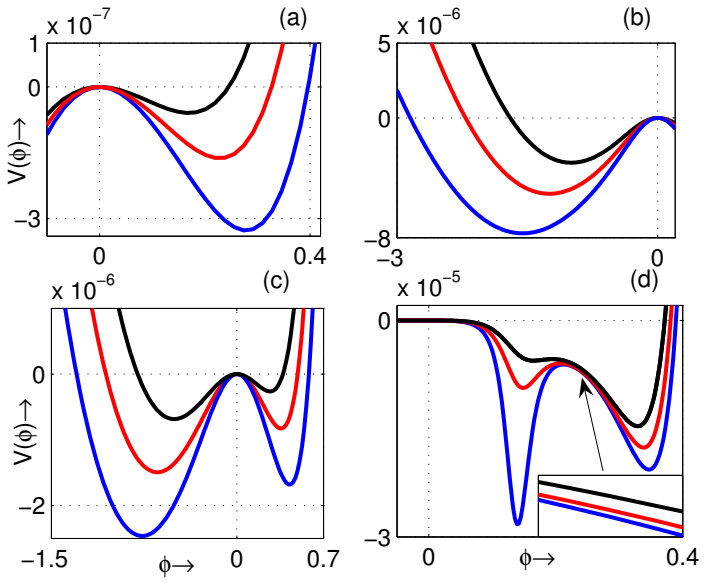

Figure 3.18: $V(\phi)$ vs. ϕ curve for different values of M with fixed values of γ, σ, β_e β_p, ω_c and l_z, when other values of parameters (n_{sc}, n_{pc}, n_{dc}, σ_{pc} and σ_{sc}) are varied.

0.01, 0.5).

Figure 3.15(d) represents the variation of the amplitude of the coexistence of NPSW and PPSW for various β_e (for black curve $\beta_e = 0$, for red curve $\beta_e = 0.25$ and for blue curve $\beta_e = 0.55$). Figure 3.15(d) states that the amplitude of both NPSW and PPSW diminishes with growing β_e for $0 < \beta_e < 0.57$ for (n_{sc}, n_{pc}, σ_{pc}, σ_{sc}, β_p, ω_c, l_z)=(0.05, 0.9, 0.09, 0.001, 0.1, 0.01, 0.5). Although the rate of diminishing of the amplitude of the PPSW is not clearly visible from this figure 3.15(d) and the NPDL does not exist for any values of β_e when (n_{sc}, n_{pc}, σ_{pc}, σ_{sc}, β_p, ω_c, l_z)=(0.05, 0.9, 0.09, 0.001, 0.1, 0.01, 0.5).

Figure 3.15(e) represents the variation of the amplitude of the coexistence of NPSW and PPSW for various σ_{sc} (for black curve $\sigma_{sc} = 0.0005$, for red curve $\sigma_{sc} = 0.001$ and for blue curve $\sigma_{sc} = 0.001132$). Figure 3.15(e) states that the amplitude of NPSW grows with growing σ_{sc}, whereas the amplitude of PPSW diminishes with growing σ_{sc} for $0.00001 < \sigma_{sc} < 0.001132$ for (n_{sc}, n_{pc}, σ_{pc}, β_p,

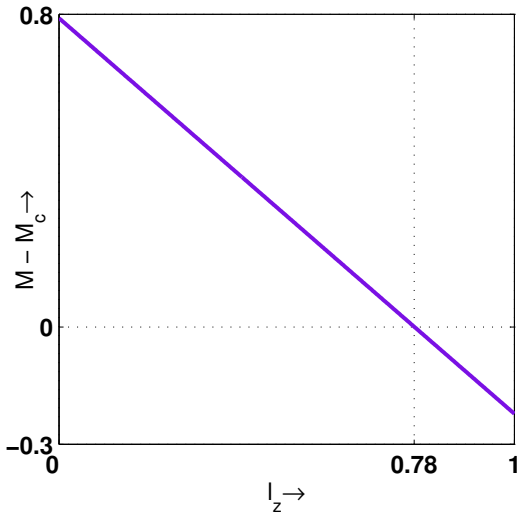

Figure 3.19: $M - M_c$ vs. l_z for $\sigma = 0.001$, $\gamma = 5/3$, $n_{sc} = 0.05$, $n_{dc} = 0.1$, $n_{pc} = 0.09$, $\sigma_{pc} = 0.09$, $\sigma_{sc} = 0.001$, $\beta_p = 0.1$, $\beta_e = 0.25$, and $M = 0.79$.

β_e, ω_c, l_z)=(0.05, 0.9, 0.09, 0.1, 0.25, 0.01, 0.5) and the system supports NPDL at $\sigma_{sc} = 0.001132$ when (n_{sc}, n_{pc}, σ_{pc}, β_p, β_e, ω_c, l_z)=(0.05, 0.9, 0.09, 0.1, 0.25, 0.01, 0.5).

Figure 3.15(f) represents the variation of the amplitude of the coexistence of NPSW and PPSW for various σ_{pc} (for black curve $\sigma_{pc} = 0.07885$, for red curve $\sigma_{pc} = 0.1$ and for blue curve $\sigma_{pc} = 0.5$). Figure 3.15(f) states that the amplitude of NPSW diminishes with growing σ_{pc}, whereas the amplitude of PPSW grows with growing σ_{pc} for $0.07885 < \sigma_{pc} < 0.99$ for (n_{sc}, n_{pc}, σ_{sc}, β_p, β_e, ω_c, l_z)=(0.05, 0.9, 0.001, 0.1, 0.25, 0.01, 0.5) and the system supports NPDL at $\sigma_{pc} = 0.07885$ when (n_{sc}, n_{pc}, σ_{sc}, β_p, β_e, ω_c, l_z)=(0.05, 0.9, 0.001, 0.1, 0.25, 0.01, 0.5).

Figure 3.15(g) represents the variation of the amplitude of the coexistence of NPSW and PPSW for various ω_c (for black curve $\omega_c = 0.008$, for red curve $\omega_c = 0.01$ and for blue curve $\omega_c = 0.012$). Figure 3.15(g) states that ω_c has no influence on the amplitude of the coexistence of NPSWs and PPSWs for (n_{sc},

n_{pc}, σ_{pc}, σ_{sc}, β_p, β_e, l_z)=(0.05, 0.9, 0.09, 0.001, 0.1, 0.25, 0.5).

Figure 3.15(h) represents the variation of the amplitude of the coexistence of NPSW and PPSW for various l_z (for black curve $l_z = 0.48185$, for red curve $l_z = 0.5$ and for blue curve $l_z = 0.52$). Figure 3.15(h) states that both the amplitude of NPSW and PPSW diminishes with growing l_z for $0.48185 < l_z < 0.543$ for (n_{sc}, n_{pc}, σ_{pc}, σ_{sc}, β_p, β_e, ω_c)=(0.05, 0.9, 0.09, 0.001, 0.1, 0.25, 0.01) and the system supports NPDL at $l_z = 0.48185$ when (n_{sc}, n_{pc}, σ_{pc}, σ_{sc}, β_p, β_e, ω_c)=(0.05, 0.9, 0.09, 0.001, 0.1, 0.25, 0.01).

The amplitude variation of PPSWs has been displayed in figure 3.16 by taking the variation of (a) n_{pc}, (b) n_{sc}, (c) β_p, (d) β_e, (e) σ_{sc}, (f) σ_{pc}, (g) ω_c and (h) l_z, and fixed values of $\sigma(= 0.001)$, $\gamma(= 5/3)$, $n_{dc}(= 0.005)$ and $M(= 0.6)$. Figure 3.16(a) represents the variation of the amplitude of PPSW for various n_{pc} (for black curve $n_{pc} = 0.05$, for red curve $n_{pc} = 0.1$ and for blue curve $n_{pc} = 0.5$). Figure 3.16(a) states that the amplitude of PPSW diminishes with growing n_{pc} for $0.0001 < n_{pc} < 0.99$ for (n_{sc}, σ_{pc}, σ_{sc}, β_p, β_e, ω_c, l_z)=(0.5, 0.9, 0.09, 0.1, 0.25, 0.01, 0.5).

Figure 3.16(b) represents the variation of the amplitude of PPSW for various n_{sc} (for black curve $n_{sc} = 0.1$, for red curve $n_{sc} = 0.2$ and for blue curve $n_{sc} = 0.5$). Figure 3.16(b) states that the amplitude of PPSW diminishes with growing n_{sc} for $0.01 < n_{sc} < 0.99$ for (n_{pc}, σ_{pc}, σ_{sc}, β_p, β_e, ω_c, l_z)=(0.09, 0.9, 0.09, 0.1, 0.25, 0.01, 0.5).

Figure 3.16(c) represents the variation of the amplitude of PPSW for various β_p (for black curve $\beta_p = 0$, for red curve $\beta_p = 0.25$ and for blue curve $\beta_p = 0.55$). Figure 3.16(c) states that the amplitude of PPSW slightly diminishes with growing β_p for $0 < \beta_p < 0.57$ for (n_{sc}, n_{pc}, σ_{pc}, σ_{sc}, β_e, ω_c, l_z)=(0.5, 0.09, 0.9, 0.09, 0.25, 0.01, 0.5).

Figure 3.16(d) represents the variation of the amplitude of PPSW for various β_e (for black curve $\beta_e = 0$, for red curve $\beta_e = 0.25$ and for blue curve $\beta_e = 0.55$).

Figure 3.16(d) states that the amplitude of PPSW diminishes with growing β_e for $0 < \beta_e < 0.57$ for (n_{sc}, n_{pc}, σ_{pc}, σ_{sc}, β_p, ω_c, l_z)=(0.5, 0.09, 0.9, 0.09, 0.1, 0.01, 0.5).

Figure 3.16(e) represents the variation of the amplitude of PPSW for various σ_{sc} (for black curve $\sigma_{sc} = 0.01$, for red curve $\sigma_{sc} = 0.1$ and for blue curve $\sigma_{sc} = 0.3$). Figure 3.16(e) states that the amplitude of PPSW diminishes with growing σ_{sc} for $0.0001 < \sigma_{sc} < 0.99$ for (n_{sc}, n_{pc}, σ_{pc}, β_p, β_e, ω_c, l_z)=(0.5, 0.09, 0.9, 0.1, 0.25, 0.01, 0.5).

Figure 3.16(f) represents the variation of the amplitude of PPSW for various σ_{pc} (for black curve $\sigma_{pc} = 0.05$, for red curve $\sigma_{pc} = 0.1$ and for blue curve $\sigma_{pc} = 0.5$). Figure 3.16(f) states that the amplitude of PPSW grows with growing σ_{pc} for $0.001 < \sigma_{pc} < 0.99$ for (n_{sc}, n_{pc}, σ_{sc}, β_p, β_e, ω_c, l_z)=(0.5, 0.09, 0.09, 0.1, 0.25, 0.01, 0.5).

Figure 3.16(g) represents the variation of the amplitude of PPSW for various ω_c (for black curve $\omega_c = 0.008$, for red curve $\omega_c = 0.01$ and for blue curve $\omega_c = 0.012$). Figure3.16 (g) states that ω_c has no influence on the amplitude of PPSW for (n_{sc}, n_{pc}, σ_{pc}, σ_{sc}, β_p, β_e, l_z)=(0.5, 0.09, 0.9, 0.09, 0.1, 0.25, 0.5).

Figure 3.16(h) represents the variation of the amplitude of PPSW for various l_z (for black curve $l_z = 0.48$, for red curve $l_z = 0.51$ and for blue curve $l_z = 0.54$). Figure 3.16(h) states that the amplitude of PPSW diminishes with growing l_z for $0.4195 < l_z < 0.585$ for (n_{sc}, n_{pc}, σ_{pc}, σ_{sc}, β_p, β_e, ω_c)=(0.5, 0.09, 0.9, 0.09, 0.1, 0.25, 0.01).

The amplitude variation of PPSSs has been displayed in figure 3.17 by taking the variation of (a) n_{pc}, (b) n_{sc}, (c) σ_{sc}, (d) σ_{pc}, (e) ω_c and (f) l_z, and fixed values of $\sigma(= 0.001)$, $\gamma(= 5/3)$, $n_{dc}(= 0.005)$ and $M(= 0.55)$. Figure 3.17(a) represents the variation of the amplitude of PPSS for various n_{pc} (for black curve $n_{pc} = 0.03$, for red curve $n_{pc} = 0.06$ and for blue curve $n_{pc} = 0.09$). Figure 3.17(a) states that the amplitude of PPSS grows with growing n_{pc} in the region of formation of

PPSS for (n_{sc}, σ_{pc}, σ_{sc}, β_p, β_e, ω_c, l_z)=(0.05, 0.2, 0.01, 0.1, 0.25, 0.01, 0.5).

Figure 3.17(b) represents the variation of the amplitude of PPSS for various n_{sc} (for black curve n_{sc} = 0.046, for red curve n_{sc} = 0.052 and for blue curve n_{sc} = 0.058). Figure 3.17(b) states that the amplitude of PPSS grows with growing n_{sc} in the region of formation of PPSS for (n_{pc}, σ_{pc}, σ_{sc}, β_p, β_e, ω_c, l_z)=(0.05, 0.2, 0.01, 0.1, 0.25, 0.01, 0.5).

Figure 3.17(c) represents the variation of the amplitude of PPSS for various σ_{sc} (for black curve σ_{sc} = 0.007, for red curve σ_{sc} = 0.01 and for blue curve σ_{sc} = 0.013). Figure 3.17(c) states that the amplitude of PPSS grows with growing σ_{sc} in the region of formation of PPSS for (n_{pc}, n_{sc}, σ_{pc}, β_p, β_e, ω_c, l_z)=(0.05, 0.05, 0.2, 0.1, 0.25, 0.01, 0.5).

Figure 3.17(d) represents the variation of the amplitude of PPSS for various σ_{pc} (for black curve σ_{pc} = 0.06, for red curve σ_{pc} = 0.1 and for blue curve σ_{pc} = 0.5). Figure 3.17(d) states that the amplitude of PPSS diminishes with growing σ_{pc} in the region of formation of PPSS for (n_{pc}, n_{sc}, σ_{sc}, β_p, β_e, ω_c, l_z)=(0.05, 0.05, 0.01, 0.1, 0.25, 0.01, 0.5).

Figure 3.17(e) represents the variation of the amplitude of PPSS for various ω_c (for black curve ω_c = 0.008, for red curve ω_c = 0.01 and for blue curve ω_c = 0.012). Figure 3.17(e) states that ω_c has no influence on the amplitude of PPSS for (n_{pc}, n_{sc}, σ_{pc}, σ_{sc}, β_p, β_e, l_z)=(0.05, 0.05, 0.2, 0.01, 0.1, 0.25, 0.5).

Figure 3.17(f) represents the variation of the amplitude of PPSS for various l_z (for black curve l_z = 0.5, for red curve l_z = 0.55 and for blue curve l_z = 0.6). Figure 3.17(f) states that the amplitude of PPSS diminishes with growing l_z in the region of formation of PPSS for (n_{pc}, n_{sc}, σ_{pc}, σ_{sc}, β_p, β_e, ω_c)=(0.05, 0.05, 0.2, 0.01, 0.1, 0.25, 0.01).

The amplitude variation of different types of soliton has been displayed in 3.18 by taking the variation of M when some parameters (n_{sc}, n_{dc}, n_{pc}, σ_{pc} and σ_{sc}) are varied, and other parameters (σ = 0.001, γ = 5/3, β_p = 0.1, β_e = 0.25, ω_c = 0.01,

$l_z = 0.5$) are fixed. Figure 3.18(a) represents PPSWs for various M (for black curve $M = 0.53$, for red curve $M = 0.54$ and for blue curve $M = 0.55$) and (n_{sc}, n_{dc}, n_{pc}, σ_{pc}, σ_{sc})=(0.5, 0.01, 0.1, 0.5, 0.07). Figure 3.18(a) states that the amplitude of PPSWs grows with growing M. Figure 3.18(b) represents NPSWs for various M (for black curve $M = 0.55$, for red curve $M = 0.57$ and for blue curve $M = 0.59$) and (n_{sc}, n_{dc}, n_{pc}, σ_{pc}, σ_{sc})=(0.5, 0.01, 0.05, 0.9, 0.05). Figure 3.18(b) states that the amplitude of NPSWs grows with growing M. Figure 3.18(c) represents the coexistence of PPSW and NPSW for various M (for black curve $M = 0.53$, for red curve $M = 0.55$ and for blue curve $M = 0.57$) and (n_{sc}, n_{dc}, n_{pc}, σ_{pc}, σ_{sc})=(0.5, 0.01, 0.1, 0.5, 0.01). Figure 3.18(c) states that the amplitude of the coexistence of PPSW and NPSW grows with growing M. Figure 3.18(d) represents PPSSs for various M (for black curve $M = 0.54$, for red curve $M = 0.57$ and for blue curve $M = 0.6$) and (n_{sc}, n_{dc}, n_{pc}, σ_{pc}, σ_{sc})=(0.05, 0.005, 0.05, 0.2, 0.01). Figure 3.18(d) states that the amplitude of PPSSs grows with growing M.

3.6 Conclusions

In this present **chapter** various types of DIA solitary waves have been discussed in a magnetized collisionless plasma consisting of negatively charged immobile dust particulates, non-isothermal positrons obeying Cairns distribution [1], isothermal electrons obeying Maxwellian distribution, non-isothermal electrons obeying Cairns distribution [1] and warm adiabatic ions. Based on the Sagdeev pseudo-potential approach, we have studied arbitrary amplitude nonlinear structures. In this five components magnetized plasma, we have seen the existence of PPSWs, PPSSs, NPSWs and NPDLs along with the coexistence of different solitary structures and supernonlinear periodic waves. The curve $V(\phi)$ w.r.t. ϕ along with their phase portraits have been displayed to ensure the existence of solitary waves.

We have seen the following effects of parameters on the amplitude of different solitary waves:

(1) Positive Potential Solitary Waves:

- The amplitude of PPSW grows with growing σ_{pc} and M in the region of formation of PPSWs.
- The amplitude of PPSW diminishes with growing n_{pc}, n_{sc}, β_p, β_e, σ_{sc} and l_z in the region of formation of PPSWs, although the amplitude variation of PPSW is negligibly small for growing β_p.
- The intensity of the magnetic field (ω_c) has no influence on the amplitude of PPSWs.

(2) Negative Potential Solitary Waves:

- The amplitude of NPSW grows with growing n_{pc}, n_{sc}, σ_{sc} and M in the region of formation of NPSWs.
- The amplitude of NPSW diminishes with growing β_p, β_e, σ_{pc} and l_z in the region of formation of NPSWs.
- The intensity of the magnetic field (ω_c) has no influence on the amplitude of NPSWs.

(3) The coexistence of Positive and Negative Potential Solitary Waves:

- Both the amplitude of NPSW and PPSW grows with growing M in the region of formation of the coexistence of NPSWs and PPSWs.
- Both the amplitude of NPSW and PPSW diminishes with growing β_p, β_e and l_z in the region of formation of the coexistence of NPSWs and PPSWs.
- The amplitude of NPSW grows, whereas the amplitude of PPSW diminishes with growing n_{pc}, n_{sc} and σ_{sc} in the region of formation of the coexistence of NPSWs and PPSWs.

- The amplitude of NPSW diminishes, whereas the amplitude of PPSW grows with growing σ_{pc} in the region of formation of the coexistence of NPSWs and PPSWs.

- The intensity of the magnetic field (ω_c) has no influence on the the amplitude of the coexistence of NPSWs and PPSWs.

(4) Positive Potential Supersolitons:

- The amplitude of PPSS grows with growing n_{pc}, n_{sc}, σ_{sc} and M in the region of formation of PPSSs.

- The amplitude of PPSS diminishes with growing σ_{pc} and l_z in the region of formation of PPSSs.

- The amplitude variation of PPSS is negligibly small with respect to the parameters β_e and β_p in the region of formation of PPSSs.

- The intensity of the magnetic field (ω_c) has no influence on the amplitude of PPSSs.

(5) Double layers: As a sequence of solitons of growing amplitude (or a sequence of supersolitons of diminishing amplitude) tends to a DL solution of same polarity provided the DL solution exists. So, it is impossible to consider the impacts of distinct parameters DL.

(6) For $M > M_c$, $(0, 0)$ corresponds to a saddle fixed point of (3.3.7), whereas $M < M_c$, $(0, 0)$ corresponds to a nonsaddle fixed point of (3.3.7). Every maximum (minimum) value of potential function $V(\phi)$ that corresponds to a saddle (nonsaddle) fixed point.

(7) It is observed that NPSW and PPSS exist simultaneously and also it is found the NPDL and PPSS exist simultaneously.

(8) Two distinct types of supernonlinear periodic waves as mentioned by Dubinov and others in the papers [89, 90] have been observed in this magnetized plasma system.

In an unmagnetized four components e-p-i-d plasma, Paul *et al.* [81] have found PPSS structures after the formation of PPDL, but in this five components magnetized e-p-i-d plasma, we have seen PPSS structures without PPDL formation.

In this **chapter**, we have not considered any specific values of the parameters, but the parameters have been normalized. As the parameters are normalized, the parameters are bounded and dimensionless. We have qualitatively analyzed the formation of various nonlinear structrues. So, anyone can use this model to analyze the system by taking the entire domain of the parameters.

Here, we have plotted the coexistence of positive and negative potential solitary waves w.r.t. distinct parameters of the system. Again we see that a pseudo particle can not move both sides of ϕ-axis at a given time and consequently, in a given interval of time it can not complete oscillations in both positive and negative sides of the ϕ-axis. Therefore, in a given time a pseudo particle will move along positive sidedirection of ϕ-axis or it will move along the negative direction of ϕ-axis. So, with respect to time, the coexistence is not possible.

From the figures 3.14(h), 3.15(h), 3.16(h) and 3.17(f), we see that the amplitude of any type of solitary structures of any polarity including supersoliton structures diminishes (grows) with growing (diminishing) l_z. In fact, from the dfinition of the Mach number M, it is clear that as M tends to M_c, the amplitude of the soliton tends to 0 and this holds good for any type of plasma system because any type of solitatary waves begin to exist for $M > M_c$. In another words, any solitary structure colapses when M tends to M_c. In figure 3.19, $M - M_c$ vs. l_z is drawn by taking fixed values of the other parameters. Figure 3.19 shows that $M - M_c$ diminishes with growing l_z and $M - M_c \to 0$ as $l_z \to 0.78$ consequently,

amplitude of the solitary structure diminishes for growing l_z starting from its lowest value 0. In figure 3.19, we see that $M > M_c$, $M = M_c$ and $M < M_c$ according to whether $0 \leq l_z < 0.78$(approximately), $l_z = 0.78$(approximately) and $0.78 < l_z \leq 1$ respectively. On the other hand, from the concluding remark of Abdikian *et al.* [376], we can say that the decrease of amplitude of the solitary wave may be due to the reflection of ions from the electrostatic field generated inside the plasma.

The results of our present investigation on arbitrary amplitude DIA nonlinear wave structures including solitons with both polarities, double layers, supersolitons and supernonlinear periodic waves may be helpful to distinguish the signals obtained from different astrophysical environments including the Jupiter's atmosphere and the auroral region of the upper Earth's ionosphere. In **Chapter-1**, we have extensively discussed the source of various five components e-p-i-d plasma system. Although there is no direct evidence for the existence of the positive potential supersoliton structures and supernonlinear periodic wave structures in laboratory plasmas and space, but we are able to identify the signature for the formation of nonlinear wave structures with the help of next-generation satellites.

Chapter 4

Modulation instability of obliquely propagating dust-ion acoustic waves in five components magnetized plasma ‖

In this **Chapter**, using the reductive perturbation method, we have derived a nonlinear Schrödinger equation to study the modulational instability of DIA waves propagating obliquely to the direction of the uniform static magnetic field in a magnetized five components plasma system as defined in **Chapter-1**. The nonlinear dispersion relation of the modulated DIA wave has been analyzed to study the instability regions in the parameter plane. The instability region grows with the increasing values of the ratio of the isothermal to nonthermal electron number density. For a certain range of increasing values of the ion cyclotron frequency, the stable region increases. The instability region also grows with the increasing values of the nonthermal parameter of the hot energetic electrons. The maximum modulational growth rate of instability decreases with increasing values of the ratio of isothermal to nonthermal electron number density. The region of existence of maximum modulational growth rate of instability increases with the increasing values of the nonthermal parameter of positrons. The maximum modulational growth rate of insatiability increases with the increasing values of the ratio of positron temperature to nonthermal electron temperature.

‖ ***Communicated***

4.1 Introduction

Modulational instability of different wave modes in plasma dynamics becomes one of the most interesting topics. Many authors [127–130, 245, 377–379] have used the nonlinear Schrödinger equation (NLSE) to describe different Modulational instability (MI). Using the reductive perturbation technique, Asanol *et al.* [106] have derived a NLSE, which admits the solitary wave solution. FAST satellite observations [180, 185–187, 380, 381] indicate the presence of dominant hot electrons together with a minority of cold electrons in the auroral region. Many authors [121–123] have considered isothermal hot electrons and isothermal cold electrons to study the MI of ion acoustic (IA) waves. Two temperature electrons having the same non-Maxwellian distribution of cold and hot electron species have been considered by the authors [214, 382, 383] to study the MI of IA waves. Two different electron species at different temperatures, where one electron species follows the Maxwell-Boltzmann distribution and another electron species is nonthermally distributed [1] have been considered by several authors [55, 94, 124, 125, 163] in different multi-species plasmas. Recently, a three dimensional nonlinear Schrödinger equation (NLSE) have been derived by Dalui *et al.* [125] to describe the MI of IA waves propagating along the direction of the magnetic field in a magnetized warm plasma consisting of nonthermal and isothermal electrons. In another work, Dalui and Bandyopadhyay [126] have established a correspondence between two NLSEs - one describes the amplitude modulation of IA waves propagating obliquely to the direction of the magnetic field and another describes the amplitude modulation of IA waves propagating along the magnetic field. Along with these two species of electrons as considered by Dalui *et al.* [125] and ions, positrons, and highly charged dust grains form a five components electron-positron-ion-dust (e-p-i-d) plasmas system which is one of the most attractive research areas in space plasma. We have already described the existence of five components e-p-i-d plasma in **Chapter-1**. Although many authors [46, 75, 77, 79, 127–130, 221, 237–239, 242, 245, 247, 249] considered four components of the e-p-i-d plasma system to study different nonlinear properties of the plasma system. Out of them, several authors [127–130, 245] have studied

modulational instability in different wave modes. All of them considered only one electron species of distinct distributions or temperatures in their e-p-i-d plasma system.

In the papers [131, 132], authors have considered an unmagnetized five components plasma system with positive ions, nonextensive positrons and electrons with two different temperatures having nonextensive distribution along with dust grains. Guo *et al.* [131] have studied MI of the planar and nonplanar IA waves by considering both negative and positive dust grains. By considering the same plasma model, and using the reductive perturbation method (RPM) [105, 106], El-Kalaawy [132] has derived a Modified NLSE which describes the low-frequency modulation of IA waves. We want to investigate the MI of DIA waves of five components e-p-i-d plasma system as considered in **Chapter-1**.

In this **chapter**, we have considered same plasma system as considered in the **Chapter-1** to study the MI of DIA waves propagating obliquely to the direction of the uniform static magnetic field in a magnetized five components plasma system composed of warm adiabatic ions, nonthermal positrons, negatively charged static dust grains, nonthermal [1] hot electrons and isothermal cold electrons. Our aim is to make a systematic development to derive an appropriate NLSE that can effectively describes the MI of DIA waves propagating along any arbitrary direction with respect to the direction of the external uniform static magnetic field. Using the NLSE, we have found the maximum modulational growth rate of instability of the modulated DIA waves propagating along any arbitrary direction.

For easy readability of this **Chapter**, we have used the same set of basic equations (1.2.1)-(1.2.4) of **Chapter- 1**. The basic equations are given in the next section along with the expression of the number density of nonthermal electrons, the number density of isothemal electrons, the number density nonthermal positrons and the number density of dust grains.

4.2 Basic Equations

The basic equations of ions fluid are as follows:

$$\frac{\partial n_i}{\partial t} + \overrightarrow{\nabla}.(n_i \overrightarrow{u_i}) = 0, \tag{4.2.1}$$

$$\left(\frac{\partial}{\partial t} + \overrightarrow{u_i}.\overrightarrow{\nabla}\right)\overrightarrow{u_i} + \frac{\sigma}{n_i}\overrightarrow{\nabla} P_i + \overrightarrow{\nabla}\phi - \omega_c(\overrightarrow{u_i} \times \hat{z}) = 0, \tag{4.2.2}$$

$$\frac{\partial P_i}{\partial t} + (\overrightarrow{u_i}.\overrightarrow{\nabla})P_i + \gamma P_i(\overrightarrow{\nabla}.\overrightarrow{u_i}) = 0, \tag{4.2.3}$$

$$\nabla^2\phi = n_{ce} + n_{se} - n_p - n_i + Z_d n_{d0}. \tag{4.2.4}$$

Here, $n_i, n_{ce}, n_{se}, n_p, n_d, \overrightarrow{u_i} = (u_x, u_y, u_z), \phi, P_i, (x, y, z)$ and t are the ion number density, the nonthermal electron number density, the isothermal electron number density, the nonthermal positron number density, the number density of dust grains, the ion fluid velocity, the electrostatic potential, the ion pressure, the spatial variables and time, respectively. These are normalized by $n_{i0}, n_{i0}, n_{i0}, n_{i0}, n_{i0}$, c_s, $\frac{K_B T_{pef}}{e}, n_{i0} K_B T_i, (\lambda_D, \lambda_D, \lambda_D)$ and ω_p^{-1}, respectively. Z_d is the number of electrons residing on the dust grain surface, $-e$ is the charge of an electron, $\gamma\big(=\frac{5}{3}\big)$ is the ratio of two specific heats and K_B is the Boltzmann constant, $\sigma = \frac{T_i}{T_{pef}}$, ω_c (the ion cyclotron frequncy) $= \frac{eB_0}{m_i c}$, $\omega_p = \sqrt{\frac{4\pi e^2 n_{i0}}{m_i}}$, λ_D (Debye length of the present plasma system) $= \sqrt{\frac{K_B T_{pef}}{4\pi e^2 n_{i0}}}$ and $c_s = \sqrt{\frac{K_B T_{pef}}{m_i}}$, m_i is the mass of an ion and $\overrightarrow{\nabla} = \hat{x}\frac{\partial}{\partial x} + \hat{y}\frac{\partial}{\partial y} + \hat{z}\frac{\partial}{\partial z}$.

Under the above-mentioned normalization of the dependent and independent variables, the number density of nonthermally distributed electrons, isothemally distributed electrons, nonthermally distributed positrons and dust grains are as follow:

$$n_{ce} = \overline{n}_{c0}(1 - \beta_e\sigma_c\phi + \beta_e\sigma_c^2\phi^2)\exp(\sigma_c\phi), \tag{4.2.5}$$

$$n_{se} = \overline{n}_{s0}\exp(\sigma_s\phi), \tag{4.2.6}$$

$$n_p = \overline{n}_{p0}(1 + \beta_p\sigma_p\phi + \beta_p\sigma_p^2\phi^2)\exp(-\sigma_p\phi), \tag{4.2.7}$$

$$n_d = \overline{n}_{d0}. \tag{4.2.8}$$

Here, β_e and β_p are the nonthermal parameters associated with the nonthermal velocity distributions of hot electrons and positrons, respectively. $\overline{n}_{p0} = \frac{n_{p0}}{n_{i0}}, \overline{n}_{c0} = \frac{n_{c0}}{n_{i0}}, \overline{n}_{s0} = \frac{n_{s0}}{n_{i0}}, \overline{n}_{d0} = \frac{n_{d0}}{n_{i0}}$, $\sigma_c = \frac{T_{pef}}{T_{ce}}, \sigma_s = \frac{T_{pef}}{T_{se}}$, $\sigma_p = \frac{T_{pef}}{T_p}$, where T_i, T_{ce}, T_{se} and T_p are the average temperature of ion, nonthermal electrons, isothermal electrons and nonthermal positrons, respectively. T_{pef} is given by the following expression:

$$\sum_{j=c,s,p} \frac{n_{j0}}{T_{je}} = \frac{n_{c0} + n_{s0} - n_{p0} + Z_d n_{d0}}{T_{pef}}. \tag{4.2.9}$$

$$n_{i0} - n_{c0} - n_{s0} + n_{p0} - Z_d n_{d0} = 0. \tag{4.2.10}$$

Equation (4.2.10) represents the charge neutrality condition at the equilibrium state and n_{i0}, n_{c0}, n_{s0} and n_{p0} are the equilibrium number densities of ions, nonthermal electrons, isothermal electrons, and nonthermal positrons, respectively. From the charge neutrality condition (4.2.10) and the equation of T_{pef} (4.2.9), we have these two equations given below

$$\sum_{j=c,s,p} \overline{n}_{j0}\sigma_j = 1, \tag{4.2.11}$$

$$\sum_{j=c,s} \overline{n}_{j0} - \overline{n}_{p0} + \overline{N}_{d0} = 1, \tag{4.2.12}$$

where $Z_d n_{d0} = N_{d0} \Longleftrightarrow Z_d \overline{n}_{d0} = \overline{N}_{d0}$.

Introducing the new parameters, we get $n_{sc} = \frac{n_{s0}}{n_{c0}}$, $n_{pc} = \frac{n_{p0}}{n_{c0}}$, $n_{dc} = \frac{N_{d0}}{n_{c0}}$, $\sigma_{sc} = \frac{T_{se}}{T_{ce}}$, $\sigma_{pc} = \frac{T_p}{T_{ce}}$, we have written $\overline{n}_{c0}$, $\overline{n}_{s0}$, $\overline{n}_{p0}$, $\overline{N}_{d0}$, σ_c, σ_s and σ_p as follows:

$$(\overline{n}_{c0}, \overline{n}_{s0}, \overline{n}_{p0}, \overline{N}_{d0}) = \frac{1}{1 + n_{sc} - n_{pc} + n_{dc}}(1, n_{sc}, n_{pc}, n_{dc}), \tag{4.2.13}$$

$$(\sigma_c, \sigma_s, \sigma_p) = \frac{(1 + n_{sc} - n_{pc} + n_{dc})}{\sigma_{sc}\sigma_{pc} + n_{sc}\sigma_{pc} + n_{pc}\sigma_{sc}}(\sigma_{sc}\sigma_{pc}, \sigma_{pc}, \sigma_{sc}). \tag{4.2.14}$$

Expanding the number density of nonthermal electrons (4.2.5), the number density of isothermal electrons and the number density of positrons, and, finally keeping the terms up to ϕ^3, one can write the Poisson equation (4.2.4) as follows:

$$\nabla^2\phi = h_0 + h_1\phi + h_2\phi^2 + h_3\phi^3 - n_i, \tag{4.2.15}$$

where $h_0 = 0$, $h_1 = 1 - \beta_e \overline{n}_{c0}\sigma_c - \beta_p \overline{n}_{p0}\sigma_p$, $2h_2 = \overline{n}_{c0}\sigma_c^2 + \overline{n}_{s0}\sigma_s^2 - \overline{n}_{p0}\sigma_p^2$, and $6h_3 = (1+3\beta_e)\overline{n}_{c0}\sigma_c^3 + \overline{n}_{s0}\sigma_s^3 + (1+3\beta_p)\overline{n}_{p0}\sigma_p^3$.

The equations (4.2.1) and (4.2.3) can be written as follows:

$$P_i = n_i^{\gamma}. \tag{4.2.16}$$

Using the above equation (4.2.16), the equation of motion of ion fluid (4.2.2) can be written in the following form:

$$\left(\frac{\partial}{\partial t} + \overrightarrow{u}_i.\overrightarrow{\nabla}\right)\overrightarrow{u}_i + \sigma\gamma n_i^{\gamma-2}\overrightarrow{\nabla} n_i + \overrightarrow{\nabla}\phi - \omega_c(\overrightarrow{u}_i \times \hat{z}) = 0. \tag{4.2.17}$$

In the next section, we will use the equations (4.2.1), (4.2.15) and (4.2.17) as a new set of basic equations to derive a NLSE.

4.3 Derivation of the NLSE:

Here, we consider the following stretchings of the spatial coordinates and time:

$$\xi = \epsilon(l_1 x + m_1 y + n_1 z - V_g t), \quad \tau = \epsilon^2 t, \tag{4.3.1}$$

where, $l_1^2 + m_1^2 + n_1^2 = 1$, ϵ is a small parameter, V_g is a constant and the perturbation expansion of the dependent field quantities are

$$f = f^{(0)} + \sum_{l=1}^{\infty} \epsilon^l \sum_{a=-\infty}^{\infty} f_a^{(l)}(\xi,\tau)e^{ia\psi}, \tag{4.3.2}$$

where $\psi = (kX - \omega t)$ and $X = l_1 x + m_1 y + n_1 z$. $f = n_i,\ u_x,\ u_y,\ u_z$ and ϕ with $n_i^{(0)} = 1$, $u_x^{(0)} = u_y^{(0)} = u_z^{(0)} = \phi^{(0)} = 0$. We have also used the terminology $f_{-a}^{(l)} = \overline{f_a^{(l)}}$, where 'bar' indicates the conjugate of a complex number. As described by Dalui *et al.* [124], we have used the following consistency conditions: (i) $f_0^{(1)} = 0$, (ii) $f_a^{(l)} = 0$ for $l < |a|$, (iii) $\overline{f_0^{(l)}} = 0$ for any values of l.

Substituting the perturbation expansions for $n_i,\ u_x,\ u_y,\ u_z,\ \phi$ into the equations (4.2.1), (4.2.15), and (4.2.17) and collecting the terms of different power of ϵ, we get a sequence of equations of different orders. From each equation of a particular order, one can generate another sequence of equations for different harmonics by changing the values of a.

4.3.1 First order $o(\epsilon) = 1$:

The zeroth harmonic ($a = 0$) equations for the continuity equation of ions (4.2.1), the equation describing the motion of ions (4.2.17) and the Poisson equation (4.2.15) are identically satisfied due to the consistency condition (i).

Solving the first harmonic ($a = 1$) equations of continuity equation of ions (4.2.1), the equation describing the motion of ions (4.2.17) and the Poisson equation (4.2.15), we get the following linear dispersion relation of DIA waves

$$\frac{k_{\perp}^2}{\omega^2 - \omega_c^2} + \frac{k_{\parallel}^2}{\omega^2} = \left[\frac{k^2 + h_1}{1 + \gamma\sigma(k^2 + h_1)}\right]. \tag{4.3.3}$$

4.3.2 Second order $o(\epsilon) = 2$:

First harmonic ($a = 1$)**:**

Solving the first harmonic ($a = 1$) equations of continuity equation of ions (4.2.1), the equation describing the motion of ions (4.2.17) and the Poisson equation (4.2.15), we obtain the following compatibility condition which determines the group velocity V_g, as

$$V_g = \frac{\partial\omega}{\partial k} = \left[\frac{\omega(\omega^2 - \omega_c^2)(\omega^2 - \omega_c^2 n_1^2)}{k\{\omega^4 - \omega_c^2 n_1^2(2\omega^2 - \omega_c^2)\}} - \frac{\omega^3(\omega^2 - \omega_c^2)^2\zeta^2}{k\{\omega^4 - \omega_c^2 n_1^2(2\omega^2 - \omega_c^2)\}}\right], \tag{4.3.4}$$

where $\zeta = (1 - \sigma\gamma\Lambda)$ and $\Lambda = \dfrac{k^2(\omega^2 - \omega_c^2 n_1^2)}{\omega^2(\omega^2 - \omega_c^2)}$.

Second harmonic ($a = 2$)**:**

Solving the first harmonic ($a = 1$) equations of continuity equation of ions (4.2.1), the equation describing the motion of ions (4.2.17) and the Poisson equation (4.2.15), we get

$$(\phi_2^{(2)}, n_2^{(2)}, u_{x2}^{(2)}, u_{y2}^{(2)}, u_{z2}^{(2)}) = (E_\phi, E_n, E_{x2}, E_{y2}, E_{z2})[\phi_1^{(1)}]^2, \tag{4.3.5}$$

where $g_1 = \gamma - 2$ and

$$E_\phi = \frac{2h_2\zeta^2(1 - \sigma\gamma\eta) - E_1\Lambda^2}{2E_2}, \tag{4.3.6}$$

$$E_n = (4k^2 + h_1)E_\phi + h_2, \tag{4.3.7}$$

$$E_{x2} = \omega l_1 E_c + i\omega_c m_1 E_s, \tag{4.3.8}$$

$$E_{y2} = \omega m_1 E_c - i\omega_c l_1 E_s, \tag{4.3.9}$$

$$E_{z2} = \frac{kn_1}{\omega}\left[E_\phi + \sigma\gamma E_n + \frac{\Lambda + \sigma\gamma g_1\Lambda^2}{2\zeta^2}\right], \tag{4.3.10}$$

$$E_1 = 2 + \sigma\gamma(\gamma - 2)\eta + \frac{2\omega^2(2\omega^2 + \omega_c^2) - n_1^2\omega_c^2(7\omega^2 - \omega_c^2)}{(4\omega^2 - \omega_c^2)(\omega^2 - n_1^2\omega_c^2)}, \tag{4.3.11}$$

$$E_2 = \zeta^2\{\eta - (h_1 + 4k^2)(1 - \sigma\gamma\eta)\}, \tag{4.3.12}$$

$$E_c = \frac{k}{(4\omega^2 - \omega_c^2)}\left[4(E_\phi + \sigma\gamma E_n) + \frac{\Lambda(2\omega^2 + \omega_c^2)}{(\omega^2 - \omega_c^2)\zeta^2} + \frac{2\sigma\gamma g_1\Lambda^2}{\zeta^2}\right], \tag{4.3.13}$$

$$E_s = \frac{k}{(4\omega^2 - \omega_c^2)}\left[2(E_\phi + \sigma\gamma E_n) + \frac{3\Lambda\omega^2}{(\omega^2 - \omega_c^2)\zeta^2} + \frac{\sigma\gamma g_1\Lambda^2}{\zeta^2}\right], \tag{4.3.14}$$

$$\eta = \frac{k^2(4\omega^2 - n_1^2\omega_c^2)}{\omega^2(4\omega^2 - \omega_c^2)}. \tag{4.3.15}$$

Zeroth Harmonic $(a = 0)$**:**

Solving the zeroth harmonic $(a = 0)$ equations of continuity equation of ions (4.2.1), the equation describing the motion of ions (4.2.17) and the Poisson equation (4.2.15), we obtain

$$(\phi_0^{(2)}, n_0^{(2)}, u_{x0}^{(2)}, u_{y0}^{(2)}, u_{z0}^{(2)}) = (F_\phi, F_n, F_{x0}, F_{y0}, F_{z0})|\phi_1^{(1)}|^2, \tag{4.3.16}$$

where

$$F_\phi = \frac{F_1}{F_2}, \tag{4.3.17}$$

$$F_n = h_1 F_\phi + 2h_2, \tag{4.3.18}$$

$$F_{x0} = \frac{-2\Lambda\omega k l_1}{(\omega^2 - \omega_c^2)\zeta^2}, \tag{4.3.19}$$

$$F_{y0} = \frac{-2\Lambda\omega k m_1}{(\omega^2 - \omega_c^2)(1 - \sigma\gamma\Lambda)^2}, \tag{4.3.20}$$

$$F_{z0} = \frac{n_1}{V_g}\left[F_\phi + \sigma\gamma F_n - 2k^2 + \frac{\{\sigma\gamma g_1\Lambda + 3 - \frac{2V_g k}{\omega}\}\Lambda}{\zeta^2}\right], \tag{4.3.21}$$

$$F_1 = \left[\frac{\{\sigma\gamma g_1\Lambda + 3\}\Lambda n_1^2}{\zeta^2} - 2k^2 n_1^2 - 2h_2(V_g^2 - \sigma\gamma n_1^2)\right], \tag{4.3.22}$$

$$F_2 = h_1(V_g^2 - \sigma\gamma n_1^2) - n_1^2. \tag{4.3.23}$$

4.3.3 Third order $o(\epsilon) = 3$, First Harmonic $(a = 1)$:

Solving the first harmonic $(a = 1)$ equations of continuity equation of ions (4.2.1), the equation describing the motion of ions (4.2.17) and the Poisson equation (4.2.15), we obtain the NLSE as

$$i\frac{\partial\phi_1^{(1)}}{\partial\tau} + P\frac{\partial^2\phi_1^{(1)}}{\partial\xi^2} + Q|\phi_1^{(1)}|^2\phi_1^{(1)} = 0, \tag{4.3.24}$$

where

$$P = -\frac{1}{B}\left[1 - \frac{P_1P_2 + P_3 + P_4 + P_5}{\zeta}\right], \tag{4.3.25}$$

$$Q = -\frac{1}{B}[Q_1 - 2h_2(E_\phi + F_\phi) - 3h_3], \tag{4.3.26}$$

$$B = \frac{2k^2\{\omega^4 - \omega_c^2 n_1^2(2\omega^2 - \omega_c^2)\}}{\omega^3(\omega^2 - \omega_c^2)^2\zeta^2}, \tag{4.3.27}$$

$$P_1 = \frac{V_g k\omega}{(\omega^2 - \omega_c^2)} + \frac{V_g k - \omega}{\omega} - \sigma\gamma\Lambda + \frac{\sigma\gamma V_g k^3\omega_c^2\{\omega^2 - n_1^2(2\omega^2 - \omega_c^2)\}}{\omega^3(\omega^2 - \omega_c^2)^2}, \tag{4.3.28}$$

$$P_2 = \frac{2V_g k\{\omega^4 - \omega_c^2 n_1^2(2\omega^2 - \omega_c^2)\}}{\omega^3(\omega^2 - \omega_c^2)^2\zeta^2} - \frac{2(\omega^2 - n_1^2\omega_c^2)}{\omega^2(\omega^2 - \omega_c^2)\zeta^2}, \tag{4.3.29}$$

$$P_3 = \frac{V_g^2 k^2 \omega_c^2 \{2\omega^4 - n_1^2(3\omega^4 - 2\omega^2\omega_c^2 + \omega_c^4)\}}{\omega^4(\omega^2 - \omega_c^2)^3\zeta} - \frac{V_g k \omega_c^2 \{\omega^2 - n_1^2(2\omega^2 - \omega_c^2)\}}{\omega^3(\omega^2 - \omega_c^2)^2\zeta}, \tag{4.3.30}$$

$$P_4 = \frac{(V_g k - \omega)(\omega^2 - \omega_c^2 n_1^2)}{\omega^3(\omega^2 - \omega_c^2)\zeta}, \tag{4.3.31}$$

$$P_5 = -\frac{V_g k (V_g k - \omega)(\omega^2 - \omega_c^2 n_1^2)}{\omega^2(\omega^2 - \omega_c^2)^2\zeta}, \tag{4.3.32}$$

$$\begin{aligned} Q_1 &= \frac{\Lambda}{\zeta^2}\Bigg[\frac{\sigma\gamma g_2\Lambda^3}{\zeta^2} + (1 + \sigma\gamma g_1\Lambda)(E_n + F_n) + \frac{2k(\omega^2 E_c + \omega_c^2 E_s)(l_1^2 + m_1^2)}{(\omega^2 - \omega_c^2)} \\ &+ \frac{2k\{\omega^4 - \omega_c^2 n_1^2(2\omega^2 - \omega_c^2)\}}{\omega(\omega^2 - \omega_c^2)(\omega^2 - n_1^2\omega_c^2)}(l_1 F_{x0} + m_1 F_{y0} + n_1 F_{z0}) + \frac{2kn_1}{\omega}E_{z2}\Bigg]. \end{aligned} \tag{4.3.33}$$

The expressions of the coefficient of dispersive term P and the coefficient of the nonlinear term Q of NLSE (4.3.24), we see that both P and Q are the functions of γ, σ, β_p, β_e, n_{sc}, n_{pc}, n_{dc}, σ_{sc}, σ_{pc}, ω_c and n_1 only.

To comparison with the existing literature, if we ignore the dust particles and the effect of the positron of our present system, the present system reduces to the system considered by Dalui and Bandyopadhyay [126]. We have seen the dispersive coefficient P (4.3.25) and nonlinear coefficient Q (4.3.26) of the NLSE (4.3.24) reduces to the dispersive coefficient P (40) and nonlinear coefficient Q (41) of the NLSE (39) of Dalui and Bandyopadhyay [126].

4.4 Modulational Instability

In this section, we have derived the nonlinear dispersion relation of the modulated DIA waves [124, 384], from the NLSE (4.3.24) as follows:

$$\Omega^2 = [PK^2]^2\left(1 - \frac{2Q|\phi_0|^2}{PK^2}\right), \tag{4.4.1}$$

where Ω and K are, respectively, the modulated wave frequency and modulated wave number of DIA waves. From the above nonlinear dispersion relation (4.4.1), we have the following conditions to identify the instability of the system. (i) If $PQ < 0$, then $\Omega^2 > 0$, the DIA wave is always modulationally stable for $PQ < 0$. (ii) If $PQ > 0$, then $\Omega^2 \geq 0$ or $\Omega^2 < 0$ according to whether $K \geq K_c$ or $K < K_c$, where $K_c = \sqrt{\frac{2Q|\phi_0|^2}{P}}$. The modulated DIA wave is stable or unstable according to whether $K \geq K_c$ or $K < K_c$.

Now $PQ > 0$ and $K < K_c$ implies $\Omega^2 < 0$ and therefore the modulated DIA wave is unstable for $PQ > 0$ and $K < K_c$. The growth rate of instability Γ $(= Im(\Omega))$ is given by

$$\Gamma^2 = [PK^2]^2\Big(\frac{2Q|\phi_0|^2}{PK^2} - 1\Big). \tag{4.4.2}$$

For fixed values of the coefficients of the dispersive and nonlinear terms of the NLSE (4.3.24), the growth rate of instability Γ attains its maximum value Γ_{max} at $K = \frac{K_c}{\sqrt{2}} = \sqrt{\frac{Q|\phi_0|^2}{P}}$ and the maximum growth rate of instability Γ_{max} is given by

$$\Gamma_{max} = |Q||\phi_0|^2. \tag{4.4.3}$$

4.5 Results and Discussions

In this **chapter**, we have considered a fully ionized magnetized e-p-i-d plasma system consisting of warm adiabatic ions, nonthermally distributed positrons, negatively charged immobile dust grains, and two distinct species of electrons at distinct temperatures, one of them is nonthermally [1] distributed hot electrons and another one is Boltzmann-Maxwellian distributed cold electrons. We have considered obliquely propagating dust ion acoustic (DIA) waves with respect to the direction of the uniform static magnetic field.

To study the effect of different parameters associated with the five components system, one can consider a functional relationship between n_1 and k for the equation $PQ = 0$ and for a fixed value of other parameters. We have plotted this

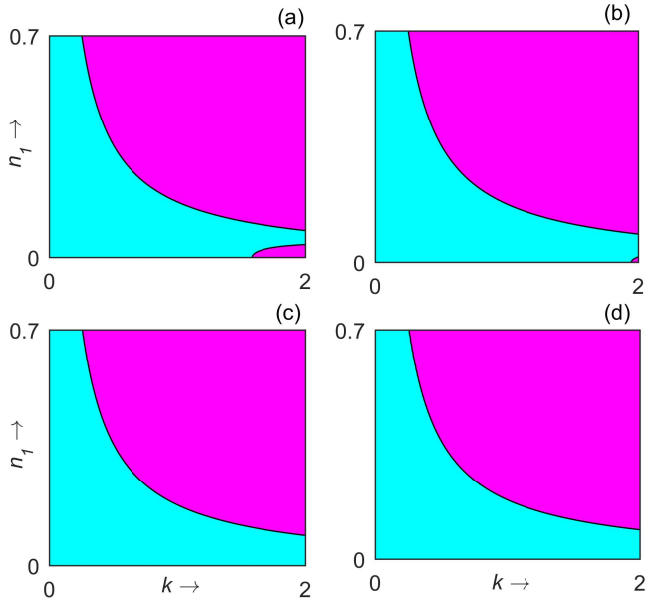

Figure 4.1: When $PQ = 0$, n_1 is plotted against k for different values of n_{pc}. Figure 4.1(a) is plotted for $n_{pc} = 0.1$, figure 4.1(b) is plotted for $n_{pc} = 0.2$, figure 4.1(c) is plotted for $n_{pc} = 0.6$ and figure 4.1(d) is plotted for $n_{pc} = 0.8$.

functional relationship of n_1 with wave number k for equation $PQ = 0$ in the figures 4.1 - 4.5.

To show the effect of n_{pc} on modulational instability (stable or unstable) we draw figure 4.1 when $PQ = 0$. In this figure, n_1 vs. k is plotted for different values of n_{pc} and for $\gamma = 5/3$, $\sigma = 0.0001$, $n_{sc} = 0.1$, $n_{dc} = 0.05$, $\sigma_{sc} = 0.1$, $\sigma_{pc} = 0.2$, $\beta_e = 0.5$, $\beta_p = 0.2$, $\omega_c = 0.2$. Figure 4.1(a) is plotted for $n_{pc} = 0.1$, figure 4.1(b) is plotted for $n_{pc} = 0.2$, figure 4.1(c) is plotted for $n_{pc} = 0.6$ and figure 4.1(d) is plotted for $n_{pc} = 0.8$. In each subfigure of figure 4.1, the curve $PQ = 0$ divides the entire region into two parts, viz., $PQ < 0$ and $PQ > 0$ in the $k - n_1$ plane. The cyan color and pink color represent the regions $PQ < 0$ and $PQ > 0$, respectively. In the region $PQ < 0$ (cyan color) the DIA is modulationally stable and in the region $PQ > 0$ (pink color) the DIA is modulationally stable and unstable depending on the conditions $K \geq K_c$ and $K < K_c$, respectively.

In figure 4.2, the effect of ω_c on modulational instability (stable or unstable) is studied. So, in figure 4.2, n_1 vs. k is plotted when $PQ = 0$ for different values of ω_c and for $\gamma = 5/3$, $\sigma = 0.0001$, $n_{sc} = 0.8$, $n_{pc} = 0.1$, $n_{dc} = 0.05$, $\sigma_{sc} = 0.1$,

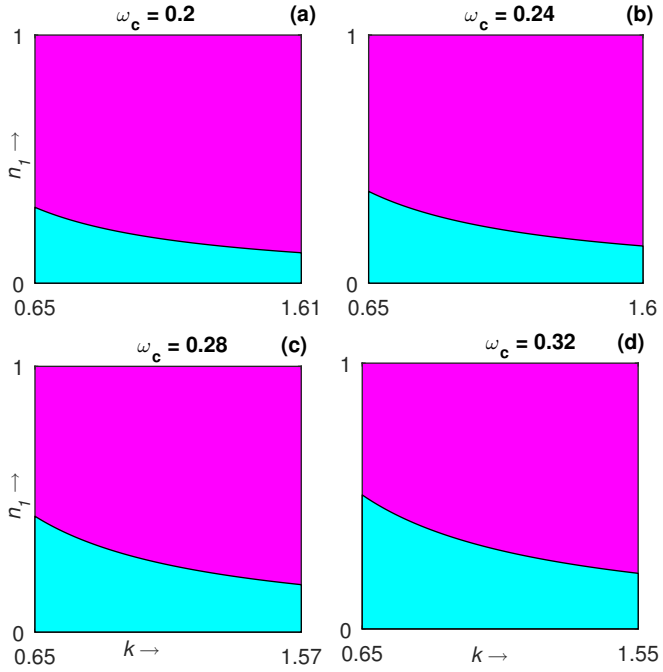

Figure 4.2: When $PQ = 0$, n_1 is plotted against k for different values of ω_c.

$\sigma_{pc} = 0.2$, $\beta_e = 0.5$, $\beta_p = 0.2$. Figure 4.2(a) is plotted for $\omega_c = 0.2$, figure 4.2(b) is plotted for $\omega_c = 0.24$, figure 4.2(c) is plotted for $\omega_c = 0.28$ and figure 4.2(d) is plotted for $\omega_c = 0.32$. In each subfigure of figure 4.2, the curve $PQ = 0$ divides the entire region into two parts, viz., $PQ < 0$ and $PQ > 0$ in the $k - n_1$ plane. The cyan and pink color represents the regions $PQ < 0$ and $PQ > 0$, respectively. In the region $PQ < 0$ (cyan color) the DIA is modulationally stable and in the region $PQ > 0$ (pink color) the DIA is modulationally stable and unstable depending on the conditions $K \geq K_c$ and $K < K_c$, respectively. From the figure, we can see that the stable region increases with increasing ω_c.

In figure 4.3, the effect of n_{sc} is studied on modulational instability. In figure 4.3, n_1 vs. k is plotted when $PQ = 0$ for different values of n_{sc} and for $\gamma = 5/3$, $\sigma = 0.0001$, $n_{pc} = 0.1$, $n_{dc} = 0.05$, $\sigma_{sc} = 0.1$, $\sigma_{pc} = 0.2$, $\beta_e = 0.5$, $\beta_p = 0.2$, $\omega_c = 0.2$. Figure 4.3(a) is plotted for $n_{sc} = 0.1$, figure 4.3(b) is plotted for $n_{sc} = 0.3$, figure 4.3(c) is plotted for $n_{sc} = 0.5$ and figure 4.3(d) is plotted for $n_{sc} = 0.8$. In figure 4.3, the curve $PQ = 0$ divides the entire region into two parts, viz., $PQ < 0$ and $PQ > 0$ in the $k - n_1$ plane. The cyan color and pink color

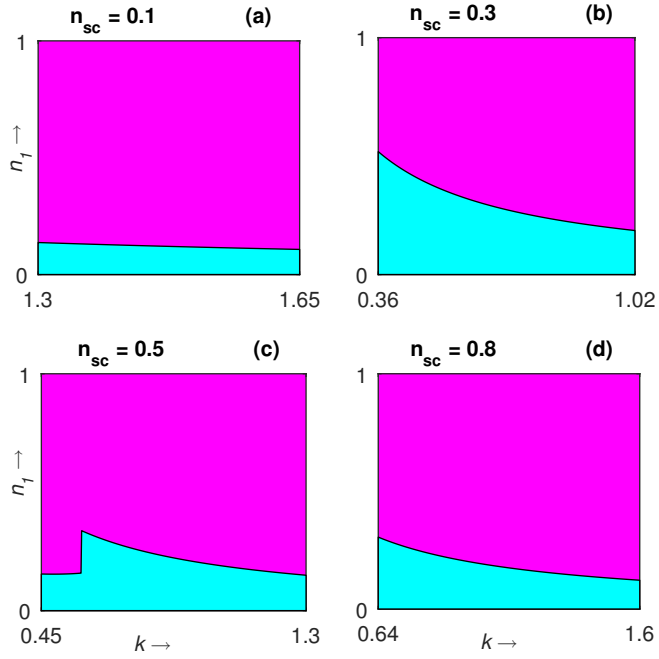

Figure 4.3: When $PQ = 0$, n_1 is plotted against k for different values of n_{sc}.

represent the regions $PQ < 0$ and $PQ > 0$, respectively. In the region $PQ < 0$ (cyan color) the DIA waves are modulationally stable and in the region $PQ > 0$ (pink color) the DIA waves are modulationally stable and unstable depending on the conditions $K \geq K_c$ and $K < K_c$, respectively. From figure 4.3, we have seen that for increasing values of n_{sc} the instability region of the modulated DIA waves increases.

In figure 4.4, the effect of σ_{pc} is studied on instability regions of the modulated DIA waves. In figure 4.4, n_1 vs. k is plotted when $PQ = 0$ for $\gamma = 5/3$, $\sigma = 0.0001$, $n_{sc} = 0.8$, $n_{pc} = 0.1$, $n_{dc} = 0.05$, $\sigma_{sc} = 0.1$, $\beta_e = 0.5$, $\beta_p = 0.2$ and $\omega_c = 0.2$, and for different values of σ_{pc}. Figures 4.4(a), 4.4(b) 4.4(c) and 4.4(d) are plotted for $\sigma_{pc} = 0.15$, $\sigma_{pc} = 0.2$, $\sigma_{pc} = 0.25$, and $\sigma_{pc} = 0.3$, respectively. The DIA waves are modulationally stable for any point (k, n_1) lying within cyan colour regions of figure 4.4. Again, for any point (k, n_1) lying within the regions $PQ > 0$, DIA waves are modulationally stable or unstable according to whether $K \geq K_c$ or $K < K_c$.

In figure 4.5, the effect of the nonthermal parameter of energetic electrons

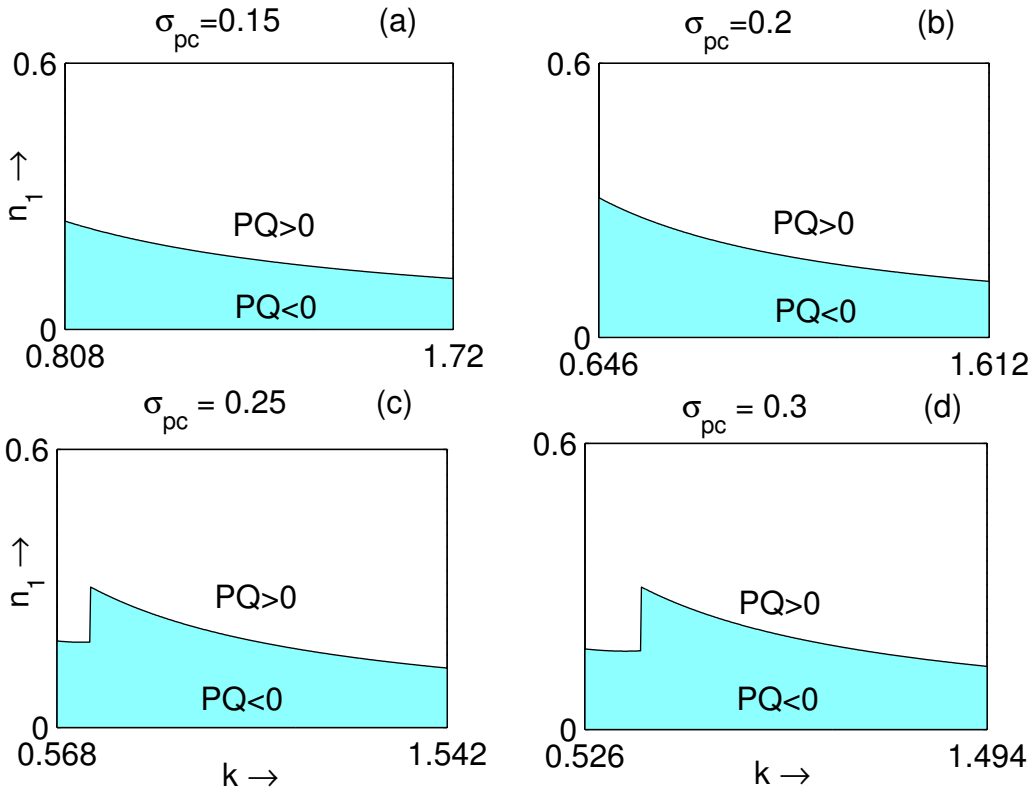

Figure 4.4: When $PQ = 0$, n_1 is plotted against k for different values of σ_{pc}.

(β_e) is studied on instability regions of the modulated DIA waves. In figure 4.5, n_1 vs. k is plotted when $PQ = 0$ for $\gamma = 5/3$, $\sigma = 0.0001$, $n_{sc} = 0.8$, $n_{pc} = 0.1$, $n_{dc} = 0.05$, $\sigma_{sc} = 0.1$, $\sigma_{pc} = 0.2$, $\beta_p = 0.2$ and $\omega_c = 0.2$, and for different values of β_e. Figures 4.5(a), 4.5(b), 4.5(c), and 4.5(d) are plotted for $\beta_e = 0$, $\beta_e = 0.2$, $\beta_e = 0.4$, and $\beta_e = 0.57$, respectively. In figure 4.5, the curve $PQ = 0$ divides the entire region into two parts, viz., $PQ < 0$ and $PQ > 0$ in the $k - n_1$ plane. The cyan color and white color represent the regions $PQ < 0$ and $PQ > 0$ respectively. In the region $PQ < 0$ (cyan color) the DIA waves are modulationally stable and in the region $PQ > 0$ (white color) the DIA waves are modulationally stable and unstable depending on the conditions $K \geq K_c$ and $K < K_c$, respectively. From figure 4.5, we see the length of the interval of k for which modulated DIA waves are unstable increases with increasing nonthermal

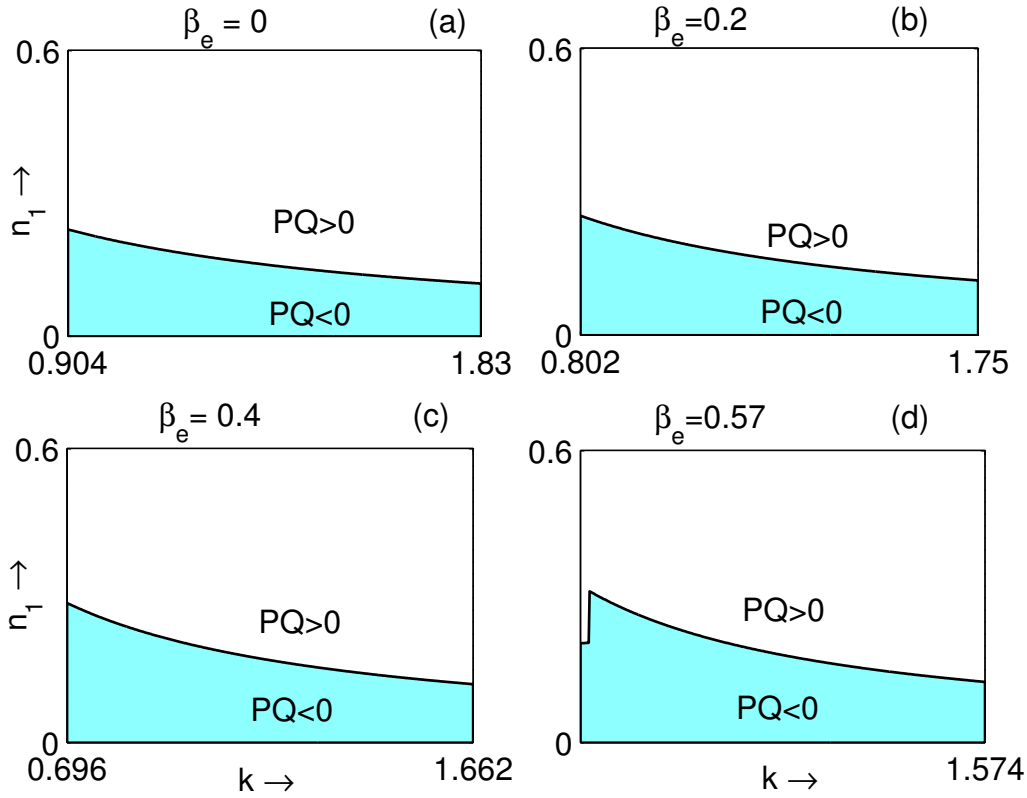

Figure 4.5: When $PQ = 0$, n_1 is plotted against k for different values of β_e.

parameter of the energetic electrons (β_e).

In the region $PQ > 0$, the modulated DIA waves are unstable if $K < K_c$. Within the region for which $PQ > 0$ and $K < K_c$, we want to study the effect of different parameters on the maximum modulation growth rate of instability. For this reason, Figs. 4.6 - 4.10 have been drawn.

In figure 4.6, the coefficient of dispersive term (P), the coefficient of nonlinear term (Q) and maximum modulational growth rate of instability ($\Gamma_{max}/|\phi_0|^2$) are plotted against k for $\gamma = 5/3$, $\sigma = 0.001$, $n_{pc} = 0.01$, $n_{dc} = 0.9$, $\sigma_{sc} = 0.1$, $\sigma_{pc} = 0.2$, $\omega_c = 0.2$, $n_1 = 0.5$, $\beta_e = 0.3$, $\beta_p = 0.2$, and for different values of n_{sc}. In this figure, we have seen that the maximum modulational growth rate of instability, i.e., $\Gamma_{max}/|\phi_0|^2$ decreases with increasing n_{sc}.

In figure 4.7, $\Gamma_{max}/|\phi_0|^2$ are plotted against k for $\gamma = 5/3$, $\sigma = 0.0001$,

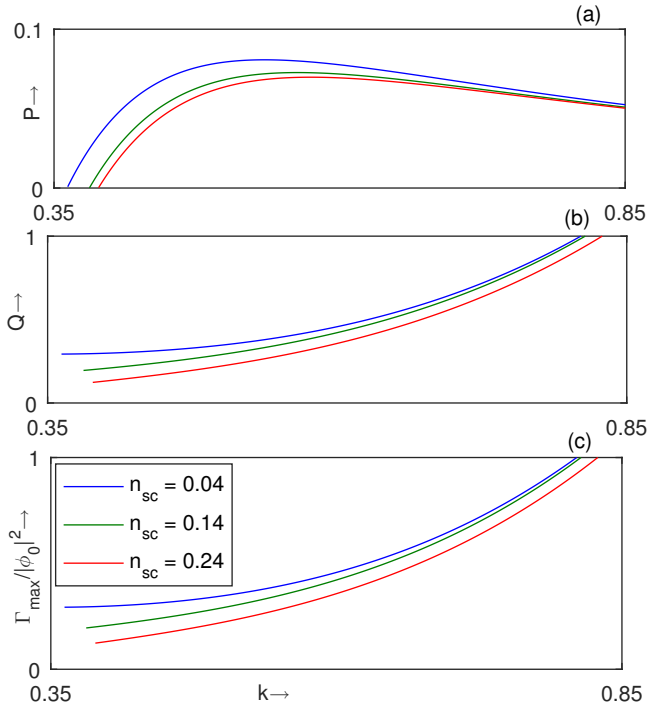

Figure 4.6: P, Q and $\Gamma_{max}/|\phi_0|^2$ are plotted against k for different values of n_{sc}.

$n_{sc} = 0.8$, $n_{pc} = 0.1$, $n_{dc} = 0.05$, $\sigma_{sc} = 0.1$, $\sigma_{pc} = 0.2$, $\omega_c = 0.2$, $\beta_e = 0.5$, $\beta_p = 0.2$ and for different values of n_1. Here red, black and blue curves correspond to $n_1 = 0.3$, $n_1 = 0.325$ and $n_1 = 0.35$, respectively. In figure 4.7, we see that there is no instability for $0 < n_1 < n_1^{(c)} = 0.1974$. The maximum modulational growth rate of instability grows with n_1.

In figure 4.8, we have investigated the effect of n_{pc} on the maximum modulational growth rate of instability. In figure 4.8, $\Gamma_{max}/|\phi_0|^2$ is plotted against k for $\gamma = 5/3$, $\sigma = 0.001$, $n_{sc} = 0.8$, $n_{dc} = 0.05$, $n_1 = 0.21$, $\sigma_{sc} = 0.1$, $\sigma_{pc} = 0.2$, $\beta_e = 0.5$, $\beta_p = 0.2$, $\omega_c = 0.2$ and for different values of n_{pc}. We see that the growth rate of instability reduces with n_{pc}.

In figure 4.9, we have investigated the effect of nonthermal parameter of the positrons on the maximum modulational growth rate of instability. In figure 4.9, $\Gamma_{max}/|\phi_0|^2$ is plotted against k for $\gamma = 5/3$, $\sigma = 0.001$, $n_{sc} = 0.8$, $n_{pc} = 0.8$, $n_{dc} = 0.05$, $n_1 = 0.5$, $\sigma_{sc} = 0.1$, $\sigma_{pc} = 0.2$, $\beta_e = 0.1$, $\omega_c = 0.2$ and for different values of β_p. The maximum modulational growth rate of instability increases

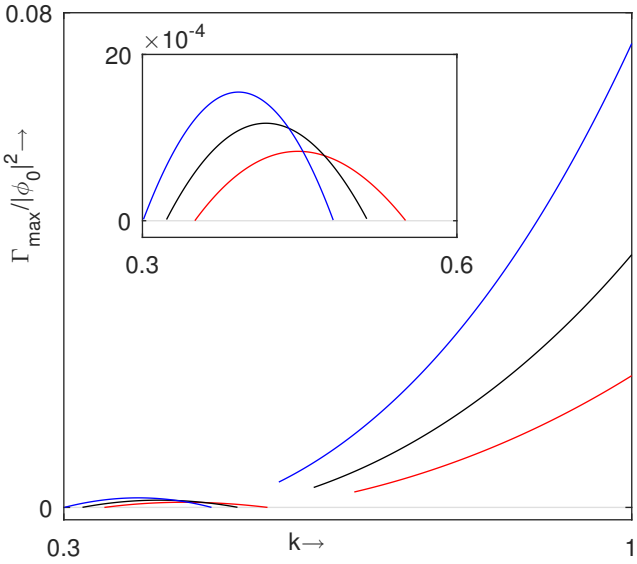

Figure 4.7: $\Gamma_{max}/|\phi_0|^2$ is plotted against k for different values of n_1.

with the nonthermal parameter β_p of the positrons. The region of existence of maximum modulational growth rate of instability increases with the nonthermal parameter. Also, the maximum modulational growth rate of instability increases with the nonthermal parameter.

In figure 4.10, we have plotted the maximum modulational growth rate of insatiability for different values of σ_{sc} and for other fixed values of $\gamma = 5/3$, $\sigma = 0.001$, $n_{sc} = 0.8$, $n_{pc} = 0.8$, $n_{dc} = 0.05$, $n_1 = 0.5$, $\sigma_{pc} = 0.2$, $\beta_e = 0.3$, $\beta_p = 0.3$, $\omega_c = 0.2$. From figure 4.10, we can conclude that the maximum modulational growth rate of insatiability increases with increasing σ_{sc}.

4.6 Conclusions

In this **chapter**, we have considered exactly the same five components e-p-i-d plasma system of **Chapter-1**. We have considered the obliquely propagating DIA waves with respect to the direction of the uniform static magnetic field.

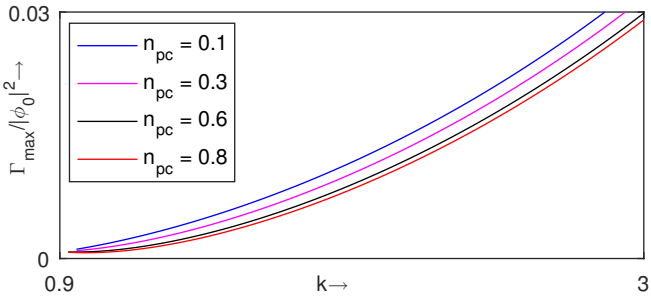

Figure 4.8: $\Gamma_{max}/|\phi_0|^2$ is plotted against k for different values of n_{pc}.

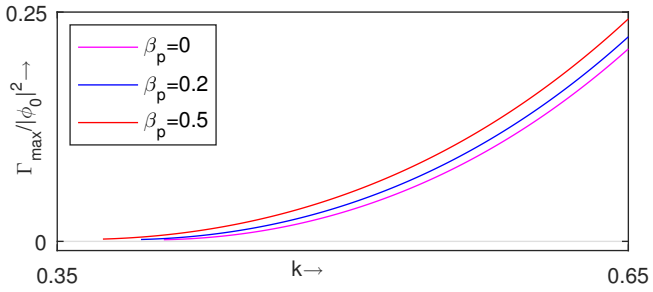

Figure 4.9: $\Gamma_{max}/|\phi_0|^2$ is plotted against k for different values of β_p.

We derived the nonlinear Schrödinger equation (NLSE) using the reductive perturbation method [105, 106]. From this NLSE, we have obtained the nonlinear dispersion relation of the modulated DIA waves.

We have derived a more general NLSE (4.3.24) and we have shown that our results also preserve the investigation of Dalui and Bandyopadhyay [126]. We have seen that the dispersive coefficient P (4.3.25) and nonlinear coefficient Q (4.3.26) of the NLSE (4.3.24) reduce to those of Dalui and Bandyopadhyay [126]: P (40) and Q (41) for NLSE (39).

We have investigated the effect of different parameters on the existence of stable and unstable regions with respect to modulated DIA waves.

- We have seen that for a certain range of increasing values of ω_c, the stable region increases for the present e-p-i-d plasma system.

- We have seen that for increasing values of n_{sc}, the instability region of the

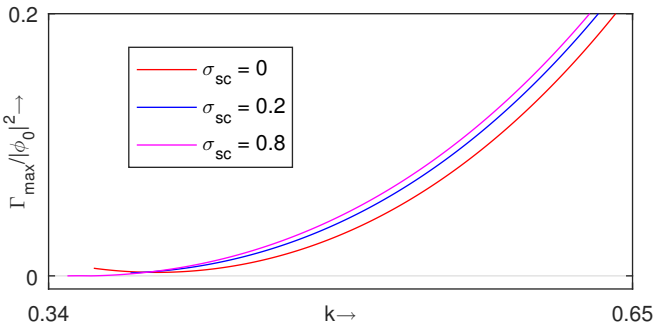

Figure 4.10: $\Gamma_{max}/|\phi_0|^2$ is plotted against k for different values of σ_{sc}.

modulated DIA waves increases.

- The interval of k for which modulated DIA waves are stable increases with increasing $\sigma_{pc} < \sigma_{pc}^{(c)}$, after that the interval of k for which modulated DIA waves are stable decreases.

- We see the interval of k for which modulated DIA waves are unstable increases with increasing nonthermal parameter of the energetic electrons.

For $PQ > 0$ and $K < K_c$, the modulated DIA waves are unstable. Within this region, we have studied the effect of different parameters on the maximum modulation growth rate of instability.

- We have observed that the maximum modulational growth rate of instability decreases with increasing n_{sc}.

- The maximum modulational growth rate of instability grows with n_1.

- The maximum modulational growth rate of instability decreases with increasing β_e.

- The region of existence of maximum modulational growth rate of instability increases with the nonthermal parameter of the positrons.

- The maximum modulational growth rate of insatiability increases with increasing σ_{sc}.

Chapter 5

Arbitrary amplitude dust-ion acoustic solitary structures in five components unmagnetized plasma [‡]

In this **Chapter**, the energy integral derived by using Sagdeev pseudo-potential technique has been analyzed to investigate the existence of arbitrary amplitude dust-ion acoustic solitons including double layers and supersolitons in a collisionless five components unmagnetized plasma system whose constituents are same as given in **Chapter-1**. The plasma system contains warm adiabatic ions, two distinct populations of electrons at different temperatures, nonthermal hot positron species, and negatively charged static dust grains. The graphical analysis of Sagdeev pseudo-potential shows the existence of positive potential supersolitons (PPSS) along with positive potential double layers (PPDLs) and positive potential solitary waves (PPSWs) whereas in the negative potential side, the system does not support negative potential supersolitons but the existence of negative potential double layers (NPDLs), negative potential solitary waves (NPSWs), the coexistence of both PPSWs and NPSWs, and super-nonlinear periodic waves have been established. To explain the existence of different DIA solitary structures, phase portraits of the dynamical system corresponding to the different DIA solitary structures have been drawn. With the help of phase portraits, the transition of PPSWs just before and just after the formation of PPDL has been discussed. We have seen that the amplitude of PPSW decreases with increasing β_e, β_p, and σ_{sc} and it increases with increasing σ_{pc} whereas there exists a critical value n_{pc}^c of n_{pc} such that the amplitude of PPSW decreases (increases) with increasing n_{pc} for $n_{pc} < n_{pc}^c$ ($n_{pc}^c < n_{pc}$) for a fixed value of the Mach number M in the region of existence of PPSWs. Effects of parameters have been considered on the amplitude of NPSWs and PPSS also.

[‡]This chapter has been published in ***Plasma Phys. Rep.*** **49, 467 (2023); https://doi.org/ 10.1134/S1063780X22601225**

5.1 Introduction

Several authors [45–47, 56, 62, 75–84, 127, 128, 148, 169–172, 218–223, 237, 238, 240–249] have considered the different electron-positron-ion-dust (e-p-i-d) plasma systems to investigate different plasma properties, that can be found in different space plasma observations [169, 170, 385–388]. In these e-p-i-d plasma systems, dust-ion acoustic (DIA) or ion-acoustic (IA) solitary structures have been studied by several authors [45–47, 56, 62, 75–84, 148, 249] considering different velocity distribution of electrons and positrons. Out of them, several authors [75–84] have investigated the arbitrary amplitude DIA solitary structures, viz., positive potential solitary waves (PPSWs), negative potential solitary waves (NPSWs), negative potential double layers (NPDLs), positive potential double layers (PPDLs), super-nonlinear periodic waves and supersolitons. In the above mentioned papers [75–84], authors have considered only one population electrons. Two different species of electrons are observed in space plasma. So, a general prescription is to consider two different species of electrons instead of one species of electrons along with the species of positrons, ions, and dust grains. In fact, different satellite observations [180, 183, 185–187, 381] ensure the existence of two different populations electrons at the auroral region. In this **chapter**, we have considered two distinct populations of electrons, the cooler electron species is Maxwellian distributed isothermal electrons whereas the hotter electron species is Cairns [1] distributed nonthermal electrons. However, Yu and Luo [188] clearly pointed out that the multispecies model for identical particles is not in general suitable for considering quasistationary nonlinear plasma structures. In fact, according to them, for phenomena on long time scales, a prior partitioning of electrons into two different species at different temperatures is possible only when these species are physically separated in the phase space or time domain of interest. So, one can consider Maxwell-Boltzmann distributed electrons and Cairns

[1] distributed electrons as two different species of electrons only when those electron species are physically separated in the phase space by external or self-consistent fields. Assuming that the condition prescribed by Yu and Luo [188] for the existence of a multispecies model for identical particles holds good, two distinct species of electrons at different temperatures have been considered by several authors [126, 163, 290, 294, 311, 315, 355, 356]. Several authors [55, 66–68, 94, 95, 98, 163, 232, 291, 295–297, 389] have investigated different IA solitary structures in a collisionless unmagnetized or magnetized plasma by considering of two different electrons species at different temperatures.

Different five components e-p-i-d plasma systems have been considered by several authors [75, 131, 132, 324]. Guo *et al.* [131] have considered a collisionless unmagnetized five components e-p-i-d plasma system consisting of two distinct populations of q- nonextensive electrons at different temperatures, q- nonextensive positrons, positive ions, positively or negatively charged static dust grains to investigate the modulational instability of ion-acoustic waves and the existence of ion-acoustic rogue waves. El-Kalaawy [132] considered the same five components e-p-i-d plasma system of Guo *et al.* [131] to study the ion-acoustic envelope solitons. The dynamics of the dust-ion acoustic anti-kink waves have been studied by Tamang [324] in a five components e-p-i-d unmagnetized collisionless plasma system consisting of two distinct populations of q- nonextensive electrons at different temperatures, Maxwellian distributed isothermal positrons, inertial ions, and negatively charged static dust grains. Before these works of the above-mentioned authors [131, 132, 324], Dubinov and Kolotkov [75] considered a collisionless unmagnetized five components e-p-i-d plasma system consisting of one species of Maxwellian distributed isothermal electrons instead of two species of electrons, two ion species - positive ions and negative ions, Maxwellian distributed isothermal positrons and negatively charged static dust grains to investigate the existence of ion-acoustic supersolitons.

Recently, a five components dusty plasma model has been considered by Moslem *et al.* [189] and Al-Yousef [190] by considering the Maxwellian electrons and ions, positive dust grains particles including protons and solar wind streaming electrons. They have applied that model in Jupiter's atmosphere to investigate the dynamics of dust grains and solar wind streaming electrons and protons. So, it can be concluded that a five components e-p-i-d plasma may be found in the Jupiter atmosphere by considering the report of Gusev *et al.* [174, 175] regarding the production of positrons from protons. Also, several authors have considered five components cometary plasma [390–393] and electronegative plasma [394].

In **Chapter-1**, we have studied small amplitude DIA solitary structures in a magnetized five components collisionless e-p-i-d plasma system consisting of warm adiabatic ions, Cairns distributed nonthermal positrons, Maxwellian distributed isothermal electrons, Cairns distributed nonthermal electrons, and negatively charged static dust grains. They have derived different evolution equations to study the solitary wave solution and also studied the existence of those evolution equations by considering different compositional parameter planes.

In this **chapter**, we have considered a collisionless unmagnetized five components e-p-i-d plasma system, which contains two distinct populations of electrons at different temperatures, one of which is Maxwellian distributed isothermal electrons and the other one is Cairns distributed nonthermal electrons, Cairns distributed nonthermal positrons, warm adiabatic ions, and negatively charged static dust grains. Our aim is to investigate the existence of arbitrary amplitude different DIA solitary structures, viz., PPSWs, NPSWs, the coexistence of both positive and negative potential solitons, PPDLs, NPDLs, supersolitons, and super-nonlinear periodic waves with respect to different parameters associated with the present plasma system. And the plasma system as considered in the present **chapter** is an extension of Paul *et al.* [81] in the following direction: Paul *et al.* [81] have considered a collisionless unmagnetized four components

e-p-i-d plasma system consisting of only one nonthermal electrons species but in this present **chapter**, we have considered a five components e-p-i-d plasma system consisting of two electrons species, one is nonthermal electrons species, and another one is isothermal electrons species.

5.2 Basic Equations

In this **chapter**, we have considered a collisionless unmagnetized five components plasma system consisting of two distinct species of electrons at distinct temperatures, one is nonthermally distributed hot electrons and another one is Boltzmann-Maxwellian distributed cold electrons, warm adiabatic ions, nonthermally distributed positrons and negatively charged immobile dust grains. We have considered the following set of basic equations of ions fluid, viz., equation of continuity of ions fluid, equation of motion of ions fluid, equation of pressure of ions fluid and Poisson equation to investigate the nonlinear behaviour of DIA waves propagating along the x-axis:

$$\frac{\partial n_i}{\partial t} + \frac{\partial}{\partial x}(n_i u_i) = 0, \tag{5.2.1}$$

$$\left(\frac{\partial}{\partial t} + u_i \frac{\partial}{\partial x}\right) u_i + \frac{\sigma}{n_i}\frac{\partial P_i}{\partial x} + \frac{\partial \phi}{\partial x} = 0, \tag{5.2.2}$$

$$\frac{\partial P_i}{\partial t} + u_i \frac{\partial P_i}{\partial x} + \gamma P_i \frac{\partial u_i}{\partial x} = 0, \tag{5.2.3}$$

$$\frac{\partial^2 \phi}{\partial x^2} = n_{ce} + n_{se} - n_p - n_i + Z_d n_{d0}. \tag{5.2.4}$$

Here n_α ($\alpha = i, ce, se, p$, and d stand for ion, nonthermal electron, isothermal electron, nonthermal positron, and dust particulates), u_i, ϕ, P_i, x, and t are the number density of α-th species, the ion fluid velocity, the electrostatic potential, the ion pressure, the spatial variables, and time respectively. These are normalized by n_{i0}, c_s, $\frac{K_B T_{pef}}{e}$, $n_{i0} K_B T_i$, λ_D, and ω_p^{-1} respectively. Z_d is the number of

negative unit charges residing on the dust grain surface, $-e$ is the charge of an electron, $\gamma(=3)$ is the ratio of two specific heats and K_B is the Boltzmann constant, $\sigma = \frac{T_i}{T_{pef}}$, $\omega_p = \sqrt{\frac{4\pi e^2 n_{i0}}{m_i}}$, $\lambda_D \left(= \sqrt{\frac{K_B T_{pef}}{4\pi e^2 n_{i0}}} \right)$ (Debye length of the present plasma system), $c_s = \sqrt{\frac{K_B T_{pef}}{m_i}}$, T_i is the average temperature of an ion, n_{i0} is the equilibrium number density of an ion and m_i is the mass of an ion.

Because of the large masses of the dust particulates in comparison with the mass of the ions (i.e., $m_d >> Z_d m_i$), the dust particulates can be considered as immobile and consequently the dust density is constant. In fact, under the above mentioned normalization of the dependent and independent variables, following Popel and Yu [357], the continuity equation of the dust grains and equation of motion of dust particulates can be written as

$$\frac{dn_d}{dt} + n_d \frac{\partial v_d}{\partial x} = 0 \text{ and } \frac{dv_d}{dt} - \frac{Z_d m_i}{m_d} \frac{\partial \phi}{\partial x} = 0 \tag{5.2.5}$$

where

$$\frac{d}{dt} = \frac{\partial}{\partial t} + v_d \frac{\partial}{\partial x}. \tag{5.2.6}$$

The second term of the left hand side of the second equation of (5.2.5) can be neglected as $m_d >> Z_d m_i$ and consequently the second equation of (5.2.5) gives $v_d =$ equlibrium value of $v_d = 0$. If $v_d = 0$, then from the first equation of (5.2.5), we get $n_d =$ equlibrium value of $n_d =$ a constant. Therefore, on the basis of the assumption $m_d >> Z_d m_i$, the dust particulates can be taken as static and the dust density can be taken as a constant. These have been reported by many authors [82, 91, 357, 359, 360, 363, 395, 396]. It is also important to note that here we are considering the DIA time scale. Again in the present problem, we have not considered the effects of variable-charge dust particulates, effects of ionization, effects of ions - dust interaction, effects of ion - neutral interaction, and effects originating from ion absorption by dust grains. These effects have been investigated by many authors [357–373, 397].

Under the above-mentioned normalization of the dependent and independent variables, the number densities of nonthermally distributed electrons, isothemally distributed electrons, nonthermally distributed positrons and dust grains are given by the following equations:

$$n_{ce} = \overline{n}_{c0}(1 - \beta_e\sigma_c\phi + \beta_e\sigma_c^2\phi^2)\exp(\sigma_c\phi), \tag{5.2.7}$$

$$n_{se} = \overline{n}_{s0}\exp(\sigma_s\phi), \tag{5.2.8}$$

$$n_p = \overline{n}_{p0}(1 + \beta_p\sigma_p\phi + \beta_p\sigma_p^2\phi^2)\exp(-\sigma_p\phi), \tag{5.2.9}$$

$$n_d = \overline{n}_{d0}. \tag{5.2.10}$$

Here, β_e and β_p are the nonthermal parameters associated with the nonthermal velocity distributions of hot electrons and positrons respectively. Also $\overline{n}_{j0} = \frac{n_{j0}}{n_{i0}}$ ($j = c, s, p$, and d stand for nonthermal electron, isothermal electron, nonthermal positron and dust particulates), where n_{j0} is the equilibrium number density of j-th species and $(\sigma_c, \sigma_s, \sigma_p) = (\frac{T_{pef}}{T_{ce}}, \frac{T_{pef}}{T_{se}}, \frac{T_{pef}}{T_p})$, where T_{ce} (T_p) and T_{se} are the average temperatures of nonthermal electron (positron) and isothermal electron respectively and T_{pef} is given by the following expression:

$$\frac{n_{c0}}{T_{ce}} + \frac{n_{s0}}{T_{se}} + \frac{n_{p0}}{T_p} = \frac{n_{c0} + n_{s0} - n_{p0} + Z_d n_{d0}}{T_{pef}}. \tag{5.2.11}$$

The equation of the charge neutrality condition is

$$n_{i0} - n_{c0} - n_{s0} + n_{p0} - Z_d n_{d0} = 0. \tag{5.2.12}$$

From the charge neutrality condition (5.2.12) and the equation of T_{pef} (5.2.11), we get following two equations:

$$\overline{n}_{c0}\sigma_c + \overline{n}_{s0}\sigma_s + \overline{n}_{p0}\sigma_p = 1, \tag{5.2.13}$$

$$\overline{n}_{c0} + \overline{n}_{s0} - \overline{n}_{p0} + \overline{N}_{d0} = 1, \tag{5.2.14}$$

where $Z_d n_{d0} = N_{d0} \Longleftrightarrow Z_d \overline{n}_{d0} = \overline{N}_{d0}$.

After that introducing the new parameters: $n_{sc} = \frac{n_{s0}}{n_{c0}}, n_{pc} = \frac{n_{p0}}{n_{c0}}, n_{dc} = \frac{N_{d0}}{n_{c0}}, \sigma_{sc} = \frac{T_{se}}{T_{ce}}, \sigma_{pc} = \frac{T_p}{T_{ce}}$, we have written $\overline{n}_{c0}, \overline{n}_{s0}, \overline{n}_{p0}, \overline{N}_{d0}, \sigma_c, \sigma_s$, and σ_p as follows:

$$(\overline{n}_{c0}, \overline{n}_{s0}, \overline{n}_{p0}, \overline{N}_{d0}) = \frac{1}{1 + n_{sc} - n_{pc} + n_{dc}}(1, n_{sc}, n_{pc}, n_{dc}), \tag{5.2.15}$$

$$(\sigma_c, \sigma_s, \sigma_p) = \frac{(1 + n_{sc} - n_{pc} + n_{dc})}{\sigma_{sc}\sigma_{pc} + n_{sc}\sigma_{pc} + n_{pc}\sigma_{sc}}(\sigma_{sc}\sigma_{pc}, \sigma_{pc}, \sigma_{sc}). \tag{5.2.16}$$

In the present plasma system, the linear dispersion relation of DIA wave is

$$\frac{\omega^2}{k^2} = M_D^2 \left[\frac{1 + \frac{\sigma\gamma}{M_c^2}\lambda_D^2 k^2}{1 + \lambda_D^2 k^2} \right], \tag{5.2.17}$$

where $M_D^2 = M_c^2 c_s^2$, and $M_c^2 = \sigma\gamma + \dfrac{1}{1 - \beta_e \overline{n}_{c0}\sigma_c - \beta_p \overline{n}_{p0}\sigma_p}$.

Here, the wave frequency and wave number of the plane wave perturbation are denoted by ω and k, respectively.

5.3 Energy Integral

To investigate the steady state DIA arbitrary amplitude, we consider the transformation $\xi = x - Mt$ to make all the dependent variables depend only on a single variable, where M (Mach number) is the dimensionless velocity of the wave frame normalized by the linearized DIA speed (c_s). And using the boundary conditions

$$\left(n_i, P_i, u_i, \phi, \frac{d\phi}{d\xi}\right) \to (1, 1, 0, 0, 0) \quad \text{as} \quad |\xi| \to \infty,$$

we get the following energy integral with $V(\phi)$ as the Sagdeev potential or pseudo-potential:

$$\frac{1}{2}\left(\frac{d\phi}{d\xi}\right)^2 + V(\phi) = 0, \tag{5.3.1}$$

where

$$V(\phi) = V_i + \frac{\overline{n}_{p0}}{\sigma_p} V_p - \frac{\overline{n}_{c0}}{\sigma_c} V_{ce} - \frac{\overline{n}_{s0}}{\sigma_s} V_{se} - \overline{N}_{d0} V_d, \tag{5.3.2}$$

$$V_i = (M^2 + \sigma) - n_i(M^2 + 3\sigma - 2\phi - 2\sigma n_i^2), \tag{5.3.3}$$

$$n_i = \frac{\sqrt{2}M}{\sqrt{\phi_M - \phi} + \sqrt{\psi_M - \phi}}, \tag{5.3.4}$$

$$\phi_M = \frac{(M + \sqrt{3\sigma})^2}{2}, \tag{5.3.5}$$

$$\psi_M = \frac{(M - \sqrt{3\sigma})^2}{2}, \tag{5.3.6}$$

$$V_p = (1 + 3\beta_p) - (1 + 3\beta_p + 3\beta_p\sigma_p\phi + \beta_p\sigma_p^2\phi^2)\exp(-\sigma_p\phi), \tag{5.3.7}$$

$$V_{ce} = (1 + 3\beta_e - 3\beta_e\sigma_c\phi + \beta_e\sigma_c^2\phi^2)\exp(\sigma_c\phi) - (1 + 3\beta_e), \tag{5.3.8}$$

$$V_{se} = \exp(\sigma_s\phi) - 1, \tag{5.3.9}$$

$$V_d = \phi. \tag{5.3.10}$$

Equation (5.3.1) is known as energy integral. For the existence of a positive (negative) potential solitary wave solution of (5.3.1), the following conditions hold good:

(a) $V(\phi) = V^{'}(\phi) = 0$ and $V^{''}(\phi) < 0$ at $\phi = 0$.

(b) $V(\phi_m) = 0$, $V^{'}(\phi_m) > 0$ ($V^{'}(\phi_m) < 0$) for some $\phi_m > 0$ ($\phi_m < 0$). This condition is responsible for the oscillation of the particle within the interval $\min\{0, \phi_m\} < \phi < \max\{0, \phi_m\}$.

(c) $V(\phi) < 0$ for all $0 < \phi < \phi_m (\phi_m < \phi < 0)$. This condition is necessary to define the equation (5.3.1) within the interval $\min\{0, \phi_m\} < \phi < \max\{0, \phi_m\}$. Also for the existence of a positive (negative) potential double layer solution of (5.3.1),

we must replace the second condition by $V(\phi_m) = 0,\ V^{'}(\phi_m) = 0,\ V^{''}(\phi_m) < 0$ for some $\phi_m > 0$ ($\phi_m < 0$).

Here, $M > M_c$ ($M < M_c$) is the necessary conditions for the existence of different solitary wave solutions at the supersonic speed (subsonic speed) of the waves of the energy integral (5.3.1), where

$$M_c = \sqrt{3\sigma + \frac{1}{1 - \beta_e \overline{n}_{c0}\sigma_c - \beta_p \overline{n}_{p0}\sigma_p}}. \tag{5.3.11}$$

From the expression of n_i as given by equation (5.3.4), we see that n_i is well-defined if and only if $\phi \leq \psi_M$.

In figure 5.1, n_i is plotted against ϕ for different values M with $M > M_c$ and $\phi \leq \psi_M$. This figure shows that $n_i > 1$ for $\phi > 0$ whereas $n_i < 1$ for $\phi > 0$ and $n_i = 1$ for $\phi = 0$. Here it is important to note that ion density is normalized by n_{i0} (unperturbed ion number density) and $\phi = 0$ is the equilibrium electrostatic potential. Therefore $n_i > 1$ implies the positive ion density perturbation and $n_i < 1$ implies the negative ion density perturbation. So in our present **chapter**, there is a possibility to get solitary structures of both positive and negative polarities including double layers and supersoliton structures of both polarities. But we have seen that although the present system supports the negative potential double layers but it is not possible to get negative potential supersolitons. Considering the isothermal distribution of electrons, [357] reported that the dual existence of two types of wave structures is not possible in the case of impurity-free plasma. The only bright ion-acoustic soliton can exist in this case. Authors have shown that the structure with positive electrostatic potential corresponds to a positive ion density perturbation which gives a bright soliton for ion density when the plasma is free from the impurity. But Cairns *et al.* [1, 50, 398] have shown in a series of papers that both positive and negative ion density perturbation can exist if one can take nonthermal velocity distribution of electrons as prescribed by Cairns et al [1]. In fact, Verheest and others [69, 72, 102, 155, 168, 292, 351, 399–402] have

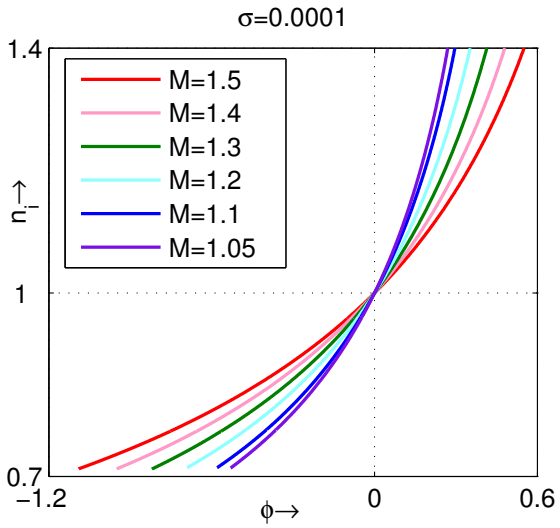

Figure 5.1: n_i is drawn against ϕ for $\sigma = 0.0001$ (the violet, blue, sky-blue, green, magenta, and red curves correspond to $M = 1.05, M = 1.1, M = 1.2, M = 1.3, M = 1.4$, and $M = 1.5$, respectively).

investigated a series of problems to study the coexistence of solitary structures including double layers and supersolitons by considering the nonthermal distribution of electrons as prescribed by Cairns et al [1]. In this present **chapter**, we have considered two populations of electrons at different temperatures, the hotter one is cairns distributed and the cooler one is isothermally distributed.

In figure 5.2(a), we have drawn $V(\phi)$ against ϕ for $\gamma = 3$, $\sigma = 0.0001$, $n_{sc} = 0.0515$, $n_{pc} = 0.055$, $n_{dc} = 0.005$, $\sigma_{sc} = 0.095$, $\sigma_{pc} = 0.19$, $\beta_e = 0.4$, $\beta_p = 0.1$, and for different values of M. Here, the magenta, blue, red, sky-blue, and black curves correspond to $M = 1.143, M = 1.15, M = 1.16, M = 1.17$, and $M = 1.173875$, respectively. From this figure 5.2(a), we see that there exists an interval $M_c < M < M^{(c)}$, such that within this interval, positive potential solitary waves (PPSWs) exist, where $M^{(c)} = 1.173875$, and we also see that the

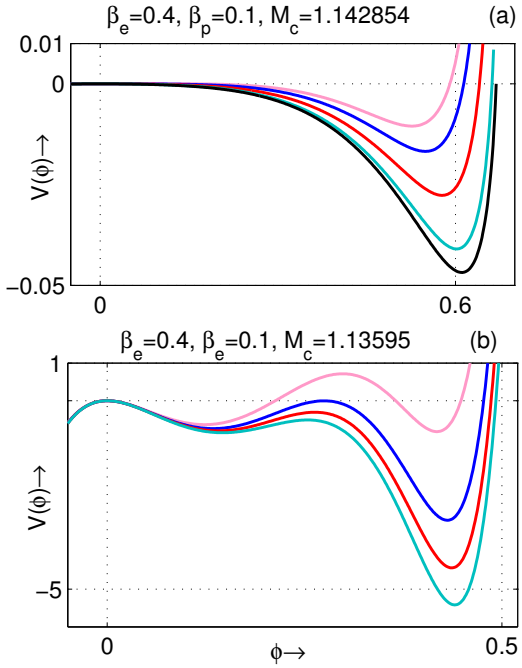

Figure 5.2: $V(\phi)$ is drawn against ϕ for $\gamma = 3$, $\sigma = 0.0001$, $n_{sc} = 0.0515$, $n_{pc} = 0.055$, $n_{dc} = 0.005$, $\sigma_{sc} = 0.095$, $\beta_e = 0.4$, and $\beta_p = 0.1$, and (a) for $\sigma_{pc} = 0.19$ (the magenta, blue, red, sky-blue, and black curves correspond to $M = 1.143$, $M = 1.15, M = 1.16, M = 1.17$, and $M = 1.173875$, respectively) and (b) for $\sigma_{pc} = 0.129$ (the magenta, blue, red, and sky-blue curves correspond to $M = 1.1605$, $M = 1.1613$, $M = 1.1617$, and $M = 1.162$, respectively).

amplitude of PPSWs increases with increasing the values of M. For the greater value of $M^{(c)}$ the system does not support any PPSW in case of the same value of other parameters.

In figure 5.2(b), we have drawn $V(\phi)$ against ϕ for $\gamma = 3$, $\sigma = 0.0001$, $n_{sc} = 0.0515$, $n_{pc} = 0.055$, $n_{dc} = 0.005$, $\sigma_{sc} = 0.095$, $\sigma_{pc} = 0.129$, $\beta_e = 0.4$, $\beta_p = 0.1$ and for different values of M. Here, the magenta, blue, red and sky-blue curves correspond to $M = 1.1605, 1.1613, 1.1617$ and 1.162, respectively and from this figure 5.2(b), we have seen that there exist a positive potential double layer (PPDL). Here, the red curve ($M = 1.1613 = M_{PPDL}$) indicates the existence of PPDL. From figure 5.2(b), we can conclude that after the formation of a double

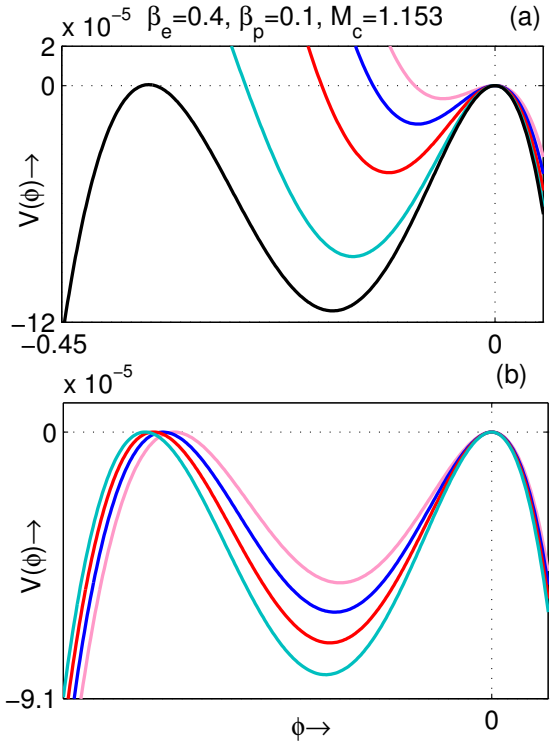

Figure 5.3: $V(\phi)$ is drawn against ϕ for $\gamma = 3$, $\sigma = 0.0001$, $n_{sc} = 0.0515$, $n_{pc} = 0.055$, $n_{dc} = 0.005$, $\sigma_{sc} = 0.095$, $\beta_e = 0.4$, and (a) for $\sigma_{pc} = 0.45$, $\beta_p = 0.1$ (the magenta, blue, red, sky-blue, and black curves correspond to $M = 1.1615, M = 1.17, M = 1.175, M = 1.18$, and $M = 1.18224$, respectively) and (b) for $\sigma_{pc} = 0.39$ and different values of β_p and M (the magenta, blue, red, and sky-blue curves correspond to $\beta_p = 0.1, \beta_p = 0.2, \beta_p = 0.3, \beta_p = 0.4$ and the corresponding value of M_c and M_{NPDL} are respectively $M_c = 1.1517$ and $M_{NPDL} = 1.171514$, $M_c = 1.1582$ and $M_{NPDL} = 1.180635$, $M_c = 1.1648$ and $M_{NPDL} = 1.189972$, and $M_c = 1.1714765$ and $M_{NPDL} = 1.199526$).

layer confirms the existence of a sequences of supersolitons.

In figure 5.3(a), we have drawn $V(\phi)$ against ϕ for $\gamma = 3$, $\sigma = 0.0001$, $n_{sc} = 0.0515$, $n_{pc} = 0.055$, $n_{dc} = 0.005$, $\sigma_{sc} = 0.095$, $\sigma_{pc} = 0.45$, $\beta_e = 0.4$ and $\beta_p = 0.1$. Here, the magenta, blue, red, sky-blue, and black curves correspond to $M = 1.165, 1.17, 1.175, 1.18$, and 1.18224, respectively. From this figure, we see that the black curve ($M = 1.18224$) indicates the NPDL structure and the negative potential solitary waves (NPSWs) exist within the interval $1.1637 \leq M < M_{NPDL}$, and we see that the amplitude of NPSWs increases with

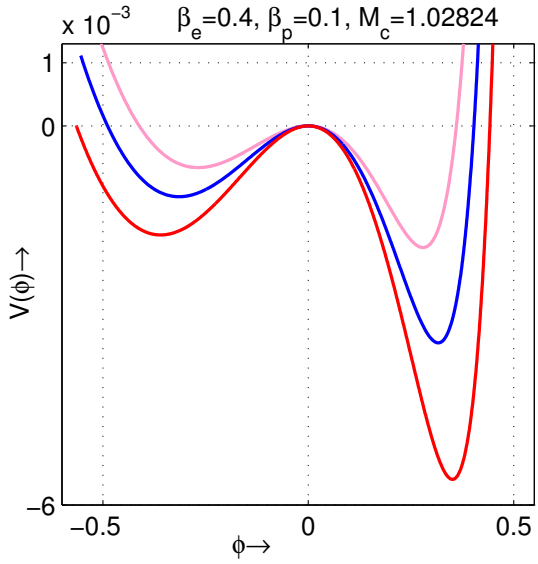

Figure 5.4: $V(\phi)$ is drawn against ϕ for $\gamma = 3$, $\sigma = 0.0001$, $n_{sc} = 0.615$, $n_{pc} = 0.00055$, $n_{dc} = 0.6$, $\sigma_{pc} = 0.39$, $\sigma_{sc} = 0.095$, $\beta_e = 0.4$, and $\beta_p = 0.1$. Here, the magenta, blue, and red curves correspond to $M = 1.06, M = 1.07$, and $M = 1.0806$, respectively.

increasing values of M.

In figure 5.3(b), we have drawn $V(\phi)$ against ϕ for $\gamma = 3$, $\sigma = 0.0001$, $n_{sc} = 0.0515$, $n_{pc} = 0.055$, $n_{dc} = 0.005$, $\sigma_{sc} = 0.095$, $\sigma_{pc} = 0.39$, $\beta_e = 0.4$, and for different values of β_p and M. Here, the magenta, blue, red, and sky-blue curves correspond to $\beta_p = 0.1, \beta_p = 0.2, \beta_p = 0.3, \beta_p = 0.4$, and the corresponding values of M_c and M_{NPDL} are respectively, $M_c = 1.1517$ and $M_{NPDL} = 1.171514$, $M_c = 1.1582$ and $M_{NPDL} = 1.180635$, $M_c = 1.1648$ and $M_{NPDL} = 1.189972$, and $M_c = 1.1714765$ and $M_{NPDL} = 1.199526$. From figure 5.3(b), we get different NPDL structures for different values of β_p.

In figure 5.4, we have drawn $V(\phi)$ against ϕ for $\gamma = 3$, $\sigma = 0.0001$, $n_{sc} = 0.615$, $n_{pc} = 0.00055$, $n_{dc} = 0.6$, $\sigma_{sc} = 0.095$, $\sigma_{pc} = 0.39$, $\beta_e = 0.4$, $\beta_p = 0.1$, and for different values of M. Here, the magenta, blue, and red curves correspond to

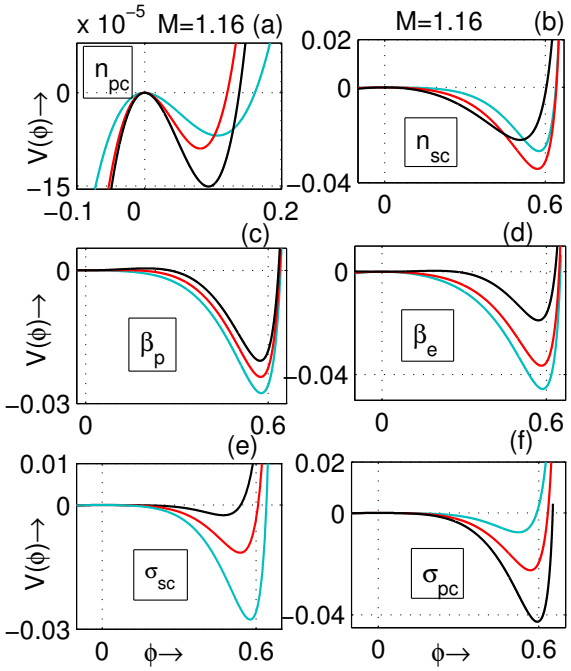

Figure 5.5: The amplitude of PPSW is drawn against ϕ for $\gamma = 3$, $\sigma = 0.0001$, $n_{dc} = 0.005$, and $M = 1.16$ in (a) for different values of n_{pc} (the sky-blue, red, and black curves correspond to $n_{pc} = 0.1$, $n_{pc} = 0.2$, and $n_{pc} = 0.4$, respectively), (b) for different values of n_{sc} (the sky-blue, red, and black curves correspond to $n_{sc} = 0.05$, $n_{sc} = 0.08$, and $n_{sc} = 0.2$, respectively), (c) for different values of β_p (the sky-blue, red, and black curves correspond to $\beta_p = 0.1$, $\beta_p = 0.3$, and $\beta_p = 0.5$, respectively), (d) for different values of β_e (the sky-blue, red, and black curves correspond to $\beta_e = 0.2$, $\beta_e = 0.3$, and $\beta_e = 0.5$, respectively), (e) for different values of σ_{sc} (the sky-blue, red, and black curves correspond to $\sigma_{sc} = 0.095$, $\sigma_{sc} = 0.1$, and $\sigma_{sc} = 0.105$, respectively) and (f) for different values of σ_{pc} (the sky-blue, red, and black curves correspond to $\sigma_{pc} = 0.15$, $\sigma_{pc} = 0.18$, and $\sigma_{pc} = 0.22$, respectively).

$M = 1.06, M = 1.07$, and $M = 1.0806$, respectively. From figure 5.4, we see the coexistence of PPSWs and NPSWs structures. From this figure 5.4, we see that the solitary waves of both polarities exist within the interval $M_c < M < M^{(c)} = 1.0806$, where $M_c = 1.02824$. For $M > M^{(c)}$ only the positive potential solitary waves are formulated.

In figure 5.5, the amplitude of PPSW is drawn against ϕ for (a) for different values of n_{pc}, (b) for different values of n_{sc}, (c) for different values of β_p, (d) for different values of β_e, (e) for different values of σ_{sc}, and (f) for different values of

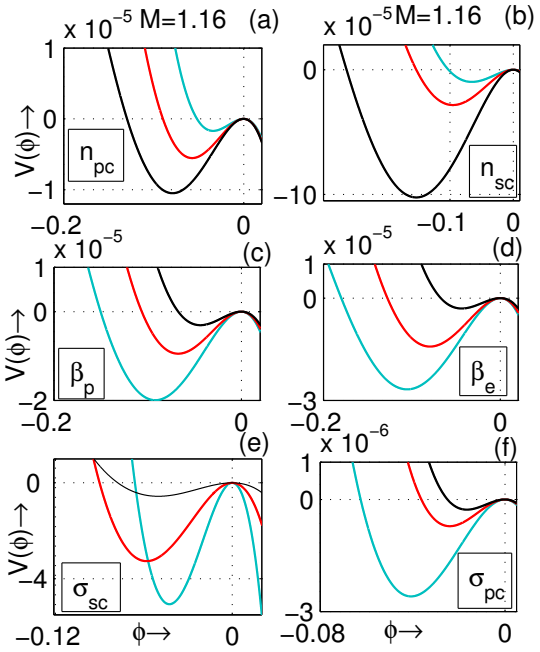

Figure 5.6: The amplitude of NPSW is drawn against ϕ for $\gamma = 3$, $\sigma = 0.0001$, $n_{dc} = 0.005$, and $M = 1.16$ in (a) for different values of n_{pc} (the sky-blue, red, and black curves correspond to $n_{pc} = 0.05$, $n_{pc} = 0.06$, and $n_{pc} = 0.07$, respectively), (b) for different values of n_{sc} (the sky-blue, red, and black curves correspond to $n_{sc} = 0.055$, $n_{sc} = 0.06$, and $n_{sc} = 0.07$, respectively), (c) for different values of β_p (the sky-blue, red, and black curves correspond to $\beta_p = 0.01$, $\beta_p = 0.05$, and $\beta_p = 0.1$, respectively), (d) for different values of β_e (the sky-blue, red, and black curves correspond to $\beta_e = 0.385$, $\beta_e = 0.39$, and $\beta_e = 0.4$, respectively), (e) for different values of σ_{sc} (the sky-blue, red, and black curves correspond to $\sigma_{sc} = 0.01$, $\sigma_{sc} = 0.05$, and $\sigma_{sc} = 0.09$, respectively) ,and (f) for different values of σ_{pc} (the sky-blue, red, and black curves correspond to $\sigma_{pc} = 0.4$, $\sigma_{pc} = 0.5$, and $\sigma_{pc} = 0.6$, respectively).

σ_{pc}. Other values of the parameters are $\gamma = 3$, $\sigma = 0.0001$, $n_{dc} = 0.005$, and $M = 1.16$. In figure 5.5(a), the sky-blue, red, and black curves correspond to $n_{pc} = 0.1, 0.2$, and 0.4, respectively. From figure 5.5(a), we have seen that the amplitude of PPSW decreases with increasing n_{pc} within $0.0479 < n_{pc} < 0.2 = n_{pc}^{(c)}$ and for $n_{pc}^{(c)} < n_{pc} < 0.99$ the amplitude of PPSW increases with increasing n_{pc}. In figure 5.5(b), the sky-blue, red, and black curves correspond to $n_{sc} = 0.05, 0.08$, and 0.2, respectively. From figure 5.5(b), we have seen that the amplitude of PPSW increases with increasing n_{sc} within $0.0274 < n_{sc} < 0.08 = n_{sc}^{(c)}$ and for

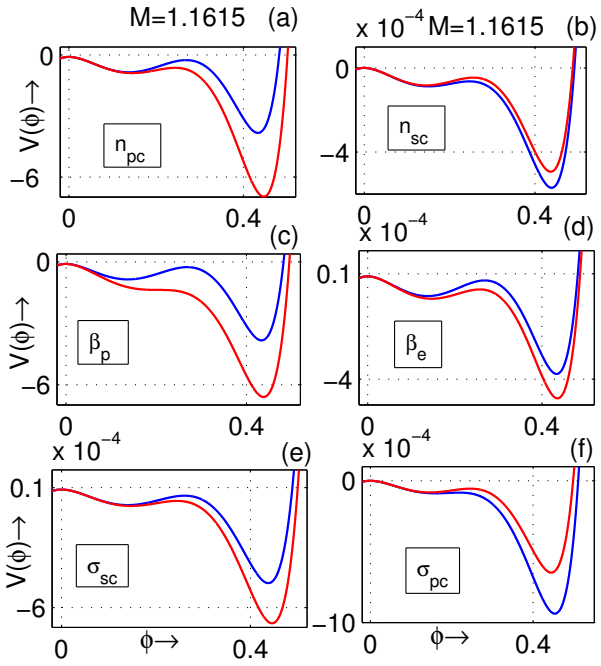

Figure 5.7: The amplitude of PPSS is drawn against ϕ for $\gamma = 3$, $\sigma = 0.0001$, $n_{dc} = 0.005$, and $M = 1.1615$ in (a) for different values of n_{pc} (the red and blue curves correspond to $n_{pc} = 0.0545$ and $n_{pc} = 0.055$, respectively), (b) for different values of n_{sc} (the red and blue curves correspond to $n_{sc} = 0.0518$ and $n_{sc} = 0.052$, respectively), (c) for different values of β_p (the red and blue curves correspond to $\beta_p = 0.08$ and $\beta_p = 0.1$, respectively), (d) for different values of β_e (the red and blue curves correspond to $\beta_e = 0.398$ and $\beta_e = 0.4$, respectively), (e) for different values of σ_{sc} (the red and blue curves correspond to $\sigma_{sc} = 0.0947$ and $\sigma_{sc} = 0.0949$, respectively), and (f) for different values of σ_{pc} (the red and blue curves correspond to $\sigma_{pc} = 0.13$ and $\sigma_{pc} = 0.131$, respectively).

$n_{sc}^{(c)} < n_{sc} < 0.99$ the amplitude of PPSW decreases with increasing n_{sc}. In figure 5.5(c), the sky-blue, red, and black curves correspond to $\beta_p = 0.1, 0.3$, and 0.5, respectively. From figure 5.5(c), we have seen that the amplitude of PPSW decreases with increasing β_p. In figure 5.5(d), the sky-blue, red, and black curves correspond to $\beta_e = 0.2, 0.3$, and 0.5, respectively. From figure 5.5(d), we have seen that the amplitude of PPSW decreases with increasing β_e. In figure 5.5(e), the sky-blue, red, and black curves correspond to $\sigma_{sc} = 0.095, 0.1$, and 0.105, respectively. From figure 5.5(e), we have seen that the amplitude of PPSW

decreases with increasing σ_{sc} within the interval $0.09142 < \sigma_{sc} < 0.13$. In figure 5.5(f), the sky-blue, red, and black curves correspond to $\sigma_{pc} = 0.15, 0.18$, and 0.22, respectively. From figure 5.5(f), we have seen that the amplitude of PPSW increases with increasing σ_{pc} within the interval $0.13 < \sigma_{pc} < 0.2245$.

In figure 5.6, the amplitude of NPSW is drawn against ϕ for (a) for different values of n_{pc}, (b) for different values of n_{sc}, (c) for different values of β_p, (d) for different values of β_e, (e) for different values of σ_{sc}, and (f) for different values of σ_{pc}. Other values of the parameters are $\gamma = 3$, $\sigma = 0.0001$, $n_{dc} = 0.005$, and $M = 1.16$. In figure 5.6(a), the sky-blue, red, and black curves correspond to $n_{pc} = 0.05, 0.06$, and 0.07, respectively. From figure 5.6(a), we have seen that the amplitude of NPSW increases with increasing n_{pc}. In figure 5.6(b), the sky-blue, red, and black curves correspond to $n_{sc} = 0.055, 0.06$, and 0.07, respectively. From figure 5.6(b), we have seen that the amplitude of NPSW increases with increasing n_{sc}. In figure 5.6(c), the sky-blue, red, and black curves correspond to $\beta_p = 0.01, 0.05$, and 0.1, respectively. From figure 5.6(c), we have seen that the amplitude of NPSW decreases with increasing β_p. In figure 5.6(d), the sky-blue, red, and black curves correspond to $\beta_e = 0.385, 0.39$, and 0.4, respectively. From figure 5.6(d), we have seen that the amplitude of NPSW decreases with increasing β_e. In figure 5.6(e), the sky-blue, red, and black curves correspond to $\sigma_{sc} = 0.01, 0.05$, and 0.09, respectively. From figure 5.6(e), we have seen that the amplitude of NPSW increases with increasing σ_{sc} within $\sigma_{sc} < \sigma_{sc}^{(c)}$ and for $\sigma_{sc} > \sigma_{sc}^{(c)}$, the amplitude of NPSW decreases with increasing σ_{sc}. In figure 5.6(f), the sky-blue, red, and black curves correspond to $\sigma_{pc} = 0.4, 0.5$, and 0.6, respectively. From figure 5.6(f), we have seen that the amplitude of NPSW decreases with increasing σ_{pc}.

In figure 5.7, the amplitude of PPSS is drawn against ϕ (a) for different values of n_{pc}, (b) for different values of n_{sc}, (c) for different values of β_p, (d) for different values of β_e, (e) for different values of σ_{sc}, and (f) for different values

of σ_{pc}. Other values of the parameters are $\gamma = 3$, $\sigma = 0.0001$, $n_{dc} = 0.005$, and $M = 1.1615$. In figure 5.7(a), the red and blue curves correspond to $n_{pc} = 0.0545$ and 0.055, respectively. From figure 5.7(a), we have seen that the amplitude of PPSS decreases with increasing n_{pc}. In figure 5.7(b), the red and blue curves correspond to $n_{sc} = 0.0518$ and 0.052, respectively. From figure 5.7(b), we have seen that the amplitude of PPSS increases with increasing n_{sc}. In figure 5.7(c), the red and blue curves correspond to $\beta_p = 0.08$ and 0.1, respectively. From figure 5.7(c), we have seen that the amplitude of PPSS decreases with increasing β_p. In figure 5.7(d), the red and blue curves correspond to $\beta_e = 0.398$ and 0.4, respectively. From figure 5.7(d), we have seen that the amplitude of PPSS decreases with increasing β_e. In figure 5.7(e), the red and blue curves correspond to $\sigma_{sc} = 0.0947$ and 0.0949, respectively. From figure 5.7(e), we have seen that the amplitude of PPSS decreases with increasing σ_{sc}. In figure 5.7(f), the red and blue curves correspond to $\sigma_{pc} = 0.13$ and 0.131, respectively. From figure 5.7(f), we have seen that the amplitude of PPSS increases with increasing σ_{pc}.

5.4 Solitary Structures and Phase Portraits

Differentiating (5.3.1) with respect to ϕ, we get a second-order differential equation of ϕ, and this second-order differential equation can be decomposed into the following two coupled equation

$$\frac{d\phi}{d\xi} = \psi, \qquad \frac{d\psi}{d\xi} = -V^{'}(\phi). \tag{5.4.1}$$

In figures 5.8(a)-5.11(a) and 5.14(a)-5.18(a), $V(\phi)$ is drawn with respect to ϕ whereas in figures 5.8(b)-5.11(b) and 5.14(b)-5.18(b), phase portraits of (5.4.1) have been drawn. One can draw the phase portraits of (5.4.1) to confirm the different DIA solitary structures. One can find that there is a one-one correspondence between the separatrix of the phase portrait of figures 5.8(b)-5.11(b)

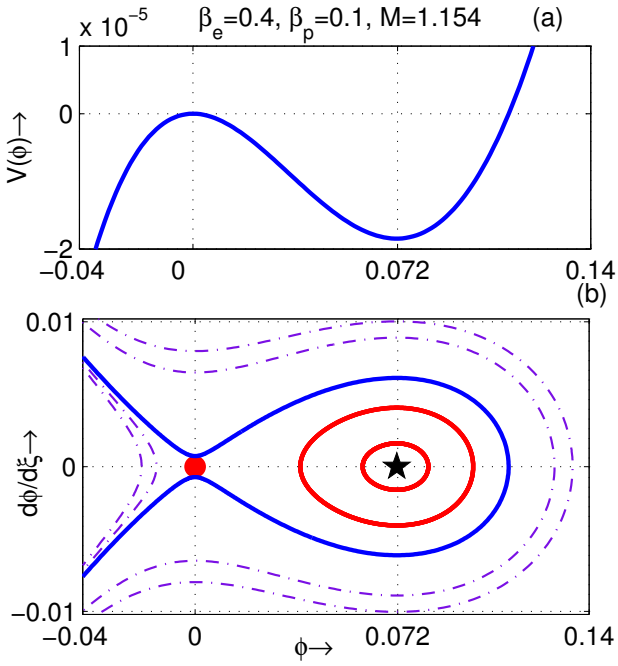

Figure 5.8: $V(\phi)$ (on top) and the phase portrait of the system (5.4.1) (on bottom) are drawn against ϕ for $M = 1.154$, $\gamma = 3$, $\sigma = 0.0001$, $n_{sc} = 0.0515$, $n_{pc} = 0.055$, $n_{dc} = 0.005$, $\sigma_{sc} = 0.095$, $\sigma_{pc} = 0.129$, $\beta_e = 0.4$, and $\beta_p = 0.1$.

and 5.14(b)-5.18(b), with the curve $V(\phi)$ against ϕ of figures 5.8(a)-5.11(a) and 5.14(a)-5.18(a).

Here the origin $(0, 0)$ is an unstable (stable) equilibrium point of the phase portrait of (5.4.1) for the supersonic (subsonic) speed of the waves, i.e., for $M > M_c$ ($M < M_c$) described by the figures (5.8)-(5.11), and figures (5.14)-(5.16) (the figure (5.17), and the figure (5.18)).

Figure 5.8(a) depicts the formation of PPSW before the formation of PPDL, whereas figure 5.8(b) depicts the corresponding phase portrait which contains only one unstable equilibrium point at the origin and a stable equilibrium point. From the ϕ axis of 5.8(b), it is clear that there is only one separatrix that appears to pass through the origin (0, 0), and enclose the stable equilibrium point, viz.,(0.071693, 0).

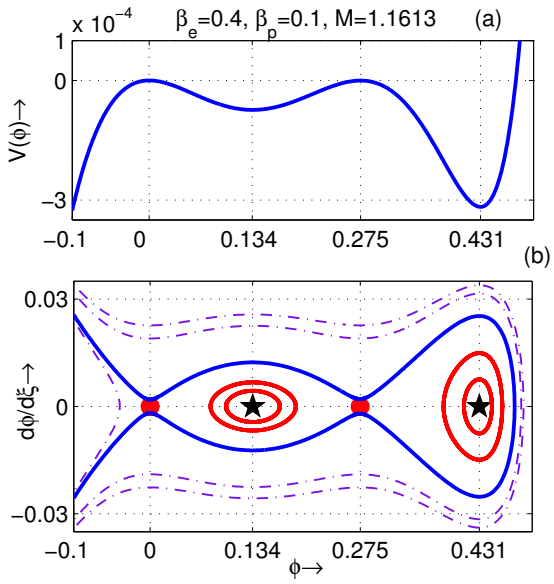

Figure 5.9: $V(\phi)$ (on top) and the phase portrait of the system (5.4.1) (on bottom) are drawn against ϕ for $M = 1.1613$, $\gamma = 3$, $\sigma = 0.0001$, $n_{sc} = 0.0515$, $n_{pc} = 0.055$, $n_{dc} = 0.005$, $\sigma_{sc} = 0.095$, $\sigma_{pc} = 0.129$, $\beta_e = 0.4$, and $\beta_p = 0.1$.

Figure 5.9(a) depicts the PPDL, whereas figure 5.9(b) depicts that the corresponding phase portrait that indicates that the separatrix corresponding to the double layer solution appears to pass through two unstable equilibrium points (0, 0) and (0.27478, 0), and it encloses another two stable equilibrium points (0.13435, 0) and (0.43099, 0). Here the blue curve in both the upper panel and lower panel depicts that there is a one-one correspondence between the separatrix of figure 5.9(b), with the curve $V(\phi)$ against ϕ of figure 5.9(a).

Figure 5.10(a) depicts the PPSS, whereas figure 5.10(b) shows the corresponding phase portrait of PPSS [88, 90]. Following the definition of PPSS as given by Dubinov and Kolotkov, we can analyze the phase portrait of PPSS. From figure 5.10(b), we see that there are two separatrices as shown in the blue curve and magenta curve. The blue separatrix appears to pass through the origin (0, 0), and the magenta separatrix appears to pass through the non-zero unstable

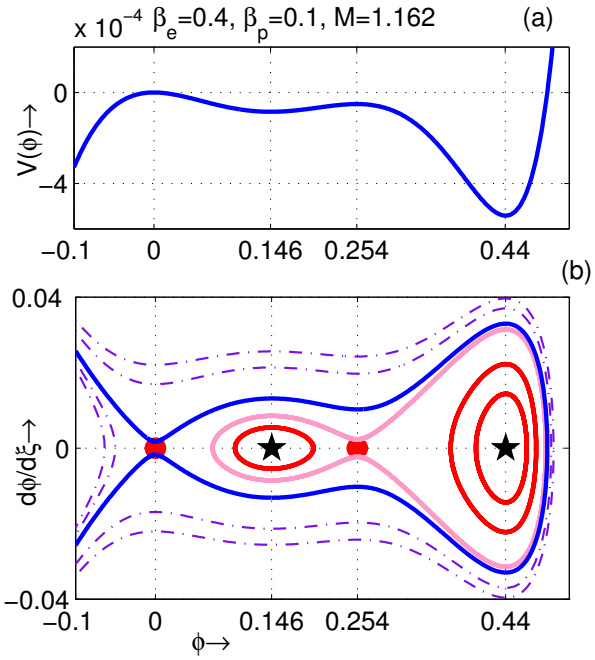

Figure 5.10: $V(\phi)$ (on top) and the phase portrait of the system (5.4.1) (on bottom) are drawn against ϕ for $M = 1.162$, $\gamma = 3$, $\sigma = 0.0001$, $n_{sc} = 0.0515$, $n_{pc} = 0.055$, $n_{dc} = 0.005$, $\sigma_{sc} = 0.095$, $\sigma_{pc} = 0.129$, $\beta_e = 0.4$, and $\beta_p = 0.1$.

equilibrium point (0.25382, 0). The blue separatrix envelopes the magenta separatrix and two stable equilibrium points, viz., (0.14635, 0) and (0.44034, 0). The magenta separatrix encloses two stable equilibrium points.

Figure 5.11(a) depicts the PPSW after the formation of PPDL and sequences of PPSS structures, whereas figure 5.11(b) depicts that the corresponding phase portrait which contains only one unstable equilibrium point at the origin and a stable equilibrium point. From the ϕ axis of 5.11(b), it is clear that there is only one separatrix that appears to pass through the origin (0, 0), and encloses a stable equilibrium point, viz.,(0.46131, 0).

We have also drawn the unstable equilibrium points and stable equilibrium points of (5.4.1) on the ϕ-axis in figure (5.12), for the increasing values of M where $M = M_{PPDL} + \epsilon$. Here $\epsilon = 0$ represents the equilibrium point for a

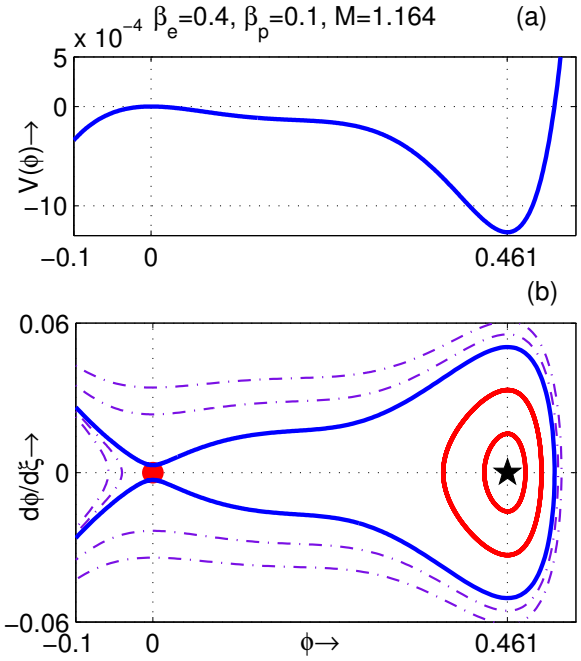

Figure 5.11: $V(\phi)$ (on top) and the phase portrait of the system (5.4.1) (on bottom) are drawn against ϕ for $M = 1.164$, $\gamma = 3$, $\sigma = 0.0001$, $n_{sc} = 0.0515$, $n_{pc} = 0.055$, $n_{dc} = 0.005$, $\sigma_{sc} = 0.095$, $\sigma_{pc} = 0.129$, $\beta_e = 0.4$, and $\beta_p = 0.1$.

double layer solution at $M = M_{PPDL}$ of (5.4.1). For increasing values of M, the distance between the stable equilibrium point (close to the non-zero unstable equilibrium point) and the non-zero unstable equilibrium point decreases, and ultimately both of them vanish from the system. Finally, the system contains only one unstable equilibrium point at the origin and a stable equilibrium point. This figure also depicts the transition from supersolitions to solitary structures after the formation of a double layer and confirms the existence of a sequence of supersolitons.

In figure (5.13), ϕ is drawn against ξ for $\gamma = 3$, $\sigma = 0.0001$, $n_{sc} = 0.0515$, $n_{pc} = 0.055$, $n_{dc} = 0.005$, $\sigma_{sc} = 0.095$, $\sigma_{pc} = 0.129$, $\beta_e = 0.4$, and $\beta_p = 0.1$ and two values of M before and after the formation of PPDL. The red curve represents the solitons before the formation of PPDL for $M = 1.1614$, whereas the blue curve

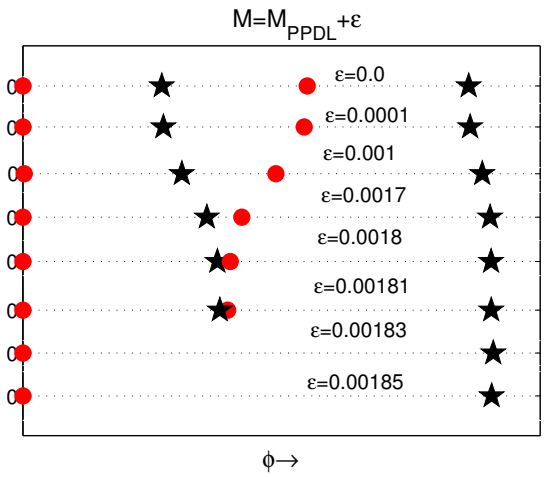

Figure 5.12: Saddle points (solid red circles) and stable equilibrium points (solid black stars) for the dynamical system have been drawn on the ϕ axis for different values of $M = 1.1613 + \epsilon$ when $\gamma = 3$, $\sigma = 0.0001$, $n_{sc} = 0.0515$, $n_{pc} = 0.055$, $n_{dc} = 0.005$, $\sigma_{sc} = 0.095$, $\sigma_{pc} = 0.129$, $\beta_e = 0.4$, and $\beta_p = 0.1$.

represents the solitons after the formation of PPDL for $M = 1.1612$. From that figure, we see that the amplitudes of solitary waves before and after the formation of PPDL have a finite jump.

Figure 5.14(a) depicts NPSW before the formation of NPDL, and 5.14(b) depicts that the corresponding phase portrait that contains only one stable equilibrium point. From the ϕ axis of 5.14(b), it is clear that one separatrix that appears to pass through the origin (0, 0), and encloses a stable equilibrium point, viz.,(-0.12821, 0) on the negative side on the ϕ axis and there is another separatrix that appears to pass through the unstable equilibrium point (-0.28756, 0), and encloses the separatrix that appears to pass through the origin.

Figure 5.15(a) depicts the NPDL, whereas figure 5.15(b) depicts the corresponding phase portrait which shows that the separatrix corresponding to the double layer solution appears to pass through two unstable equilibrium points

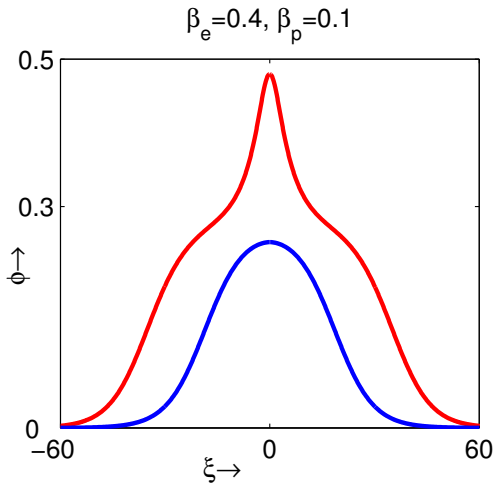

Figure 5.13: ϕ is drawn against ξ for $\gamma = 3$, $\sigma = 0.0001$, $n_{sc} = 0.0515$, $n_{pc} = 0.055$, $n_{dc} = 0.005$, $\sigma_{sc} = 0.095$, $\sigma_{pc} = 0.129$, $\beta_e = 0.4$, and $\beta_p = 0.1$. The red curve corresponds to $M = 1.1614$, and the blue curve corresponds to $M = 1.1612$.

(0, 0) and (-0.2818, 0), and it encloses the stable equilibrium point (-0.13412, 0). Here the blue curve in both the upper panel and lower panel depicts that there is a one-one correspondence between the separatrix of figure 5.15(b) with the curve $V(\phi)$ against ϕ of figure 5.15(a).

Figure 5.16(a) depicts the coexistence of solitary waves of both polarities, whereas figure 5.16(b) depicts the corresponding phase portrait to the coexistence of solitary waves of both polarities. From the phase portrait, we see there is only one blue separatrix. The blue separatrix appears to start and end at the unstable equilibrium point (0, 0). The blue separatrix encloses two stable equilibrium points, one stable equilibrium point (0.23587, 0) lies on the positive side of ϕ-axis, and the other stable equilibrium point(-0.21559, 0) lies on the negative side of ϕ-axis.

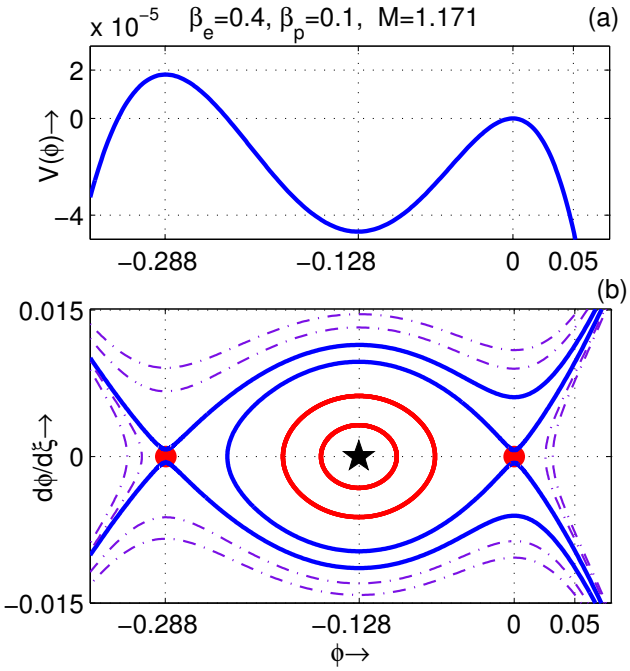

Figure 5.14: $V(\phi)$(on top) and the phase portrait of the system (5.4.1) (on bottom) are drawn against ϕ for $M = 1.171$, $\gamma = 3$, $\sigma = 0.0001$, $n_{sc} = 0.0515$, $n_{pc} = 0.055$, $n_{dc} = 0.005$, $\sigma_{sc} = 0.095$, $\sigma_{pc} = 0.39$, $\beta_e = 0.4$, and $\beta_p = 0.1$.

We have drawn the figure (5.17) and figure (5.18) for the subsonic speed of the waves, i.e., for $M < M_c$ for different values of parameters.

Figure 5.17(a) depicts the $V(\phi)$ vs ϕ curve for $M = 1.11708$, $\gamma = 3$, $\sigma = 0.0001$, $n_{sc} = 0.0515$, $n_{pc} = 0.15$, $n_{dc} = 0.005$, $\sigma_{sc} = 0.095$, $\sigma_{pc} = 0.9$, $\beta_e = 0.4$, $\beta_p = 0.1$ and for the value of $M_c = 1.1501$, whereas the figure 5.17(b) depicts the corresponding phase portrait. Figure 5.17(b) depicts the phase portrait of super-nonlinear periodic waves [89, 90]. From figure 5.17(b), we have seen that there are two separatrices, as shown in the blue curve and magenta curve. The blue separatrix appears to pass through a non-zero unstable equilibrium point $(-0.6049, 0)$, and the magenta separatrix appears to pass through another non-zero unstable equilibrium point (0.25703, 0). The blue separatrix envelopes the magenta separatrix. And there are two stable equilibrium points, viz., origin (0,

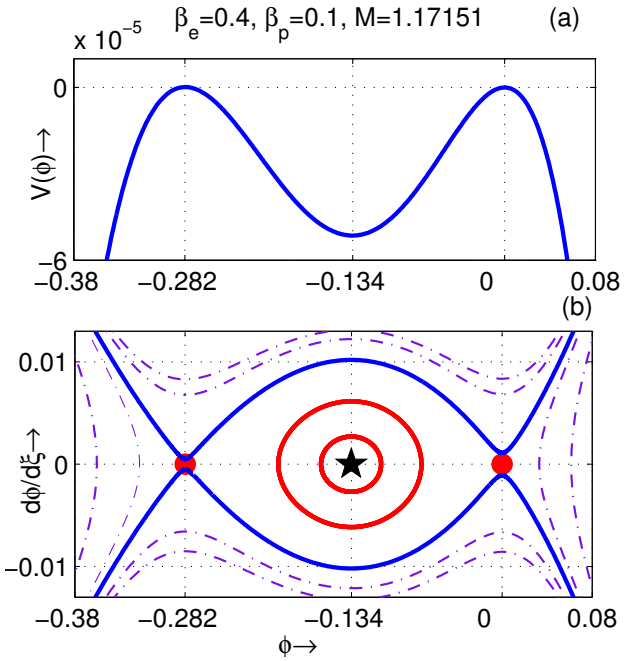

Figure 5.15: $V(\phi)$ (on top) and the phase portrait of the system (5.4.1) (on bottom) are drawn against ϕ for $M = 1.17151$, $\gamma = 3$, $\sigma = 0.0001$, $n_{sc} = 0.0515$, $n_{pc} = 0.055$, $n_{dc} = 0.005$, $\sigma_{sc} = 0.095$, $\sigma_{pc} = 0.39$, $\beta_e = 0.4$, and $\beta_p = 0.1$.

0) and (0.41416, 0), which are enclosed by the magenta separatrix. The magenta separatrix is surrounded by sequences of sky-blue closed curves that are due to super-nonlinear periodic waves.

Figure 5.18(a) also depicts $V(\phi)$ vs ϕ curve for $M = 1.13$, $\gamma = 3$, $\sigma = 0.0001$, $n_{sc} = 0.075$, $n_{pc} = 0.162$, $n_{dc} = 0.005$, $\sigma_{sc} = 0.093$, $\sigma_{pc} = 0.6$, $\beta_e = 0.38$, $\beta_p = 0.4$, and for the value of $M_c = 1.1434672$, whereas figure 5.18(b) depicts the corresponding phase portrait. Figure 5.18(b) depicts the phase portrait of super-nonlinear periodic waves [89, 90]. From figure 5.18(b), we have seen that there are two separatrices as shown in the blue curve and magenta curve. The blue separatrix appears to pass through a non-zero unstable equilibrium point (-0.42851, 0), and the magenta separatrix appears to pass through another non-zero unstable equilibrium point (0.1654, 0). The blue separatrix envelopes the

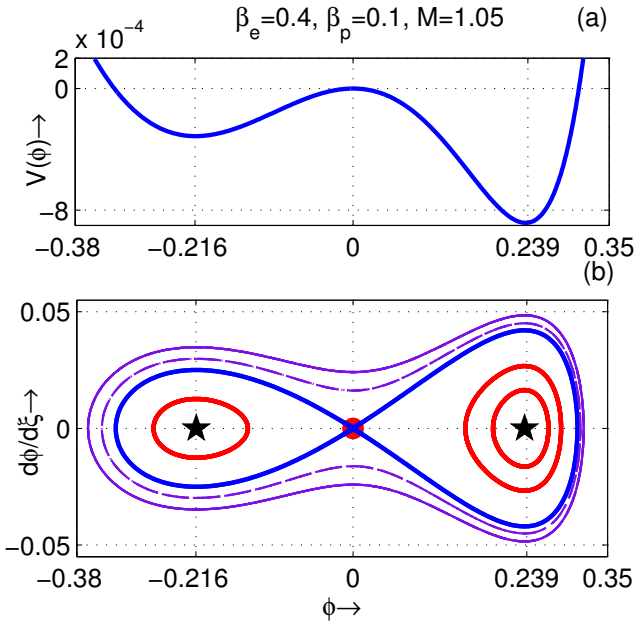

Figure 5.16: $V(\phi)$ (on top) and the phase portrait of the system (5.4.1) (on bottom) are drawn against ϕ for $M = 1.05$, $\gamma = 3$, $\sigma = 0.0001$, $n_{sc} = 0.61$, $n_{pc} = 0.00055$, $n_{dc} = 0.6$, $\sigma_{sc} = 0.095$, $\sigma_{pc} = 0.39$, $\beta_e = 0.4$, and $\beta_p = 0.1$.

magenta separatrix. And there are two stable equilibrium points, viz., (0, 0) and (0.3713, 0), which are enclosed by the magenta separatrix. The magenta separatrix is surrounded by sequences of sky-blue closed curves that are due to super-nonlinear periodic waves.

5.5 Conclusions

In this **chapter**, we have studied the existence of different solitary structures in a collisionless unmagnetized five components e-p-i-d plasma consisting of warm adiabatic ions, nonthermal positrons, negatively charged static dust grains, and two distinct populations of electrons at different temperatures. Using the Sagdeev pseudo-potential technique, the energy integral equation has been derived. We have observed the existence of PPSWs, NPSWs, the coexistence of both PPSWs

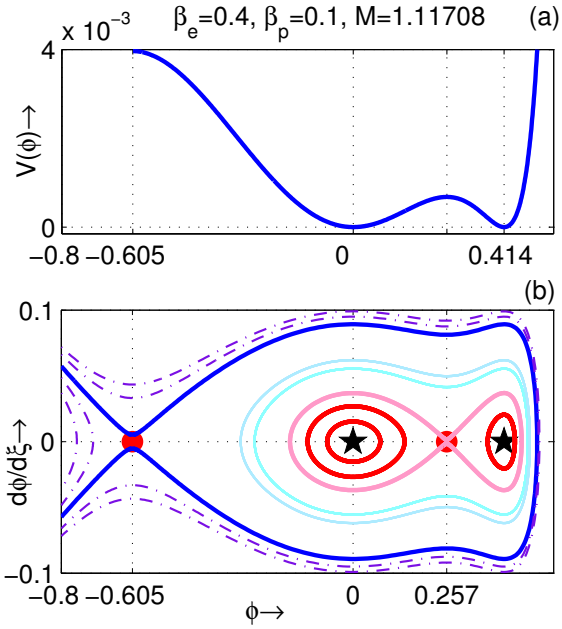

Figure 5.17: $V(\phi)$ (on top) and the phase portrait of the system (5.4.1) (on bottom) are drawn against ϕ for $M = 1.11708$, $\gamma = 3$, $\sigma = 0.0001$, $n_{sc} = 0.0515$, $n_{pc} = 0.15$, $n_{dc} = 0.005$, $\sigma_{sc} = 0.095$, $\sigma_{pc} = 0.9$, $\beta_e = 0.4$, and $\beta_p = 0.1$.

and NPSWs, NPDLs, PPDLs, supersolitons, and super-nonlinear periodic waves. However, considering the dust dynamics, paper [367] reported the existence of large amplitude hybrid DIA solitary structures.

We have the following observations on the amplitude of solitary structures:

(1) Effects of β_e:

(A) ON PPSW: The amplitude of PPSW decreases with increasing β_e within the domain of existence PPSW. For $\gamma = 3$, $n_{sc} = 0.0515$, $n_{pc} = 0.055$, $n_{dc} = 0.005$, $\sigma = 0.0001$, $\sigma_{sc} = 0.095$, $\sigma_{pc} = 0.19$, $\beta_p = 0.1$, and $M = 1.16$, the interval of existence of β_e is $(0.1407, 0.57)$, i.e., $0.1407 < \beta_e < 0.57$. Therefore, for the fixed values of the above parameters, the amplitude of PPSW decreases with increasing β_e when β_e is restricted by the inequality $0.1407 < \beta_e < 0.57$.

(B) ON NPSW: The amplitude of NPSW decreases with increasing β_e within the

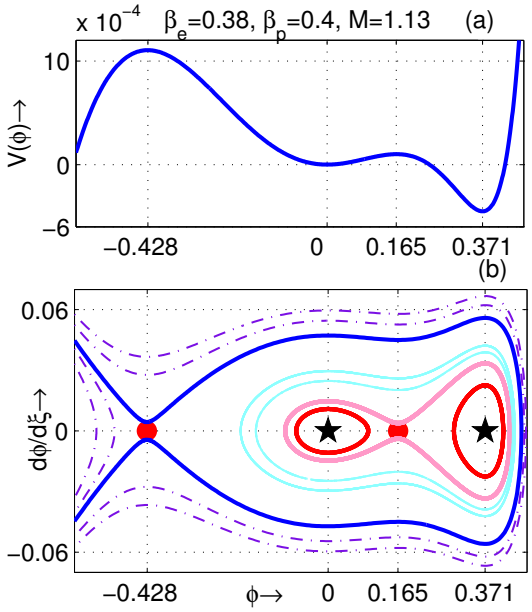

Figure 5.18: $V(\phi)$ (on top) and the phase portrait of the system (5.4.1) (on bottom) are drawn against ϕ for $M = 1.13$, $\gamma = 3$, $\sigma = 0.0001$, $n_{sc} = 0.075$, $n_{pc} = 0.162$, $n_{dc} = 0.005$, $\sigma_{sc} = 0.093$, $\sigma_{pc} = 0.6$, $\beta_e = 0.38$, and $\beta_p = 0.4$.

domain of existence NPSW. For $\gamma = 3$, $n_{sc} = 0.0515$, $n_{pc} = 0.055$, $n_{dc} = 0.005$, $\sigma = 0.0001$, $\sigma_{sc} = 0.095$, $\sigma_{pc} = 0.39$, $\beta_p = 0.1$, and $M = 1.16$, the amplitude of NPSW decreases with increasing β_e when $0.385 < \beta_e < 0.42$.

(C) ON PPSS: The amplitude of PPSS decreases with increasing β_e within the domain of existence PPSS. For $\gamma = 3$, $n_{sc} = 0.0515$, $n_{pc} = 0.055$, $n_{dc} = 0.005$, $\sigma = 0.0001$, $\sigma_{sc} = 0.095$, $\sigma_{pc} = 0.129$, $\beta_p = 0.1$, and $M = 1.1615$, the amplitude of PPSS decreases with increasing β_e when $0.395 < \beta_e < 0.4005$.

(2) Effects of β_p:

(A) ON PPSW: The amplitude of PPSW decreases with increasing β_p within the domain of existence PPSW. For $\gamma = 3$, $n_{sc} = 0.0515$, $n_{pc} = 0.055$, $n_{dc} = 0.005$, $\sigma = 0.0001$, $\sigma_{sc} = 0.095$, $\sigma_{pc} = 0.19$, $\beta_e = 0.4$, and $M = 1.16$, the amplitude of PPSW decreases with increasing β_p when $0 < \beta_p < 0.57$.

(B) ON NPSW: The amplitude of NPSW decreases with increasing β_p within the

domain of existence NPSW. For $\gamma = 3$, $n_{sc} = 0.0515$, $n_{pc} = 0.055$, $n_{dc} = 0.005$, $\sigma = 0.0001$, $\sigma_{sc} = 0.095$, $\sigma_{pc} = 0.39$, $\beta_e = 0.4$, and $M = 1.16$, the amplitude of NPSW decreases with increasing β_p when $0 < \beta_p < 0.2$.

(C) ON PPSS: The amplitude of PPSS decreases with increasing β_p within the domain of existence PPSS. For $\gamma = 3$, $n_{sc} = 0.0515$, $n_{pc} = 0.055$, $n_{dc} = 0.005$, $\sigma = 0.0001$, $\sigma_{sc} = 0.095$, $\sigma_{pc} = 0.129$, $\beta_e = 0.4$, and $M = 1.1615$, the amplitude of PPSS decreases with increasing β_p when $0.07 < \beta_p < 0.101$.

(3) Effects of σ_{sc}:

(A) ON PPSW: The amplitude of PPSW decreases with increasing σ_{sc} within the domain of existence PPSW. For $\gamma = 3$, $n_{sc} = 0.0515$, $n_{pc} = 0.055$, $n_{dc} = 0.005$, $\sigma = 0.0001$, $\sigma_{pc} = 0.19$, $\beta_e = 0.4$, $\beta_p = 0.1$, and $M = 1.16$, the amplitude of PPSW decreases with increasing σ_{sc} when $0.0914 < \sigma_{sc} < 0.13$.

(B) ON NPSW: The amplitude of NPSW increases with increasing σ_{sc} for the interval $\sigma_{sc}^{(s)} < \sigma_{sc} < \sigma_{sc}^{(c)}$ whereas the amplitude of NPSW decreases with increasing σ_{sc} within the interval $\sigma_{sc}^{(c)} < \sigma_{sc} < \sigma_{sc}^{(t)}$. For $\gamma = 3$, $n_{sc} = 0.0515$, $n_{pc} = 0.055$, $n_{dc} = 0.005$, $\sigma = 0.0001$, $\sigma_{pc} = 0.39$, $\beta_e = 0.4$, $\beta_p = 0.1$, and $M = 1.16$, the values of $\sigma_{sc}^{(s)}$, $\sigma_{sc}^{(c)}$, $\sigma_{sc}^{(t)}$ are, respectively, 0.0001, 0.078 and 0.105.

(C) ON PPSS: The amplitude of PPSS decreases with increasing σ_{sc} within the domain of existence PPSS. For $\gamma = 3$, $n_{sc} = 0.0515$, $n_{pc} = 0.055$, $n_{dc} = 0.005$, $\sigma = 0.0001$, $\sigma_{pc} = 0.129$, $\beta_e = 0.4$, $\beta_p = 0.1$, and $M = 1.1615$, the amplitude of PPSS decreases with increasing σ_{sc} when $0.0945 < \sigma_{sc} < 0.0951$.

(4) Effects of σ_{pc}:

(A) ON PPSW: The amplitude of PPSW increases with increasing σ_{pc} within the domain of existence PPSW. For $\gamma = 3$, $n_{sc} = 0.0515$, $n_{pc} = 0.055$, $n_{dc} = 0.005$, $\sigma = 0.0001$, $\sigma_{sc} = 0.095$, $\beta_e = 0.4$, $\beta_p = 0.1$, and $M = 1.16$, the amplitude of PPSW increases with increasing σ_{pc} when $0.13 < \sigma_{pc} < 0.2245$.

(B) ON NPSW: The amplitude of NPSW decreases with increasing σ_{pc} within the domain of existence NPSW. For $\gamma = 3$, $n_{sc} = 0.0515$, $n_{pc} = 0.055$, $n_{dc} = 0.005$,

$\sigma = 0.0001$, $\sigma_{sc} = 0.095$, $\beta_e = 0.4$, $\beta_p = 0.1$, and $M = 1.16$, the amplitude of NPSW decreases with increasing σ_{pc} when $0.327 < \sigma_{pc} < 0.65$.

(C) ON PPSS: The amplitude of PPSS increases with increasing σ_{pc} within the domain of existence PPSS. For $\gamma = 3$, $n_{sc} = 0.0515$, $n_{pc} = 0.055$, $n_{dc} = 0.005$, $\sigma = 0.0001$, $\sigma_{sc} = 0.095$, $\beta_e = 0.4$, $\beta_p = 0.1$, and $M = 1.1615$, the amplitude of PPSS increases with increasing σ_{pc} when $0.129 < \sigma_{pc} < 0.132$.

(5) Effects of $\mathbf{n_{pc}}$:

(A) ON PPSW: The amplitude of PPSW decreases with increasing n_{pc} for $n_{pc}^{(s)} < n_{pc} < n_{pc}^{(c)}$ whereas the amplitude of PPSW increases with increasing n_{pc} for $n_{pc}^{(c)} < n_{pc} < n_{pc}^{(t)}$. For $\gamma = 3$, $n_{sc} = 0.0515$, $n_{dc} = 0.005$, $\sigma = 0.0001$, $\sigma_{sc} = 0.095$, $\sigma_{pc} = 0.19$, $\beta_e = 0.4$, $\beta_p = 0.1$, and $M = 1.16$, the values of $n_{pc}^{(s)}$, $n_{pc}^{(c)}$, $n_{pc}^{(t)}$ are, respectively, 0.0479, 0.2 and 0.99.

(B) ON NPSW: The amplitude of NPSW increases with increasing n_{pc} within the domain of existence NPSW. For $\gamma = 3$, $n_{sc} = 0.0515$, $n_{dc} = 0.005$, $\sigma = 0.0001$, $\sigma_{sc} = 0.095$, $\sigma_{pc} = 0.39$, $\beta_e = 0.4$, $\beta_p = 0.1$, and $M = 1.16$, the amplitude of NPSW increases with increasing n_{pc} when $0.035 < n_{pc} < 0.0675$.

(C) ON PPSS: The amplitude of PPSS decreases with increasing n_{pc} within the domain of existence PPSS. For $\gamma = 3$, $n_{sc} = 0.0515$, $n_{dc} = 0.005$, $\sigma = 0.0001$, $\sigma_{sc} = 0.095$, $\sigma_{pc} = 0.129$, $\beta_e = 0.4$, $\beta_p = 0.1$, and $M = 1.1615$, the amplitude of PPSS decreases with increasing n_{pc} when $0.053 < n_{pc} < 0.055$.

(6) Effects of $\mathbf{n_{sc}}$:

(A) ON PPSW: The amplitude of PPSW increases with increasing n_{sc} for $n_{sc}^{(s)} < n_{sc} < n_{sc}^{(c)}$ whereas the amplitude of PPSW decreases with increasing n_{sc} for $n_{sc}^{(c)} < n_{sc} < n_{sc}^{(t)}$. For $\gamma = 3$, $n_{pc} = 0.055$, $n_{dc} = 0.005$, $\sigma = 0.0001$, $\sigma_{sc} = 0.095$, $\sigma_{pc} = 0.19$, $\beta_e = 0.4$, $\beta_p = 0.1$ and $M = 1.16$, the values of $n_{sc}^{(s)}$, $n_{sc}^{(c)}$, $n_{sc}^{(t)}$ are, respectively, 0.0274, 0.08 and 0.99.

(B) ON NPSW: The amplitude of NPSW increases with increasing n_{sc} within the domain of existence NPSW. For $\gamma = 3$, $n_{pc} = 0.055$, $n_{dc} = 0.005$, $\sigma = 0.0001$,

$\sigma_{sc} = 0.095$, $\sigma_{pc} = 0.39$, $\beta_e = 0.4$, $\beta_p = 0.1$, and $M = 1.16$, the amplitude of NPSW increases with increasing n_{sc} when $0.05 < n_{sc} < 0.079$.

(C) ON PPSS: The amplitude of PPSS increases with increasing n_{sc} within the domain of existence PPSS. For $\gamma = 3$, $n_{pc} = 0.055$, $n_{dc} = 0.005$, $\sigma = 0.0001$, $\sigma_{sc} = 0.095$, $\sigma_{pc} = 0.129$, $\beta_e = 0.4$, $\beta_p = 0.1$, and $M = 1.1615$, the amplitude of PPSS increases with increasing n_{sc} when $0.0514 < n_{sc} < 0.0525$.

(7) Effects of M:

The amplitude of any solitary structures increases with increasing M within the domain of existence of solitary structures.

(8) Effects of different parameters on double layers

It is not possible to consider the effects of different parameters of the system on the double layer solution. Because a double layer soliton exists for fixed values of the parameters of the system or in other words a sequence of solitary structures of increasing amplitude (NPSW or PPSW) or decreasing amplitude (PPSS) converges to the double layer soliton if it exists. Solitary structures (before the formation of the double layer) of increasing amplitude end with a double layer. Soliton structures (after the formation of the double layer) of decreasing amplitude end with a double layer soliton.

(9) We have also studied the coexistence of opposite polarities.

(10) Phase portrait analysis of DIA waves through the coupled equation (5.4.1) **shows the following facts:**

(A) For supersonic speed of the waves ($M > M_c$), the origin (0, 0) is an unstable equilibrium point, whereas, for the subsonic speed of the waves ($M < M_c$), the origin (0, 0) is a stable equilibrium point.

(B) Every minimum value of the potential function $V(\phi)$ corresponds to a stable equilibrium point, whereas, maximum value of potential function $V(\phi)$ corresponds to an unstable equilibrium point.

(C) Every closed curve about any stable equilibrium point corresponds to a periodic wave solution, whereas, a separatrix that appears to pass through the unstable equilibrium point at the origin (0, 0) enclosing a stable equilibrium point corresponds to a solitary waves.

(D) The separatrix through (0, 0) which encloses another separatrix and more than one stable equilibrium points corresponds to a supersolitons.

(E) For the subsonic speed ($M < M_c$), we have observed existence of a separatrix passes through a non-zero unstable equilibrium point enveloping the another separatrix that appears to pass through the another non-zero unstable equilibrium point. The inner separatrix encloses at least two stable equilibrium points, one of which is (0, 0). Any closed curve within inner and outer separatrix as shown by sky-blue colour in the figures 5.17(b) and 5.18(b) are due to super-nonlinear periodic waves.

(F)From the phase portraits of the figures 5.8(b) and 5.11(b), i.e, before and after the formation of PPDL, it is clear that there is no characteristic difference between these two figures. In both figures, there is only one separatrix passing through the origin enclosing a stable equilibrium point.

(11) There is a jump-type discontinuity between the amplitudes of positive potential solitary structures just before and just after the formation of PPDL, i.e, the amplitude of soliton after the formation of PPDL is much greater than that of the soliton before the formation of PPDL.

(12) Smooth transition: PPSW (before the formation of PPDL) $\rightarrow$ PPDL $\rightarrow$ PPSS $\rightarrow$ PPSW (after the formation of PPDL) has been confirmed for the present five components plasma model using the stable and unstable equilibrium points lie on the ϕ axis and that confirms the existence of a sequence of supersolitons. For negative potential solitary structures, we also have smooth transitions from NPSWs to NPDLs only if NPDLs exists.

Chapter 6

Arbitrary amplitude DIA nonlinear wave structures at $M = M_c$ in an unmagnetized five components plasma ¶

In this Chapter, we have investigated the arbitrary amplitude dust-ion acoustic (DIA) nonlinear wave structures at the acoustic (sonic) speed $M = M_c$ in a collisionless unmagnetized five components electron-positron-ion-dusty (e-p-i-d) plasma system as consider in **Chapter -5**. The present plasma system confirms the existence of NPSWs, PPSWs and NPDLs at the acoustic speed $M = M_c$. We have studied the effect of different parameters of the system on the amplitude of PPSWs, NPSWs and NPDLs at $M = M_c$. We have also analyzed the difference between various DIA nonlinear wave structures at supersonic speed, subsonic speed and sonic speed through phase portraits of the dynamical system corresponding to nonlinear DIA wave structures.

¶ ***Communicated***

6.1 Introduction

In unmagnetized plasma, arbitrary amplitude ion acoustic (IA) or dust-ion acoustic (DIA) solitary structures at the supersonic ($M > M_c$) speed and supernonlinear periodic waves at the subsonic ($M < M_c$) speed have been studied by several authors [56, 75, 77, 79, 81, 82, 89, 91, 166, 297, 298, 322]. They have studied different kinds of nonlinear wave structures including supersolitons, double layers and supernonlinear periodic waves. At the sonic speed ($M = M_c$) of the wave, some authors [83, 102, 103, 146, 298, 403–406] have observed dust acoustic (DA), IA and DIA solitary structures by considering various unmagnetized plasmas. By considering a collisionless unmagnetized plasma system, positive potential DA solitary structure was observed by Verheest and Hellberg [102] at the sonic speed. This was the first observation of DA solitary structure at the sonic speed. Later Das *et al.* [103] established analytically the conditions for the existence of solitary structures at the sonic speed for any unmagnetized collisionless plasma system. In the same paper, they have considered DA solitary structures at the acoustic speed by using the conditions proved in this paper. Using the results of Das *et al.* [103], Paul *et al.* [83] studied DIA solitary structures at the sonic speed in a collisionless unmagnetized four components plasma system. For the first time, Debnath and Bandyopadhyay [101] studied IA solitary waves at acoustic speed in a collisionless magnetized plasma. In the present **chapter**, we have studied DIA nonlinear wave structures at sonic speed for the plasma system considered in **Chapter -5**.

For easy readability of this **Chapter**, we have used the same set of basic equations (5.2.1)-(5.2.4) of **Chapter- 5**. The basic equations are given in the next section along with the expression of the number density of nonthermal electrons, the number density of isothemal electrons, the number density nonthermal positrons and the number density of dust grains.

6.2 Basic Equations

In this **chapter**, we have considered an unmagnetized collisionless five components plasma system consisting of adiabatic warm ions, nonthermal positrons nonthermal electrons, isothermal electrons and negatively charged immobile dust grains. Basically, we have considered the same plasma system of **Chapter-5**. We have considered the following equations for ion fluid:

$$\frac{\partial n_i}{\partial t} + \frac{\partial}{\partial x}(n_i u_i) = 0, \tag{6.2.1}$$

$$\left(\frac{\partial}{\partial t} + u_i \frac{\partial}{\partial x}\right) u_i + \frac{\sigma}{n_i}\frac{\partial P_i}{\partial x} + \frac{\partial \phi}{\partial x} = 0, \tag{6.2.2}$$

$$\frac{\partial P_i}{\partial t} + u_i \frac{\partial P_i}{\partial x} + \gamma P_i \frac{\partial u_i}{\partial x} = 0, \tag{6.2.3}$$

$$\frac{\partial^2 \phi}{\partial x^2} = n_{ce} + n_{se} - n_p - n_i + Z_d n_{d0}. \tag{6.2.4}$$

where the equation (6.2.1) represents the continuity equation for ions, the equation (6.2.2) represents the equation of motion for ions, the equation (6.2.3) represents the pressure equation of ions fluid and the equation (6.2.4) represents the Poisson equation.

The equations (6.2.1)-(6.2.4) are supplemented by the following equations of number density of nonthermal positrons, number density of nonthermal electrons, number density of isothemal electrons and number density of the dust grains, respectively:

$$n_p = \overline{n}_{p0}(1 + \beta_p \sigma_p \phi + \beta_p \sigma_p^2 \phi^2) \exp(-\sigma_p \phi), \tag{6.2.5}$$

$$n_{ce} = \overline{n}_{c0}(1 - \beta_e \sigma_c \phi + \beta_e \sigma_c^2 \phi^2) \exp(\sigma_c \phi), \tag{6.2.6}$$

$$n_{se} = \overline{n}_{s0} \exp(\sigma_s \phi), \tag{6.2.7}$$

$$n_d = \overline{n}_{d0}. \tag{6.2.8}$$

Here, n_θ ($\theta = i, se, ce, p$ and d for ions, isothermal electrons, nonthermal electrons, nonthermal positrons and dust particulates) is the number density of θ-th species of particles, u_i is the ion fluid velocity along x - axis, the electrostatic potential is ϕ, the ion pressure is P_i, the spatial variable is x, and time is t, respectively. Here, n_θ, u_i, ϕ, P_i, x and t are normalized by n_{i0}, c_s, $\frac{K_B T_{pef}}{e}$, $n_{i0} K_B T_i$, λ_D and ω_p^{-1}, respectively. The number of negative unit charges residing on the dust grain surface is denoted by Z_d, the charge of an electron is $-e$, the ratio of two specific heats is $\gamma(= 3)$, the Boltzmann constant is K_B, $\sigma = \frac{T_i}{T_{pef}}$, $\lambda_D \left(= \sqrt{\frac{K_B T_{pef}}{4\pi e^2 n_{i0}}} \right)$ (Debye length of the plasma system), $\omega_p = \sqrt{\frac{4\pi e^2 n_{i0}}{m_i}}$, $c_s = \sqrt{\frac{K_B T_{pef}}{m_i}}$, the average temperature of an ion is T_i, the equilibrium number density of an ion is n_{i0}, the mass of an ion is m_i and the nonthermal parameter β_p (β_e) is associated with the nonthermal velocity distributions of hot positrons (electrons). Also $\overline{n}_{j0} = \frac{n_{j0}}{n_{i0}}$ ($j = c, s, p$ and d for nonthermal electrons, isothermal electrons, nonthermal positrons and dust particulates), where n_{j0} is the equilibrium number density of j-th species and $\sigma_k = \frac{T_{pef}}{T_k}$ ($k = se, ce$ and p for isothermal electrons, nonthermal electrons and nonthermal positrons), where T_k is the average temperature of k-th species. T_{pef} is given by the following equation:

$$\frac{n_{c0}}{T_{ce}} + \frac{n_{s0}}{T_{se}} + \frac{n_{p0}}{T_p} = \frac{n_{c0} + n_{s0} - n_{p0} + Z_d n_{d0}}{T_{pef}}. \tag{6.2.9}$$

The charge neutrality condition is given by

$$n_{c0} + n_{s0} + Z_d n_{d0} - n_{i0} - n_{p0} = 0. \tag{6.2.10}$$

Introducing the new variables $\overline{n}_{j0}$ and σ_k, condition of charge neutrality (6.2.10) and equation (6.2.9), can be written in the following form:

$$\overline{n}_{c0}\sigma_c + \overline{n}_{s0}\sigma_s + \overline{n}_{p0}\sigma_p = 1, \tag{6.2.11}$$

$$\overline{n}_{c0} + \overline{n}_{s0} - \overline{n}_{p0} + \overline{N}_{d0} = 1, \tag{6.2.12}$$

where $Z_d n_{d0} = N_{d0} \Longleftrightarrow Z_d \overline{n}_{d0} = \overline{N}_{d0}$.

We have introduced the following new parameters $n_{sc} = \frac{n_{s0}}{n_{c0}}, n_{pc} = \frac{n_{p0}}{n_{c0}}, n_{dc} = \frac{N_{d0}}{n_{c0}}, \sigma_{sc} = \frac{T_{se}}{T_{ce}}, \sigma_{pc} = \frac{T_p}{T_{ce}}$.

Solving (6.2.11) and (6.2.12), we get

$$(\overline{n}_{c0}, \overline{n}_{s0}, \overline{n}_{p0}, \overline{N}_{d0}, \sigma_c, \sigma_s, \sigma_p) = \left(\Lambda, \Lambda n_{sc}, \Lambda n_{pc}, \Lambda n_{dc}, \Gamma\sigma_{sc}\sigma_{pc}, \Gamma\sigma_{pc}, \Gamma\sigma_{sc}\right), \tag{6.2.13}$$

where

$$\Lambda = \frac{1}{1 + n_{sc} - n_{pc} + n_{dc}}, \Gamma = \frac{(1 + n_{sc} - n_{pc} + n_{dc})}{\sigma_{sc}\sigma_{pc} + n_{sc}\sigma_{pc} + n_{pc}\sigma_{sc}}.$$

6.3 Energy Integral

To study the arbitrary amplitude DIA waves at sonic speed, we consider the same transformation of Paul *et al.* [83] and we apply the following boundary conditions

$$\left(n_i, u_i, \phi, \frac{d\phi}{d\xi}, P_i\right) \to (1, 0, 0, 0, 1) \text{ as } \xi \to -\infty \text{ or } \infty.$$

Shifting the basic equation in the wave frame, we get the following energy integral:

$$\frac{1}{2}\left(\frac{d\phi}{d\xi}\right)^2 + V(\phi) = 0. \tag{6.3.1}$$

Where $V(\phi)$ is known as the Sagdeev pseudo-potential and the expression of $V(\phi)$ is

$$V(M, \phi) = V(\phi) = V_i + \frac{\overline{n}_{p0}}{\sigma_p}V_p - \frac{\overline{n}_{c0}}{\sigma_c}V_{ce} - \frac{\overline{n}_{s0}}{\sigma_s}V_{se} - \overline{N}_{d0}V_d, \tag{6.3.2}$$

where

$$V_i = (M^2 + \sigma) - n_i(M^2 + 3\sigma - 2\phi - 2\sigma n_i^2), \tag{6.3.3}$$

$$n_i = \frac{\sqrt{2}M}{\sqrt{\phi_M - \phi} + \sqrt{\psi_M - \phi}}, \tag{6.3.4}$$

$$\phi_M = \frac{(M + \sqrt{3\sigma})^2}{2}, \tag{6.3.5}$$

$$\psi_M = \frac{(M - \sqrt{3\sigma})^2}{2}, \tag{6.3.6}$$

$$V_p = (1 + 3\beta_p) - (1 + 3\beta_p + 3\beta_p\sigma_p\phi + \beta_p\sigma_p^2\phi^2)\exp(-\sigma_p\phi), \tag{6.3.7}$$

$$V_{ce} = (1 + 3\beta_e - 3\beta_e\sigma_c\phi + \beta_e\sigma_c^2\phi^2)\exp(\sigma_c\phi) - (1 + 3\beta_e), \tag{6.3.8}$$

$$V_{se} = \exp(\sigma_s\phi) - 1, \tag{6.3.9}$$

$$V_d = \phi. \tag{6.3.10}$$

Equation (6.3.1) is known as energy integral. According to the prescription of the authors [91, 101], it is important to note that $V(M, \phi)$ satisfies the following conditions:

$$V(M_c, 0) = 0, V'(M_c, 0) = 0, V''(M_c, 0) = 0, \tag{6.3.11}$$

where

$$M_c = \sqrt{3\sigma + \frac{1}{1 - \beta_e\overline{n}_{c0}\sigma_c - \beta_p\overline{n}_{p0}\sigma_p}}. \tag{6.3.12}$$

In figure 6.1, the variation of the amplitude of PPSW is drawn against ϕ at $M = M_c$ for fixed values of $\gamma = 3$, $\sigma = 0.1$, $n_{dc} = 0.1$ and non-identical values of (a) β_e, (b) β_p, (c) n_{sc}, (d) n_{pc}, (e) σ_{sc} and (f) σ_{pc}. In figure 6.1(a), the change of the amplitude of PPSW is plotted against ϕ at $M = M_c$ for non-identical values of β_e. For $\beta_e = 0.35$, $\beta_e = 0.4$ and $\beta_e = 0.45$, we, respectively, get the black curve, magenta curve and blue curve. From figure 6.1(a), we have seen that for increasing values of β_e the amplitude of PPSW grows. In figure 6.1(b), the change of the amplitude of PPSW is plotted against ϕ at $M = M_c$ for non-identical values of β_p. For $\beta_p = 0$, $\beta_p = 0.1$ and $\beta_p = 0.3$, we, respectively, get the black curve, magenta curve and blue curve. From figure 6.1(b), we have seen that for increasing values of β_p the amplitude of PPSW grows. In figure 6.1(c), the change of the amplitude of PPSW is plotted against ϕ at $M = M_c$ for non-identical values of n_{sc}. For $n_{sc} = 0.11$, $n_{sc} = 0.13$ and $n_{sc} = 0.15$, we, respectively,

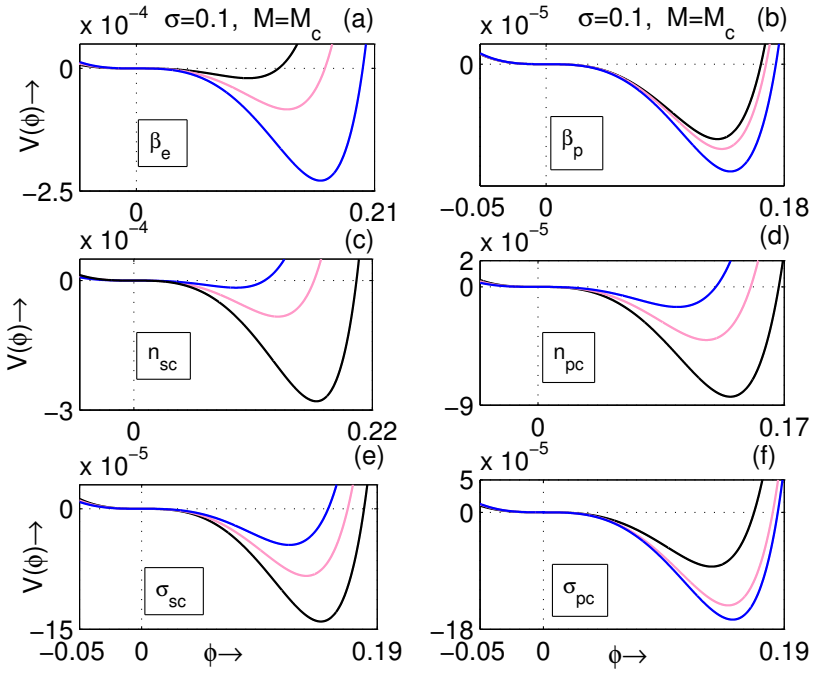

Figure 6.1: $V(\phi)$ vs. ϕ curves for $\gamma = 3$, $\sigma = 0.1$, $n_{dc} = 0.1$ in (a) for non-identical values of β_e, (b) for non-identical values of β_p, (c) for non-identical values of n_{sc}, (d) for non-identical values of n_{pc}, (e) for non-identical values of σ_{sc} and (f) for non-identical values of σ_{pc}.

get the black curve, magenta curve and blue curve. From figure 6.1(c), we have seen that the increasing values of n_{sc} the amplitude of PPSW diminishes. In figure 6.1(d), the change of the amplitude of PPSW is plotted against ϕ at $M = M_c$ for non-identical values of n_{pc}. For $n_{pc} = 0.01$, $n_{pc} = 0.015$ and $n_{pc} = 0.02$, we, respectively, get the black curve, magenta curve and blue curve. From figure 6.1(d), we have seen that for increasing values of n_{pc} the amplitude of PPSW diminishes. In figure 6.1(e), the change of the amplitude of PPSW is plotted against ϕ at $M = M_c$ for non-identical values of σ_{sc}. For $\sigma_{sc} = 0.085$, $\sigma_{sc} = 0.09$ and $\sigma_{sc} = 0.095$, we, respectively, get the black curve, magenta curve and blue curve. From figure 6.1(e), we have seen that for increasing values of σ_{sc} the amplitude of PPSW diminishes. In figure 6.1(f), the change of the amplitude of PPSW is plotted against ϕ at $M = M_c$ for non-identical values of σ_{pc}. For $\sigma_{pc} = 0.2$, $\sigma_{pc} = 0.4$ and $\sigma_{pc} = 0.6$, we, respectively, get the black curve, magenta

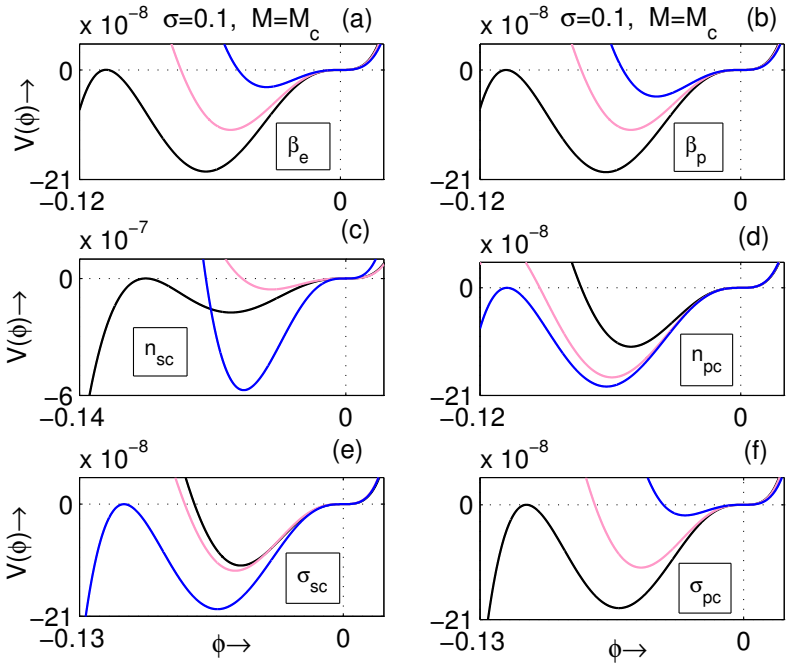

Figure 6.2: $V(\phi)$ vs. ϕ curves for $\gamma = 3$, $\sigma = 0.1$, $n_{dc} = 0.09$ in (a) for non-identical values of β_e, (b) for non-identical values of β_p, (c) for non-identical values of n_{sc}, (d) for non-identical values of n_{pc}, (e) for non-identical values of σ_{sc} and (f) for non-identical values of σ_{pc}.

curve and blue curve. From figure 6.1(f), we have seen that for increasing values of σ_{pc}, the amplitude of PPSW grows.

In figure 6.2, the variation of the amplitude of NPSW is drawn against ϕ at $M = M_c$ for constant values of $\gamma = 3$, $\sigma = 0.1$, $n_{dc} = 0.09$ and non-identical values of (a) β_e, (b) β_p, (c) n_{sc}, (d) n_{pc}, (e) σ_{sc} and (f) σ_{pc}. In figure 6.2(a), the change of the amplitude of NPSW is plotted against ϕ at $M = M_c$ for non-identical values of β_e. For $\beta_e = 0.149355$, $\beta_e = 0.15$ and $\beta_e = 0.1515$, we, respectively, get the black curve, magenta curve and blue curve. From figure 6.2(a), it is found that for increasing values of β_e the amplitude of NPSW diminishes, and at $\beta_e = 0.149355$ the NPDL exists. In figure 6.2(b), the change of the amplitude of NPSW is plotted against ϕ at $M = M_c$ for non-identical values of β_p. For $\beta_p = 0.06708$, $\beta_p = 0.1$ and $\beta_p = 0.15$, we, respectively, get the black curve, magenta curve and blue curve. From figure 6.2(b), we have seen that for increasing values of

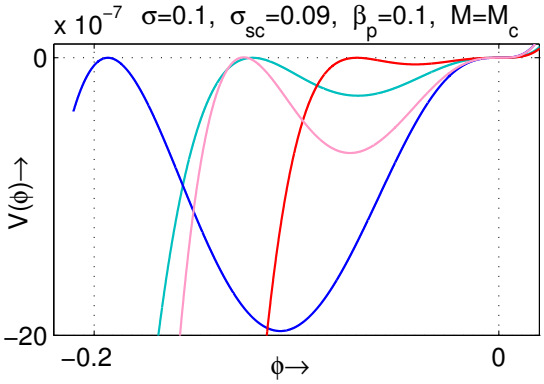

Figure 6.3: $V(\phi)$ vs. ϕ curves at $M = M_c$ for fixed value of γ, σ, σ_{sc}, β_p and non-identical values of other parameters. The blue curves correlate to $n_{sc} = 0.0652858$, $n_{pc} = 0.02$, $n_{dc} = 0.001$, $\sigma_{pc} = 0.9$, $\beta_e = 0.2$, the magenta curves correlate to $n_{sc} = 0.136797$, $n_{pc} = 0.01$, $n_{dc} = 0.1$, $\sigma_{pc} = 0.1$, $\beta_e = 0.32$, the sky blue curves correlate to $n_{sc} = 0.05554978$, $n_{pc} = 0.02$, $n_{dc} = 0.02$, $\sigma_{pc} = 0.9$, $\beta_e = 0.2$ and red curves correlate to $n_{sc} = 0.113916$, $n_{pc} = 0.01$, $n_{dc} = 0.1$, $\sigma_{pc} = 0.1$, $\beta_e = 0.3$.

β_p the amplitude of NPSW diminishes, and at $\beta_p = 0.06708$ the NPDL exists. In figure 6.2(c), the change of the amplitude of NPSW is plotted against ϕ at $M = M_c$ for non-identical values of n_{sc}. For $n_{sc} = 0.059515$, $n_{sc} = 0.061$ and $n_{sc} = 0.105$, we, respectively, get the black curve, magenta curve and blue curve. From figure 6.2(c), we have seen that for increasing values of n_{sc} the amplitude of NPSW diminishes within a certain interval after that the amplitude of NPSW grows within the domain of existence, and at $n_{sc} = 0.059515$ the NPDL exists. In figure 6.2(d), the change of the amplitude of NPSW is plotted against ϕ at $M = M_c$ for non-identical values of n_{pc}. For $n_{pc} = 0.01$, $n_{pc} = 0.0102$ and $n_{pc} = 0.01024505$, we, respectively, get the black curve, magenta curve and blue curve. From figure 6.2(d), we have seen that for increasing values of n_{pc} the

amplitude of NPSW grows, and at $n_{pc} = 0.01024505$ the NPDL exists. In figure 6.2(e), the change of the amplitude of NPSW is plotted against ϕ at $M = M_c$ for non-identical values of σ_{sc}. For $\sigma_{sc} = 0.09$, $\sigma_{sc} = 0.09005$ and $\sigma_{sc} = 0.09009963$, we, respectively, get the black curve, magenta curve and blue curve. From figure 6.2(e), we have seen that for increasing values of σ_{sc} the amplitude of NPSW grows, and at $\sigma_{sc} = 0.09009963$ the NPDL exists. In figure 6.2(f), the change of the amplitude of NPSW is plotted against ϕ at $M = M_c$ for non-identical values of σ_{pc}. For $\sigma_{pc} = 0.487704$, $\sigma_{pc} = 0.5$ and $\sigma_{pc} = 0.55$, we, respectively, get the black curve, magenta curve and blue curve. From figure 6.2(f), we have seen that for increasing values of σ_{pc}, the amplitude of NPSW diminishes, and at $\sigma_{pc} = 0.487704$ the NPDL exists.

In figure 6.3, $V(\phi)$ is drawn against ϕ at $M = M_c$ for fixed values of γ, σ, σ_{sc}, β_p and different values of other parameters, where $\gamma = 3$, $\sigma = 0.1$, $\sigma_{sc} = 0.09$ and $\beta_p = 0.1$. The blue curve correlates to $n_{sc} = 0.0652858$, $n_{pc} = 0.02$, $n_{dc} = 0.001$, $\sigma_{pc} = 0.9$ and $\beta_e = 0.2$, the magenta curve correlates to $n_{sc} = 0.136797$, $n_{pc} = 0.01$, $n_{dc} = 0.1$, $\sigma_{pc} = 0.1$ and $\beta_e = 0.32$, the sky blue curve correlates to $n_{sc} = 0.05554978$, $n_{pc} = 0.02$, $n_{dc} = 0.02$, $\sigma_{pc} = 0.9$ and $\beta_e = 0.2$, and red curves correlate to $n_{sc} = 0.113916$, $n_{pc} = 0.01$, $n_{dc} = 0.1$, $\sigma_{pc} = 0.1$ and $\beta_e = 0.3$. From figure 6.3, we see that for different sets of parameters, different NPDLs exist.

6.4 Solitary Structures and Phase Portraits

To confirm the existence of different solitary structures, we draw the phase portrait of the dynamical system described by the energy integral (6.3.1). Differentiating equation (6.3.1) with respect to ϕ, we get a second order differential equation which is equivalent to the following system of equations:

$$\frac{d\phi}{d\xi} = \psi, \quad \frac{d\psi}{d\xi} = -V^{'}(\phi). \tag{6.4.1}$$

At the sonic speed, we have plotted the phase portrait of dynamical system described by (6.4.1).

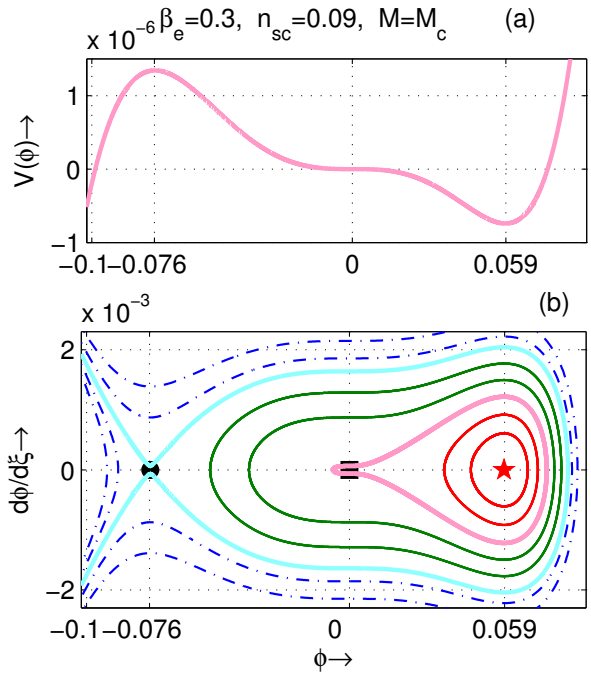

Figure 6.4: Pseudopotential $V(\phi)$ and the phase portrait of (6.4.1) are plotted against ϕ for $M = M_c$, $\gamma = 3$, $\sigma = 0.1$, $n_{sc} = 0.09$, $n_{pc} = 0.01$, $n_{dc} = 0.1$, $\sigma_{sc} = 0.09$, $\sigma_{pc} = 0.1$, $\beta_e = 0.3$ and $\beta_p = 0.1$.

For $\gamma = 3$, $\sigma = 0.1$, $n_{pc} = 0.01$, $n_{dc} = 0.1$, $\sigma_{sc} = 0.09$, $\sigma_{pc} = 0.1$, $\beta_e = 0.3$, $\beta_p = 0.1$ and increasing values of n_{sc}, we have plotted solitary structures and the associated phase portrait of system (6.4.1) as shown in figures (6.4)-(6.6).

In figure 6.4(a), $V(\phi)$ vs. ϕ curve at $M = M_c$ shows the presence of a PPSW and the associated phase portrait given in figure 6.4(b), ensures its existence. From the phase portrait, we see that the origin represents the point of inflexion (marked as black square) and there are another two equilibrium points. One of them is the saddle point (marked as a black circle) and another one is a stable equilibrium point (marked as a red star). Two separatrices are seen from figure 6.4(b). The magenta separatrix tends to pass through the point of inflexion (0, 0) and it encloses the stable equilibrium point (0.058829, 0). At $M = M_c$, this magenta separatrix correlates to positive potential solitary structure as obtained

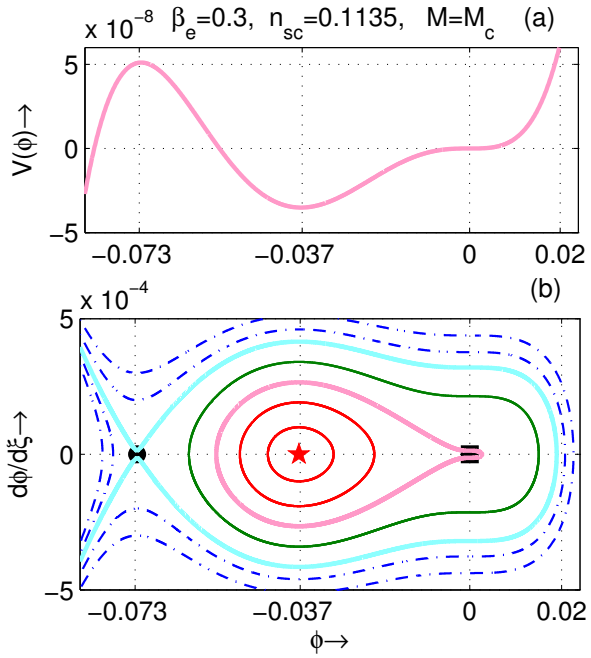

Figure 6.5: Pseudopotential $V(\phi)$ and the phase portrait of (6.4.1) are plotted against ϕ for $M = M_c$, $\gamma = 3$, $\sigma = 0.1$, $n_{sc} = 0.1135$, $n_{pc} = 0.01$, $n_{dc} = 0.1$, $\sigma_{sc} = 0.09$, $\sigma_{pc} = 0.1$, $\beta_e = 0.3$ and $\beta_p = 0.1$.

in figure 6.4(a). In fact, the minimum point of $V(\phi)$ corresponds to a stable equilibrium point(marked by a red star), whereas maximum point $V(\phi)$ corresponds to an unstable (saddle) point (marked by a black circle). The sky blue separatrix tends to pass through the saddle point (-0.07573, 0) and it encloses the magenta separatrix that starts and ends at (0, 0). From figure 6.4(b), we see that there are infinitely many green curves between these two separatrices, and each green curve correlates to a supernonlinear periodic wave at the sonic speed.

In figure 6.5(a), $V(\phi)$ vs. ϕ curve at $M = M_c$ shows the presence of an NPSW and figure 6.5(b) shows the associated phase portrait of this $V(\phi)$ vs. ϕ curve. From the phase portrait, we see that the origin represents the point of inflexion (marked as a black square) and there are another two equilibrium points. One of them is the saddle point (marked as a black circle) and another one is a stable equilibrium point (marked as a red star). We have observed two separatrices in

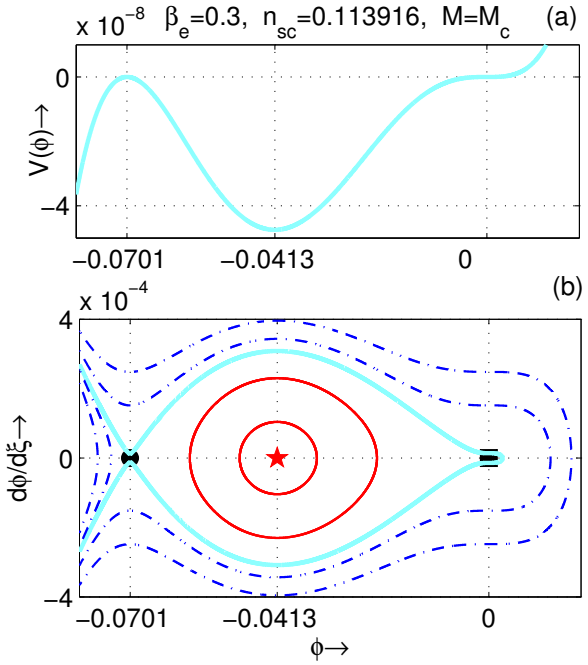

Figure 6.6: Pseudopotential $V(\phi)$ and the phase portrait of (6.4.1) are plotted against ϕ for $M = M_c$, $\gamma = 3$, $\sigma = 0.1$, $n_{sc} = 0.113916$, $n_{pc} = 0.01$, $n_{dc} = 0.1$, $\sigma_{pc} = 0.1$, $\sigma_{sc} = 0.09$, $\beta_e = 0.3$ and $\beta_p = 0.1$.

figure 6.5(b). The magenta separatrix tends to pass through the point of inflexion (0, 0) and it encloses the stable equilibrium point (-0.037, 0). At $M = M_c$, this magenta separatrix correlates to the negative potential solitary structure. The sky blue separatrix tends to pass through the saddle equilibrium point (-0.073, 0) and it encloses the magenta separatrix which starts and ends at (0, 0). From figure 6.5(b), we see that there are infinitely many green curves between these two separatrices that correlate to a supernonlinear periodic wave at the sonic speed.

In figure 6.6(a), $V(\phi)$ vs. ϕ curve at $M = M_c$ shows the presence of an NPDL and figure 6.6(b) the associated phase portrait of the $V(\phi)$ vs. ϕ curve. From the phase portrait, we see that the origin represents the point of inflexion (marked as a black square) and there are another two equilibrium points. One of them is the saddle point (marked as a black circle) and another one is a stable equilibrium point (marked as a red star). Here, we have observed only one separatrix. The

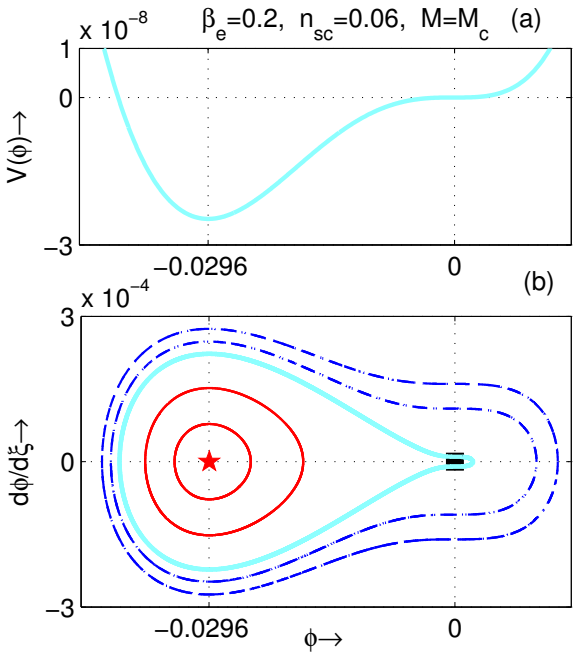

Figure 6.7: Pseudopotential $V(\phi)$ and the phase portrait of (6.4.1) are plotted against ϕ for $M = M_c$, $\gamma = 3$, $\sigma = 0.1$, $n_{sc} = 0.06$, $n_{pc} = 0.02$, $n_{dc} = 0.02$, $\sigma_{pc} = 0.9$, $\sigma_{sc} = 0.09$, $\beta_e = 0.2$ and $\beta_p = 0.1$.

separatrix tends to pass through the point of inflexion (0, 0) and the saddle point (-0.070099, 0) and it encloses the stable equilibrium point (-0.041337, 0). At $M = M_c$, this sky blue separatrix correlates to a negative potential double layer solution.

Figures (6.7) -(6.12) confirm similar types of solitary structures as described in figures (6.4) -(6.6) for different values of the parameters as given in each figure caption.

6.5 Conclusions

Considering a collisionless unmagnetized five components plasma system, DIA solitary structures have been studied at the sonic speed. We have found the existence of PPSWs, NPSWs along with supernonlinear periodic waves and NPDL.

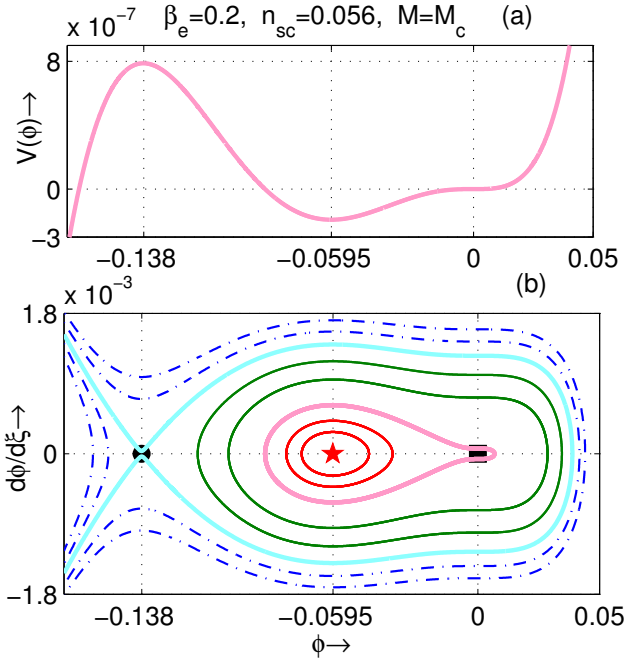

Figure 6.8: Pseudopotential $V(\phi)$ and the phase portrait of (6.4.1) are plotted against ϕ for $M = M_c$, $\gamma = 3$, $\sigma = 0.1$, $n_{sc} = 0.056$, $n_{pc} = 0.02$, $n_{dc} = 0.02$, $\sigma_{pc} = 0.9$, $\sigma_{sc} = 0.09$, $\beta_e = 0.2$ and $\beta_p = 0.1$.

(1) We have seen the following effects of parameters on the amplitude of PPSW at the sonic speed:

(I) Effect of β_e: At $M = M_c$, the amplitude of PPSW grows with increasing β_e within the domain of existence PPSW. For $\gamma = 3$, $\sigma = 0.1$, $n_{sc} = 0.13$, $n_{pc} = 0.01$, $n_{dc} = 0.1$, $\sigma_{sc} = 0.09$, $\sigma_{pc} = 0.2$, $\beta_p = 0.1$, the interval of existence of β_e is $(0.255, 0.566)$. Therefore, for the fixed values of above parameters, the amplitude of PPSW grows with increasing β_e for $0.255 < \beta_e < 0.566$.

(II) Effect of β_p: At $M = M_c$, the amplitude of PPSW grows with increasing β_p within the domain of existence PPSW. For $\gamma = 3$, $\sigma = 0.1$, $n_{sc} = 0.13$, $n_{pc} = 0.01$, $n_{dc} = 0.1$, $\sigma_{sc} = 0.09$, $\sigma_{pc} = 0.2$, $\beta_e = 0.4$, the interval of existence of β_p is $(0, 0.57)$. Therefore, for the fixed values of above parameters, the amplitude of PPSW grows with increasing β_p for $0 < \beta_p < 0.57$.

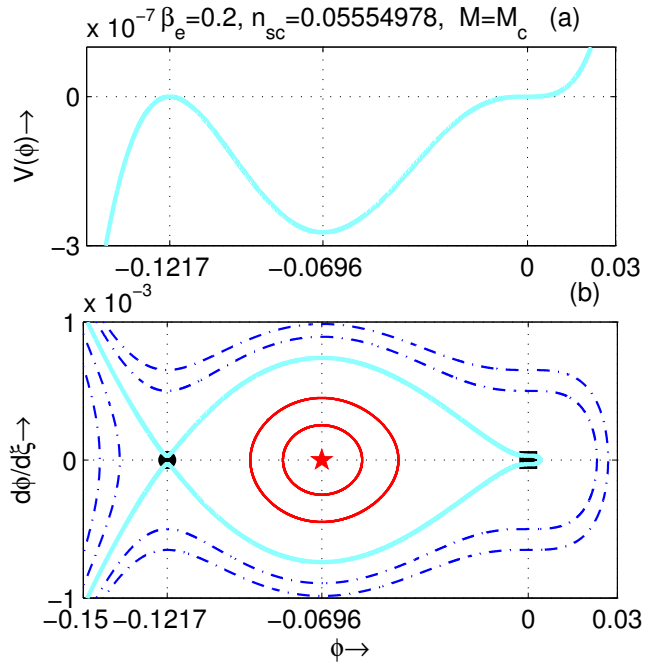

Figure 6.9: Pseudopotential $V(\phi)$ and the phase portrait of (6.4.1) are plotted against ϕ for $M = M_c$, $\gamma = 3$, $\sigma = 0.1$, $n_{sc} = 0.05554978$, $n_{pc} = 0.02$, $n_{dc} = 0.02$, $\sigma_{pc} = 0.9$, $\sigma_{sc} = 0.09$, $\beta_e = 0.2$ and $\beta_p = 0.1$.

(III) Effect of $\mathbf{n_{sc}}$: At $M = M_c$, the amplitude of PPSW decreases with increasing n_{sc} within the domain of existence PPSW. For $\gamma = 3$, $\sigma = 0.1$ $n_{pc} = 0.01$, $n_{dc} = 0.1$, $\sigma_{sc} = 0.09$, $\sigma_{pc} = 0.2$, $\beta_e = 0.4$, $\beta_p = 0.1$, the interval of existence of n_{sc} is $(0.0836, 0.85)$. Therefore, for the fixed values of above parameters, the amplitude of PPSW diminishes with increasing n_{sc} for $0.0836 < n_{sc} < 0.85$.

(IV) Effect of $\mathbf{n_{pc}}$: At $M = M_c$, the amplitude of PPSW diminishes with increasing n_{pc} within the domain of existence PPSW. For $\gamma = 3$, $\sigma = 0.1$, $n_{sc} = 0.13$, $n_{dc} = 0.1$, $\sigma_{sc} = 0.09$, $\sigma_{pc} = 0.2$, $\beta_e = 0.4$, $\beta_p = 0.1$, the interval of existence of n_{pc} is $(0, 0.033)$. Therefore, for the above mentioned fixed values of parameters, the amplitude of PPSW diminishes with increasing n_{pc} for $0 < n_{pc} < 0.033$.

(V) Effect of σ_{sc}: At $M = M_c$, the amplitude of PPSW diminishes with increasing σ_{sc} within the domain of existence PPSW. For $\gamma = 3$, $\sigma = 0.1$, $n_{sc} = 0.13$,

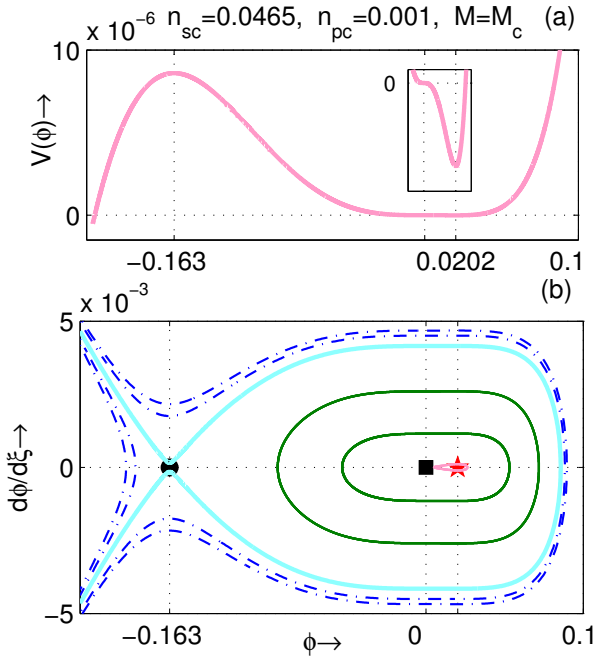

Figure 6.10: Pseudopotential $V(\phi)$ and the phase portrait of (6.4.1) are plotted against ϕ for $M = M_c$, $\gamma = 3$, $\sigma = 0.1$, $n_{sc} = 0.0465$, $n_{pc} = 0.001$, $n_{dc} = 0.001$, $\sigma_{pc} = 0.9$, $\sigma_{sc} = 0.09$, $\beta_e = 0.2$ and $\beta_p = 0.1$.

$n_{pc} = 0.01$, $n_{dc} = 0.1$, $\sigma_{pc} = 0.2$, $\beta_e = 0.4$, $\beta_p = 0.1$, the interval of existence of σ_{sc} is $(0.0589, 0.1126)$. Therefore, for the above mentioned fixed values the parameters, the amplitude of PPSW diminishes with increasing σ_{sc} for $0.0589 < \sigma_{sc} < 0.1126$.

(VI) Effect of σ_{pc}: At $M = M_c$, the amplitude of PPSW grows with increasing σ_{pc} within the domain of existence PPSW. For $\gamma = 3$, $\sigma = 0.1$, $n_{sc} = 0.13$, $n_{pc} = 0.01$, $n_{dc} = 0.1$, $\sigma_{sc} = 0.09$, $\beta_e = 0.4$, $\beta_p = 0.1$, the interval of existence of σ_{pc} is $(0.079, 0.99)$. Therefore, for the fixed values of above parameters, the amplitude of PPSW grows with increasing σ_{pc} for $0.079 < \sigma_{pc} < 0.99$.

(2) We have seen the following effects of parameters on the amplitude of NPSW at the sonic speed:

(I) Effect of β_e: At $M = M_c$, the amplitude of NPSW diminishes with increasing β_e within the domain of existence NPSW. For $\gamma = 3$, $\sigma = 0.1$, $n_{sc} = 0.06$,

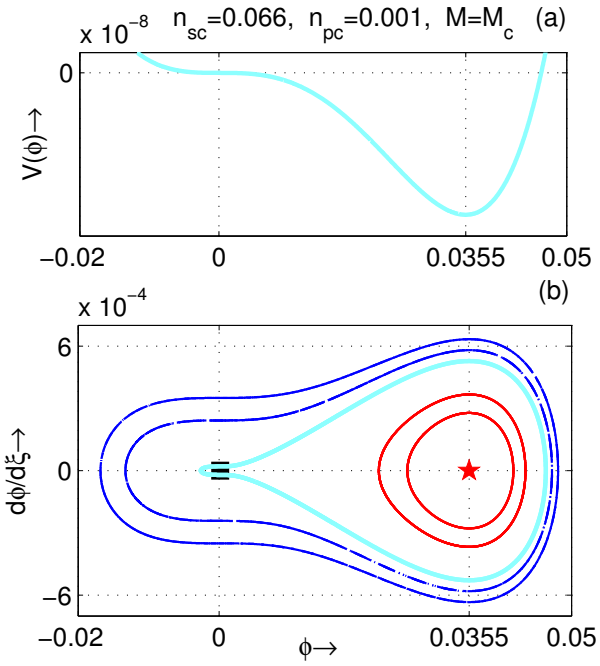

Figure 6.11: Pseudopotential $V(\phi)$ and the phase portrait of (6.4.1) are plotted against ϕ for $M = M_c$, $\gamma = 3$, $\sigma = 0.1$, $n_{sc} = 0.066$, $n_{pc} = 0.001$, $n_{dc} = 0.001$, $\sigma_{pc} = 0.9$, $\sigma_{sc} = 0.09$, $\beta_e = 0.2$ and $\beta_p = 0.1$.

$n_{pc} = 0.01$, $n_{dc} = 0.09$, $\sigma_{sc} = 0.09$, $\sigma_{pc} = 0.5$, $\beta_p = 0.1$, the interval of existence of β_e is $(0.149356, 0.1556)$. Therefore, for the above mentioned fixed values of the parameters, the amplitude of NPSW diminishes with increasing β_e for $0.149356 < \beta_e < 0.1556$ and at $\beta_e = 0.149355$, there exists a NPDL.

(II) Effect of β_p: At $M = M_c$, the amplitude of NPSW diminishes with increasing β_p within the domain of existence NPSW. For $\gamma = 3$, $\sigma = 0.1$, $n_{sc} = 0.06$, $n_{pc} = 0.01$, $n_{dc} = 0.09$, $\sigma_{sc} = 0.09$, $\sigma_{pc} = 0.5$, $\beta_e = 0.15$, the interval of existence of β_p is $(0.06709, 0.4)$. Therefore, for the above mentioned fixed values of the parameters, the amplitude of NPSW diminishes with increasing β_p for $0.06709 < \beta_p < 0.4$ and at $\beta_p = 0.06708$, there exists a NPDL.

(III) Effect of n_{sc}: At $M = M_c$, the amplitude of NPSW diminishes with increasing n_{sc} for $(n_{sc}^{(s)} < n_{sc} < n_{sc}^{(c)})$ whereas the amplitude of NPSW grows with increasing n_{sc} for $(n_{sc}^{(c)} < n_{sc} < n_{sc}^{(t)})$. For $\gamma = 3$, $\sigma = 0.1$, $n_{pc} = 0.01$,

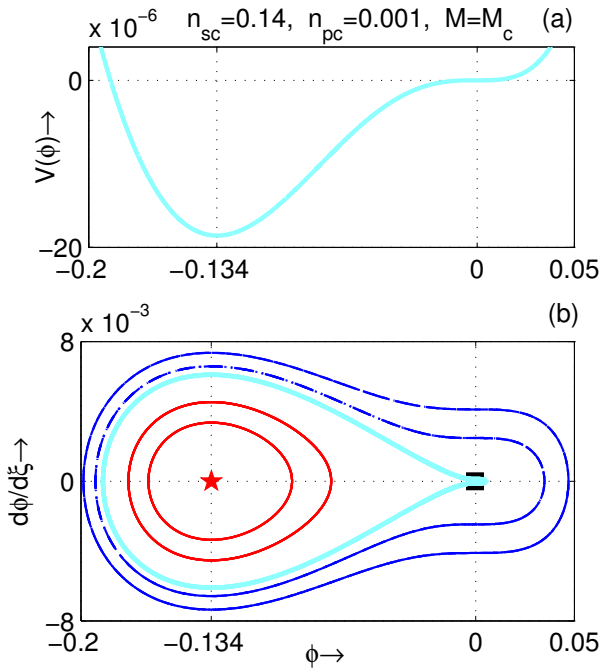

Figure 6.12: Pseudopotential $V(\phi)$ and the phase portrait of (6.4.1) are plotted against ϕ for $M = M_c$, $\gamma = 3$, $\sigma = 0.1$, $n_{sc} = 0.14$, $n_{pc} = 0.001$, $n_{dc} = 0.001$, $\sigma_{pc} = 0.9$, $\sigma_{sc} = 0.09$, $\beta_e = 0.2$ and $\beta_p = 0.1$.

$n_{dc} = 0.09$, $\sigma_{sc} = 0.09$, $\sigma_{pc} = 0.5$, $\beta_e = 0.15$, $\beta_p = 0.1$ the values of $n_{sc}^{(s)}$, $n_{sc}^{(c)}$, $n_{sc}^{(t)}$ are, respectively, 0.059516, 0.08 and 0.1391 and at $n_{sc} = 0.059515$, there exists a NPDL.

(IV) Effect of $\mathbf{n_{pc}}$: At $M = M_c$, the amplitude of NPSW grows with increasing n_{pc} within the domain of existence NPSW. For $\gamma = 3$, $\sigma = 0.1$, $n_{sc} = 0.06$, $n_{dc} = 0.09$, $\sigma_{sc} = 0.09$, $\sigma_{pc} = 0.5$, $\beta_e = 0.15$, $\beta_p = 0.1$, the interval of existence of n_{pc} is $(0.00735, 0.01024504)$. Therefore, for the above mentioned fixed values of the parameters, the amplitude of NPSW grows with increasing n_{pc} for $0.00735 < n_{pc} < 0.01024504$ and at $n_{pc} = 0.01024505$, there exists a NPDL.

(V) Effect of σ_{sc}: At $M = M_c$, the amplitude of NPSW grows with increasing σ_{sc} within the domain of existence NPSW. For $\gamma = 3$, $\sigma = 0.1$, $n_{sc} = 0.06$, $n_{pc} = 0.01$, $n_{dc} = 0.09$, $\sigma_{pc} = 0.5$, $\beta_e = 0.15$, $\beta_p = 0.1$, the interval of existence of σ_{sc} is $(0.089, 0.09009962)$. Therefore, for the above mentioned fixed values of the

parameters, the amplitude of NPSW grows with increasing σ_{sc} for $0.089 < \sigma_{sc} < 0.09009962$ and at $\sigma_{sc} = 0.09009963$, there exists a NPDL.

(VI) Effect of σ_{pc}: At $M = M_c$, the amplitude of NPSW diminishes with increasing σ_{pc} within the domain of existence NPSW. For $\gamma = 3$, $\sigma = 0.1$, $n_{sc} = 0.06$, $n_{pc} = 0.01$, $n_{dc} = 0.09$, $\sigma_{sc} = 0.09$, $\beta_e = 0.15$, $\beta_p = 0.1$, the interval of existence of σ_{pc} is $(0.487705, 0.68)$. Therefore, for the above mentioned fixed values of the parameters, the amplitude of NPSW diminishes with increasing σ_{pc} for $0.487705 < \sigma_{sc} < 0.68$ and at $\sigma_{sc} = 0.487704$, there exists a NPDL. .

In the all above six cases : (I) - (VI), sequence of NPSWs converges to a NPDL solution.

(3) At the sonic speed of the wave, we have also studied the phase portrait of different DIA solitons through the coupled equations (6.4.1). We have seen in **Chapter-5**, that for subsonic speed (supersonic speed) of the waves $M < M_c (M > M_c)$ the origin (0, 0) is a stable (unstable) equilibrium point, whereas, for sonic speed ($M = M_c$) of the wave, the origin (0, 0) is the point of inflexion.

(4) From the phase portrait of DIA double layers at sonic speed, we have seen the separatrix of the phase portrait tends to pass through an unstable equilibrium point which starts and ends at the point of inflexion. This separatrix encloses at least one stable equilibrium point.

(5) We have studied the phase portrait of corresponding DIA solitary structures for different sets of values of parameters.

The findings of our current study on arbitrary amplitude DIA nonlinear wave structures at sonic speed including double layers and supernonlinear periodic waves will be helpful to distinguish the signals coming from the Jupiter atmosphere and the auroral region of the upper Earth's ionosphere. We anticipate that the next generation satellite will be able to identify the signature of the above nonlinear wave forms discussed in this chapter.

References

[1] R A Cairns, A A Mamum, R Bingham, R Boström, R O Dendy, C M C Nairn, and P K Shukla. *Geophys. Res. Lett.*, 22:2709, 1995.

[2] D J Korteweg and G De Vries. *Phil. Mag.*, 39:422, 1895.

[3] W H Munk. *Ann. N. Y. Acad. Sci.*, 51:376, 1949.

[4] J H Adlam and J E Allen. *Phil. Mag.*, 3:448, 1958.

[5] N J Zabusky and M D Kruskal. *Phys. Rev. Lett.*, 15:240, 1965.

[6] H Washimi and T Taniuti. *Phys. Rev. Lett.*, 17:996, 1966.

[7] M Q Tran. *Plasma Phys.*, 16:1167, 1974.

[8] G C Das and S G Tagare. *Plasma Phys.*, 17:1025, 1975.

[9] B N Goswami and B Buti. *Plasma Phys.*, 19:53, 1977.

[10] S Watanabe. *J. Phys. Soc. Jpn.*, 53:950, 1984.

[11] S G Tagare and R Virupakshi Reddy. *J. Plasma Phys.*, 35:219, 1986.

[12] S G Tagare. *J. Plasma Phys.*, 36:301, 1986.

[13] F Verheest. *J. Plasma Phys.*, 39:71, 1988.

[14] K P Das and F Verheest. *J. Plasma Phys.*, 41:139, 1989.

[15] G Rowlands. *J. Plasma Phys.*, 3:567, 1969.

[16] E. Infeld. *J. Plasma Phys.*, 8:105, 1972.

[17] E Infeld and G Rowlands. *J. Plasma Phys.*, 10:293, 1973.

[18] E Infeld. *J. Plasma Phys.*, 33:171, 1985.

[19] G Ghosh and K P Das. *J. Plasma phys.*, 59:333, 1998.

[20] K P Das, F W Sluijter, and F Verheest. *Phys. Scr.*, 45:358, 1992.

[21] A A Mamun and R A Cairns. *J. Plasma Phys.*, 56:175, 1996.

[22] D Chakraborty and K P Das. *J. Plasma Phys.*, 60:151, 1998.

[23] S Munro and E J Parkes. *J. Plasma Phys.*, 62:305, 1999.

[24] A Bandyopadhyay and K P Das. *J. Plasma Phys.*, 62:255, 1999.

[25] A A Mamun, S M Russell, C A Mendoza-Briceno, M N Alam, T K Datta, and A K Das. *Planet. Space Sci.*, 48:163, 2000.

[26] A Bandyopadhyay and K P Das. *Phys. Plasmas*, 7:3227, 2000.

[27] A Bandyopadhyay and K P Das. *Phys. Scr.*, 63:145, 2001.

[28] D Chakraborty and K P Das. *Phys. Plasmas*, 10:2236, 2003.

[29] J Das, A Bandyopadhyay, and K P Das. *J. Plasma Phys.*, 72:587, 2006.

[30] M G M Anowar and A A Mamun. *Phys. Plasmas*, 15:102111, 2008.

[31] M G M Anowar and A A Mamun. *IEEE Trans. Plasma Sci.*, 37:1638, 2009.

[32] M G M Anowar and A A Mamun. *J. Plasma Phys.*, 75:475, 2009.

[33] M Shalaby, S K El-Labany, E F El-Shamy, W F El-Taibany, and M A Khaled. *Phys. Plasmas*, 16:123706, 2009.

[34] Sk A Islam, A Bandyopadhyay, and K P Das. *J. Plasma Phys.*, 75:593, 2009.

[35] W F El-Taibany, N A El-Bedwehy, and E F El-Shamy. *Phys. Plasmas*, 18:033703, 2011.

[36] O Rahman, A A Mamun, and K S Ashrafi. *Astrophys. Space Sci.*, 335:425, 2011.

[37] A A Mamun, S S Duha, and P K Shukla. *J. Plasma Phys.*, 77:617, 2011.

[38] M M Haider and A A Mamun. *Phys. Plasmas*, 19:102105, 2012.

[39] T Akhter, M M Hossain, and A A Mamun. *Phys. Plasmas*, 19:093707, 2012.

[40] S Akter, M M Haider, S S Duha, M Salahuddin, and A A Mamun. *Phys. Scr.*, 88:015501, 2013.

[41] M M Haider. *Contrib. Plasma Phys.*, 53:234, 2013.

[42] N R Kundu, M M Masud, K S Ashrafi, and A A Mamun. *Astrophys. Space Sci.*, 343:279, 2013.

[43] T S Gill, P Bala, and A S Bains. *Astrophys. Space Sci.*, 357:63, 2015.

[44] N Shahmohammadi and D Dorranian. *Contrib. Plasma Phys.*, 55:643, 2015.

[45] S Sardar, A Bandyopadhyay, and K P Das. *Phys. Plasmas*, 23:073703, 2016.

[46] S Sardar, A Bandyopadhyay, and K P Das. *Phys. Plasmas*, 23:123706, 2016.

[47] S Sardar, A Bandyopadhyay, and K P Das. *Phys. Plasmas*, 24:063705, 2017.

[48] D N Gao, J P Wu, and W S Duan. *Contrib. Plasma Phys.*, 61:e202100010, 2021.

[49] R Sarma. *Astrophys. Space Sci.*, 367:29, 2022.

[50] R A Cairns, A A Mamun, R Bingham, and P K Shukla. *Phys. Scr.*, T63:80, 1996.

[51] A Bandyopadhyay and K P Das. *J. Plasma Phys.*, 65:131, 2001.

[52] A Bandyopadhyay and K P Das. *J. Plasma Phys.*, 68:285, 2002.

[53] A A Mamun and P K Shukla. *Phys. Plasmas*, 9:1468, 2002.

[54] D K Singh and H K Malik. *Plasma Phys. Control. Fusion*, 49:1551, 2007.

[55] Sk A Islam, A Bandyopadhyay, and K P Das. *J. Plasma Phys.*, 74:765, 2008.

[56] S Ghosh and R Bharuthram. *Astrophys. Space Sci.*, 314:121, 2008.

[57] H K Malik, R Kumar, and K E Lonngren. *IEEE Trans. Plasma Sci.*, 38:1073, 2010.

[58] P Eslami, M Mottaghizadeh, and H R Pakzad. *Phys. Scr.*, 84:015504, 2011.

[59] F Verheest, M A Hellberg, and W A Hereman. *Phys. Rev. E*, 86:036402, 2012.

[60] I Tasnim, M M Masud, and A A Mamun. *Plasma Phys. Rep.*, 40:723, 2014.

[61] H Kaur, T S Gill, and P Bala. *Pramana*, 89:1–6, 2017.

[62] R Maity and B Sahu. *Z Naturforsch A*, 76:1077, 2021.

[63] R Z Sagdeev. *Rev Plasma Phys., Volume 4.* Edited by M. A. Leontovich, Consultants Bureau New York, 1966.

[64] P K Shukla and M Y Yu. *J. Math. Phys.*, 19:2506, 1978.

[65] B Buti. *Phys. Lett. A*, 76:251, 1980.

[66] R Bharuthram and P K Shukla. *Phys. Fluids*, 29:3214, 1986.

[67] S Baboolal, R Bharuthram, and M A Hellberg. *J. Plasma Phys.*, 40:163, 1988.

[68] S Baboolal, R Bharuthram, and M A Hellberg. *J. Plasma Phys.*, 41:341, 1989.

[69] F Verheest. *Phys. Plasmas*, 18:083701, 2011.

[70] M A Hellberg, T K Baluku, F Verheest, and I Kourakis. *J. Plasma Phys.*, 79:1039, 2013.

[71] F Verheest, M A Hellberg, and I Kourakis. *Phys. Plasmas*, 20:012302, 2013.

[72] F Verheest, M A Hellberg, and I Kourakis. *Phys. Rev. E*, 87:043107, 2013.

[73] F Verheest. *J. Plasma Phys.*, 80:787, 2014.

[74] F Verheest, G S Lakhina, and M A Hellberg. *Phys. Plasmas*, 21:062303, 2014.

[75] A E Dubinov and D Y Kolotkov. *IEEE Trans. Plasma Sci.*, 40:1429, 2012.

[76] S A El-Tantawy and W M Moslem. *Phys. Plasmas*, 18:112105, 2011.

[77] A E Dubinov, D Y Kolotkov, and M A Sazonkin. *Tech. Phys.*, 57:585, 2012.

[78] N S Saini, B S Chahal, and A S Bains. *Astrophys. Space Sci.*, 347:129, 2013.

[79] A Paul and A Bandyopadhyay. *Astrophys. Space Sci.*, 361:1, 2016.

[80] G Banerjee and S Maitra. *Phys. Plasmas*, 23:123701, 2016.

[81] A Paul, A Bandyopadhyay, and K P Das. *Phys. Plasmas*, 24:013707, 2017.

[82] A Paul, A Das, and A Bandyopadhyay. *Plasma Phys. Rep.*, 43:218, 2017.

[83] A Paul, A Bandyopadhyay, and K P Das. *Plasma Phys. Rep.*, 45:466, 2019.

[84] G Banerjee and S Maitra. *AJAMC*, 1:27, 2020.

[85] C R Choi, C M Ryu, N C Lee, and D Y Lee. *Phys. Plasmas*, 12:022304, 2005.

[86] C R Choi, C M Ryu, N C Lee, D Lee, and Y Kim. *Phys. Plasmas*, 12:072301, 2005.

[87] A E Dubinov, I D Dubinova, and V A Gordienko. *Phys. Plasmas*, 13:082111, 2006.

[88] A E Dubinov and D Y Kolotkov. *Plasma Phys. Rep.*, 38:909, 2012.

[89] A E Dubinov, D Y Kolotkov, and M A Sazonkin. *Plasma Phys. Rep.*, 38:833, 2012.

[90] A E Dubinov and D Y Kolotkov. *Rev. Mod. Plasma Phys.*, 2:1–46, 2018.

[91] A Das, A Bandyopadhyay, and K P Das. *J. Plasma Phys.*, 78:149, 2012.

[92] S Maitra and R Roychoudhury. *Phys. Plasmas*, 13:112302, 2006.

[93] M Shahmansouri and H Alinejad. *Phys. Plasmas*, 19:123701, 2012.

[94] O R Rufai, R Bharuthram, S V Singh, and G S Lakhina. *Phys. Plasmas*, 21:082304, 2014.

[95] O R Rufai, R Bharuthram, S V Singh, and G S Lakhina. *Commun. Nonlinear Sci. Numer. Simul.*, 19:1338, 2014.

[96] O R Rufai, A S Bains, and Z Ehsan. *Astrophys. Space Sci.*, 357:1, 2015.

[97] O R Rufai, R Bharuthram, S V Singh, and G S Lakhina. *Phys. Plasmas*, 23:032309, 2016.

[98] S Dalui, S Sardar, and A Bandyopadhyay. *Z Naturforschung A*, 76:455, 2021.

[99] D Debnath, A Bandyopadhyay, and K P Das. *Phys. Plasmas*, 25:033704, 2018.

[100] D Debnath and A Bandyopadhyay. *Astrophys. Space Sci.*, 365:72, 2020.

[101] D Debnath and A Bandyopadhyay. *Z Naturforsch A*, 76:985, 2021.

[102] F Verheest and M A Hellberg. *Phys. Plasmas*, 17:102312, 2010.

[103] A Das, A Bandyopadhyay, and K P Das. *J. Plasma Phys.*, 78:565, 2012.

[104] T Taniuti and H Washimi. *Phys. Rev. Lett.*, 21:209, 1968.

[105] T Taniuti and N Yajima. *J. Math. Phys.*, 10:1369, 1969.

[106] N Asano, T Taniuti, and N Yajima. *J. Math. Phys.*, 10:2020, 1969.

[107] M Kako. *J. Phys. Soc. Japan*, 33:1678, 1972.

[108] M Kako, Y Furutani, Y H Ichikawa, and T Taniuti. *J. Phys. Soc. Japan*, 35:1526, 1973.

[109] M Kako. *Prog. Theor. Phys. Suppl.*, 55:120, 1974.

[110] Y H Ichikawa and M Kako. *Prog. Theor. Phys. Suppl.*, 55:233, 1974.

[111] T Kakutani and N Sugimoto. *Phys Fluids*, 17:1617, 1974.

[112] G Murtaza and M Salahuddin. *Plasma Phys.*, 24:451, 1982.

[113] R S Chhabra and S R Sharma. *Phys. Fluids*, 29:128, 1986.

[114] R Bharuthram and P K Shukla. *Phys. Rev. A*, 35:1433, 1987.

[115] M K Mishra, R S Chhabra, and S R Sharma. *Phys. Rev. A*, 41:2176, 1990.

[116] R S Chhabra, M K Mishra, and S R Sharma. *Phys. Rev. A*, 42:2292, 1990.

[117] J K Xue, W S Duan, and L He. *Chin Phys*, 11:1184, 2002.

[118] X Jukui and T Rongan. *Phys. Scr.*, 67:74, 2003.

[119] X Jukui. *Chaos, Solitons Fractals*, 18:849, 2003.

[120] T Rongan and J K Xue. *Phys. plasmas*, 11:3939, 2004.

[121] A Esfandyari-Kalejahi and H Asgari. *Phys. plasmas*, 12:102302, 2005.

[122] A Esfandyari-Kalejahi, I Kourakis, and M Akbari-Moghanjoughi. *J. Plasma Phys.*, 76:169, 2010.

[123] I Kourakis and P K Shukla. *J. Phys. A*, 36:11901, 2003.

[124] S Dalui, A Bandyopadhyay, and K P Das. *Phys. Plasmas*, 24:042305, 2017.

[125] S Dalui, A Bandyopadhyay, and K P Das. *Phys. Plasmas*, 24:102310, 2017.

[126] S Dalui and A Bandyopadhyay. *Astrophys. Space Sci.*, 364:182, 2019.

[127] Md Rahman, N A Chowdhury, A Mannan, A A Mamun, et al. *Galaxies*, 9:31, 2021.

[128] M N Haque, A Mannan, and A A Mamun. *Contrib. Plasma Phys.*, 59, 2019.

[129] M N Haque and A Mannan. *IEEE Trans. Plasma Sci.*, 48:2591, 2020.

[130] W F El-Taibany, N A El-Bedwehy, N A El-Shafeay, and S K El-Labany. *Galaxies*, 9, 2021.

[131] S Guo, L Mei, and A Sun. *Ann. Phys.*, 332:38, 2012.

[132] O H El-Kalaawy. *Eur. Phys. J. Plus*, 133:1, 2018.

[133] S Watanabe. *J. Plasma Phys.*, 17:487, 1977.

[134] H Ikezi, K Schwarzenegger, A L Simons, Yukiharu Ohsawa, and T Kamimura. *Phys. Fluids*, 21:239, 1978.

[135] J H Binsack. PhD thesis, Massachusetts Institute of Technology, 1966.

[136] V M Vasyliunas. *J. Geophys. Res.*, 73:2839, 1968.

[137] R L Mace and M A Hellberg. *Phys. Plasmas*, 2:2098, 1995.

[138] R L Mace, M A Hellberg, and R A Treumann. *J. Plasma Phys.*, 59:393, 1998.

[139] R L Mace, G Amery, and M A Hellberg. *Phys. Plasmas*, 6:44, 1999.

[140] M A Hellberg and R L Mace. *Phys. Plasmas*, 9:1495, 2002.

[141] A F Viñas, Richard L Mace, and Robert F Benson. *J. Geophys. Res. Space Phys.*, 110:A06202, 2005.

[142] T K Baluku and M A Hellberg. *Phys. Plasmas*, 15:123705, 2008.

[143] N S Saini, I Kourakis, and M A Hellberg. *Phys. Plasmas*, 16:062903, 2009.

[144] A Berbri and M Tribeche. *Phys. Plasmas*, 16:053703, 2009.

[145] A Berbri and M Tribeche. *Phys. Plasmas*, 16:053701, 2009.

[146] T K Baluku, M A Hellberg, I Kourakis, and N S Saini. *Phys. Plasmas*, 17:053702, 2010.

[147] G Livadiotis and D J McComas. *Astrophys. J.*, 741:88, 2011.

[148] S A El-Tantawy, N A El-Bedwehy, and W M Moslem. *Phys. Plasmas*, 18:052113, 2011.

[149] A Danehkar, N S Saini, M A Hellberg, and I Kourakis. *Phys. Plasmas*, 18:072902, 2011.

[150] T K Baluku and M A Hellberg. *Phys. Plasmas*, 19:012106, 2012.

[151] I Kourakis, S Sultana, and M A Hellberg. *Plasma Phys. Control. Fusion*, 54:124001, 2012.

[152] S Sultana, I Kourakis, and M A Hellberg. *Plasma Phys. Control. Fusion*, 54:105016, 2012.

[153] G Williams, F Verheest, M A Hellberg, M G M Anowar, and I Kourakis. *Phys. Plasmas*, 21:092103, 2014.

[154] A Das, A Bandyopadhyay, and K P Das. *Phys. Plasmas*, 16:073703, 2009.

[155] F Verheest and S R Pillay. *Phys. Plasmas*, 15:013703, 2008.

[156] A A Mamun, R A Cairns, and P K Shukla. *Phys. Plasmas*, 3:2610, 1996.

[157] T S Gill, P Bala, H Kaur, N S Saini, S Bansal, and J Kaur. *Eur. Phys. J. D*, 31:91, 2004.

[158] S V Singh and G S Lakhina. *Nonlinear Process. Geophys.*, 11:275, 2004.

[159] S R Pillay and F Verheest. *J. Plasma Phys.*, 71:177, 2005.

[160] R Sabry, W M Moslem, and Padma Kant Shukla. *Phys. Plasmas*, 16:032302, 2009.

[161] H R Pakzad. *Phys. Lett. A*, 373:847–850, 2009.

[162] F Verheest, M A Hellberg, and T K Baluku. *Phys. Plasmas*, 19:032305, 2012.

[163] S V Singh and G S Lakhina. *Commun. Nonlinear Sci. Numer. Simulat.*, 23:274, 2015.

[164] F Verheest and M A Hellberg. *Phys. Plasmas*, 24:022306, 2017.

[165] A Paul, A Das, and A Bandyopadhyay. *Plasma Phys. Rep.*, 43:218, 2017.

[166] A Paul and A Bandyopadhyay. *Indian J. Phys.*, 92:1187, 2018.

[167] Y Ghai, N S Saini, and B Eliasson. *Phys. Plasmas*, 25:013704, 2018.

[168] M Tribeche, R Amour, and P K Shukla. *Phys. Rev. E*, 85:037401, 2012.

[169] W H Zurek. *Astrophys. J.*, 289:603, 1985.

[170] J C Higdon, R E Lingenfelter, and R E Rothschild. *Astrophys. J.*, 698:350, 2009.

[171] P K Shukla. *Phys. Scr.*, 77:068201, 2008.

[172] H Alfvén. *Cosmic plasma*, volume 82. Taylor & Francis, 1981.

[173] P K Shukla and M Marklund. *Phys. Scr.*, T113:36, 2004.

[174] A A Gusev, U B Jayanthi, I M Martin, G I Pugacheva, and W N Spjeldik. *Braz. J. of Phy.*, 30:590, 2000.

[175] A A Gusev, U B Jayanthi, I M Martin, G I Pugacheva, and W N Spjeldvik. *J. Geophys. Res.: Space Phys.*, 106:26111, 2001.

[176] R Boström, G Gustafsson, B Holback, G Holmgren, H Koskinen, and P M Kintner. *Phys. Rev. Lett.*, 61:82, 1988.

[177] R Boström. *IEEE Trans. Plasma Sci.*, 20:756, 1992.

[178] M Temerin, K Cerny, W Lotko, and F S Mozer. *Phys. Rev. Lett.*, 48:1175, 1982.

[179] H Matsumoto, H Kojima, T Miyatake, Y Omura, M Okada, I Nagano, and M Tsutsui. *Geophys. Res. Lett.*, 21:2915, 1994.

[180] J P McFadden, C W Carlson, R E Ergun, F S Mozer, L Muschietti, I Roth, and E Moebius. *J. Geophys. Res.*, 108:8018, 2003.

[181] J R Franz, P M Kintner, and J S Pickett. *Geophys. Res. Lett.*, 25:1277, 1998.

[182] C A Cattell, J Dombeck, J R Wygant, M K Hudson, F S Mozer, M A Temerin, W K Peterson, C A Kletzing, et al. *Geophys. Res. Lett.*, 26:425, 1999.

[183] R E Ergun, C W Carlson, J P McFadden, F S Mozer, G T Delory, W Peria, C C Chaston, M Temerin, et al. *Geophys. Res. Lett.*, 25:2025, 1998.

[184] R E Ergun, C W Carlson, J P McFadden, F S Mozer, G T Delory, W Peria, C C Chaston, M Temerin, et al. *Geophys. Res. Lett.*, page 2061, 1998.

[185] G T Delory, R E Ergun, C W Carlson, L Muschietti, C C Chaston, W Peria, J P McFadden, and R Strangeway. *Geophys. Res. Lett.*, 25:2069, 1998.

[186] R Pottelette, R E Ergun, R A Treumann, M Berthomier, C W Carlson, J P McFadden, and I Roth. *Geophys. Res. Lett.*, 26:2629, 1999.

[187] P O Dovner, A I Eriksson, R Boström, and B Holback. *Geophys. Res. Lett.*, 21:1827, 1994.

[188] M Y Yu and H Luo. *Phys. Plasmas*, 15:024504, 2008.

[189] W M Moslem, R E Tolba, and S Ali. *Phys. Scr.*, 94:075601, 2019.

[190] H A Al-Yousef, B M Alotaibi, R E Tolba, and W M Moslem. *Results Phys.*, 21, 2021.

[191] G Slathia, K Singh, and N S Saini. *IEEE Trans. Plasma Sci*, 50:1723, 2022.

[192] G Slathia, K Singh, and N S Saini. *J. Astrophys. Astron.*, 43:63, 2022.

[193] F Sayed and A A Mamun. *Phys. Plasmas*, 14:014501, 2007.

[194] A Rahman, A A Mamun, and S M K Alam. *Astrophys. Space Sci.*, 315:243, 2008.

[195] G Mandal and P Chatterjee. *Z. Naturforsch. A*, 65:85, 2010.

[196] S Z Alamri. *Z. Naturforsch. A*, 74:227, 2019.

[197] M Farooq, M Ahmad, and Q Jan. *Contrib. Plasma Phys*, 61:e202000170, 2021.

[198] T Taniuti and C C Wei. *J. Phys. Soc. Jpn*, 24:941, 1968.

[199] W Malfliet and W Hereman. *Phys. Scr.*, 54:563, 1996.

[200] A R Seadawy. *Comput. Math. Appl.*, 67:172, 2014.

[201] A R Seadawy. *Phys. A: Stat. Mech. Appl.*, 455:44, 2016.

[202] A R Seadawy, M Arshad, and Dianchen Lu. *Eur. Phys. J. Plus*, 132:162, 2017.

[203] A R Seadawy, Dianchen Lu, and Chen Yue. *J. Taibah Univ. Sci.*, 11:623, 2017.

[204] Abdullah, A R Seadawy, and J Wang. *Mod. Phys. Lett. A*, 33:1850145, 2018.

[205] B Ghanbari, A Yusuf, M Inc, and D Baleanu. *Adv. Differ. Equ*, 2019:49, 2019.

[206] A Jhangeer, M Munawar, M B Riaz, and D Baleanu. *Results Phys.*, 19:103330, 2020.

[207] E C Whipple, T G Northrop, and D A Mendis. *J. Geophys. Res.*, 90:7405, 1985.

[208] C K Goertz. *Rev. Geophys.*, 27:271, 1989.

[209] N N Rao, P K Shukla, and M Y Yu. *Planet. Space Sci.*, 38:543, 1990.

[210] F Verheest. *Planet. Space Sci.*, 40:1, 1992.

[211] N N Rao. *J. Plasma Phys.*, 53:317, 1995.

[212] P K Shukla. *Phys. Plasmas*, 8:1791, 2001.

[213] S K Maharaj, R Bharuthram, S V Singh, S R Pillay, and G S Lakhina. *Phys. Plasmas*, 15, 2008.

[214] S Sultana, S Islam, and A A Mamun. *Astrophys. Space Sci.*, 351:581, 2014.

[215] M S Alam, M M Masud, and A A Mamun. *Astrophys. Space Sci.*, 349:245, 2014.

[216] N S Saini and P Sethi. *Phys. Plasmas*, 23(10), 2016.

[217] N Paul, K K Mondal, R Ali, and P Chatterjee. *Indian J. Phys.*, 95:2855, 2021.

[218] N Jehan, W Masood, and A M Mirza. *Phys. Scr.*, 80:035506, 2009.

[219] M M Masud, S Sultana, and A A Mamun. *Astrophys. Space Sci.*, 348:99, 2013.

[220] A S Bains, N S Saini, and T S Gill. *Astrophys. Space Sci.*, 343:293, 2013.

[221] A N Dev, M K Deka, R K Kalita, and J Sarma. *The Eur. Phys. J. Plus*, 135:1, 2020.

[222] B Boro, A N Dev, R Sarma, B K Saikia, and N C Adhikary. *Plasma Phys. Rep.*, 47:557–567, 2021.

[223] S Banik, R K Shikha, A A Noman, N A Chowdhury, A Mannan, T S Roy, and A A Mamun. *Eur. Phys. J. D*, 75:1–6, 2021.

[224] W C Feldman, J R Asbridge, S J Bame, M D Montgomery, and S P Gary. *J. Geophys. Res.*, 80:4181, 1975.

[225] W D Jones, A Lee, S M Gleman, and H J Doucet. *Phys. Rev. Lett.*, 35:1349, 1975.

[226] N Hershkowitz. *Space Sci. Rev.*, 41:351, 1985.

[227] Y Nishida and T Nagasawa. *Phys. Fluids*, 29:345, 1986.

[228] G Hairapetian and R L Stenzel. *Phys. Rev. Lett.*, 65.

[229] B N Goswami and B Buti. *Phys. Lett. A*, 57:149, 1976.

[230] K Nishihara and M Tajiri. *J. Phys. Soc. Japan*, 50:4047, 1981.

[231] Yashvir, T N Bhatnagar, and S R Sharma. *J. Plasma Phys.*, 33:209, 1985.

[232] S Baboolal, R Bharuthram, and M A Hellberg. *J. Plasma Phys.*, 44:1, 1990.

[233] L L Yadav, R S Tiwari, and S R Sharma. *J. Plasma Phys.*, 51:355, 1994.

[234] L L Yadav, R S Tiwari, K P Maheshwari, and S R Sharma. *Phys. Rev. E*, 52:3045, 1995.

[235] S G Tagare. *Phys. Plasmas*, 7:883, 2000.

[236] F S Mozer, R Ergun, M Temerin, C Cattell, J Dombeck, and J Wygant. *Phys. Rev. Lett.*, 79:1281, 1997.

[237] A Esfandyari-Kalejahi, M Afsari-Ghazi, K Noori, and S Irani. *Phys. Plasmas*, 19:082308, 2012.

[238] H Y Wang and K B Zhang. *J. Korean Phys. Soc.*, 64:1677, 2014.

[239] M Jamshidi, M R Rouhani, and H Hakimi Pajouh. *Phys. Scr.*, 90:025604, 2015.

[240] H Y Wang and K B Zhang. *Pramana*, 84:145, 2015.

[241] E Saberian, A Esfandyari-Kalejahi, and M Afsari-Ghazi. *Plasma Phys. Rep.*, 43:83, 2017.

[242] K Singh, N Kaur, and N Saini. *Phys. Plasmas*, 24:063703, 2017.

[243] B Kaur and N S Saini. *Z Naturforschung A*, 73:215, 2018.

[244] S M Motevalli, T Mohsenpour, and N Dashtban. *Contrib. Plasma Phys.*, 59:111, 2019.

[245] A A Noman, N A Chowdhury, A Mannan, and A A Mamun. *Contrib. Plasma Phys.*, 59, 2019.

[246] S K Paul, N A Chowdhury, A Mannan, and A A Mamun. *Pramana*, 94:58, 2020.

[247] B Boro, A N Dev, B K Saikia, and N C Adhikary. *Plasma Phys. Rep.*, 46:641, 2020.

[248] S Thakur, C Das, and S Chandra. *IEEE Trans. Plasma Sci.*, 2021.

[249] A Shome and G Banerjee. *Ricerche di Matematica*, 2021.

[250] E Infeld and G Rowlands. *Proceedings of the Royal Society of London. A. Math. Phys. Sci.*, 366:537, 1979.

[251] E W Laedke and K H Spatschek. *J. Plasma Phys.*, 28:469, 1982.

[252] S Munro and E J Parkes. *J. Plasma Phys.*, 64:411, 2000.

[253] W S Duan. *Phys. Plasmas*, 8:3583, 2001.

[254] W S Duan. *Chaos Solitons Fractals*, 14:503, 2002.

[255] S Munro and E J Parkes. *J. Plasma Phys.*, 70:543, 2004.

[256] E J Parkes and S Munro. *J. Plasma Phys.*, 71:695, 2005.

[257] F Tian-Jun. *Commun. Theor. Phys.*, 47:333, 2007.

[258] J Das, A Bandyopadhyay, and K P Das. *Phys. Plasmas*, 14:092304, 2007.

[259] J H Chen and W S Duan. *Phys. Plasmas*, 14:083702, 2007.

[260] W S Duan, J H Chen, X R Hong, and G X Wan. *Commun. Theor. Phys.*, 47:149, 2007.

[261] J H Chen and W S Duan. *Phys. Plasmas*, 17:063701, 2010.

[262] M M Haider, S Akter, S S Duha, and A A Mamun. *Cent. Eur. J. Phys.*, 10:1168, 2012.

[263] G Williams and I Kourakis. *Phys. Plasmas*, 20:122311, 2013.

[264] J Das, A Bandyopadhyay, and K P Das. *J. Plasma Phys.*, 80:89, 2014.

[265] N Akhtar, W F El-Taibany, S Mahmood, E E Behery, S A Khan, S Ali, and S Hussain. *J. Plasma Phys.*, 81:905810518, 2015.

[266] P Goldstein and E Infeld. *J. Plasma Phys.*, 82, 2016.

[267] O H El-Kalaawy, S M Moawad, and Shrouk Wael. *Results Phys.*, 7:934, 2017.

[268] S K El-Labany, W M Moslem, and N K Elneely. *Adv. Space Res.*, 66:266, 2020.

[269] M Khalid, A Althobaiti, S K Elagan, S A Alkhateeb, E A Elghmaz, and S A El-Tantawy. *Symmetry*, 13:2232, 2021.

[270] D N Gao, J B Yue, J P Wu, W Sh Duan, and Z Z Li. *Plasma Phys. Rep.*, 47:48, 2021.

[271] S A El-Tantawy, A H Salas, and C H Jairo E. *Plos one*, 16:e0254816, 2021.

[272] N A Zedan, A Atteya, W F El-Taibany, and S K El-Labany. *Waves Random Complex Media*, 32:728, 2022.

[273] S Sardar and A Bandyopadhyay. In *Nonlinear Dynamics and Applications: Proceedings of the ICNDA 2022*, page 193. Springer, 2022.

[274] A R Seadawy, S T R Rizvi, and H Zahed. *Mathematics*, 11:1074, 2023.

[275] M A Allen and G Rowlands. *J. Plasma Phys.*, 50:413, 1993.

[276] M A Allen and G Rowlands. *J. Plasma Phys.*, 53:63, 1995.

[277] J A Pava. *Nonlinear dispersive equations: existence and stability of solitary and periodic travelling wave solutions*. Number 156. American Mathematical Soc., 2009.

[278] Q M Huang, Y T Gao, and Lei Hu. *Appl. Math. Comput.*, 352:270, 2019.

[279] F Haq, K Shah, Qasem M Al-Mdallal, and F Jarad. *Eur. Phys. J. Plus*, 134:461, 2019.

[280] I Ali, A R Seadawy, S T R Rizvi, M Younis, and K Ali. *Int. J. Mod. Phys.*, 34:2050283, 2020.

[281] A R Seadawy and N Cheemaa. *Indian J. Phys.*, 94:117, 2020.

[282] Y J Feng, Y T Gao, L Q Li, and T T Jia. *Eur. Phys. J. Plus*, 135:272, 2020.

[283] H Liu, H Khan, R Shah, A A Alderremy, S A, and D Baleanu. *Complexity*, 2020, 2020.

[284] S T R Rizvi, A R Seadawy, F Ashraf, M Younis, H Iqbal, and D Baleanu. *Results Phys.*, 19:103661, 2020.

[285] G Akram, M Sadaf, and I Zainab. *Mod. Phys. Lett. B*, 36:2150520, 2022.

[286] M Alquran and R Alhami. *Nonlinear Dyn*, 109:1985, 2022.

[287] M M Hossain, Md A N Sheikh, et al. *Partial Differential Equations in Applied Mathematics*, 6:100422, 2022.

[288] D C Nandi, M S Ullah, M Z Ali, et al. *Heliyon*, 8:e10924, 2022.

[289] A R Seadawy and A Ali. *Int. J. Mod. Phys. B*, 37:2350276, 2023.

[290] H R Pakzad and M Tribeche. *Astrophys. Space Sci.*, 334:45, 2011.

[291] S K Maharaj, R Bharuthram, S V Singh, and G S Lakhina. *Phys. Plasmas*, 19:072320, 2012.

[292] F Verheest, M A Hellberg, and I Kourakis. *Phys. Plasmas*, 20:082309, 2013.

[293] G S Lakhina, S V Singh, and A P Kakad. *Phys. Plasmas*, 21:062311, 2014.

[294] S S Ghosh and A N Sekar Iyengar. *Phys. Plasmas*, 21:082104, 2014.

[295] A Saha and P Chatterjee. *Astrophys. Space Sci.*, 350:631, 2014.

[296] C P Olivier, S K Maharaj, and R Bharuthram. *Phys. Plasmas*, 22:082312, 2015.

[297] A Saha and J Tamang. *Adv. Space Res.*, 63:1596, 2019.

[298] A Saha, P Chatterjee, and S Banerjee. *Eur. Phys. J. Plus*, 135:801, 2020.

[299] S Dalui and A Bandyopadhyay. *Indian J. Phys.*, 95:367, 2021.

[300] M Irshad and M Khalid. *Eur. Phys. J. Plus*, 137:893, 2022.

[301] H Rashid, U Zakir, F Hadi, and A Zeeshan. *Arab. J. Sci. Eng*, 48:835, 2023.

[302] M K Mishra, R S Tiwari, and S K Jain. *Phys. Rev. E*, 76:036401, 2007.

[303] J F Zhang, Y Y Wang, and L Wu. *Phys. Plasmas*, 16:062102, 2009.

[304] P Chatterjee, U N Ghosh, K Roy, S V Muniandy, C S Wong, and B Sahu. *Phys. Plasmas*, 17:122314, 2010.

[305] S Ghosh and R Bharuthram. *Astrophys. Space Sci.*, 331:163, 2011.

[306] A Rasheed, N L Tsintsadze, and G Murtaza. *Phys. Plasmas*, 18:112701, 2011.

[307] P Eslami, M Mottaghizadeh, and H R Pakzad. *Phys. Plasmas*, 18:102313, 2011.

[308] S K Jain and M K Mishra. *J. Plasma Phys.*, 79:661, 2013.

[309] Md M Rahman, Md S Alam, and A A Mamun. *Eur. Phys. J. Plus*, 129, 2014.

[310] B Ghosh and S Banerjee. *Indian J. Phys.*, 89:1307, 2015.

[311] M A Hossen and A A Mamun. *IEEE Trans. Plasma Sci.*, 44:643, 2016.

[312] S Lashgarinezhad, A H Sari, and D Dorranian. *Chaos, Solitons Fractals*, 103:261, 2017.

[313] C Lavanya. *Braz. J. Phys.*, 52:38, 2022.

[314] H G Abdelwahed. *J. Taibah Univ. Sci.*, 17:2210347, 2023.

[315] M S Alam, M M Masud, and A A Mamun. *Chin. Phys. B*, 22:115202, 2013.

[316] H Ainejad, M Mahdavi, and M Shahmansouri. *Eur. Phys. J. Plus*, 129, 2014.

[317] S A Ema, M Ferdousi, S Sultana, and A A Mamun. *Eur. Phys. J. Plus*, 130:46, 2015.

[318] L B Gogoi and P N Deka. *Phys. Plasmas*, 24:033708, 2017.

[319] S Roy, R R Kairi, and S Raut. *Braz. J. Phys.*, 51:1651, 2021.

[320] A Hussein and M M Selim. *Eur. Phys. J. Plus*, 136:797, 2021.

[321] S N Naeem, A Qamar, M Khalid, and A Rahman. *Eur. Phys. J. Plus*, 136:1205, 2021.

[322] A Sinha and B Sahu. *Adv. Space Res.*, 67:1244, 2021.

[323] M Khalid, E A Elghmaz, and L Shamshad. *Braz. J. Phys.*, 53:2, 2023.

[324] J Tamang. In *Advanced Computational and Communication Paradigms*, page 375. Springer, 2018.

[325] Y Chen and M Y Yu. *Phys. Plasmas*, 1:1868, 1994.

[326] S Mahmood and S Hussain. *Phys. Plasmas*, 14:082303, 2007.

[327] S A El-Tantawy, N A El-Bedwehy, S Khan, S Ali, and W M Moslem. *Astrophys. Space Sci.*, 342:425, 2012.

[328] A Saha and P Chatterjee. *Astrophys. Space Sci.*, 349:813, 2014.

[329] M Sayyar, H Zahed, S J Pestehe, and S Sobhanian. *Phys. Plasmas*, 23:073704, 2016.

[330] F Farhad Kiyaei and D Dorranian. *Phys. Plasmas*, 24:012107, 2017.

[331] M Farooq and M Ahmad. *Phys. Plasmas*, 24:123707, 2017.

[332] G Yashika, K Nimardeep, K Singh, and N S Saini. *Plasma Sci. Technol.*, 20:074005, 2018.

[333] Abdullah, A R Seadawy, and J Wang. *Braz. J. Phys.*, 49:67, 2019.

[334] M Farooq, A Mushtaq, and J Qasim. *Contrib. Plasma Phys*, 59:122, 2019.

[335] O Rahman and M M Haider. *Theor. Phys.*, 4:47, 2019.

[336] S K El-Labany, W F El-Taibany, E E Behery, and R Abd-Elbaki. *Sci. Rep.*, 10:16152, 2020.

[337] M A El-Borie, M Abd-Elzaher, and A Atteya. *Chin. J. Phys.*, 63:258, 2020.

[338] J K Chawla, P C Singhadiya, and R S Tiwari. *Pramana*, 94:13, 2020.

[339] M Shamir and G Murtaza. *Eur. Phys. J. Plus*, 135:394, 2020.

[340] H K Malik, R Srivastava, S Kumar, and D Singh. *J. Taibah Univ. Sci.*, 14:417, 2020.

[341] Md A Salam, M A Akbar, M Z Ali, and M M Haider. *Result. Phys.*, 26:104376, 2021.

[342] O R Rufai, R Bharuthram, and S K Maharaj. *Phys. Plasmas*, 28:052901, 2021.

[343] N S Saini, K Singh, and P Sethi. *Laser Particle Beams*, 2021:e21, 2021.

[344] Md R Hassan and S Sultana. *Contrib. Plasma Phys*, 61(9):e202100065, 2021.

[345] A Atteya, M A El-Borie, G D Roston, A-A S El-Helbawy, P K Prasad, and A Saha. *Z. Naturforsch. A*, 76:757, 2021.

[346] P K Prasad and A Saha. *J. Astrophys. Astron.*, 42:9, 2021.

[347] M Khalid, A Ullah, A Kabir, H Khan, M Irshad, and S M Shah. *EPL*, 138:63001, 2022.

[348] Md A Salam, M A Akbar, M Z Ali, et al. *Phys. Scr.*, 97:125605, 2022.

[349] W F El-Taibany, P K Karmakar, A A Beshara, M A El-Borie, S A Gwaily, and A Atteya. *Sci. Rep.*, 12:19078, 2022.

[350] H A Alyousef, Muhammad Khalid, and Abdul Kabir. *Europhys. Lett*, 139:53002, 2022.

[351] M Khalid, M Khan, A Rahman, and F Hadi. *Indian J. Phys.*, 96:1783, 2022.

[352] S Y El-Monier, A S El-Helbawy, Moamen M Elsayed, and M Saad. *Phys. Scr.*, 98:065602, 2023.

[353] A N Das, S Saha, S Raut, and P Talukdar. *Plasma Phys. Rep.*, 49:454, 2023.

[354] B Pradhan, A Gowrisankar, A Abdikian, S Banerjee, and A Saha. *Phys. Scr.*, 2023.

[355] H G Abdelwahed. *Astrophys. Space Sci.*, 341:491, 2012.

[356] Y W Hou, M X Chen, M Y Yu, and B Wu. *Plasma Phys. Rep.*, 42:900, 2016.

[357] S I Popel and M Y Yu. *Contrib. Plasma Phys.*, 35:103, 1995.

[358] J X Ma and M Y Yu. *Phys. Plasmas*, 1:3520, 1994.

[359] S I Popel, M Y Yu, and V N Tsytovich. *Phys. Plasmas*, 3:4313, 1996.

[360] S I Popel, V N Tsytovich, and M Y Yu. *Astrophys. Space Sci.*, 256:107, 1997.

[361] S Ghosh, S Sarkar, M Khan, and M R Gupta. *Phys. Lett. A*, 274:162, 2000.

[362] J Vranješ, B P Pandey, and S Poedts. *Phys. Rev. E*, 64:066404, 2001.

[363] S I Popel, A P Golub, T V Losseva, R Bingham, and S Benkadda. *Phys. Plasmas*, 8:1497, 2001.

[364] A A Mamun and P K Shukla. *IEEE Trans. Plasma Sci.*, 30:720, 2002.

[365] S I Popel, S N Andreev, A A Gisko, A P Golub, and T V Losseva. *Plasma Phys. Rep.*, 30:284, 2004.

[366] E F El-Shamy. *Chaos, Solitons Fractals*, 25:665, 2005.

[367] T V Losseva, S I Popel, A P Golub, and P K Shukla. *Phys. Plasmas*, 16:093704, 2009.

[368] H Alinejad. *Astrophys. Space Sci.*, 331:611, 2011.

[369] H Alinejad, M Tribeche, and M A Mohammadi. *Phys. Lett. A*, 375:4183, 2011.

[370] S A Elwakil, M A Zahran, E K El-Shewy, and A E Mowafy. *Adv Space Res.*, 48:1067, 2011.

[371] T V Losseva, S I Popel, and A P Golub. *Plasma Phys. Rep.*, 38:729, 2012.

[372] M Kamran, F Sattar, M Khan, R Khan, and M Ikram. *Res. Phys.*, 21:103808, 2021.

[373] T V Losseva, S I Popel, and A P Golub. *Plasma Phys. Rep.*, 46:1089, 2020.

[374] F Verheest, T Cattaert, and M A Hellberg. *Phys. Plasmas*, 12:082308, 2005.

[375] F Sayed and A A Mamun. *Pramana*, 70:527, 2008.

[376] A Abdikian, J Tamang, and A Saha. *Phys. Scr.*, 96:095605, 2021.

[377] K Singh and N S Saini. *Frontiers Phys.*, page 511, 2020.

[378] A A Noman, Md K Islam, M Hassan, S Banik, N A Chowdhury, A Mannan, and A A Mamun. *Gases*, 1:106, 2021.

[379] S Jahan, M N Haque, N A Chowdhury, A Mannan, and A A Mamun. *Universe*, 7:63, 2021.

[380] R E Ergun, C W Carlson, J P McFadden, F S Mozer, G T Delory, W Peria, C C Chaston, M Temerin, R Elphic, R Strangeway, R Pfaff, C A Cattell, D Klumpar, E Shelley, W Peterson, E Moebius, and L Kistler. *Geophys. Res. Lett.*, 25:2025, 1998.

[381] R E Ergun, C W Carlson, J P McFadden, F S Mozer, G T Delory, W Peria, C C Chaston, M Temerin, R Elphic, R Strangeway, R Pfaff, C A Cattell, D Klumpar, E Shelley, W Peterson, E Moebius, and L Kistler. *Geophys. Res. Lett.*, 25:2061, 1998.

[382] H Alinejad, M Mahdavi, and M Shahmansouri. *Astrophys. Space Sci.*, 352:571, 2014.

[383] Shalini, N S Saini, and A P Misra. *Phys. Plasmas*, 22:092124, 2015.

[384] S Dalui, P Kumar, and D Sharma. *Phys. Scr.*, 98:025606, 2023.

[385] M Horányi, G Morfill, and E Grün. *Nature*, 363:144, 1993.

[386] M Horányi, T W Hartquist, O Havnes, D A Mendis, and G E Morfill. *Rev. Geophys.*, 42, 2004.

[387] S M Krimigis, J F Carbary, E P Keath, T P Armstrong, L J Lanzerotti, and G Gloeckler. *J. Geophys. Res.: Space Phys.*, 88:8871, 1983.

[388] H Alfvén. In *Evolution in the Universe*, page 31, 1982.

[389] Katsunobu N. and Masayoshi T. *J. Phys. Soc. Japan*, 50:4047, 1981.

[390] S Sebastian, G Sreekala, M Michael, N P Abraham, S Antony, G Renuka, and C Venugopal. *Int. J. Scientific Res.*, 3:1301, 2014.

[391] S Sijo, M Manesh, G Sreekala, T W Neethu, G Renuka, and C Venugopal. *Phys. Plasmas*, 22:123704, 2015.

[392] M Michael, S Gopinathan, S Sebastian, N T Willington, A Varghese, R Gangadharan, C Venugopal, et al. *JAMP*, 3:1431, 2015.

[393] N T Willington, A Varghese, A C Saritha, N S Philip, and C Venugopal. *Adv Space Res*, 68:4292, 2021.

[394] R Kohli, N S Saini, and T S Gill. *Astrophys. Space Sci.*, 363:193, 2018.

[395] S I Popel and M Y Yu. *Phys. Rev. E*, 50:3060, 1994.

[396] S I Popel, A P Golub, T V Losseva, A V Ivlev, S A Khrapak, and G Morfill. *Phys. Rev. E*, 67:056402, 2003.

[397] A Abdikian and M Eghbali. *Indian J. Phys.*, 97:7, 2022.

[398] R A Cairns, R Bingham, R O Dendy, C M C Nairn, P K Shukla, and A A Mamun. *J. de Physique*, 5:C6–43, 1995.

[399] A A Mamun. *Phys. Rev. E*, 55:1852, 1997.

[400] C A Mendoza-Briceno, S M Russel, and A A Mamun. *Planet. Space Sci.*, 48:599, 2000.

[401] A A Mamun and P K Shukla. *Phys. Rev. E*, 80:037401, 2009.

[402] R K Shikha, M M Orani, and A A Mamun. *Results Phys.*, 27:104507, 2021.

[403] T K Baluku, M A Hellberg, and F Verheest. *Europhys. Lett.*, 91:15001, 2010.

[404] F Verheest and M A Hellberg. *Phys. Plasmas*, 22:012301, 2015.

[405] F Verheest and C P Olivier. *Phys. Plasmas*, 24:113708, 2017.

[406] C P Olivier, F Verheest, and S K Maharaj. *J. Plasma Phys.*, 83:905830605, 2017.